Imperial College of Science, Technology and Medicine

Department of Chemistry

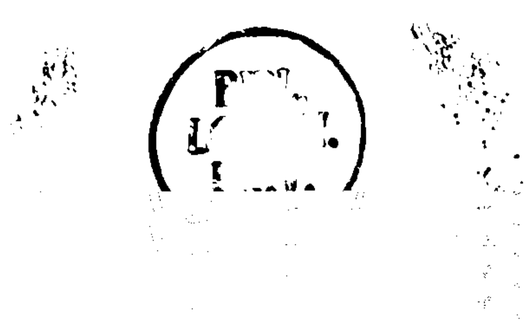
Applications of Microwave Dielectric Heating in Chemistry

by

Benjamin Stephen James Halstead

Submitted for the Degree of Doctor of Philosophy

and for the Diploma of Imperial College



Abstract

This Thesis describes some applications of microwave dielectric heating in chemistry.

In Chapter One the origins of microwave dielectric heating are described briefly and some current applications to synthesis are reviewed.

In Chapter Two the apparatus used in the synthetic experiments is described, including the adaptation of a Fischer-Porter vessel for use in the CEM STAR 2 oven. Several successful organometallic syntheses have been performed, generating good yields in reaction times significantly shorter than conventional procedures. A systematic study of the substitution of Group 6 hexacarbonyls by pyridine and 2,2-bipyridine has been used to evaluate the alternative procedures offered by the range of currently available ovens and vessels.

In Chapter Three the synthesis of high nuclearity carbonyl clusters by microwave dielectric heating is examined. Starting from small clusters and using PTFE autoclaves a variety of products may be synthesised, depending on the solvent employed, with metal cores of 6 to 11 atoms. Reaction times are short and yields are good to excellent. The reactions also show slightly greater selectivity than conventional reflux procedures with only one or two minor products. Cluster synthesis has also been studied in solvent-free conditions. An examination of several of the experimental parameters of the system has been made and the potential of the technique is discussed.

In Chapter Four the origins of microwave dielectric heating are examined in greater detail. The relationship between the dielectric constants and molecular structure for many common solvents is discussed, using a wide range of literature data augmented by recent measurements in out laboratory. The relationship between the dielectric constants and the observed experimental heating rates is discussed for a series of solvents.

Chapter Five strays from the general theme of the Thesis, examining the metal-metal bonding for $M_2(CO)_{10}$ and $MM'(CO)_{10}$ (where M and M' = Mn or Tc) using Density Functional Theory based molecular orbital calculations. Although differences in the molecular orbitals are observed for the mixed metal species, the calculated metal-metal

bond length and energy does not significantly differ from the average of the two homometallic systems, in contrast to the experimentally observed measurements for $MnRe(CO)_{10}$

Acknowledgements

Firstly I must thank Mike for his help and support during the last five years. I also couldn't have completed this Thesis without much help and encouragement from past and present members of the Mingos group; particularly Paul Dyson, who initiated the cluster experiments, Crispin Roche and Steven Tarlton, who recorded some of the NMR spectra, Phil Dyer mentored the hexacarbonyl substitutions, Sami Gabriel began the dielectric measurements and performed the high frequency scans for Chapter 4, Ramon Vilar and John McGrady gave invaluable advice during the ADF stages of the DFT studies and Pascal Harper has made heroic efforts to upgrade the group PC's to a state where the Thesis will actually print. Other members of the group have provided help and advice and generally done their best to keep me sane, especially Phil Blakeman.

The resolution of Chapter 4 would have been impossible without the help of Ian Gould and Edward Griffiths. Garry Rumbles group lent us disk recovery software at several crucial moments. The vast majority of departmental technicians were very helpful when faced by my questions. The Imperial glassblowers did a splendid job; I apologise for continually shattering their work.

The whole of the sixth floor provided a great working atmosphere and friends from school and UEA kept me supplied with beer and company, with special thanks to Nik and Sam and Dave.

My family have provided an enormous amount of emotional and financial support; I owe them a great debt. Thanks to one and all.

Table of Contents

Abstract 2
Acknowledgements 4
Table of Contents 5
List of Figures 7
List of Tables 9
List of Abbreviations 11

Chapter One Introduction 13

1.1. Introduction 13
1.2. Kinetic Studies 14
1.3. Organic Syntheses 19
1.4. Solid-Liquid Solvent-Free Phase Transfer Catalysis 24
1.5. Synthesis of Inorganic Solids 27
1.6. Catalysis 35
1.7. Microwave Plasma Chemistry 40
1.8. Microwave Enhanced Deuteriation 42
1.9. Polymer Applications 43
1.10. Summary 46
1.11. References 47

Chapter Two Description Of Apparatus And Reactions 49

2.1. Introduction 49
2.2. Apparatus 49
2.2.1. CEM MDS 2000 49
2.2.2. CEM STAR 2 52
2.2.3. New Vessels 54
2.3. Vessel evaluation 57
2.3.1. Introduction 57
2.3.2. Pressure development 57
2.3.3. Test reactions 59
2.4. Substitution reactions of Group 6 Metal hexacarbonyls 61
2.4.1 Pyridine 61
2.4.2. 2,2'-bipyridine 65
2.5. Limitations of the new vessel 68
2.5.1 Vessel failures 68
2.5.2 Seal failure 71
2.6. Summary 71
2.7. Experimental 73
2.8. References 77

Chapter Three Transition Metal Carbonyl Cluster Synthesis 78

3.1. Introduction 78
3.2. Carbonyl Cluster Synthesis 78

3.3. Cluster Structures 81
3.4. Dielectric Thermolysis 85
3.4.1. Ruthenium 86
3.4.2. Osmium 91
3.4.3. Iridium 94
3.4.4. Summary 95
3.5. Surface-mediated Syntheses 96
3.5.1. Ruthenium 98
3.5.2. Osmium 100
3.5.3. Summary 104
3.6. Experimental 106
3.7. References 111

Chapter Four Dielectric Parameters and their Influence on Solvent Heating 112

4.1. Introduction 112
4.2. Fundamental Theory 113
4.2.1. Dielectric Polarisation 114
4.3. Aqueous Systems 118
4.3.1. Water-alcohol and water-carbohydrate mixtures 120
4.3.1. Aqueous protein solutions 121
4.3.1. Ionic solutions 122
4.4. Organic Solvents 123
4.4.1. Alcohols 123
4.4.2. Nitriles, esters, ketones and chlorohydrocarbons 126
4.4.3. Aromatic Compounds 129
4.4.4. Polyalcohols 130
4.4.5. Intramolecular rotations 131
4.5. Relaxation 133
4.6. Heating Rates 138
4.7. Temperature dependence 148
4.8. Summary 151
4.9. Experimental 152
4.10. References 153

Chapter Five Density-functional study of the di-metal decacarbonyls of group 7 155

5.1. Introduction 155
5.2. Evaluation of calculation accuracy. 156
5.3. Investigation of the mixed metal system 158
5.4. Relaxation of the mono-metallic fragments 168
5.5. Conclusion 171
5.6. Theoretical Methods 173
5.7. References 174

List of Figures

Figure 1.1: The effects of heating rate on selectivity. (a) Theoretical model: (b) Experimental results from the sulfonation of naphthalene. 15
Figure 1.2. Average temperature profiles with and without superheating areas. 16
Figure 1.3. Kinetical curves with and without superheating areas 16
Figure 1.4. Yields of esterification with Montmorillonite KSF at 140 °C under microwave (MW), conventional heating (CH) and ultrasound (US) conditions. 18
Figure 1.5. Growth curves for ZSM-5: (a) seeded, TPABr, microwave; (b) seeded, inorganic, microwave; (c) seeded, TPABr, thermal; (d) unseeded, TPABr, microwave; (e) unseeded, TPABr, thermal, (f) unseeded, inorganic, thermal 32

Figure 2.1: Schematic illustration of the MDS 2000 microwave oven 50
Figure 2.2: Lined Digestion Vessel (LDV) 51
Figure 2.3: STAR 2 Microwave Oven 53
Figure 2.4: Modified Fisher Porter Vessel (Vessel **2)** 55
Figure 2.5: Detail of vessel head 56
Figure 2.6: Variation of pressure with time for **Vessel 1** and **Vessel 2.** 58
Figure 2.7: Temperature traces for **Vessel 2** 58
Figure 2.8: ROSA reactor 64
Figure 2.9: Vessel 2, showing clamp and support points. 68
Figure 2.10 Some possible simple alterations for **Vessel 2** 70

Figure 3.1. Structures of $[H_4Os_{10}(CO)_{24}]^{2-}$, a condensed cluster with face centred cubic packing and $[Pt_{15}(CO)_{30}]^{2-}$, a columnar cluster. 82
Figure 3.2. Examples of clusters with interstitial atoms 82
Figure 3.3. Examples of ring and three-connected cluster compounds. 83
Figure 3.4. *closo, nido* and *arachno* polyhedra derived from the octahedron. 84
Figure 3.5. Metal core of $[HOs_8(CO)_{22}]^-$. 85
Figure 3.6. Structure of $[HRu_6(CO)_{18}]^-$. 87
Figure 3.7. Structure of $[H_2Ru_{10}(CO)_{25}]^{2-}$. 88
Figure 3.8. Structure of the metal core in $[HRu_{11}(CO)_{27}]^{3-}$ 89
Figure 3.9. Osmium and ruthenium carbonyl clusters with bridging and terminal halides 92
Figure 3.10. Apparatus for surface mediated reactions in a STAR 2 oven 97

Figure 4.1. Application of a sinusoidal electric field to liquid ideal dielectric (top) and the induced Maxwell displacement current (bottom) 114
Figure 4.2. Phase diagrams for a) an ideal dielectric where the energy is transmitted without loss b) where there is a phase displacement δ c) the relationship between ε^*, ε' and ε'' 115
Figure 4.3. The variation of ε' and ε'' with frequency for water at 20 °C 119
Figure 4.4. Schematic illustration of the dielectric spectrum of an aqueous protein solution. 121

Figure 4.5. Experimental values of the permittivity and total loss factor for KCl solutions with differing concentrations 122
Figure 4.6. Dielectric spectra for water and a range of alcohols 126
Figure 4.7. Possible localised relaxation processes for Ph_3CX 131
Figure 4.8. Dielectric absorption of tri-tert-butylphenol in decalin (0.76 M) at 20 °C 132
Figure 4.9. Plots of relaxation time τ vs. $3V\eta$ for a) a series of alkanenitriles and a series of halobenzenes; b) a series of alcohols. 134
Figure 4.10. Measured dielectric constants for benzyl alcohol and the fitted curves for two Debye relaxations. 135
Figure 4.11. Measured dielectric constants for n-octanol and the fitted curves using the Cole-Davidson equation 136
Figure 4.12. Plot of observed temperature rise vs. dielectric parameters for a series of alcohols 141
Figure 4.13. Plot of absorbed power vs. dielectric parameters for a series of alcohols 142
Figure 4.14. Plot of observed temperature rise vs. dielectric parameters for a series of alkanenitriles 144
Figure 4.15. Plot of absorbed power vs. dielectric parameters for a series of alkanenitriles 144
Figure 4.16. Plot of temperature rise vs. dielectric parameters for a series of halobenzenes 146
Figure 4.17. Plot of absorbed power vs. dielectric parameters for a series of halobenzenes 146
Figure 4.18. Variation of temperature rise against tan δ and $\varepsilon\varepsilon$ for samples of constant volume 147
Figure 4.19. Variation of the loss factor as a function of temperature 150

Figure 5.1. Optimised geometry for $MnTc(CO)_{10}$, using a 3-21g* basis set. 159
Figure 5.2. e_3 π^* oribtal for $Mn_2(CO)_{10}$. 162
Figure 5.3. e_1 π orbital for $Mn_2(CO)_{10}$ 163
Figure 5.4. a_1 σ orbital for $Mn_2(CO)_{10}$ 163
Figure 5.5. e_2 δ orbital for $Mn_2(CO)_{10}$ 164
Figure 5.6. Highest occupied molecular orbital (a_1) for $MnTc(CO)_{10}$ 165
Figure 5.7. Relative energy levels for the upper occupied orbitals of $M_2(CO)_{10}$ 165
Figure 5.8. Low-lying e orbital for $MnTc(CO)_{10}$, centred on the $Tc(CO)_5$ fragment. 166
Figure 5.9. High-energy e orbital for $MnTc(CO)_{10}$, centred on Mn. 166
Figure 5.10. Ligand back-bonding orbitals (b_1 and b_2) for MnTc. 167
Figure 5.11. Optimised geometries for the $M(CO)_5$ radicals, using GAUSSIAN 98 and a 3-21g* basis set a) M = Mn b) M = Tc 169

List of Tables

Table 1.1. Temperature of 50 cm^3 of solvent, after heating from room temperature for 1 minute at 560W. 14
Table 1.2. Influence of the heating mode on reaction yields for different esterification catalysts. 17
Table 1.3. Synthesis of Schiff bases from 5-amino-2-toluenesulfonamide by three methods. 20
Table 1.4. Dielectric Synthesis of dioxolanes 21
Table 1.5. Synthesis of organomercurial compounds. 22
Table 1.6. Oxidation of β,β-disubstituted enamines 23
Table 1.7. Selective dealkylation of aromatic esters 25
Table 1.8. Synthesis of aryloxyacetic acids under microwave irradiation without the use of organic solvent. 26
Table 1.9. Glasses formed by microwave heating. 35
Table 1.10. Comparison of conventional (furnace) and microwave heating methods for the catalytic oxidation of *o-xylene* to PAN over V_2O_5/SiO_2. 36
Table 1.11. Product distribution of microwave catalysis of carbon dioxide and water. 38
Table 1.12. Rate constants for the addition of chloro compounds to alkenes under microwave (k_m) and conventional (k_c) conditions, in the presence of [$Cu(2\text{-}PhNH_2)_2Cl$] catalyst. 40
Table 1.13. Deuteriation of selected aromatics (PhX) under microwave conditions. 43

Table 2.1: Results for a series of organometallic transformations 60
Table 2.2: Substitution of $M(CO)_6$ by pyridine. Heated under reflux at atmospheric pressure conditions in the STAR 2 oven 62
Table 2.3: Substitution of $M(CO)_6$ by pyridine. Heated under pressure in the MDS 2000 oven 63
Table 2.4: Substitution of $M(CO)_6$ by pyridine. Heated under pressure in the STAR 2 oven, **Vessel 2** 65
Table 2.5: Substitution of $M(CO)_6$ by bipyridine under reflux conditions. (literature data in italics) 66
Table 2.6: Substitution of $M(CO)_6$ by bipyridine in an autoclave (CEM LDV) 67

Table 3.1. Preparation of high nuclearity ruthenium clusters by reflux thermolysis. 79
Table 3.2. Preparation of osmium carbonyl clusters by reflux thermolysis. 80
Table 3.3. Preparation of carbonyl clusters on inorganic surfaces. 81
Table 3.4. Preparation of high nuclearity ruthenium clusters by dielectric heating. 86
Table 3.5. Preparation of Osmium clusters by dielectric thermolysis 91
Table 3.6. Preparation of Iridium clusters by dielectric heating. 95
Table 3.7. Alumina supported $Ru_3(CO)_{12}$ heated to 100°C in **Vessel 3** 98

Table 3.8. Alumina supported $Os_3(CO)_{12}$ heated to 200 °C with a range of surface dispersions 101
Table 3.9. Alumina supported $Os_3(CO)_{12}$, heated to 200 °C, for 20 minutes, with an uneven surface dispersion. (Overall Os ratio 2.5 % w/w) 102
Table 3.10. Alumina supported $Os_3(CO)_{12}$ heated to 200 °C for a range of times, surface dispersion 1 % Os w/w 102
Table 3.11. Alumina supported $Os_3(CO)_{12}$, heated for 20 minutes 103

Table 4.1. Relaxation times (at 20 °C) and dielectric properties of aliphatic alcohols compared with water 124
Table 4.2 Values of static permittivity (ε_s) and Kirkwood correlation factor g for some non-aqueous solvents. 125
Table 4.3. Relaxation times of some nitriles. 127
Table 4.4. Relaxation times of a series of oxygenated solvents. 128
Table 4.5. Relaxation times of some halogenated alkanes 129
Table 4.6. Relaxation times and dielectric properties of simple aromatic compounds 129
Table 4.7. Relaxation times and dielectric properties of glycols. 130
Table 4.8. Structure and dielectric parameters of three methoxybenzylamines 132
Table 4.9. Data required for the evaluation of Debye's equation for dielectric relaxation times 134
Table 4.10. Data from the dielectric heating experiments for a range of alcohols. 140
Table 4.11. Data from the dielectric heating experiments for a range of alkanenitriles. 143
Table 4.12. Data from the dielectric heating experiments for a range of halobenzenes. 145
Table 4.13. Relaxation times and dielectric properties of linear alcohols at 2.45 GHz as a function of temperature 148

Table 5.1. Geometries for $Mn_2(CO)_{10}$ 156
Table 5.2. Geometries for $Tc_2(CO)_{10}$ 157
Table 5.3. Experimental M-M Bond Dissociation Enthalpies for $Mn_2(CO)_{10}$ in kJ mol^{-1} 157
Table 5.4. Calculated Energy contributions to the M-M Bond Dissociation Enthalpies (D_e) for $Mn_2(CO)_{10}$ in kJ mol^{-1} 158
Table 5.5. Comparative geometries for calculated $Mn_2(CO)_{10}$, $Tc_2(CO)_{10}$ and $MnTc(CO)_{10}$ 159
Table 5.6. Calculated Energy contributions to the M-M Bond Dissociation Enthalpies (D_e) for $M_2(CO)_{10}$ and $MM'(CO)_{10}$ in kJ mol^{-1} 160
Table 5.7. Experimental bond dissociation energies in kJ mol^{-1}. 161
Table 5.8. Comparative geometric parameters for $Mn_2(CO)_{10}$ and $Mn(CO)_5$, calculated using GAUSSIAN 94 and a 6-311^+g* basis set. 168
Table 5.9. Geometric parameters for $M(CO)_5$, optimised using GAUSSIAN 98 and a 3-21g* basis set. 170
Table 5.10. Comparative geometries for $M(CO)_5$ optimised under C_{4v} and C_{2v} symmetries using ADF 2.3 171

List of Abbreviations

TPSA	toluene-*p*-sulfonic acid
dmf	dimethylformamide
dmso	dimethylsulfoxide
TPABr	tetrapropylammonium bromide
PTFE	polytetrafluoroethylene
LDV	lined digestion vessel
bipy	2,2-bipyridine
py	pyridine
pec	polyhedral electron count
PPN	$(PPh_3)_2N^+$
ps	pico seconds
D	Debye
DFT	Density Functional Theory

This Thesis is dedicated to the memory of Jon Cunliffe

Chapter One

Introduction

1.1. Introduction

The interaction between microwave radiation and polar solvents (particularly water) has been known since the early days of the magnetron[1] and domestic ovens utilising this effect have been widespread since the 1980's. Interest in the application of dielectric heating to chemical transformations has grown steadily since the early 1980's to the extent that specific reviews on organic synthesis[2], inorganic solid state chemistry[3,4], catalysis[5] and 'solvent-free' synthesis[6] have appeared, alongside a steady stream of more general reviews.[7,8,9,10]

The detailed physical basis of dielectric heating is examined in Chapter Four. In essence, a molecule with a permanent dipole in an electric field will rotate such that the dipole and field are aligned. If the oscillation of the electric field is comparable to the response time of the molecular dipole, a molecular torque is generated, leading to energy absorption. Microwave ovens generally operate at 2.45 GHz as the surrounding frequencies are reserved for RADAR and telecommunication use. At this frequency small inorganic and organic molecules with permanent dipoles show strong heating effects (see Table 1.1.).

The dielectric properties of materials are defined by the parameters ε', the dielectric constant and ε", the dielectric loss. The dielectric constant describes the ability of the material to be polarised by the electric field whereas the dielectric loss measures the efficiency with which the energy of the electromagnetic radiation is converted into heat.

Table 1.1. Temperature of 50 cm^3 of solvent, after heating from room temperature for 1 minute at 560W.

Solvent	Temperature / °C	Boiling point / °C	Solvent	Temperature / °C	Boiling point / °C
Water	81	100	Acetic acid	110	119
Methanol	65	65	Ethyl acetate	73	77
Ethanol	78	78	Chloroform	46	61
1-propanol	97	97	Acetone	56	56
1-butanol	109	117	dmf	131	153
1-pentanol	106	137	Diethyl ether	32	35
1-hexanol	92	158	Hexane	25	68
1-chlorobutane	76	78	Heptane	26	98
1-bromobutane	95	101	CCl_4	28	77

Data from ref. 10.

The ratio of ε'' to ε' is described as the energy dissipation factor or loss tangent and generally written tan δ.

1.2. Kinetic Studies

Chemical reactions performed under microwave conditions are often reported as resulting in dramatically reduced timescales with 10 to 100-fold reductions.[7] In early work this was attributed to a 'non-thermal' effect of dielectric activation,[11] however such an effect is not now generally recognised. Careful examination of the reaction conditions under both heating regimes is required to fully evaluate these effects.

Stuerga *et al*[12] examined the kinetics for a system where two reversible reactions compete for the same reactant. The model derived, after allowing for differing activation energies and rate constants in the forward and reverse reactions, shows product selectivity to be dependent on dT/dt (see Figure 1.1). Theoretical results agree well with those obtained from the sulfonation of naphthalene to give 1- and 2-naphthalene sulfuric acids (NSA). The selectivity is a direct result of the heating rate and theoretically independent

of the heating method. However, the effect is only observable under the steep temperature ramping obtained from microwave heating.

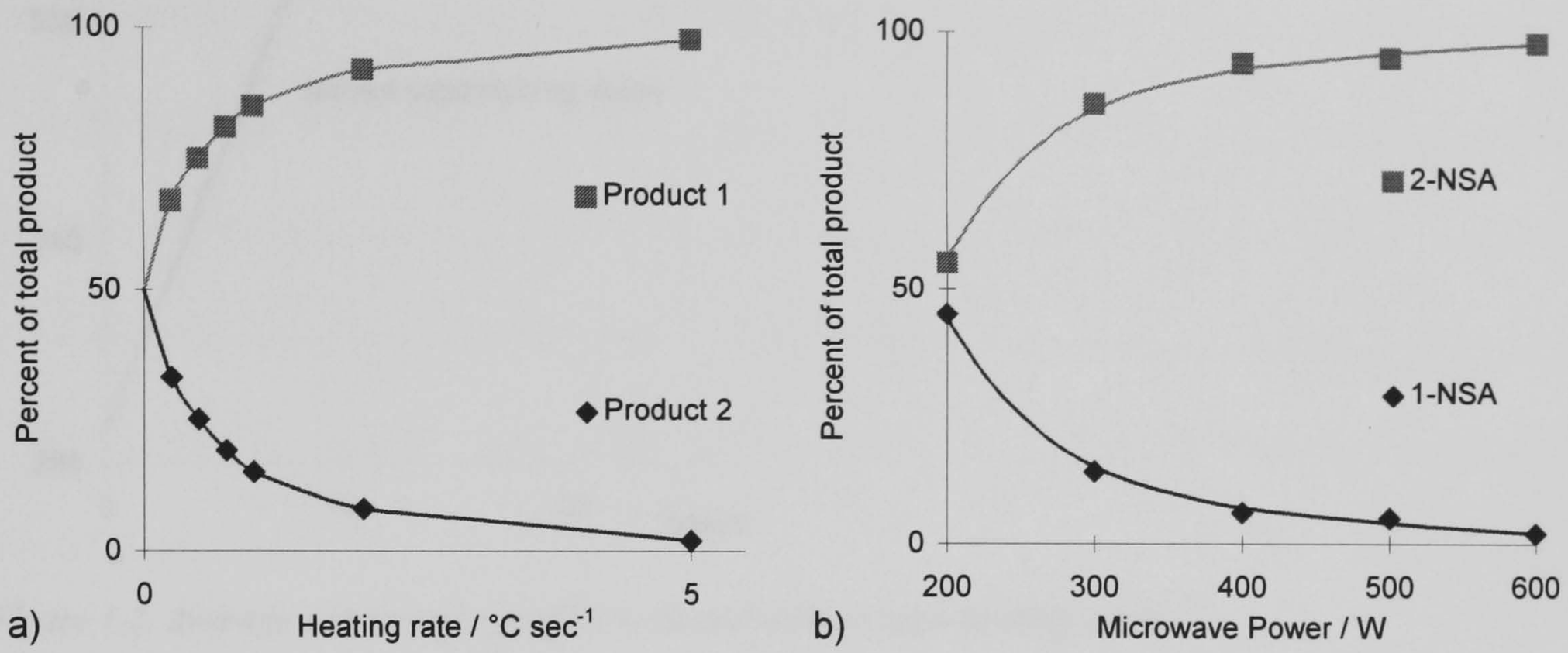


Figure 1.1: The effects of heating rate on selectivity.
(a) Theoretical model:
(b) Experimental results from the sulfonation of naphthalene.[12]

Stuerga and Gaillard[13] have also examined the possible kinetic effects of localised superheating ('hot-spots'). Alumina, treated with 0.1 % potassium acetate to enhance the dielectric absorption, was heated in a 200W monomode cavity for 30 s. In order to minimise the difference between core and surface temperatures, the alumina sample surface was only 2 mm thick. Surface temperature was monitored with an infra-red camera. The surface temperature was observed to vary between 50 and 120 °C, with thermal gradients between 7 °C cm^{-1} and 70 °C cm^{-1}.

The measured overall temperature, for a model experiment with a base temperature of 340 K and a ramp time of 10 s is shown in Figure 1.2. When 'hot spots' with a population of 2 % and a temperature gradient of 70 °C are added to the model, the overall temperature barely changes.

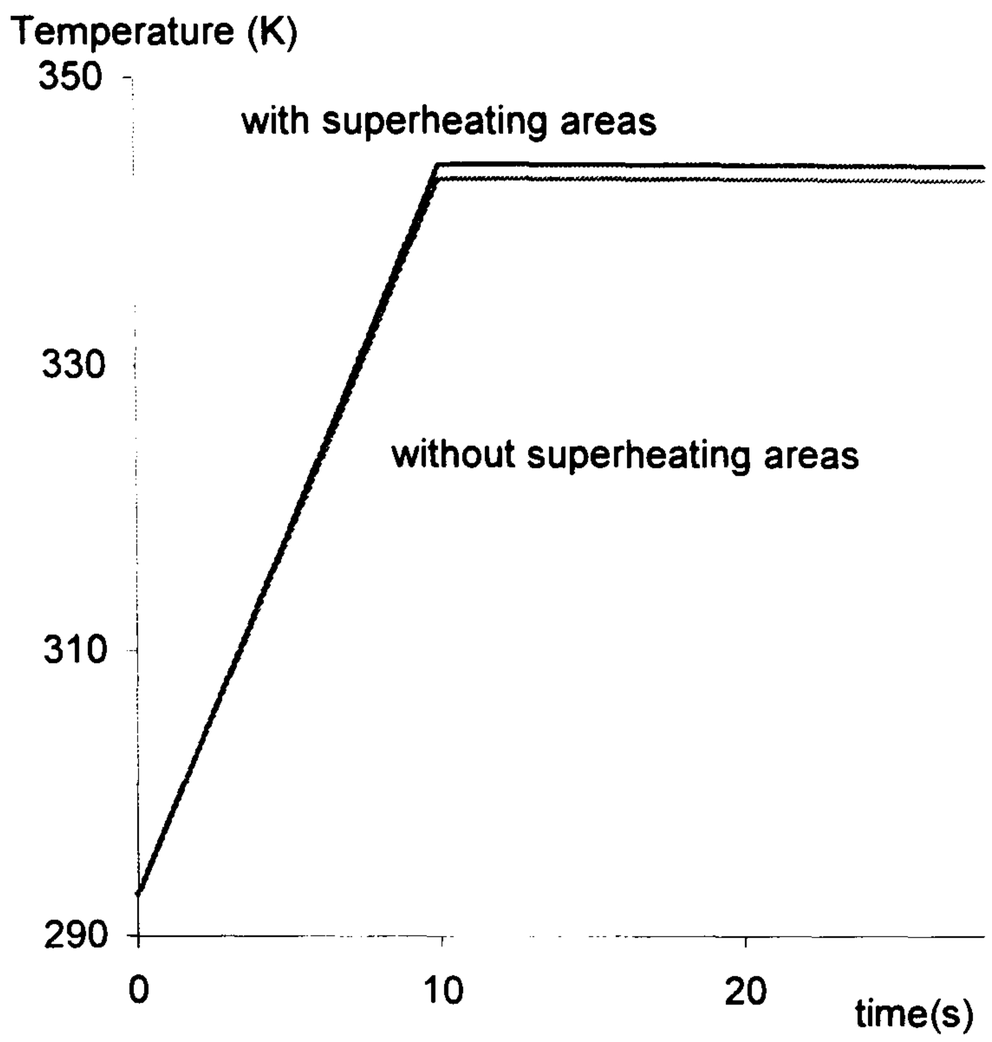


Figure 1.2. Average temperature profiles with and without superheating areas.[13]

However, for a model reaction of the form

$$R_1 + R_2 \xrightarrow{A,E} P$$

with A, the pre-exponential factor, set to 1.45×10^{13} $mol^{-1}s^{-1}$ and E, the activation energy, set as 80 kJ mol^{-1} the plots for reaction progression shown in Figure 1.3. were

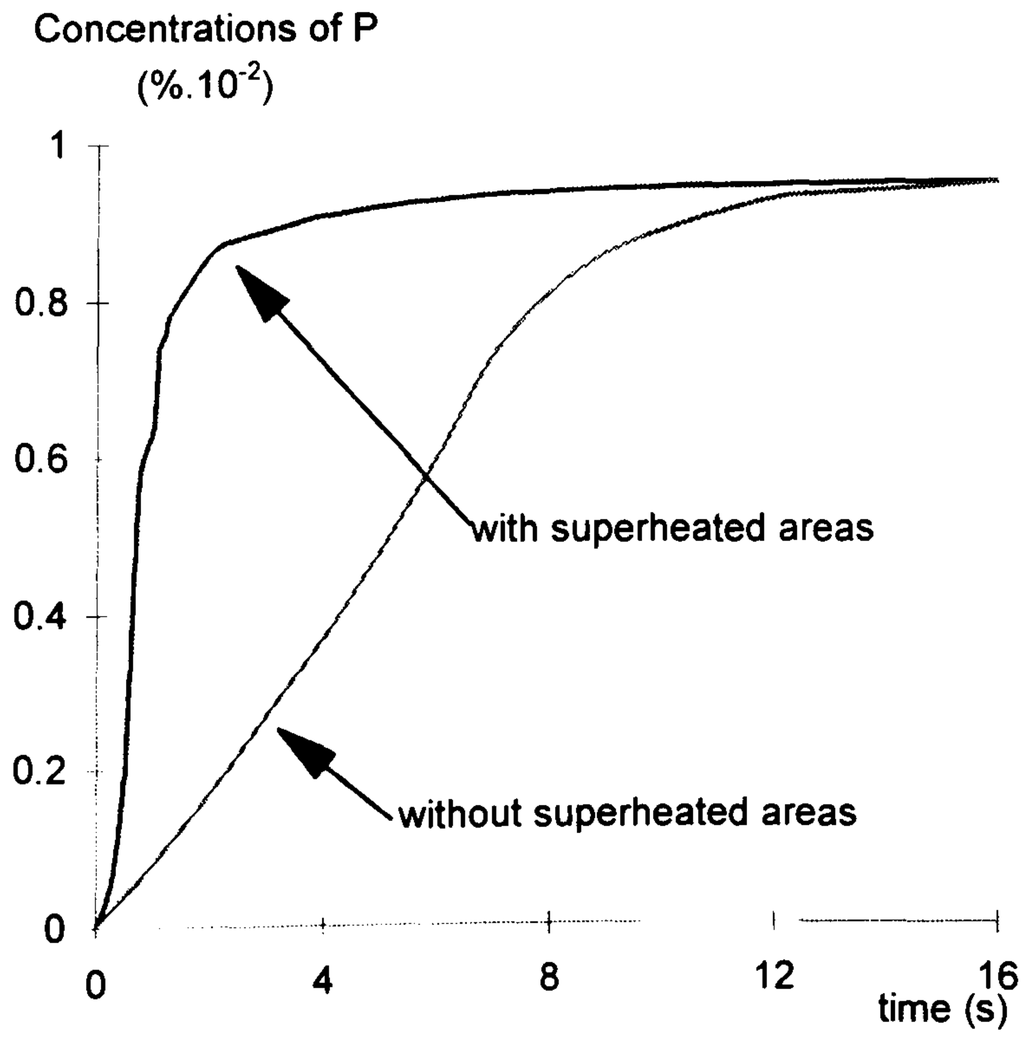


Figure 1.3. Kinetical curves with and without superheating areas[13]

calculated. For these parameters, typical of conventional reaction conditions, the difference in average temperature is negligible whilst the effect on reaction rate is large.

Galema *et al*[14] have examined the esterification of stearic acid under homogenous and heterogeneous conditions. For a homogenous reaction between stearic acid and n-butanol, catalysed by toluene-*p*-sulfonic acid, no difference in activation energy is observed for dielectrically or conventionally heated experiments. For a heterogeneous system, heated for 2 hours at 140 °C, the higher yields seen under dielectric heating conditions are summarised in Table 1.2.

Table 1.2. Influence of the heating mode on reaction yields for different esterification catalysts.[14]

Catalyst	Reaction time / min	$Y_{(d)}$	$Y_{(c)}$	$Y_{(d)}/Y_{(c)}$
TPSA[a]	60	91	89	1.0
$Fe_2(SO_4)_3$[b]	120	71	50	1.4
$TiBu_4$[b]	120	78	60	1.3
KF[b]	120	85	64	1.3
Montmorillonite KSF[b]	120	95	82	1.2

a) Homogenous reaction conditions

b) Heterogeneous reaction conditions

$Y_{(d)}$ -Yield under dielectric heating

$Y_{(c)}$ -Yield under conventional heating

The higher yields for the dielectrically heated heterogeneous reactions were attributed to localised hot-spots, unobtainable under conventional heating conditions. Nevertheless, better yields are still obtained using homogenous catalysts. If graphite (a strong microwave absorber) was added to the heterogeneous systems, in order to enhance the hot-spot effects, yields of 95 % were observed after only 5 minutes.

The effect of ultrasound activation of heterogeneous systems was also examined. Ultrasound activation is believed to improve mass transfer at the catalyst surface and thus

would be expected to be complementary to microwave activation. This has been shown to be the case for the reaction on Montmorillonite KSF and is illustrated in Figure 1.4.

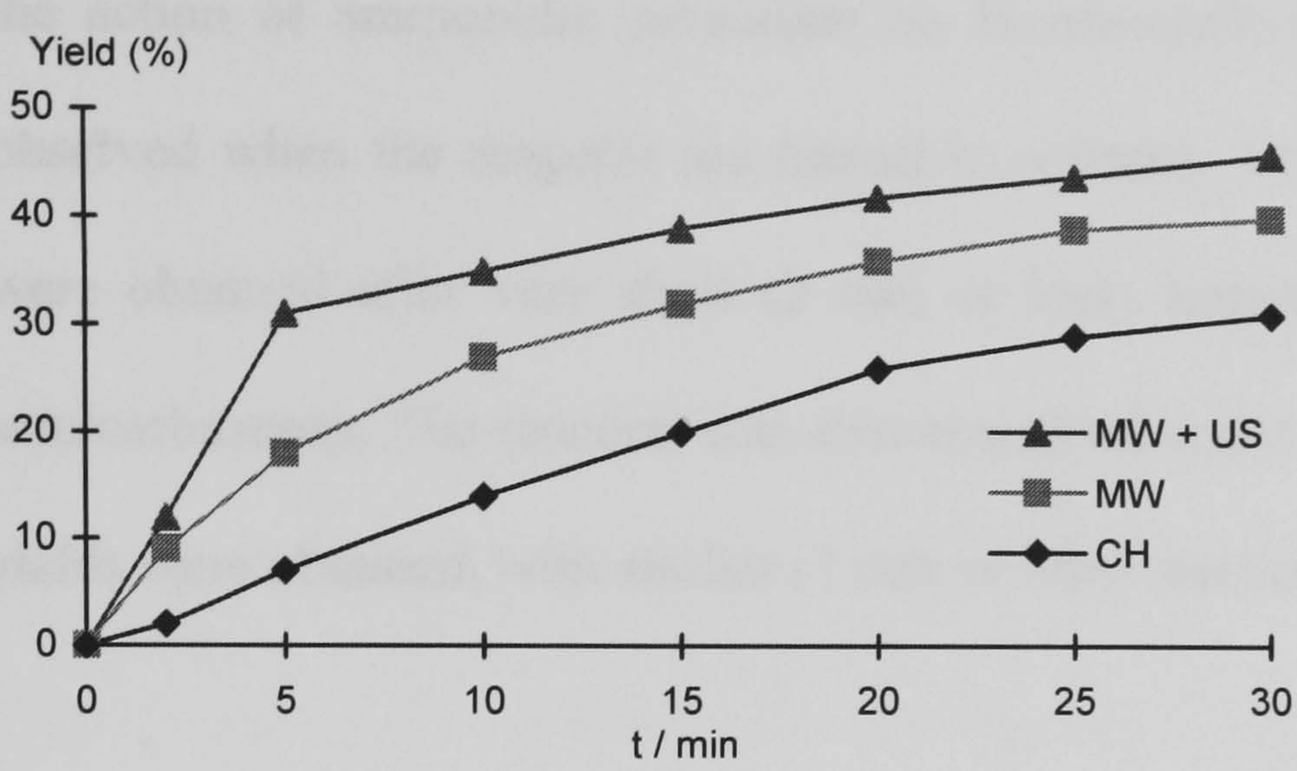
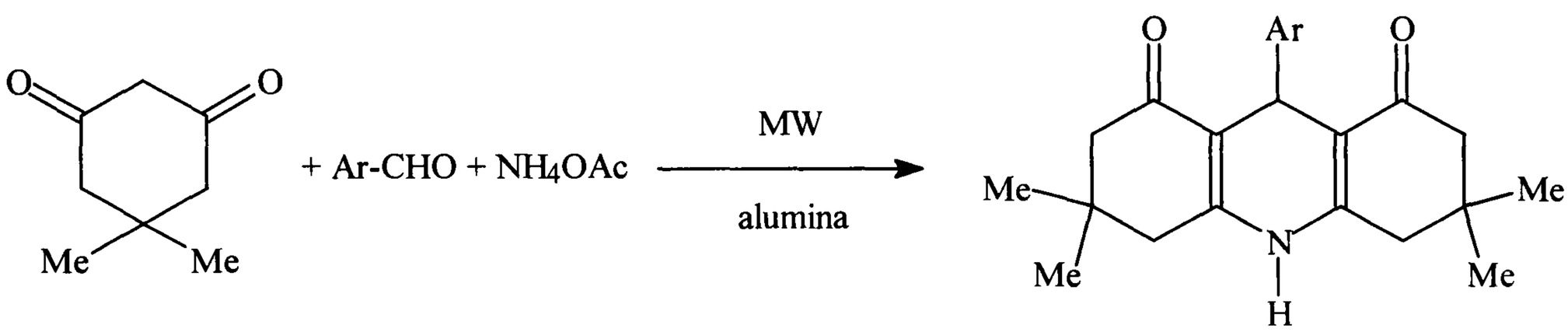


Figure 1.4. Yields of esterification with Montmorillonite KSF at 140 °C under microwave (MW), conventional heating (CH) and ultrasound (US) conditions.[14]

Marken *et al*[15] have examined the effect of short pulses of microwave radiation on the ferrocyanide/ferricyanide redox couple. When the oxidation of 2 mM $[Fe(CN)_6]^{4-}$ at 25 mm diameter Pt electrode in aqueous 1 M KCl was subjected to 0.6 s pulses of 24 W of microwave radiation sudden and temporary increases in the redox current, apparently induced by the microwaves, were seen. Similar pulses were seen for the reduction of $[Fe(CN)_6]^{3-}$. The short pulses are insufficient to heat the bulk solution and the redox current rapidly returns to the 'steady state' value. These effects are attributed to localised heating at the Pt electrode. By reference to the equilibrium potential it is possible to estimate the electrode temperature during pulses; for 24 W superheating to 120 °C is observed. The results are highly dependent on electrode size; for a 50 μm disc smaller temperature rises are observed whereas for a 1 μm disc no localised heating is observed at all.

1.3. Organic Syntheses

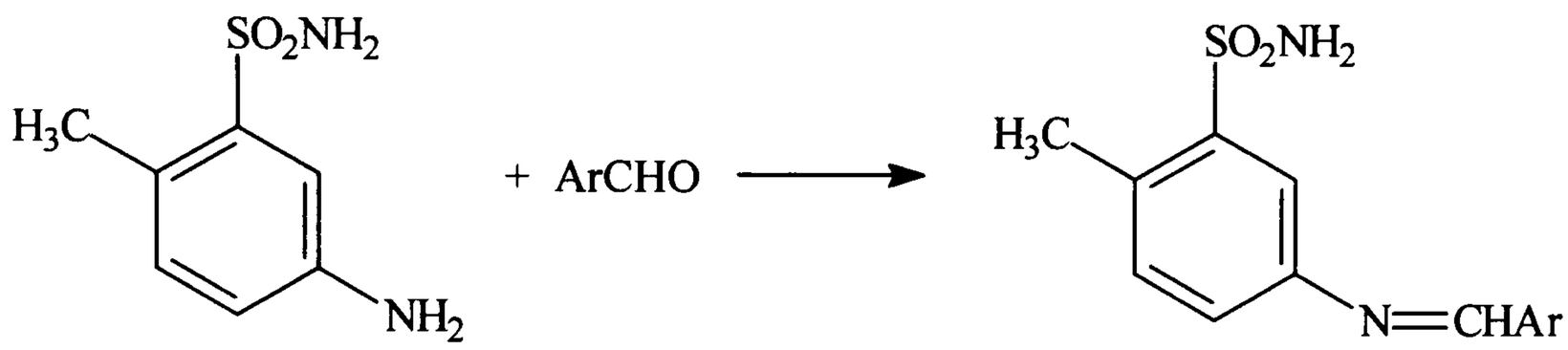
Semicarbazones and hydrazones have been oxidised to the corresponding ketones by the action of ammonium persulfate on Montmorillonite K10 clay.[16] No reaction was observed when the reagents are heated in solution. Good (60 - 80 %) yields of ketone were obtained after very short (2 min or less) heating periods, for a wide variety of semicarbazones. The reaction was also examined under ultrasonic activation: comparable yields were obtained, with similar (3 min or less) reaction times.



Scheme 1.1

Decahydroacridine derivatives have been prepared according to Scheme 1.1. using microwave irradiated alumina as a support material.[17] Catalytic amounts of dmf were used to enhance the heating rate in the early stages of reaction. Good yields were achieved after 5 minutes of dielectric heating. By comparison the conventional synthesis requires heating at reflux for several hours.

Ochoa *et al*[18] have studied the synthesis of a range of Schiff bases, derived from aminotoluenesulfonamide (Scheme 1.2.) under a variety of dielectric and conventional heating methods. The conventional synthesis which involved a reflux in ethanol, was compared with a solvent free microwave method, both with and without catalytic amounts of dmf (0.4 mL of dmf with 20 mmol 5-amino-2-toluenesulfonamide) as a heat transfer agent. The solvent free method was also examined under conventional heating methods.



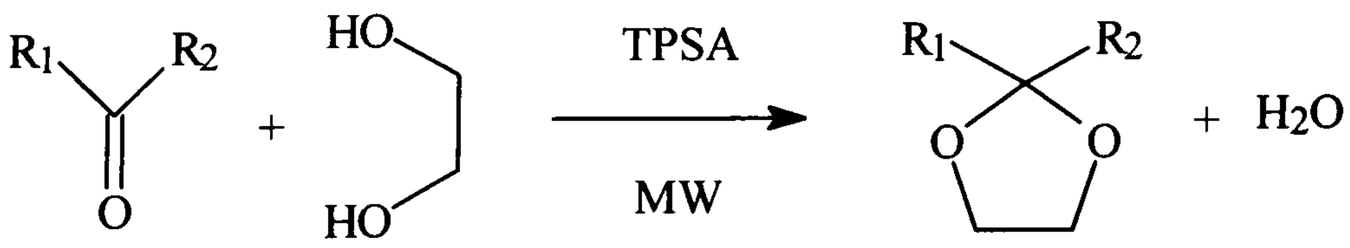
Scheme 1.2.

The results, shown in Table 1.3. demonstrate the clear advantages of the microwave method and the value of dmf as a heat transfer agent for samples that do not heat strongly in a microwave field.

Table 1.3. Synthesis of Schiff bases from 5-amino-2-toluenesulfonamide by three methods.[18]

Ar	EtOH-reflux		Microwave-dmf		Microwave-no dmf		Oil bath dmf	
	Yield (%)	time (min)	Yield (%)	time (min)	Yield (%)	time (min)	Yield (%)	time (min)
p-$NO_2C_6H_4$	80	180	98	1	40	1	5	1
o-ClC_6H_4	75	240	90	2	22	2	6	2
2-furyl	70	300	72	2	20	3	5	3
5-(*p*-$NO_2C_6H_4$)-2-furyl	75	240	96	2	40	2	10	2
5-NO_2-2-furyl	75	120	96	2	20	2	5	2
5-NO_2-2-thienyl	87	180	92	1	30	1	10	1

Dioxolanes have been synthesised from both aldehydes and ketones (see Scheme 1.3.) using a monomode reactor[19] or a standard domestic oven.[20] Some results are summarised in Table 1.4. Comparison between the methodologies is problematical as no temperature data were reported for the multimode system.

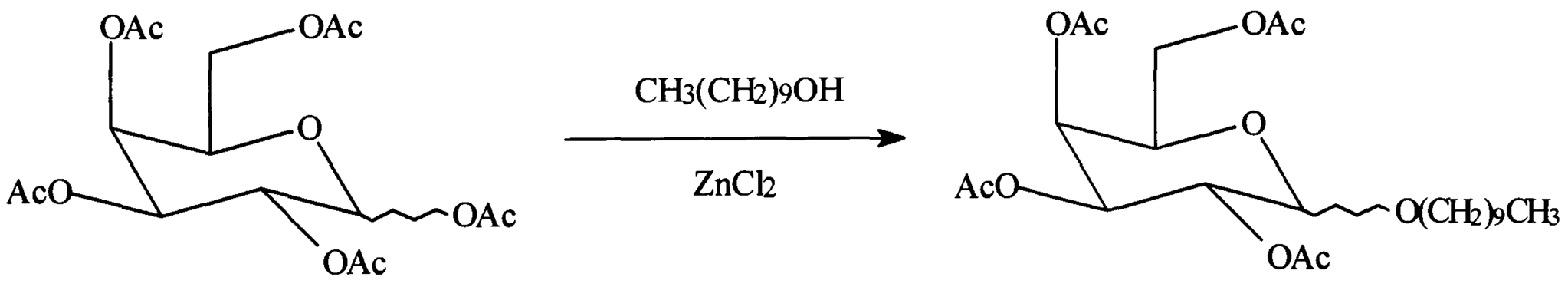


Scheme 1.3.

Table 1.4. Dielectric Synthesis of dioxolanes

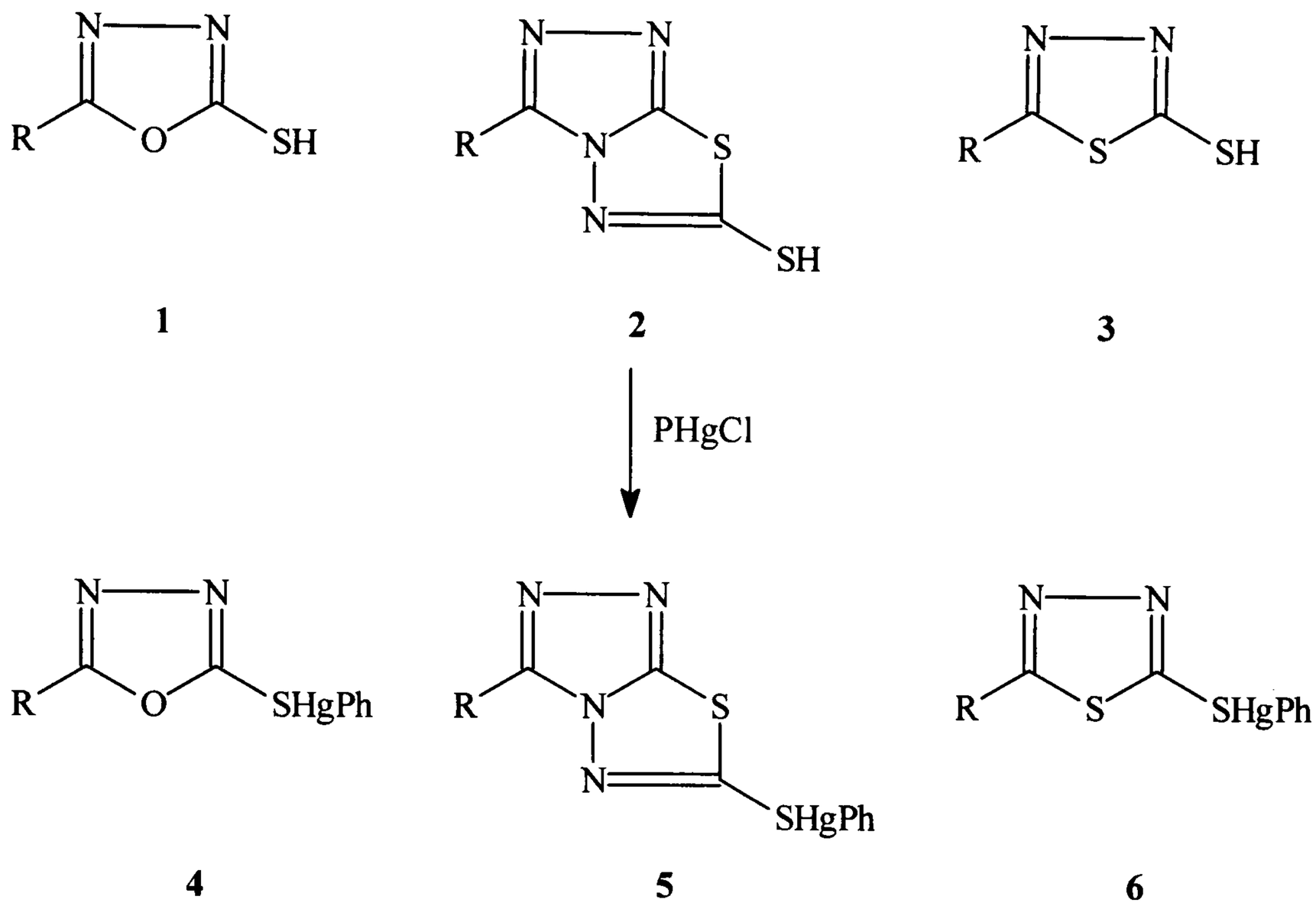
R_1	R_2	Ratio of Ethylene Glycol:carbanone	Oven	Conditions	Yield %	Ref.
Ph	H	1.5	Monomode	80 °C	80	19
Ph	H	10 - 15	Domestic (multimode)	650 W	81	20
Ph	CH_3	3	Monomode	120 °C	90	19
Ph	CH_3	10 - 15	Domestic (multimode)	650 W	71	20

Scheme 1.4. shows the glycosylation of peracetylated D-glucopyranose. This has been performed in a monomode oven, giving yields of 74 % after only 3 minutes.[21] The temperature must be held below 115 °C to prevent decomposition of the alkylglucoside, this requires a specialised microwave oven. If the reaction is performed using an oil bath heater no product is formed after 3 minutes and even after 5 hours the yield is only 25 %. The reaction has been extended to include the peracetylated D-galactose, D-mannose and N-troc-D-glucosamine (troc = 2,2,2-trichloroethoxycarbonyl) and similar results have been obtained.



Scheme 1.4.

A variety of organomercurial compounds, with potential anti-fungal activity, have been synthesised according to Scheme 1.5. using either conventional reflux in dmso or simply heating in dmf in a domestic microwave oven.[22] The results, summarised in Table 1.5, show the remarkable reductions in reaction times that may be achieved with very simple equipment; reactions requiring several hours under dmso reflux can be performed in the microwave in under 5 minutes.



1 2 3

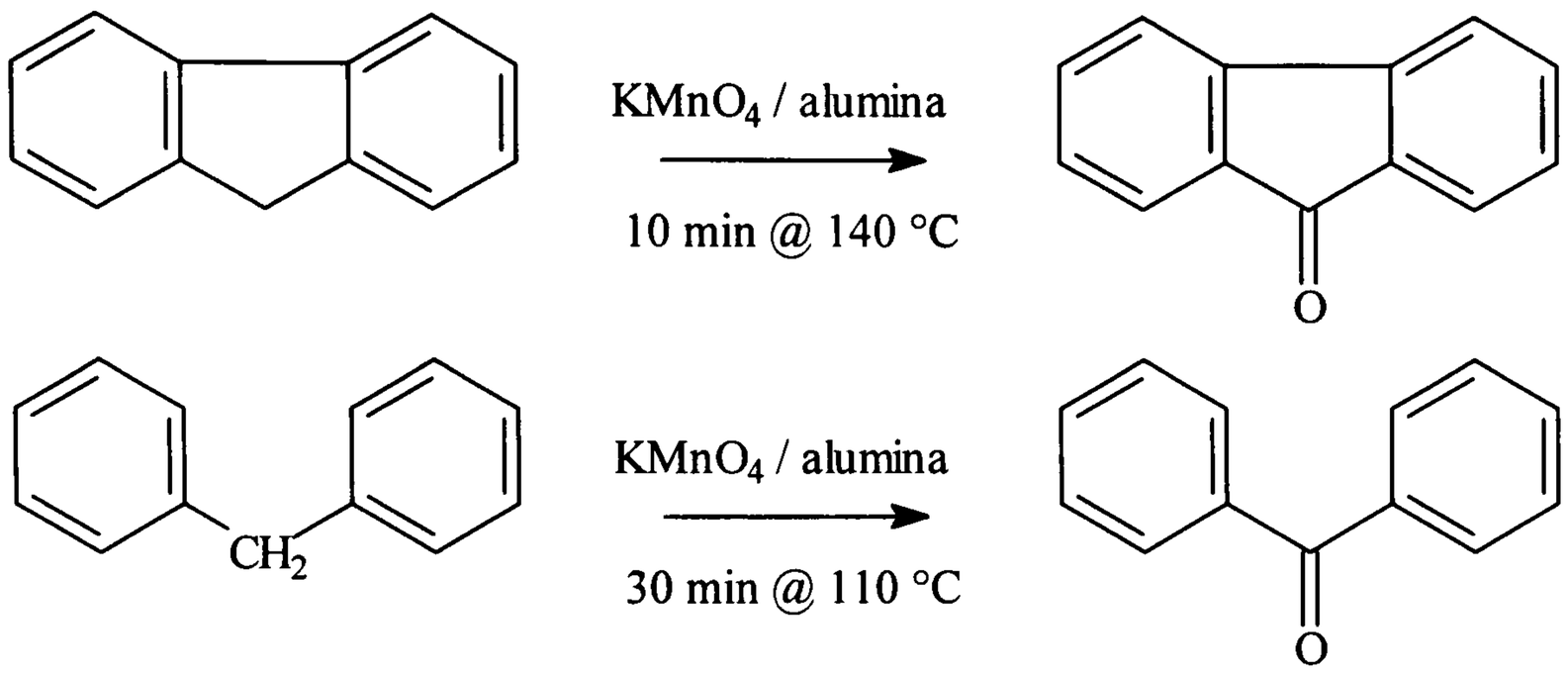
4 5 6

Scheme 1.5.

Table 1.5. Synthesis of organomercurial compounds.[22]

Compound	DMSO reflux		Dielectric heating	
	time (hour)	Yield (%)	time (min)	Yield (%)
4a	4.0	80	2.0	88
4b	4.5	76	2.5	85
4c	4.5	73	3.0	81
5a	6.0	78	2.5	89
5b	6.5	75	3.0	83
5c	7.0	70	3.5	80
6a	8.0	68	3.0	80
6b	8.5	70	3.5	85
6c	9.0	72	4.0	90

The oxidation of arenes to ketones requires several days treatment with $KMnO_4$ in 1,2-dichloroethane at room temperature.[23] By dispersing the reactants on alumina and heating in a monomode microwave reactor the reaction, shown in Scheme 1.6, is completed within minutes.[24] The major changes in reaction conditions do not make this a fair comparison. If the 'dry media' system is heated by conventional means yields of less

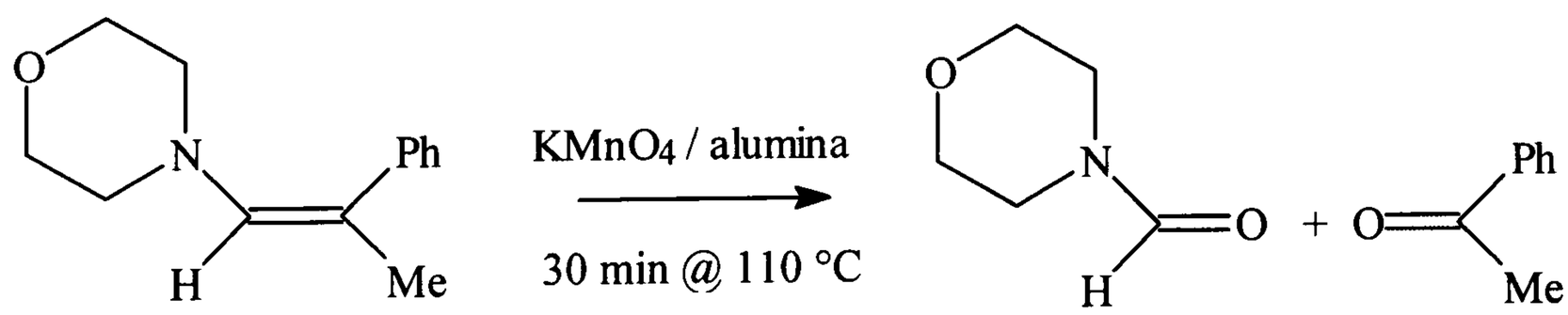


Scheme 1.6.

than 60 % are achieved in the time frame required for the microwave experiments. This technique has also been extended to *β,β*-disubstituted enamines[25] (Scheme 1.7.). Comparative results for a variety of heating methods are given in Table 1.6., a monomode microwave reactor operating at 300 W gave the highest yield.

Table 1.6. Oxidation of β,β-disubstituted enamines

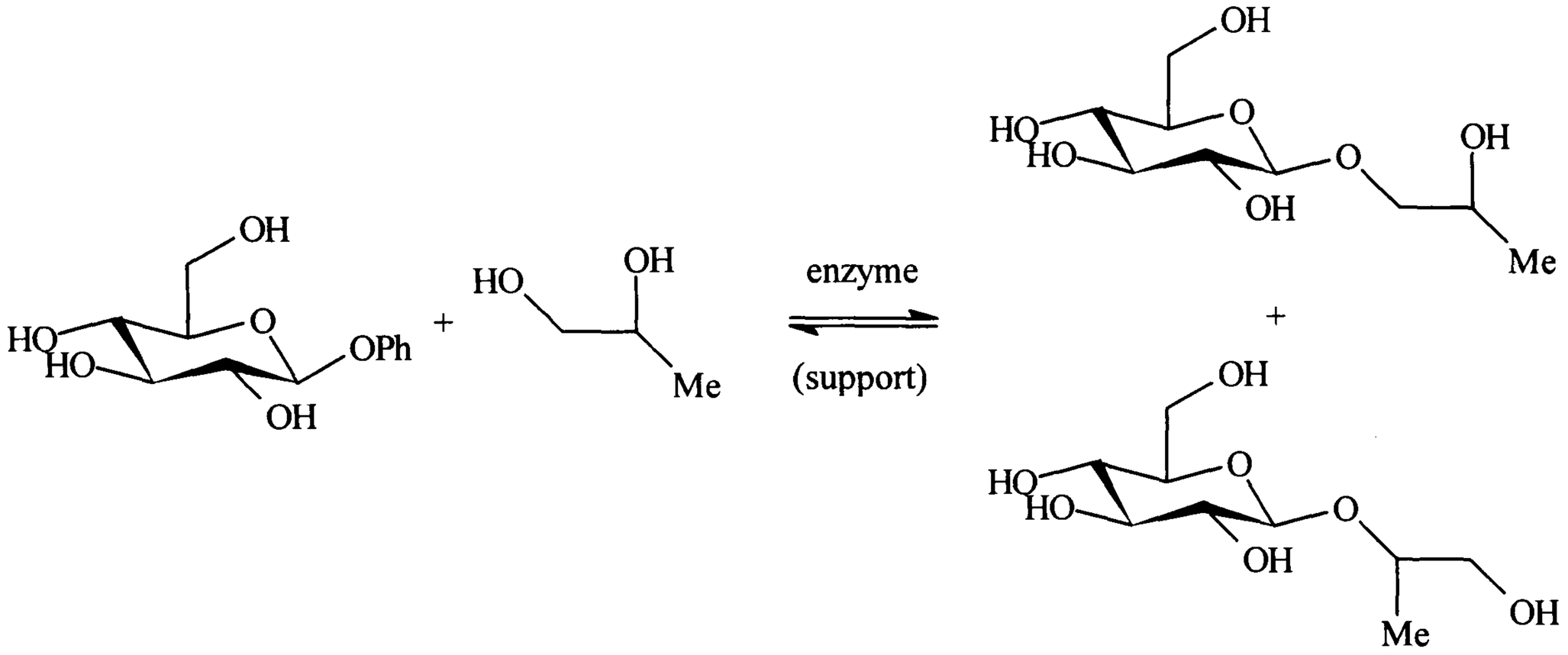
Heating mode	Conditions		Yield
Domestic microwave oven	255 W		73 %
Monomode microwave reactor	300 W	140 °C	83 %
Classical heating		140 °C	< 2 %



Scheme 1.7.

Recent developments in enzyme catalysis have included the production of enzymes immobilised upon a support,[26] such as *Psuedomonas* lipase (PL) dispersed inside Hyflo Super Cell (HSC) which consists of diatmeous silica of pH 8.5 -9.0. Normally enzymes require a narrow range of operating temperatures, generally less than 40 °C, to preserve

their activity, however the supported versions are stable up to 100 °C. As well as offering significant advantages in their own right such supported enzymes are tailor-made for 'dry media' dielectric syntheses, provided an oven with suitable temperature control is used.



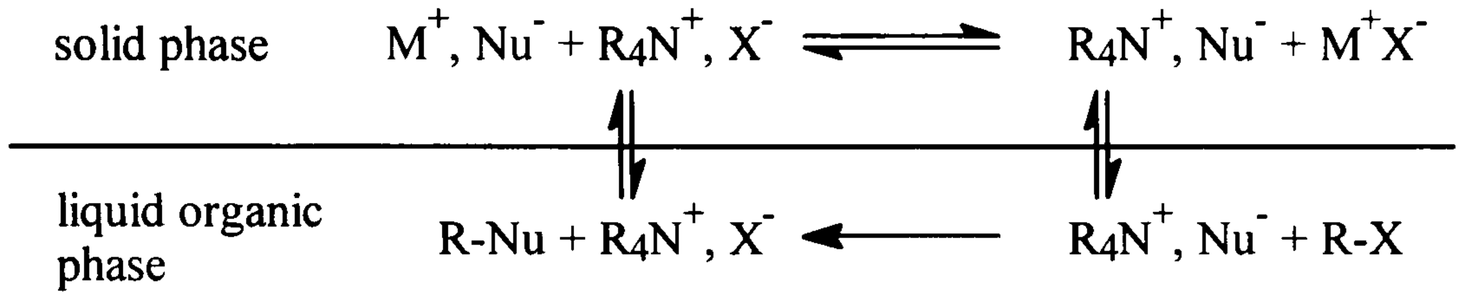
Scheme 1.8.

Scheme 1.8. shows the transesterification of phenyl-β-D-glucoside, using *Sulfolobus solfataricus* as the enzyme. This reaction requires 100 fold molar excesses of acceptor for classical synthesis (75 °C in acetonitrile), giving a yield of 60 % after 40 hours. By contrast, a microwave synthesis gave quantitative yields after 2 hours at 110 °C and only required 10 equivalents of acceptor.[27] For reactions using neutral alumina as support and impregnating the reagents from an aqueous suspension it is possible to recover the enzyme. This method gives 81 % conversion and 8 % hydrolysis after one hour; a conventionally heated system only yielded 40 % conversion.

1.4. Solid-Liquid Solvent-Free Phase Transfer Catalysis

For organic reactions with anionic nucleophiles and liquid electrophiles, addition of solvent to disperse the nucleophile also dilutes the electrophile, reducing reactivity. An alternative approach is to include catalytic amounts of a tetra-alkylammonium salt or

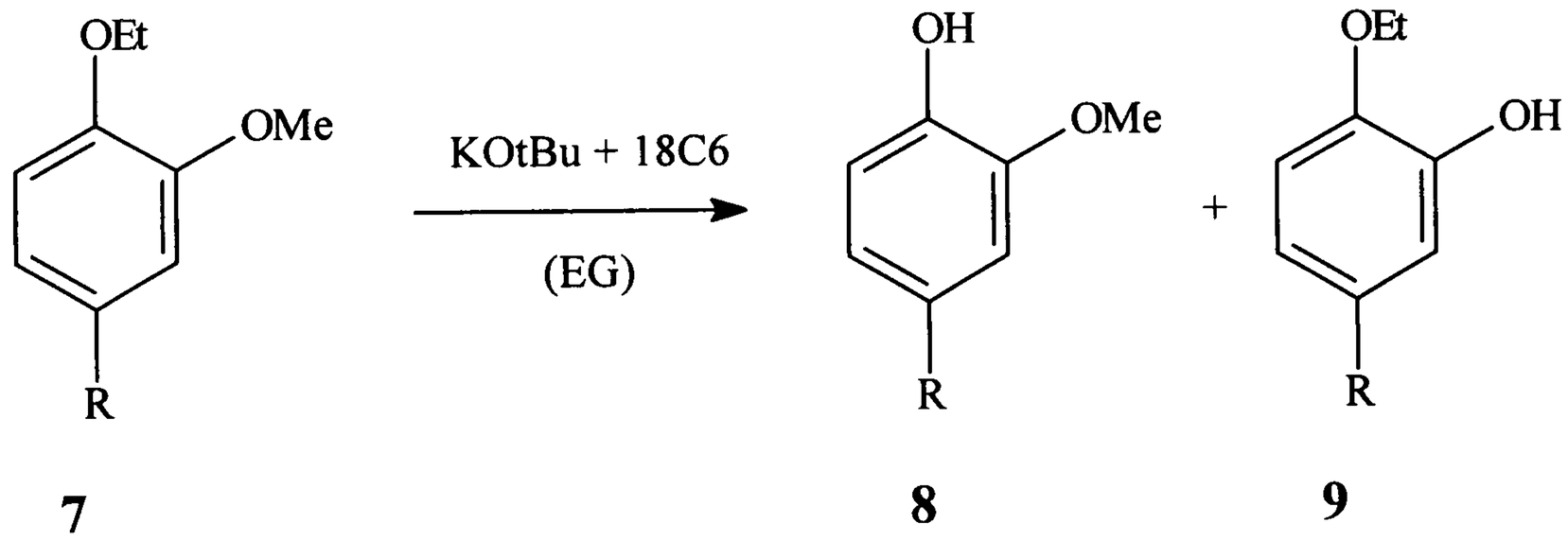
cation complexing agent. This is added, in equimolar amounts to both phases. Reaction then takes place in the organic phase (R-X) as shown in Scheme 1.9.



Scheme 1.9.

Ethyliseugenol (**7a**) and ethoxyanisole (**7b**) can be selectively dealkylated to **9** using KO^{t}Bu in the presence of 18-6 crown ether. Addition of ethylene glycol (EG) reverses the selectivity, giving the demethylated product, **8** (Scheme 1.10.). Better yields are obtained

a R = CH=CH-CH_3
b R = H



7 **8** **9**

Scheme 1.10.

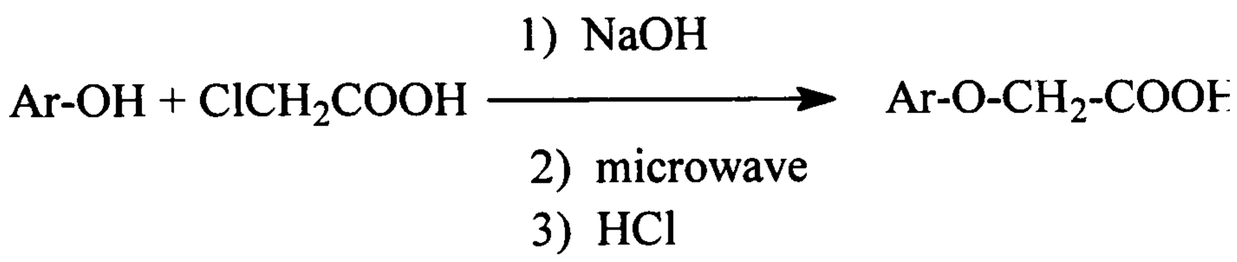
Table 1.7. Selective dealkylation of aromatic esters[*]

Ether	Reaction Conditions	Time (min)	T (°C)	Products (%)		
				7	**8**	**9**
7a	MW monomode reactor (60 W)	20	139	9		**82**
	Oil bath	20	139	32		52
	MW monomode reactor (60 W) + EG (2 mL)	60	228	6	**56**	3
	Sand bath + EG (2 mL)	60	228	70	2	
7b	MW monomode reactor (60 W)	20	120	7		**90**
	Oil bath	20	120	48		50
	MW monomode reactor (60 W) + EG (2 mL)	75	180		**72**	23
	Oil bath + EG (2 mL)	75	180	98		

* **1** (5 mmol), KO^{t}Bu (2 equiv.) and 18-C-6 (10 %)

using a monomode microwave reactor (Table 1.7).[28]

Villemin and Hammadi[29] have examined the synthesis of aryloxyacetic acids, which can be used either as plant growth hormones (4-chlorophenoxyacetic and 2-napthoxyacetic acids) or, for the more potent compounds, herbicides (2,4D and 2,4,5-T).



Scheme 1.11.

Equal amounts of an aryl alcohol and chloroacetic acid are neutralised by 50 % sodium hydroxide. The aqueous solution is then removed under moderately reduced pressures, leaving the wet solid. After irradiation for 4-7 minutes the mixture is redissolved in a minimum of water and the product precipitated by acidification to pH 3, using hydrochloric acid.

Table 1.8. Synthesis of aryloxyacetic acids under microwave irradiation without the use of organic solvent.[29]

Phenol	Yield (%)
phenol	97
4-methoxyphenol	93
4-chlorophenol	98
3,5-dimethylphenol	95
2,3-dichlorophenol	95
1-napthol	98
2-napthol	95

Table 1.8. shows some results for a series of phenols; not only are the yields an improvement on conventional techniques but also no organic solvent is required during the reaction or workup.

1.5. Synthesis of Inorganic Solids

A wide variety of inorganic solid-state reactions have been examined using dielectric heating techniques.[3] Ceramic SiC has been made from its elements in ten minutes.[30] If air is not excluded up to 15 % impurity of SiO_2 is also formed. If the reaction is performed under I_2 only monophasic β SiC is generated. Other carbides synthesised in this manner include TiC and Mo_2C. TiC and SiC have also been synthesised using a carbothermal reduction of the metal oxides as the initial step.[31] This approach has also been used for NbC and TaC.

Several chalcogenides have been synthesised by dielectric heating. Fine powders of the elements were sealed in evacuated quartz ampoules and heated for ten minutes or less. Reactions using sulfur and selenium gave a blue discharge, attributed to formation of a chalcogenide plasma.[32] A wide range of chromium chalcogenides were synthesised in this way as well as MnS, Fe_7S_8, TaS_2 and SnS_2, most of which required further annealing. Nonetheless, the overall reaction time was usually reduced by several days. Other compounds synthesised by this technique include PbSe, PbTe, ZnS, ZnSe, Ag_2S[33] and ZnTe.[34] Reaction times are typically of the order of 30 minutes, rather than a day or more. Absorption of impurities from the ampoules was minimised, as a consequence of the rapid heating rate and also the volumetric nature of dielectric heating, *i.e.* energy is transmitted throughout the sample, consequently the reagents are generally at a higher temperature

than that of the ampoules. This technique has also been applied to tertiary chalcogenides such as $CuInS_2$ and $CuInSe_2$:[35] Here the initial step is believed to be the formation of CuS and melting of the indium. Further reaction then occurs within the indium solution.

$LiMn_2O_4$ has been prepared by microwave irradiation of a mixture of LiI and MnO_2 for 6 minutes, giving the monophasic cubic spinel (an important cathode material) in high purity. The use of Li as reactant generates an *in situ* iodine atmosphere, preventing oxidation. By comparison, use of $LiCO_3$ yields only a defect spinel phase.[3]

For systems where the reactants do not heat in a microwave field at ambient temperatures, secondary initiators have been used. Graphite or amorphous carbon powder has been commonly used for this purpose. The reactants are ground together, pelletised and then coated with carbon. In the reaction of Na_2CO_3 and Nb_2O_5[36] it is believed that the initial heating of a carbon layer (which burns off) raises the temperature to a point where the Nb_2O_5 couples effectively with the microwaves, A rapid reaction then ensues, resulting in $NaNbO_3$ pellets with good crystallinity and phase purity. This technique has also been applied to $LiNbO_3$, $KNbO_3$, $BaTiO_3$ and $PbTiO_3$. $BaTiO_3$ has also been synthesised by microwave irradiation of $Ba(OCOCH_3)_2$ and $Ti(OC_3H_7)_4$.[37].

Phosphates are not generally microwave active; after heating for 5 minutes in a domestic microwave oven neither $Na_2HPO_4{\cdot}2H_2O$, KH_2PO_4 or $(NH_4)_2HPO_4$ had reached a temperature beyond 50 °C.[38] $Na_3PO_4{\cdot}12H_2O$ initially heats very rapidly due to the microwave coupling to the water of crystallisation but this is lost with two minutes and no further heating takes place. By comparison $NaH_2PO_4{\cdot}2H_2O$ loses three water molecules, in the process raising the temperature to ~700 K where the resulting $NaPO_3$ has a

sufficiently high tan δ to couple with microwaves. Five minutes irradiation results in molten $NaPO_3$ with a temperature of ~1000K. Thus $NaZr_2(PO_4)_3$ may be synthesised from ZrO_2 and $NaH_2PO_4 \cdot 2H_2O$ after 8 minutes of microwave heating.

Inorganic nitrides have attracted attention in recent years as materials with a wide range of applications. However, the inertness of N_2 makes direct synthesis from the elements difficult, usually requiring high temperatures. AlN has been synthesised by heating aluminium powder (mixed with carbon as an initiator) in a domestic microwave oven under a flow of nitrogen. The reaction proceeds rapidly and at a much lower temperature (1173K) than required by conventional methods. However the AlN surface formed blocks further reaction; six stages of grinding, followed by ten minutes of irradiation are needed for complete conversion.[39] An alternative approach is to use ammonia as the nitrogen source: GaN, a possible blue laser material, has been synthesised from Ga_2O_3 irradiated under flowing ammonia, carbon black is used as an initiator and reducing agent.[40] TiN and VN may also be prepared by this method, requiring less than half an hour of heating.

Many synthetic minerals are produced by long hydrothermal reactions. Dielectric heating has been found to dramatically reduce the time required: hydroxyapatite (HAp, $Ca_{10}(OH)_2(PO_4)_6$), the main inorganic substiuent of mammal bone, has been synthesised by simply mixing an aqueous suspension of $Ca(OH)_2$ with $(NH_4)_2HPO_4$ in a beaker and heating the mixture at a power level sufficient to boil the water off gently.[41] Reaction is complete within 25 minutes. The significant decrease in reaction time has been attributed to disruption of the Ca^{2+} aquation sheath by microwave coupling to the water molecules.

This has the effect of denuding the Ca^{2+} ions and enabling them to interact with the phosphate and hydroxyl ions much more readily than when they (Ca^{2+} ions) have to get out of the aquation sheath themselves.

Dealuminated Y zeolite (DAY) supported CuO and CuCl are sorbents for SO_2, with applications in gas separation. Since the DAY zeolite is hydrophobic, deposition from an aqueous solution is not possible and an alternative thermal processing method is required. By raising the temperature to approximately $^2/_3$ of the melting point of the precursor, sufficient energy is gained to allow diffusion throughout the support. This method is not generally effective for active species with high melting points. A dielectric heating approach to this problem has been developed.[42] CuCl, and $Cu(NO_3)_2$ were (respectively) mixed with DAY zeolite and heated in a domestic microwave oven for 30 minutes. For low relative amounts of $Cu(NO_3)_2$ (less than 10 % w/w) an even surface dispersion was obtained (as indicated by the lack of $Cu(NO_3)_2$ peaks in XRD spectra). Some nantokite (cubic CuCl) peaks were observed in the CuCl samples, nonetheless to obtain comparable quality samples by conventional heating would require several days heating.

Urania and thoria (UO_2 and ThO_2) share the calcium fluoride crystal structure and have similar lattice parameters. Thus solid solutions with a wide range of compositions may be formed, with potential applications as nuclear fuels for thermal breeder and high gas temperature reactors. Rao *et al.*[43] have recently examined the effectiveness of dielectric heating, using the PVA aided denitration method for the synthesis of thoria and urania. Aqueous nitrate solutions of uranium and thorium were mixed with an aqueous solution of polyvinyl alcohol and heated in a domestic microwave oven until the mixture was completely charred. The product was then calcined in air and sintered under argon.

All experiments used a microwave oven for the initial reaction. Microwave calcination of the denitrited mixture was found to lead to solid solutions with a lower surface area than those prepared by conventional heating. However, the microwave samples showed higher phase purity, attributed to the reduction in processing time (2 minutes rather than 4 hours); all samples had comparable densities after sintering. Dielectric heating was less successful in the sintering stage, consistent results were difficult to obtain and the pellet densities were usually lower than those produced by conventional heating. This has been attributed to practical difficulties in controlling the atmosphere and pellet temperature: thoria couples poorly to microwaves, such that low urania (U/(U + Th) = 0.15) samples would not heat in a domestic microwave oven.

There has been considerable interest in the microwave synthesis of zeolites in recent years.[4] Cundy *et al*[44] have reported the synthesis of [Al]ZSM-5, from an unseeded reaction mixture within 3 hours at 170 °C, some three times faster than the conventional method. Hexagonal NaY zeolite (EMT) is generally very difficult to synthesise, requiring longer reaction times (4 - 12 days) at low temperatures (110 °C) to minimise the formation of amorphous phases. At similar temperatures to the conventional method no reduction in reaction time is observed under dielectric heating conditions. On raising the temperature to 115 °C the required crystallisation time halves, with very crystalline samples being formed in 2.5 days. Dielectric synthesis of NaY zeolite shows a selectivity for the FAU structure at high temperatures; conventional methods use a temperature of 100 °C to minimise the formation of P-type zeolites. Such syntheses typically require ten hours of heating. Microwave heating at 150 °C for 20 minutes gave a crystalline sample of NaY, whilst conventional heating of the same reaction mixture produced only a P-type

zeolite. Similar results are achieved for high silica zeolites, with a sample with $SiO_2/Al_2O_3 = 4.7$ synthesised after 1.5 hours heating at 150 °C.

For many zeolite syntheses a bottleneck is observed at the nucleation stage. This is commonly overcome by the addition of seed crystals to the reaction mixture. In Figure 1.5. the crystalline growth curves for ZSM-5, synthesised both with and without and organic template (tetrapropylammonium bromide, TPABr)[45] are shown. Under conventional heating conditions, addition of seed material reduces the crystallisation time from 5.5 hours to 2 hours (curves (e) and (c), respectively). However, for a microwave synthesis the effect is even more dramatic and the total synthesis time falls from 3 hours to 3 minutes (curves (d) and (a)). Part of the effect may be attributed purely to thermal lag - conventionally heated autoclaves require 30 minutes to reach their set temperatures, rather than three minutes for a microwave system. Another suggested cause is hot-spots occurring at the colloid surfaces.

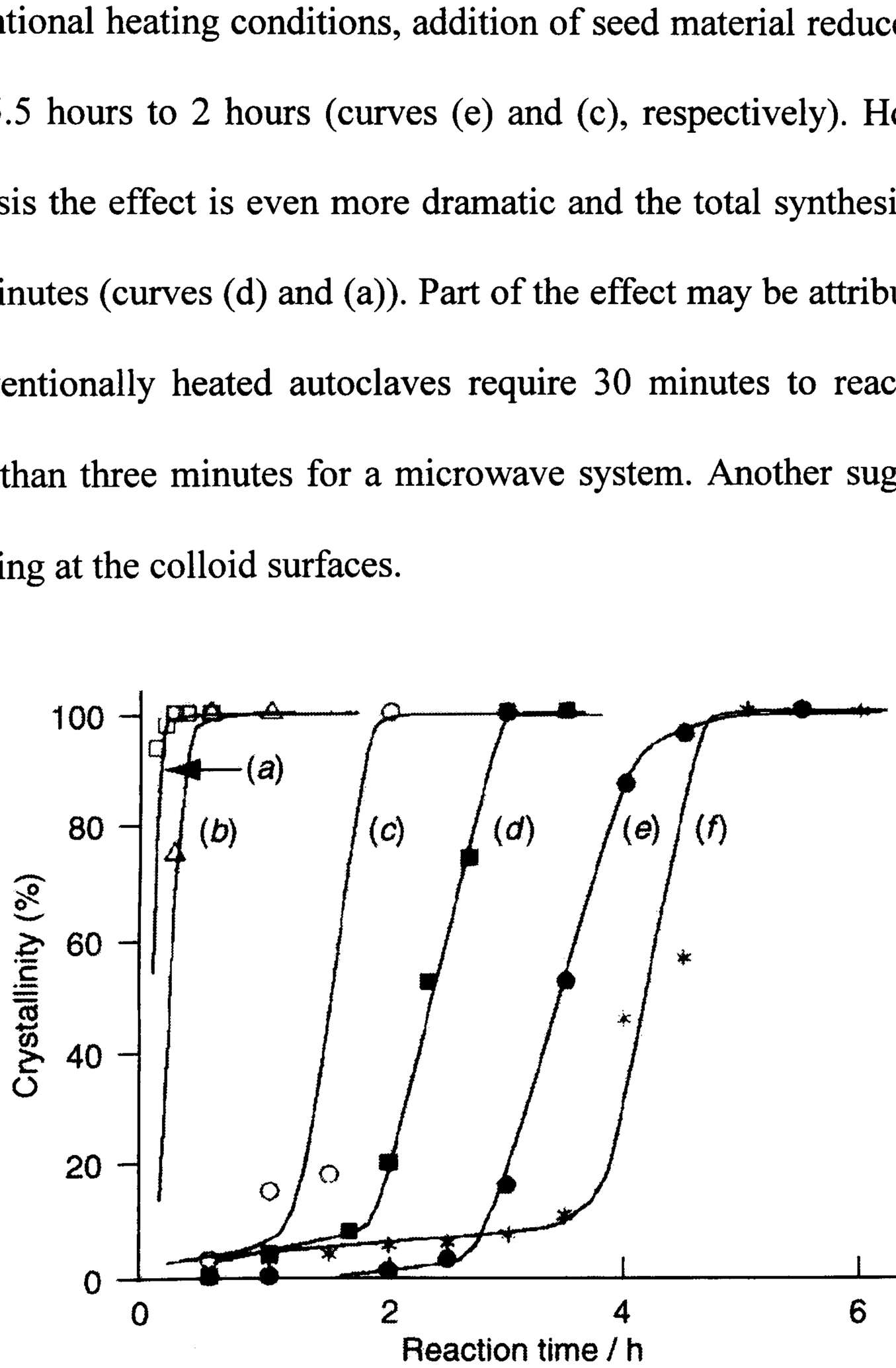


Figure 1.5. Growth curves for ZSM-5: (a) seeded, TPABr, microwave; (b) seeded, inorganic, microwave; (c) seeded, TPABr, thermal; (d) unseeded, TPABr, microwave; (e) unseeded, TPABr, thermal, (f) unseeded, inorganic, thermal

Nanometre sized particles of $AlPO_4$-5 molecular sieves have been synthesised by dielectric heating and reaction times of less than 2 hours at 150 - 160 °C were noted.[46] Average particles sizes of 50 nm or less were found, lower than that obtained by conventional methods.

Koegler *et al* have examined the growth of orientated silicate-1 crystals on silicon wafers under dielectric heating.[47] Conventional heating methods need three hours, with the reaction temperature inside the autoclave not reaching the required level (165 °C) for the first two hours. Dielectric heating of the reaction mixture in Teflon autoclaves reaches the reaction temperature within 30s, allowing close control of the reaction conditions. By using a reaction mixture with a high template (TPABr) concentration a continuous layer, less than 100 nm thick, may be grown after only 25 minutes heating at 155 °C.

Open structure compounds, such as hollandite ($K_2Mn_8O_{16}\cdot nH_2O$) and todorokite ($MgMn^{2+}{}_2Mn^{4+}{}_{4.5}O_{12}\cdot 4.5H_2O$) require a week of conventional heating but have been synthesised in a day under dielectric heating conditions.[48] The samples prepared under microwave conditions also show far less contamination by impurities such as bixbyite (Mn_2O_3).

Dielectric heating has been shown to greatly reduce the time required for intercalation reactions. Aluminium ions have been intercalated into Montmorillonite clay by heating an aqueous suspension of the clay and aluminium chlorohydrate for 15 minutes in a sealed vessel.[49] Samples prepared in this way show greater surface areas than those prepared using conventional techniques. The aluminium is introduced as the chlorohydrate, which is added to an aqueous suspension of the clay. By comparison the intercalation of lithium

into transition metal sulfides uses butyllithium, with the sulfides suspended in the microwave transparent solvents *n*-hexane or benzene.[50] The overall temperature of these reactions does not rise above 60 °C, nonetheless for MoS_2 the reaction is complete in 6 minutes rather than the 24 hours required by conventional methods.

An unusually selective reaction occurs between microwave irradiated graphite mixed with layered oxides; only the interlayer oxygen is removed. Thus MoO_3 (to MoO_2), CrO_3 (to Cr_2O_3), V_2O_5 (to VO_2), α-$VOPO_4 \cdot 2H_2O$ (to VPO_4) and $Ag_6Mo_{10}O_{33}$ (to Ag + MoO_2) are all reduced after less than 5 minutes irradiation, with a final temperature below 1000K.[51] Non-layered oxides, such as WO_3, show no loss of oxygen under similar conditions, nor does the reaction proceed any further. The suggested mechanism involves intercalation of a graphite layer into the oxide as the initial step.

The syntheses of many inorganic glasses are suited to dielectric heating. The starting materials frequently show a greater susceptibility to microwave techniques than those of the product melts, leading to a self-regulation in the temperature profile.[52] Some results are summarised in Table 1.9., for the glasses which have also been synthesised in conventional furnaces, comparable glass transition temperatures (T_g) are obtained. All of the melts are formed in less than 10 minutes.

AgI is a strong microwave absorber; glasses containing this component may be melted in a microwave oven. For the AgI : Ag_2O : B_2O_3 : SiO_2 system the glasses formed by dielectric heating show a red shift of ca. 10 nm by comparison to conventionally produced samples.[53] This effect is reversible - conventionally prepared glasses remelted in a microwave will show the red shift whilst microwave synthesised glasses remelted in a box

furnace lose the tint. FTIR spectra indicate a different BO_4 environment and ^{109}Ag NMR shows spin-lattice relaxation times (T_1) about a factor of two shorter within the microwave melted samples. Microwave and thermal melting occur by quite distinct mechanisms and it is proposed that differences in the local motion of Ag^+ and I^- ions in the melt may be responsible.

Table 1.9. Glasses formed by microwave heating.[52]

Glass System	T_g (K)	time (min)
x PbO : (100-x) V_2O_5 [x = 40 - 50]	520 - 522	5
50 GeO_2 : 50 V_2O_5	491	6
33 BaO : 67 V_2O_5	551	5
30 Na_2O : 30 B_2O_3 : 40 V_2O_5	470	6
50 AgI : 25 Ag_2O : 25 MoO_3	348	5
50 AgI : 25 Ag_2O : 25 WO_3	419	6
50 AgI : 25 Ag_2O : 25 CrO_3	298	3
50 AgI : 33 Ag_2O : 17 GeO_2	392	5
60 AgI : 20 Ag_2O : 10 MoO_3 : 10 WO_3	345	3
60 AgI : 20 Ag_2O : 10 MoO_3 : 10 V_2O_5	351	2
40 AgI : 30 Ag_2O : 15 WO_3 : 15 B_2O_3	460	5
30 CuI : 35 Cu_2O : 35 MoO_3 (in air)	390	3
x B_2O_3 : (45-x) PbO : 55 V_2O_5 [x = 0 - 20]	520 - 515	7
x SiO_2 : (45-x) PbO : 55 V_2O_5 [x = 0 - 15]	520 - 531	5
x ZnO_2 : (45-x) PbO : 55 V_2O_5 [x = 0 - 40]	520 - 541	5
x MoO_3 : (45-x) PbO : 55 V_2O_5 [x = 0 - 35]	520 - 515	5
x CuO : (45-x) PbO : 55 V_2O_5 [x = 0 - 20]	520 - 536	5
x WO_3 : (45-x) PbO : 55 V_2O_5 [x = 0 - 15]	520 - 531	5
x Bi_2O_3 : (45-x) PbO : 55 V_2O_5 [x = 0 - 10]	520 - 537	4

1.6. Catalysis

The use of dielectric heating in catalysis covers both catalyst preparation and use. For catalysts prepared by impregnation of a support by a solution of the active species, dielectric drying of the sample offers several advantages. Microwaves heat evenly throughout the sample (provided it is neither very lossy nor very large). The temperature gradient which is generated leads to a higher temperature at the centre of the sample. This

results in faster, more even drying; for V_2O_5 supported on silica heating in a domestic oven at 150 W for 5 min and then 600 W for 5 minutes gives far better dispersed samples.[54] No V_2O_5 crystallite signals were detected in XRD of the microwaved samples and SEM morphology showed even particle sizes. The conventional drying method is 383 K for 2 hours, followed by calcining at 670 K for 4 hours. The samples prepared by dielectric heating give twice the yield (28 % rather than 15 %) and conversion (30 % rather than 18 %) when compared to conventionally prepared samples for the catalytic oxidation of *o*-xylene to phthalic anhydride.

For microwave heating of catalytic processes another effect is seen. Many heterogeneous catalysts consist of metals supported on an inorganic oxide. The active catalyst site is generally a far stronger absorber of microwave energy than that of the support. Yin *et al* report that oxidation of *o*-xylene to phthalic anhydride (PAN) over a V_2O_5/SiO_2 system shows doubled yields and conversions at a lower temperature than that required for conventional heating (see Table 1.10.).

Table 1.10. Comparison of conventional (furnace) and microwave heating methods for the catalytic oxidation of o-*xylene to PAN over V_2O_5/SiO_2.*

	Conventional Heating	Microwave Heating
Yield (mol %)	28	67
Conversion (mol %)	30	71
Temperature (K)	653	563

These results are attributed to the formation of 'hot-spots' at the active site. An estimation of the temperature gradient can be made for this system. At high temperatures the selectivity for PAN drops rapidly. In conventionally heated systems the optimum temperature is 653 K, whereas for the microwave system it is 90 degrees lower. This interpretation is still the subject of some controversy. Perry *et al.*[55] have published

calculations suggesting that the rate of heat transfer, for a system at 1 atm., is too fast to allow the build up of discrete hot-spots on the active particles.

Mingos *et al.*[56] have recently examined the decomposition of H_2S, over γ–alumina supported MoS_2. Conversion efficiencies 3 times greater than those observed using conventional heating techniques were observed, consistent with a temperature at the active sites 200 K higher than the measured, bulk value. Furthermore, after high temperature reactions (the maximum measured bulk temperature was 1073 K) considerable alteration of the catalyst was observed. The formation of crystallites of α-alumina and some hexagonal crystals of MoS_2 suggests temperatures of at least 1273 K and 1458 K, respectively. Migration of the MoS_2 particles was also observed; forming spheres as large as 1000 μm, containing MoS_2 and alumina. Thus it has been suggested that hot-spots involving both the lossy catalyst particles and support, with sizes ranging from 100 μm to 1000 μm and temperatures of 100 - 200 K above the bulk temperature may be formed under dielectric heating.

Wan has proposed the use of short duration pulses of microwave energy into a reactor featuring a microwave active catalytic component dispersed over an inactive substrate.[5] Ideally, such a system would have an extremely high temperature gradient between the active sites and the bulk medium leading to high selectivity. In an experiment, approximately mimicking photosynthesis, carbon dioxide and water are passed over a supported nickel catalyst. The product distribution obtained after 29s is shown in Table 1.11: although the formation of methane as primary product is unsurprising the high selectivity for C_4 alcohols has no comparison in standard syngas processes.

Table 1.11. Product distribution of microwave catalysis of carbon dioxide and water.[5]

Product	Relative % Yield
Methane	55.1
Methanol	5.5
Acetone	4.7
C_3 alcohols	5.8
C_4 alcohols	28.4

Methane conversion to C_2 species over carbon has been examined using microwave and radio frequency (RF) dielectric heating.[57] High selectivities (80 -90 %) for the formation of acetylene are observed, some carbon solids and hydrogen are also produced. If hydrogen gas is introduced into the system, deposition of carbon falls rapidly and the carbon bed begins to act as a reactant rather than catalyst/heat transfer agent. At a methane/hydrogen ratio of 1:4 a reaction with the effective stoichieometry

$$CH_4 + 3C \rightarrow 2C_2H_2$$

is observed, the hydrogen is regenerated and maintains a constant partial pressure.

The catalytic transfer hydrogenation (CTH) of soybean oil uses an aqueous solution of NaO_2CH as hydrogen donor and a Pd/C catalyst. The catalyst particles are dispersed throughout the reaction mixture. Short periods of low power heating from a domestic microwave oven have been used to maintain the reaction temperature between 75 and 80 °C. When compared to a conventionally heated system, an overall rate some 8 times faster is observed under microwave heating,[58] with stearic acid (the final, saturated product) concentrations beginning to rise after 45 minutes. In the conventionally heated systems no increases in stearic acid concentration are observed after 3 hours of heating. As most of the components are strong microwave absorbers it is unlikely that 'hot-spots' with a significant temperature gradient are generated preferentially at the catalyst surface.

For the reaction to take place catalyst particles with adsorbed formate ions must interact with the oily species. It is postulated that significant differences in the oil-water interface may be present under microwave heating conditions, enhancing the exchange of reactants between phases.

Few reactions using organometallic homogenous catalysts under microwave heating conditions have been reported in the literature. The reaction

$$R\text{-}CH{=}CH_2 + CCl_3X \rightarrow R\text{-}CHCl\text{-}CH_2\text{-}CXCl_2$$

is an exception; the reported rate constants for a variety of substrates and solvents are shown in Table 1.12.[59] The temperature shown is the final temperature for the microwave system, once 90 % conversion had been achieved.

For reactions where the components are predominately non-polar (runs 1, 7 and 13) no rate enhancements are observed. The most dramatic results occur with acetonitrile as solvent, *f* values (the rate enhancement factor k_m/k_c) of greater than 20 were observed for run 6. These differences in reaction rate may be almost entirely explained by enhanced heating rates under microwave conditions. From the thermally heated results it can be seen that there are minimal solvent effects on the reaction rate, other circumstances being equal (cf. runs 2 and 3, runs 4, 5 and 6 and runs 10 and 11). In a microwave oven, use of a more polar solvent can result in dramatic effects in heating rate. Compared to acetonitrile, which may be expected to reach the reaction temperatures in 2 minutes or so, 1,1,1-trichloroethylethanoate and dichloroethane are poor microwave solvents with lower heating rates. Thus dramatic increases are observed on changing to acetonitrile (runs 4, 5

and 6). For the later systems (runs 10, 11 and 12) all of the components are microwave absorbers to some degree and the effect of changing solvent is reduced.

Table 1.12. Rate constants for the addition of chloro compounds to alkenes under microwave (k_m) *and conventional* (k_c) *conditions, in the presence of* $[Cu(2\text{-}PhNH_2)_2Cl]$ *catalyst.*

Run	Alkene	Chloro compound	Solvent	T (°C)	$k_m \bullet 10^4$ (s^{-1})	$k_c \bullet 10^4$ (s^{-1})	f[a]
1	$C_6H_5CH=CH_2$	CCl_4		30	0.0	0.00	
2		CCl_4	CH_2ClCH_2Cl	73	1.2	0.37	3.2
3		CCl_4	CH_3CN	72	3.3	0.44	7.5
4		CCl_3COOEt		85	9.3	1.30	7.1
5		CCl_3COOEt	CH_2ClCH_2Cl	83	8.7	1.20	7.2
6		CCl_3COOEt	CH_3CN	82	23.0	1.10	21.0
7	$CH_2=CHCOOMe$	CCl_4		84	0.2	0.18	1.1
8		CCl_4	CH_2ClCH_2Cl	74	1.2	0.25	4.8
9		CCl_4	CH_3CN	85	1.9	0.35	5.4
10		CCl_3COOEt		88	5.0	0.93	5.4
11		CCl_3COOEt	CH_2ClCH_2Cl	90	4.8	0.85	5.6
12		CCl_3COOEt	CH_3CN	102	5.5	0.83	6.6
13		CCl_3COOEt	C_6H_6	80	0.7	0.66	1.1

[a] f, rate enhancement factor k_m/k_c

1.7. Microwave Plasma Chemistry

Low pressure gases may form plasmas in a microwave field, giving access to unusual reaction conditions. A common problem in the direct synthesis of metal nitrides from the elements is the formation of surface nitride layers that effectively block diffusion of N_2. By using a nitrogen/hydrogen plasma, metal oxides may be reduced.[60] Using this method TiN, AlN and GaN have been synthesised; two heating stages, with intermediate grinding are still required. For Al_2O_3 substitution was still incomplete after several stages, however $Al(OH)_3$ could be completely nitrided within 24 hours.

A microwave plasma enhanced chemical vapour deposition (MPECVD) system has been described by Shih *et al*[61] and used to prepare crystalline carbon nitrides on silicon.

The process has two steps; in the initial phase a microwave plasma of CH_4/N_2 (CH_4:N_2, 3%) generated from 1500 W of input power was passed over the silicon surface with a flow rate of 100 sccm at 20 Torr, generating α- and β-Si_3N_4 layers. In the second stage the power was increased to 2000 W, the flow rate reduced to 30 sccm and a dc bias of -150 V applied to the nitrided silicon. No carbon layers were deposited in the absence of the static electric field. It is suggested that the negative dc bias enriches the dipolar and positive ionic species at the Si_3N_4 surface, facilitating the exchange between Si and plasma species such as CH, H^+ and C_2. The SiH_4 by-product then leaves the surface. Similarly a plasma of cobalt carbonyl diluted in argon may be used to deposit cobalt atoms within zeolite matrices.[62]

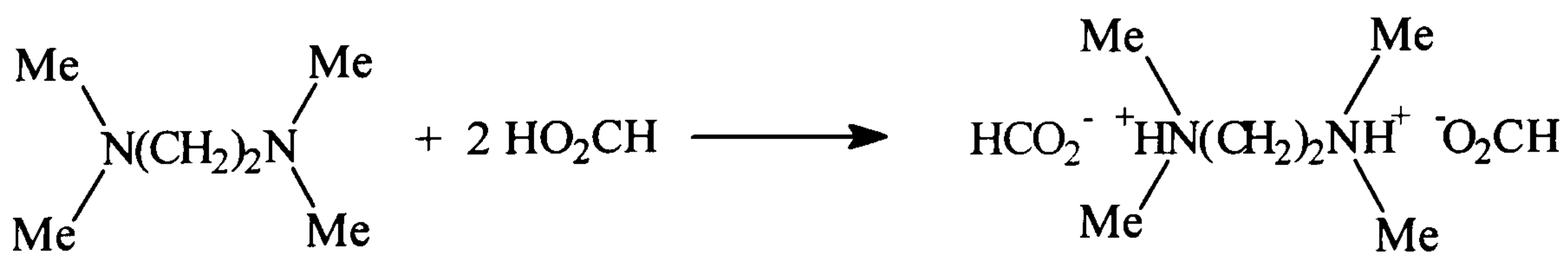
The conversion of natural gas (methane rich) to C_2+ hydrocarbons has been studied using a microwave generated plasma.[63] The conversion rate increases with the input microwave power, to a maximum of 48 % at 120 W. Increasing the power above this level results in the formation of carbon solids on the reactor wall. By adding a Pd-Ni catalyst and applying an electrical field inductance of 8V, 2A conversion rates of 64 % were achieved. The main C_2 products were ethylene, ethane and acetylene, with distributions of 37, 40 and 22 % respectively. Greater selectivity for ethane was observed in the absence of catalyst (29, 50 and 22 %) but the total conversion dropped to 46 %.

Diamy *et al*[64] have used the afterglow of a microwave generated dihydrogen plasma to reduce zeolite supported gold and palladium catalysts. The gas temperature of a microwave generated plasma drops rapidly after leaving the cavity, however the excited species (H^+, H^{2+} and H^{3+}) are carried far beyond the plasma zone. Thus the technique offers clear advantages over conventional high temperature reduction in molecular

dihydrogen which generally gives undesirably large metal particles. The experiments used a synthetic faujasite type Y zeolite and an acidified zeolite, ($Na_{0.25}H_{0.75}Y$, referred to as NaHY) as supports. All samples were treated for 30 minutes with the microwave power held at 160 W, the minimum required to maintain a stable plasma. For monometallic samples the best results were achieved using the NaY support; gold particles with an average diameter of less than 2 nm and dispersion of 43 % were detected, whereas for palladium a 78 % dispersion of 1.3 nm diameter particles was found. For mixed metal species a sample of composition $Pd_{0.8}Au_{0.2}$ supported on NaHY gave a 39 % dispersion of 2.2 nm diameter particles.

1.8. Microwave Enhanced Deuteriation

Jones *et al*[65] have reported the catalytic hydrogen transfer of α-methylcinnamic acid. This technique uses a formate as the hydrogen donor. For the reaction of α-methylcinnamic acid with ammonium formate in dmso, in the presence of Wilkinson's catalyst, the microwave synthesis is complete in 5 minutes, rather than the 30 minutes required by conventional heating at 100 °C. Furthermore, sterically hindered alkenes such as α-phenylcinnamic acid, which are reduced with difficulty using H_2 gas also respond well to this method. For reactions requiring a double hydrogen donor the diformic acid salt of tetramethylethylendiamine (TMEDA, see Scheme 1.12.) may be used.



Scheme 1.12.

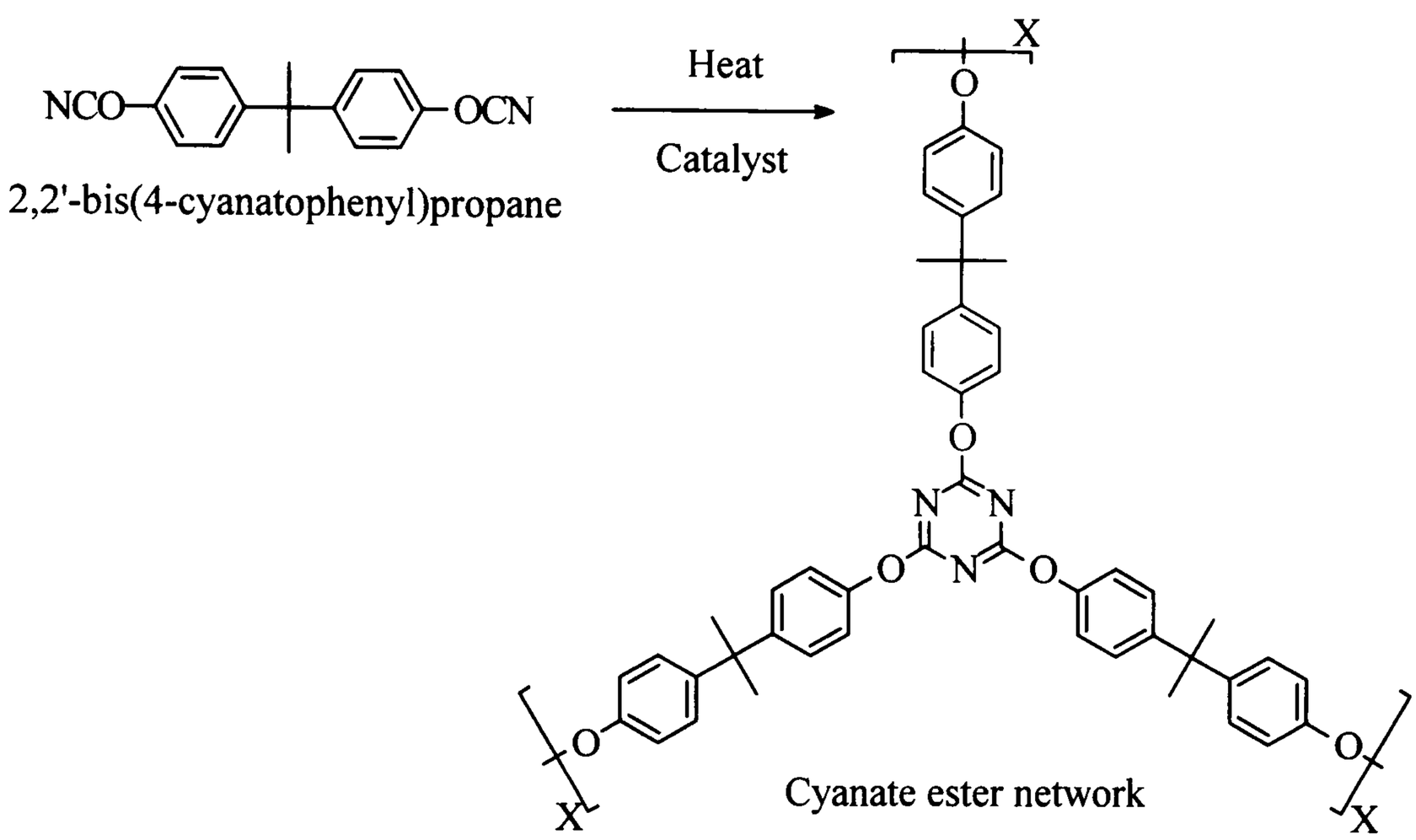
The use of D_2O as a deuterium source for simple aromatics has also been examined, using heterogeneous and homogenous catalysis.[66] The results obtained on heating several simple aromatics in D_2O for 15 minutes at low power (160 W), with PtO_2 as heterogeneous catalyst or an aqueous solution of sodium tetrachloroplatinate as a homogenous catalyst, are shown in Table 1.13. Comparative results for conventional heating are not given, although it is noted that 'temperatures in excess of 100 °C for prolonged periods, sometimes of several days duration' are customarily required.

Table 1.13. Deuteriation of selected aromatics (PhX) under microwave conditions.[66]

X	Deuteriation orientation (relative %)											
	Heterogeneous catalyst						Homogenous catalyst					
CH_3	*ortho*	(29)	*meta*	(57)	*para*	(14)						
COOH			*meta*	(100)					*meta*	(100)		
NH_2	*ortho*	(95)	*meta*	(5)			*ortho*	(65)			*para*	(35)
OH	*ortho*	(54)	*meta*	(19)	*para*	(27)	*ortho*	(86)	*meta*	(14)		
$COCH_3$	acetyl	(25)	*meta*	(50)	*para*	(25)	acetyl	(100)				
2,6-dimethoxy-benzoic acid			*meta*	(5)	*para*	(95)			*meta*	(100)		

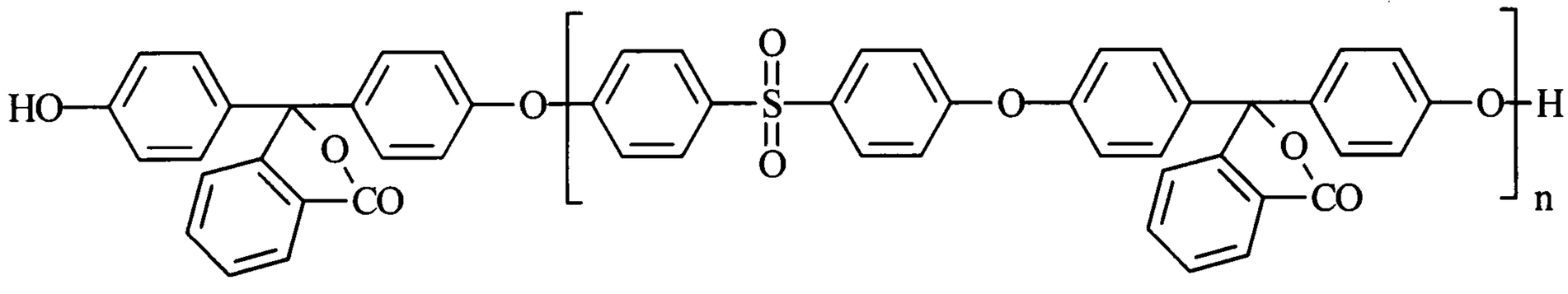
1.9. Polymer Applications

Cyanate ester networks (see Scheme 1.13.) have been cured by dielectric heating.[67] Unfortunately at the glass transition temperature (160 °C) the dielectric loss increases rapidly. This leads to thermal runaway, preventing effective control of the temperature. As a result samples of pure cyanate ester were either charred or incompletely cross-linked.



Scheme 1.13.

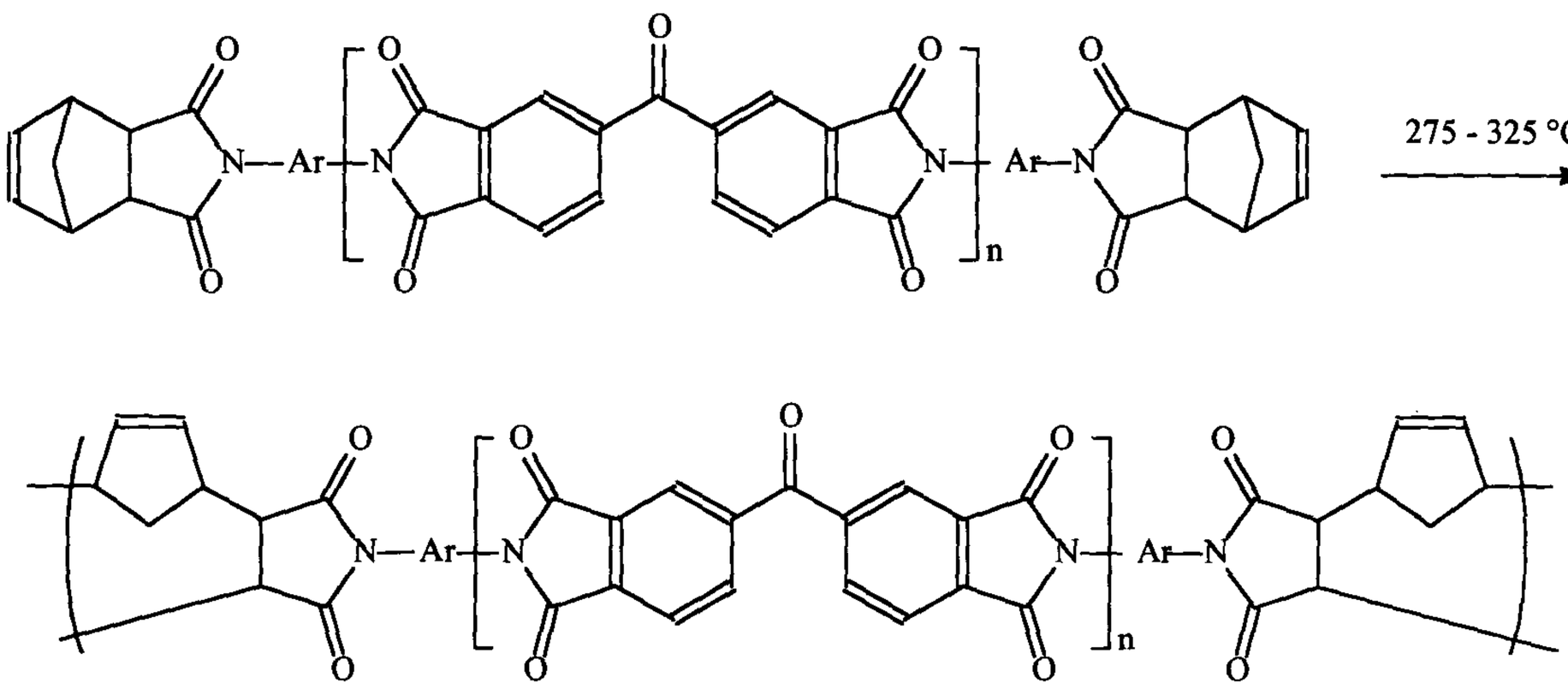
The addition of hydroxy functionalised phenolphthalein based poly(arylene ether sulfone) oligomers, with an M_n of 15,000, modified the dielectric characteristics of the mixture, allowing more even and controlled heating. For 25-30 % concentrations of thermoplastic, complete cross-linking may be achieved in 16 minutes, far quicker than conventional heating methods.



Scheme 1.14.

Dielectric heating has been investigated as a potential method for the cross-linking of LaRC RP-46 (see Scheme 1.15.), a polyimide with potential uses as a fibre reinforced composite.[68] In the full polymer infrared peaks due to the end groups are obscured, making detailed monitoring of the cross-linking problematic. Thus the bisnadimide, *N*,*N*'-

(oxyde-3,4'-phenylene)bis(5-norbornene-2,3-dicarboximide) has been used as a model compound for kinetic studies.



Cross-linked polyimide RP-46

Scheme 1.15.

Both thermal and microwave heating processes show first order kinetics, with apparently identical mechanisms. However, the microwave reaction proceeds at ten times the rate and has been calculated to have an activation energy between 74 and 84 kJ mol^{-1} noticeably lower than the value of 94 kJ mol^{-1} calculated for the conventionally heated process.[68]

1.10. Summary

In this Chapter some recent applications of microwave dielectric heating in chemical syntheses have been reviewed. The possible applications are spread over a wide range of areas and chemical techniques. The most commonly reported advantage of microwave techniques is a reduction, often dramatic, in the overall reaction time, some selectivity effects have also been shown.

The existence of an athermal microwave effect has been largely discounted. Theoretical models have been proposed which account for the observed effects either as a result of the enhanced heating rates seen under dielectric radiation or due to the formation of 'hot-spots'. The hot-spots may result either because there are areas with widely differing susceptibilities to microwaves within the samples or the wave nature of the process leads to uneven electric fields within the sample. For some aqueous reactions a specific disruption of the hydrogen bonding network has been postulated.

1.11. References

1 A.F. Harvey, *Microwave Engineering*, Academic Press, New York (1963)

2 S. Caddick, *Tetrahedron*, **51** (1995) 10403

3 K.J. Rao, B. Vaidhyanathan, M. Ganguli and P.A. Ramakrishnan, *Chem. Mater.* **11** (1999) 882

4 C.S. Cundy, *Collect. Czech. Chem. Commun.* **63** (1998) 1699

5 J.K.S. Wan, *Res. Chem. Intermed.* **19** (1993) 147

6 A. Loupy, A. Petit, J. Hamelin, F. Texier-Boullet, P. Jacquault and D. Mathé, *Synthesis* (1998) 1213

7 S.A. Galema, *Chem. Soc. Rev.* **26** (1997) 233

8 C.R. Strauss and R.W. Trainor, *Aust. J. Chem.* **48** (1995) 1665

9 D.M.P. Mingos and A.G. Whittaker, *J. Microwave Power Electromagn. Energy,* (1994) **29**, 195

10 D.M.P. Mingos and D.R. Baghurst, *Chem. Soc. Rev.* **20** (1991) 1

11 R.N. Gedye, W. Rank and K.C. Westaway, *Can. J. Chem.* **69** (1991) 706

12 D. Stuerga, K. Gonon and M. Lallemant, *Tetrahedron*, **49** (1993) 6229

13 D. Stuerga and P. Gaillard, *Tetrahedron*, **52** (1996) 5505

14 F. Chemat, M. Poux and S.A. Galema, *J. Chem. Soc. Perkin Trans. II* (1997) 2371

15 R.G. Compton, B.A. Coles and F. Marken, *Chem. Commun.* (1998) 2595

16 R.S. Varma and H.M. Meshram, *Tetrahedron Lett.* **38** (1997) 7973

17 M. Suárez, A. Loupy, E. Salfrán, L. Morán and E. Rolando, *Heterocycles,* **51** (1999) 21

18 R. Pérez, E.R. Pérez, M. Suárez, L. González, A. Loupy, M.L. Jimeno and C. Ochoa, *Org. Prep. and Proc. Int.* **29** (1997) 671

19 B. Pério, M.J. Dozias, P. Jacquault and P. Hamelin, *Tetrahedron. Lett.* **38** (1997) 2818

20 F. Matloubi-Moghaddam and A. Sharifi, *Synth. Commun.* **26** (1995) 2457

21 C. Limousin, J. Cléophax, A. Petit, A. Loupy and G. Lukacs, *J. Carbohydr. Res.* **16** (1997) 327

22 M. Kidwai, R. Kumar and Y. Goel, *Main Group Metal Chem.* **6** (1997) 367

23 D. Zhao and G.D. Lee, *Synthesis,* (1994) 915

24 A. Oussaid, A. Lopuy, J. *Chem. Res. (S)* (1997) 342

25 H. Benhaliliba, A. Derdour, J.P. Bazreau, F. Texier-Boullet, J. Hamelin, *Tetrahedron Lett.* **39** (1998) 541

26 E. Guibé-Jampel and G. Rousseau, *Tetrahedron Lett.* **28** (1987), 3563

27 M. Gelo-Pujic, E. Guibé-Jampel, A. Loupy and A. Trincone, *J. Chem. Soc. Perkin Trans. II* (1997) 1001

28 A. Oussaid, Thach Le Ngoc and A. Loupy, *Tetrahedron Lett*, **38** (1997) 2451

29 D. Villemin and M. Hammadi, *Synth. Commun.* **26** (1996) 4337

30 P.D. Ramesh, B. Vaidhyanathan, M. Ganguli and K.J. Rao, *J. Mater. Res.* **2** (1994)

31 H .Kozuja and J.D. Mackenzie, *Ceram. Trans.* **21** (1991) 387

32 A.G. Whittaker and D.M.P. Mingos, *J. Chem. Soc. Dalton. Trans.* (1995) 2073

33 B. Vaidhyanathan, M. Ganguli and K.J. Rao, *J. Mater. Res. Bull.* **30** (1995) 1173

34 S. Bhunia and D.N. Bose, *J. Cryst.Growth,* **186** (1998) 535

35 C.C. Landry and A.R. Barron, *Science*, **260** (1993) 1653

36 B. Vaidhyanathan, B. Raizada and K.J. Rao, *J. Mater.Sci. Lett.* **16** (1997) 2022

37 W.F. Kladrig and J.E. Horn, *Ceram. Int.* **16** (1990) 99

38 B. Vaidhyanathan and K.J. Rao, *J. Solid State Chem.* **132** (1997) 349

39 P.D. Ramesh, K.J. Rao, A*dv. Mater.* 7 (1995) 177

40 B. Vaidhyanathan and K.J. Rao, *Chem. Mater.* **9** (1997) 1196

41 B. Vaidhyanathan and K.J. Rao, *Bull. Mater. Sci.* **19** (1996) 1163

42 S.G. Deng and Y.S. Lin, *Chem. Eng. Sci.* **52** (1997) 1563

43 V. Chandramouli, S. Anthonysamy, P.R.Vasudeva Rao, R. Divakar and D. Sundararaman, *J. Nucl. Mater.* **254** (1998) 55

44 J.P. Zhao, C. Cundy and J. Dwyer, *Stud. Surf. Sci. Catal.* **105A** (1997) 181

45 C.S. Cundy, R.J. Plaisted and J.P. Zhao, *Chem. Commun.* (1998) 1465

46 M. Fang, H. Du, W. Xu, X. Meng and W. Pang, *Micropor. Mater.* **9** (1997) 59

47 J.H. Koegler, A. Arafat, H. van Bekkum and J.C. Jansen, *Stud. Surf. Sci. Catal.* **105C** (1997) 2163

48 S.L. Suib, E. Vileno, Q. Zhang, C. Marun and L.D. Conde, *Ceram. Trans.* **80** (1997) 331

49 G. Fetter, G. Heradia, A.M. Maubert and P. Bosch, *J. Mater. Chem.* **6** (1996) 1857

50 E. Benavente, G. Gonzales, *Mater. Res. Bull.* **32** (1997) 709

51 B. Vaidhyanathan, M. Ganguli and K.J. Rao, *J. Mater. Chem.* **6** (1996) 391

52 B. Vaidhyanathan, M. Ganguli and K.J. Rao, *J. Solid State Chem.* **113** (1994) 448

53 D.J. Duval, B.L. Phillips, M.J.E. Terjak and S.H. Risbud, *J. Solid State Chem.* **131** (1997) 173

54 Y. Liu, Y. Lu, S. Liu and Y. Yin, *Catal. Today* **51** (1999) 147

55 W.L. Perry, D.W. Cooke, J.D. Katz and A.K Datye, *Catal. Lett.* **47** (1997) 1

56 X. Zhang, D.O. Hayward and D.M.P. Mingos, *Chem. Commun.* (1999) 975

57 M.K. Ioffe, S.D. Pollington and J.K.S. Wan, *J. Catal.* **151** (1995) 349

58 S. Leskovšek, A. Šmidovnik and T. Koloini, *J. Org. Chem.* **59** (1994) 7433

59 M. Hájek, *Coll. Czech. Chem. Commun.* **62** (1997) 347

60 J.D. Houmes and H-C. zur Loye, *Chem. Mater.* **8** (1996) 2551

61 S.L Sung, T.G. Tsai, K.P. Huang, J.H. Huang and H.C. Shih, *Jpn. J. Appl. Phys.* **37A** (1998) L148

62 R.P. Zerger, K.C. McMahon, M.D. Seltzer, R.G. Michel and S.L. Suib, *J. Catal.* **99** (1986) 498

63 W. Cho, Y. Baek, D. Park, Y.C. Kim and M. Anpo, *Res. Chem. Intermed.* **24** (1998) 55

64 A.-M. Diamy, Z. Randriamanantenasoa, J.-C. Legrand, M. Polisset-Thfoin and J. Fraissard, *Chem. Phys. Lett.* **269** (1997) 327

65 M.H. Al-Qahtani, N. Cleator, T.N. Danks, R.N. Garmann, J.R. Jones, S. Stefaniak, A.D. Morgan and A.J. Simmonds, *J. Chem. Res. (S)* (1998) 400

66 J.M. Barthez, A.V. Filikov, L.B.Frederiksen, M.L. Huguet, J.R. Jones and S-Y. Lu, *Can. J. Chem.* **76** (1998) 726

67 S.A. Srinivasan, S.S. Joardar, D. Kranbeuhl, T.C. Ward and J.E. McGrath, *J. Appl. Polym. Sci.* **64** (1997) 179

68 Y. Liu, X.D. Sun, X.-Q. Xie and D.A. Scola, *J. Poly. Sci. A.* **36** (1998) 2653

Chapter Two

Description Of Apparatus And Reactions

2.1. Introduction

The experiments associated with the study of the acceleration of chemical reactions under microwave conditions, which are described in this Thesis, have used two commercially ovens manufactured by the CEM corporation. The MDS 2000 and the STAR 2. The MDS 2000 uses PTFE autoclave vessels with 100 cm^3 volumes, capable of operating at up to 200 °C and 15 atm. The STAR 2 oven uses glass vessels and the temperature can be varied between ambient and 450 °C. A thick-walled Pyrex vessel has been developed to enable the study of pressurised reactions in the STAR 2 cavity. This has proved successful for a number of simple organometallic transformations. The following sections will describe the important features of these two types of apparatus

2.2. Apparatus

2.2.1. CEM MDS 2000

The MDS 2000 is a multimode cavity operating at 630 W. It has been designed to use PTFE autoclaves and has a full pressure and temperature monitoring and control system. Although the autoclaves can withstand temperatures of 200 °C there is a danger of inelastic creep occurring in the Teflon vessels above 175 °C[1]. Thus, experiments at such high temperatures should not be performed for longer than 30 minutes.

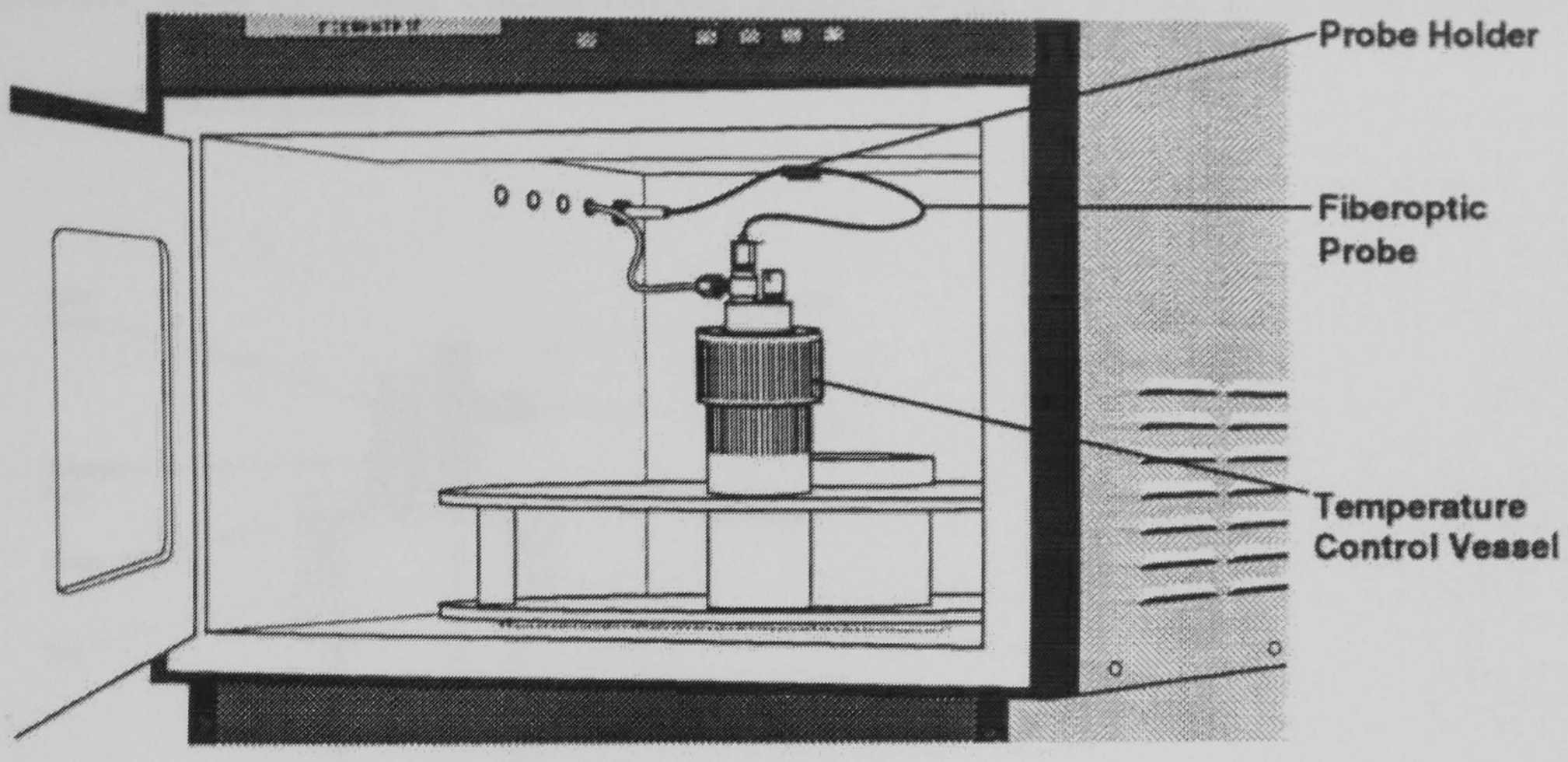


Figure 2.1: Schematic illustration of the MDS 2000 microwave oven[1]

The oven can be programmed with temperature and pressure limits in up to 5 stages. Generally the temperature limit is used as a control whilst the pressure limit is set to a high value, acting as a limiting safety measure. The reaction conditions chosen are maintained by switching the magnetron on and off, leading to oscillation about the set points of approximately 10 %. For known reaction conditions setting a pressure limit slightly below the average recorded pressure leads to reduced oscillation about the set points. Although the power can be set in 1 % intervals the reduction is achieved through standard duty-cycle switching, albeit at millisecond intervals in contrast to the 1 second intervals more normal with domestic ovens.

The Lined Digestion Vessels (see Figure 2.2) have a maximum capacity of 100 cm^3 although for safe working they should not be filled with more than 50 cm^3. At least 15 cm^3 of solvent is required to cover the thermowell sheath sufficiently to ensure accurate temperature readings. The rate of temperature rise is inversely proportional to the sample volume and the rate of pressure development is dependent on the free space volume. In

practice these opposing effects require samples sizes of between 20 and 30 cm^3 for optimum heating rates.

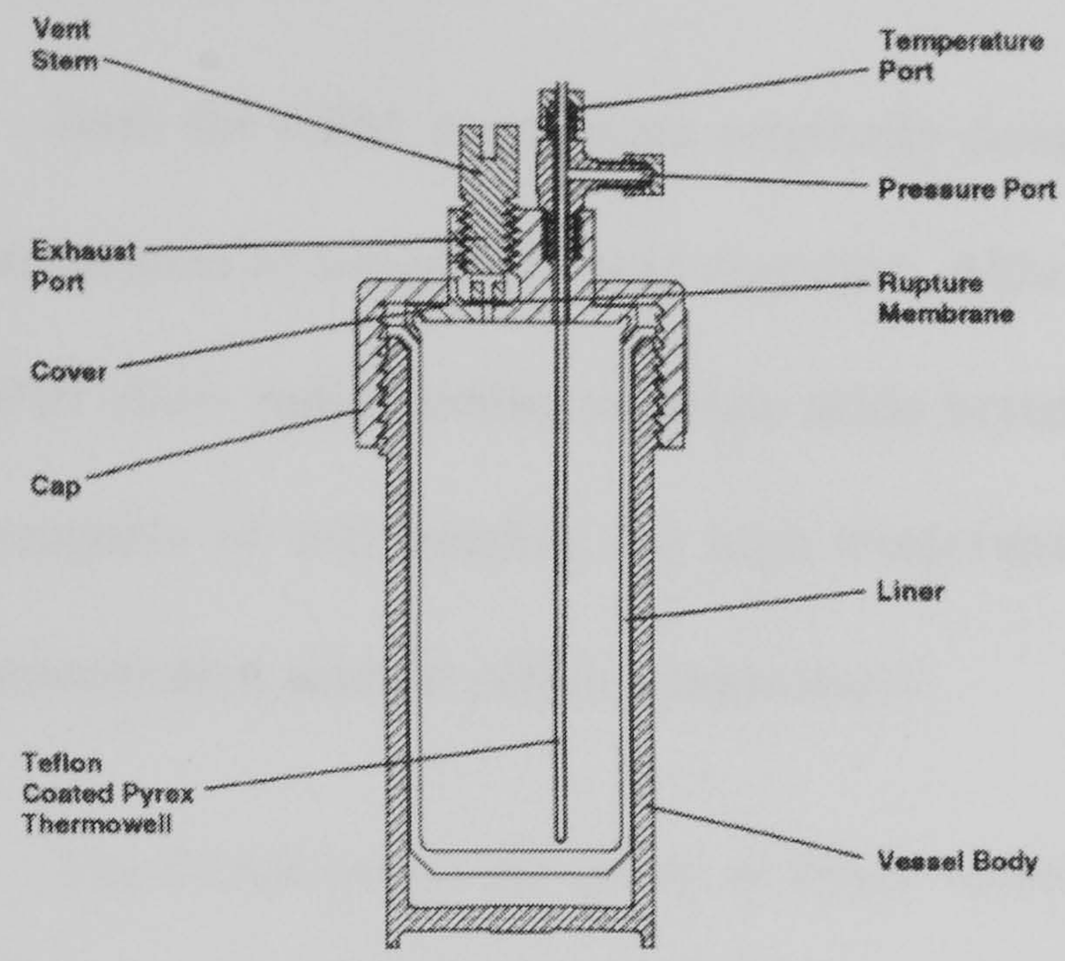


Figure 2.2: Lined Digestion Vessel (LDV)[1]

The LDV's are not easily adapted for reactions with air and moisture sensitive components. A tap is available which can be attached to the pressure sensing line, allowing some Schlenk-line manipulations, however the LDV's shape and opacity make this an awkward and difficult procedure to monitor. As the pressure sensing line is open to the atmosphere full elimination of air and moisture would require the LDV to be filled and sealed in a glove box and then run without pressure control. This approach is not advisable for reactions that produce gaseous products.

In summary; the MDS 2000 is simple to use and operate. It has been widely adopted by analytical laboratories for sample digestion. By heating solutions above their atmospheric boiling points substantial reductions in reaction time have been achieved. Also high boiling viscous solvents such as ethylene glycol may be replaced by more volatile alternatives, e.g. ethanol, for simpler processing. However, the temperature range

is limited and manipulation and control of the conditions for air or moisture sensitive systems is problematical.

2.2.2. CEM STAR 2

Both the CEM ovens were originally designed for use by analytical chemists, in the preparation of samples by acid digestion. Although the PTFE autoclaves used in the MDS 2000 allow rapid heating of dilute acids beyond their atmospheric boiling point they are incapable of withstanding the high temperatures and corrosive conditions generated by concentrated acids at reflux temperatures.

The STAR ovens use quartz or Pyrex vessels and have an infra-red temperature sensor that can be calibrated between 75 and 450 °C. Temperatures below 50 °C are not accurately registered by the sensor, particularly during the heating stages. There is an appreciable time lag in temperature measurement due to the thermal gradient across the surface of the vessel. This is most obvious in the initial stages of heating; 20 cm^3 of water heated at full power (ramp time set to 1s) is clearly boiling after 30s but the sensor reads only 60 °C. The external vessel surface does not reach the internal temperature for another 30s.

A cylindrical cavity, open at the top, is fully occupied by one vessel, with a capacity of up to 200 cm^3. The vessel is inserted through a 'choke' which allows the excess microwave energy to attenuate safely. Multistage programming, including controlled ramp and cooling stages is possible. The power within the cavity is adjusted between 0 and 100 % by the oven control mechanism. An internal, self-correcting algorithm alters

the power levels to maintain the set temperature or ramp rate. A side-effect of the design is that the microwaves within the cavity are plane-polarised.

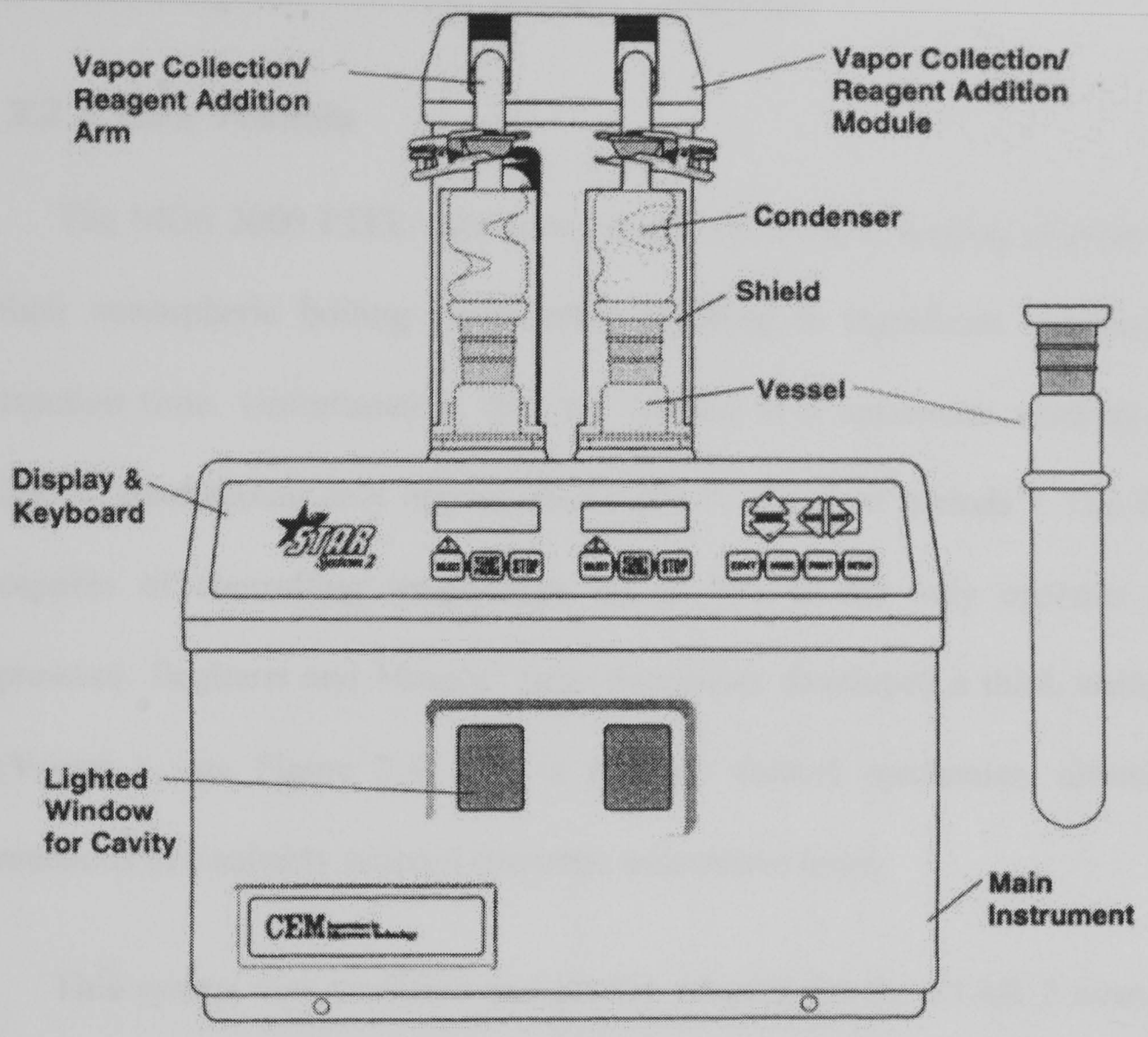


Figure 2.3: STAR 2 Microwave Oven[2]

The oven is designed for use with short condensers connected to an acid scrubber module, allowing the controlled acid char of samples. This module also has a programmable reagent addition system. In order to use organic solvents under reflux conditions or inert atmospheres, long condensers and gas lines are required to maintain reflux and allow nitrogen flow across the apparatus. Thus the reagent addition module must be removed and a short-circuit placed across the interface to bypass the automatic cut-out circuits.

In summary; the STAR 2 allows controlled heating of large samples under reflux, at temperatures between 75 and 450 °C. The vessels have standard, ground-glass necks and are easily integrated with other laboratory glassware.

2.2.3. New Vessels

The MDS 2000 PTFE autoclave vessels allow rapid heating of polar solvents above their atmospheric boiling points often resulting in significant reductions in the total reaction time. Unfortunately, they are limited to a maximum working temperature of 200 °C (and should only operate above 175 °C for short periods[1]). The STAR 2 oven is capable of controlling temperature up to 450 °C but only operates at atmospheric pressure. Baghurst and Mingos[3] have previously developed a thick walled Pyrex vessel (**Vessel 1**, see Figure 2.4) with a pressure control mechanism allowing pressurised reactions in a suitably adapted domestic microwave oven.

This system was modified and readily adapted for the STAR 2 oven as part of this research project. The final vessel (**Vessel 2**, see Figure 2.4) is 30 cm long and a solid glass flange has been added to ensure the vessel sits within the cavity at a suitable level for the infrared thermometer to be used to record and control the temperature. This flange is also necessary to trigger the STAR 2 vessel detection circuit. Initially the vessel was coated with a polymer film, to minimise glass fragmentation in the event of failure. This rapidly darkened and flaked off under experimental conditions and was subsequently abandoned.

The gas line head can be attached to various components via standard Swagelock fittings. The experimental set-up included a spring-loaded safety valve, a pressure transducer and two taps, allowing Schlenk line techniques to be used.

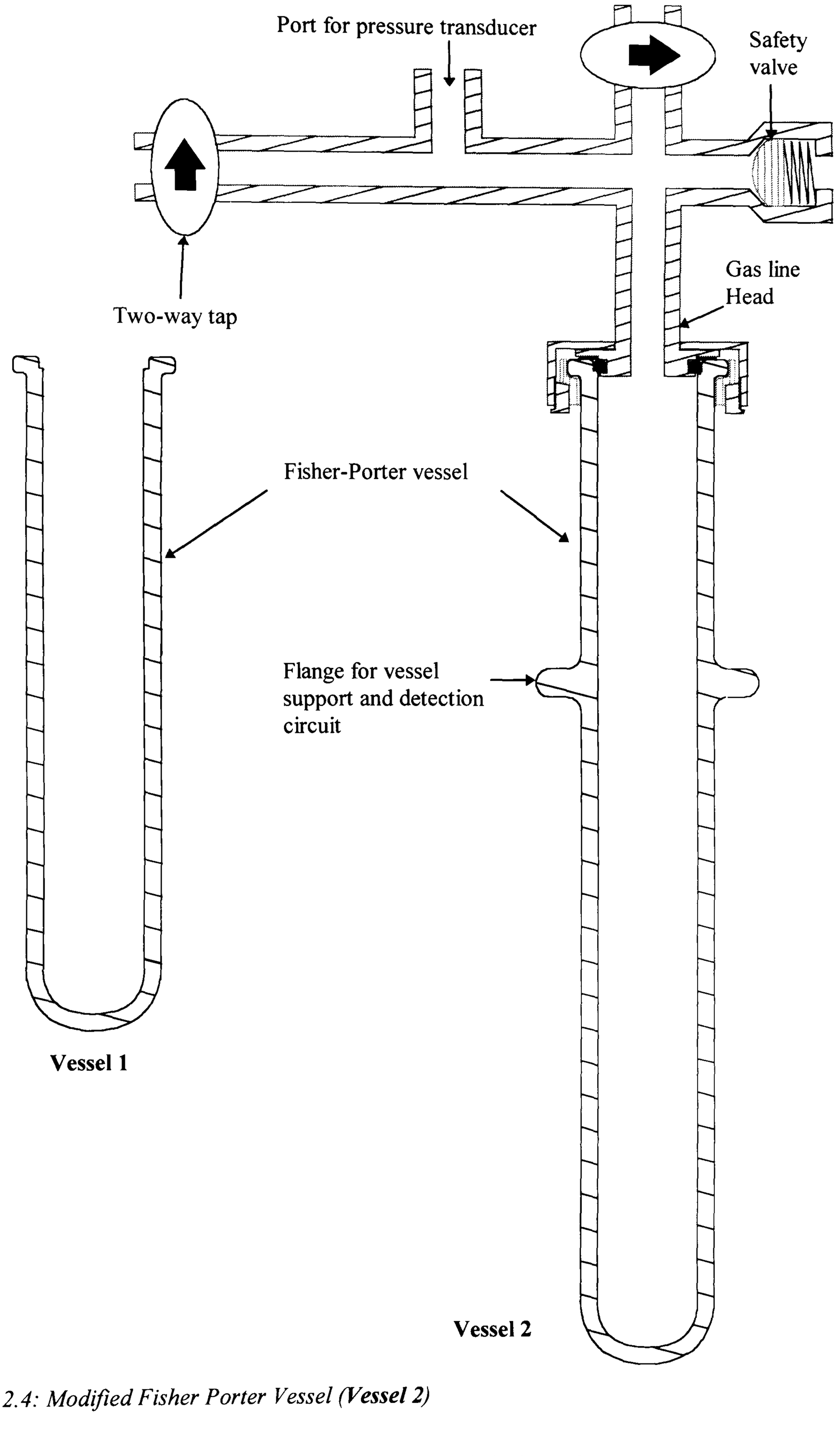


*Figure 2.4: Modified Fisher Porter Vessel (**Vessel 2**)*

The pressure transducer is connected to a digital readout. Although a circuit allowing pressure control has been developed[3] it drives a variac transformer spliced into the oven's

power supply. The STAR 2 has an internal microprocessor control mechanism incompatible with this design, although a safety cut-out system could probably be devised. As the STAR 2 controller can be driven through a suitably connected PC it is also possible that software could be developed to allow full control of temperature and pressure conditions.

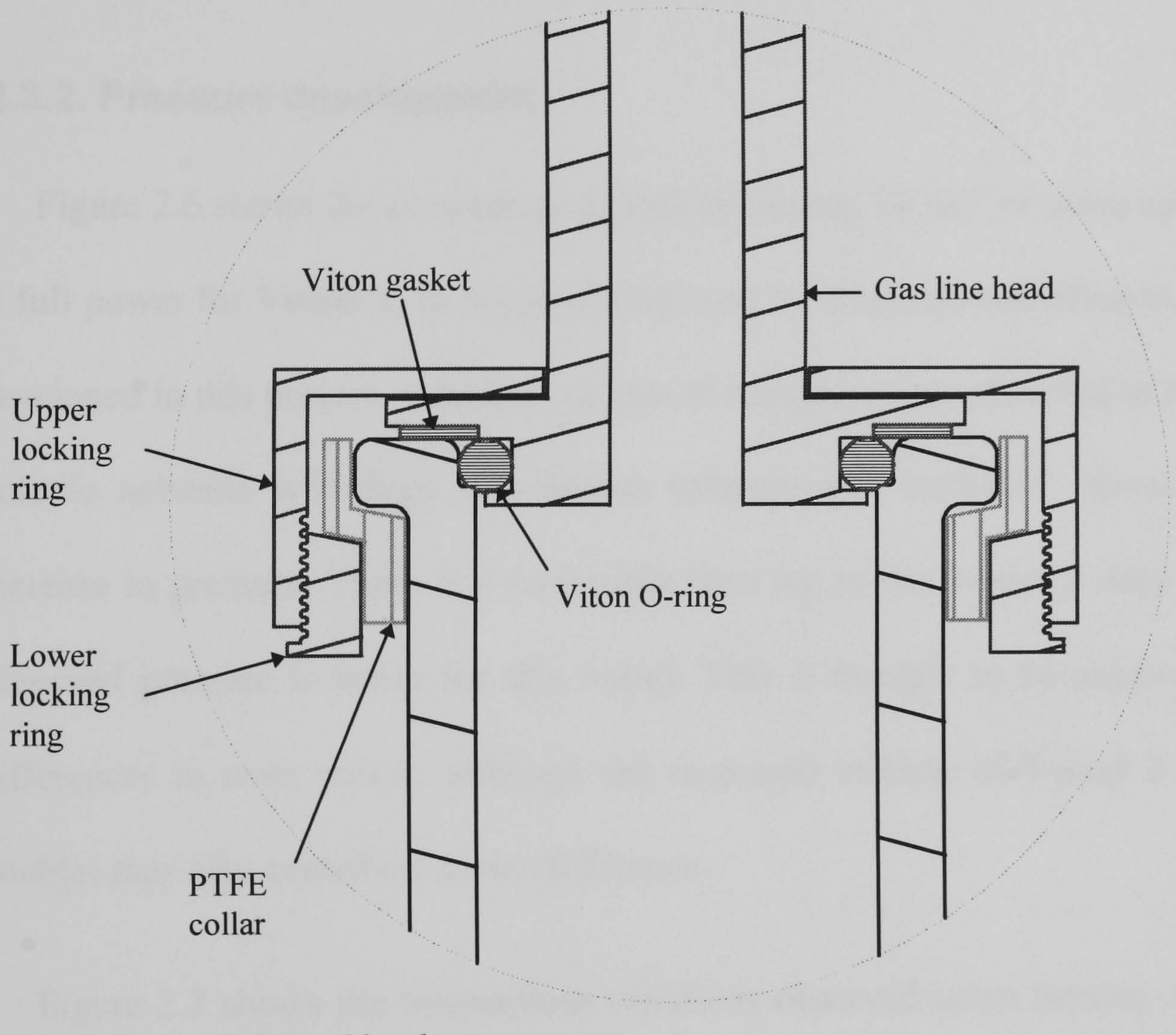


Figure 2.5: Detail of vessel head

Figure 2.5 shows a detailed diagram of the vessel head and seal. A viton O-ring is the primary seal, with a flat viton gasket to prevent contact between the glass and metal surfaces. A PTFE spacer has a similar function with respect to the lower locking ring.

2.3. Vessel evaluation

2.3.1. Introduction

In order to evaluate the effectiveness of the new vessel some comparative experiments were made using some simple inorganic and organometallic transformations first studied by Baghurst and Mingos.[3] The rate of pressure development for some common solvents was also measured and compared with earlier data.

2.3.2. Pressure development

Figure 2.6 shows the pressure generated by heating 20 cm^3 of some common solvents at full power for **Vessel 1**, as originally reported by Baghurst and Mingos,[3] and **Vessel 2**, developed in this project. A similar pattern of behaviour was observed in both cases, with volatile solvents with high loss factors (ethanol and methanol) showing the highest increase in pressure. There is a noticeable time lag in the **Vessel 2** data and overall the observed pressure is lower for this vessel. This is thought to be predominately due to differences in oven power, although the increased volume of **Vessel 2** (approximately double) may also contribute to the difference.

Figure 2.7 shows the temperature variations observed when heating 20 cm^3 of some common solvents at full power in the STAR 2 oven. There is a delay before any temperature is recorded, a consequence of the relatively high calibration limits.

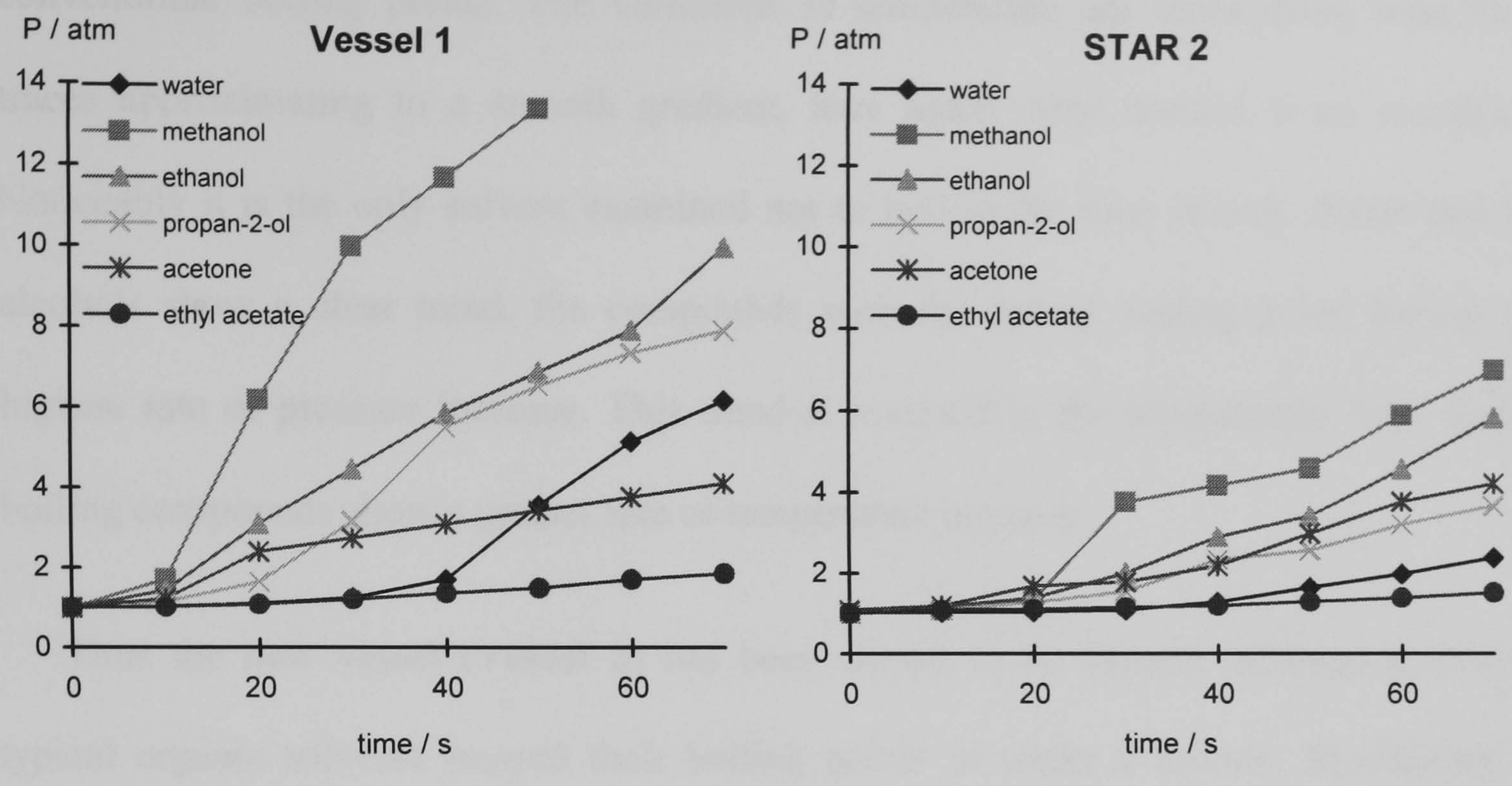


*Figure 2.6: Variation of pressure with time for **Vessel 1** and **Vessel 2.***

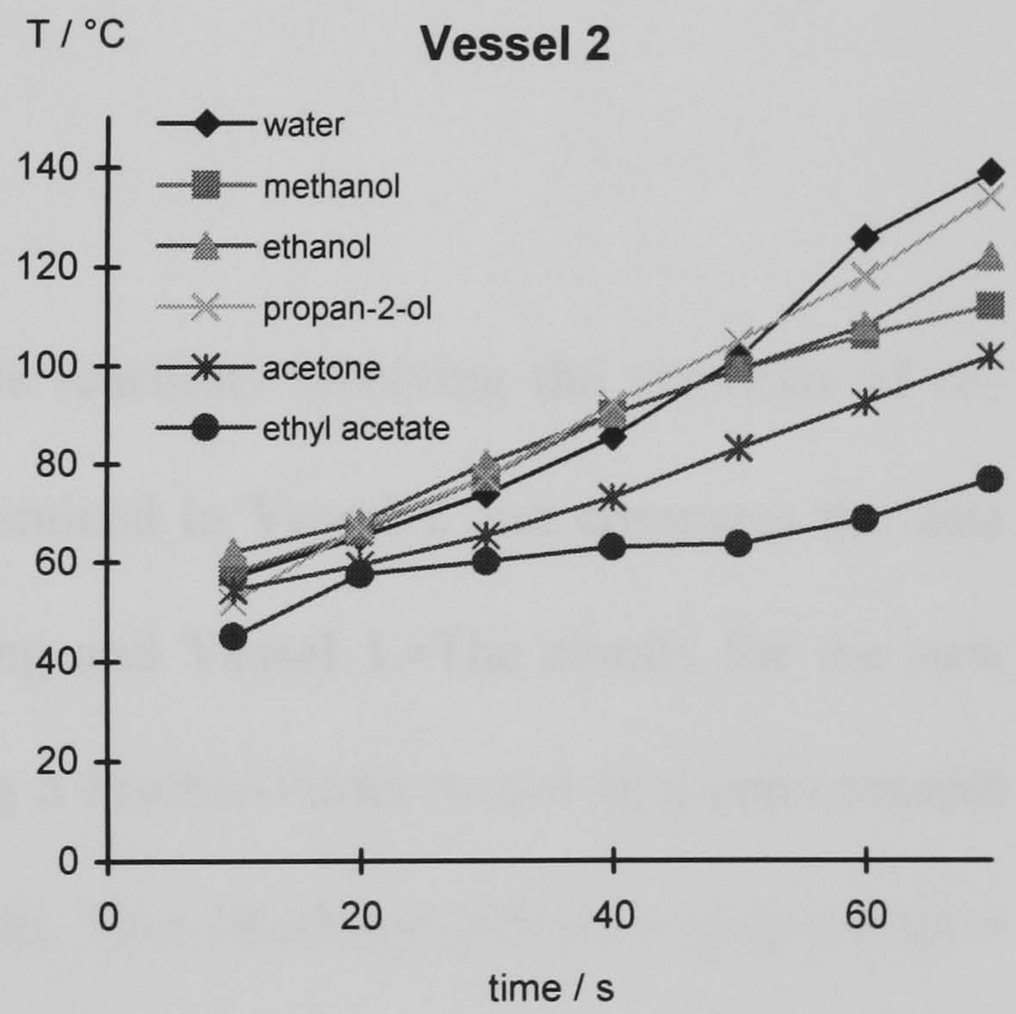


*Figure 2.7: Temperature traces for **Vessel 2***

With the exception of ethyl acetate the observed pressure increases are uneven. The first change, to a higher rate of pressure increase, appears to coincide with the onset of boiling, although this cannot be authoritatively stated. There is some uncertainty in real-time temperature values as a result of the lag associated with the infrared thermometer and organic solvents have been observed to reflux at temperatures above their

conventional boiling points. The variations in temperature are more even, with most traces approximating to a smooth gradient, here again ethyl acetate is an exception. Noticeably it is the only solvent examined not to boil in the time period. Water and the alcohols show a clear trend, the compounds with the lowest boiling point having the highest rate of pressure increase. This trend is inverted in the temperature data, higher boiling compounds show a greater rate of temperature increase.

Thus the new vessel (**Vessel 2**) has been shown to be capable of heating several typical organic solvents beyond their boiling points in under a minute. Monitoring of pressure and temperature is possible, although a distinct lag, of the order of 30 s, is observed for the temperature measurements.

2.3.3. Test reactions

Table 2.1 summarises the results for some reactions involving the synthesis of co-ordination and organometallic compounds examined in **Vessel 2** and compares the data with earlier studies using conventional heating and **Vessel 1**. The results for the new vessel are comparable to those achieved using a Fischer-Porter vessel in a conventional microwave oven in terms of both time and yield. Thus $[Ru(bipy)_3](PF_6)_2$ was synthesised in virtually quantitative yields after heating to 120 °C for 10 minutes in methanol, rather than 3 days at reflux in 95 % aqueous ethanol.[4] This is a slightly lower temperature than that used by Baghurst and Mingos,[3] in order to keep the pressure below 10 atm. For $[Ru(C_7H_8)Cl_2]_2$ a slight drop in yield is recorded although the reaction time is reduced by more than three hundredfold by comparison with the conventionally heated method.[5] The synthesis of $Mo_2(acetato)_4$ uses acetic acid as a solvent, rather than ethylene glycol.

Unsurprisingly, as the temperatures are very similar, the reduction in overall reaction time for this synthesis is much less marked than that for the earlier examples.

Table 2.1: Results for a series of organometallic transformations

	Conventional Heating	Baghurst and Mingos[3] **(Vessel 1)**	Present Work **(Vessel 2)**
$[Ru(bipy)_3](PF_6)_2$	Ref. 4		
time	72 hr	10 min.	10 min.
solvent	95 % EtOH	MeOH	MeOH
T / ° C	78	133	120
P / atm	1	12	10
Yield / %	95	87	98
$[Ru(C_7H_8)Cl_2]_2$	Ref. 5		
time	2 day	9 min.	9 min.
solvent	EtOH	EtOH	EtOH
T / ° C	50	135	133
P / atm	1	11	7.3
Yield / %	65	66	54
$Mo_2(acetato)_4$	Ref. 6		
time	8 hour	30 min.	30 min.
solvent	Ethylene glycol	CH_3CO_2H	CH_3CO_2H
T / ° C	198	195	195
P / atm	1	10	7.3
Yield / %	85	65	65

These simple experiments show that **Vessel 3** is an effective apparatus for Fischer-Porter type syntheses, using microwave dielectric heating. It can be easily used with the CEM STAR 2 oven allowing full monitoring and control of the reaction temperature. When compared to conventional heating methods dramatic reductions in overall reaction time are observed.

2.4. Substitution reactions of Group 6 Metal hexacarbonyls

2.4.1 Pyridine

The substitution of carbon monoxide, in $M(CO)_6$ (M = Cr, Mo or W) by pyridine has been studied under reflux and atmospheric pressure conditions in the STAR 2 oven and using the LDV autoclaves in the MDS 2000. For chromium no substituted compounds were isolated. Tungsten and molybdenum gave quantitative yields of the di-substituted products, $M(CO)_4py_2$. Using extended reaction times in the **Vessel 2** Pyrex autoclave a 60 % yield of the tri-substituted $W(CO)_3py_3$ compound was obtained.

Heiber and Romberg[7] reported that heating $W(CO)_6$ in pyridine under reflux for 8 hours gave $W(CO)_3py_3$ exclusively, whereas heating in an autoclave gave only $W(CO)_4py_2$. Kraihanzel and Cotton[8] reported stepwise substitution under reflux conditions. Mono or di-substituted pyridines were isolated by carefully monitoring the volume of CO evolved during the reaction. Yields of 70 % were reported for $Mo(CO)_4py_2$ and $Cr(CO)_4py_2$. Monosubtituted pyridines could also be obtained in moderate yield (45 %) by stirring a thf solution of hexacarbonyl with one equivalent of pyridine and Me_3NO.[9]

Table 2.2 summarises some results obtained when $M(CO)_6$ (M = M or W) was heated under reflux in neat pyridine using the STAR 2 oven. The solution was observed to reflux steadily at 121 °C, 6 degrees above the usually observed boiling point for pyridine. Tungsten and molybdenum hexacarbonyl rapidly dissolved in the pyridine to give red solutions. The solution reached reflux conditions without significant sublimation of the starting material being observed. This was not the case for $Cr(CO)_6$: Sublimation of the

starting material was considerable and the refluxing solution rapidly turned dark brown. The chromium compound is much more thermally sensitive and the rapid heating rates which are associated with microwave conditions appear to cause extensive decomposition. No stable products were isolated from this reaction mixture.

Table 2.2: Substitution of $M(CO)_6$ by pyridine. Heated under reflux at atmospheric pressure conditions in the STAR 2 oven

Metal	time / min.		Yield / %
Mo	30	$Mo(CO)_4py_2$	99
	60	$Mo(CO)_4py_2$	90
W	20	$W(CO)_5py$	3
		$W(CO)_4py_2$	4
	45	$W(CO)_5py$	2
		$W(CO)_4py_2$	50
	60	$W(CO)_4py_2$	80
	180	$W(CO)_4py_2$	27
		$W(CO)_3py_3$	29

Methods for the synthesis of $M(CO)_mpy_{(6-m)}$ using conventional heating emphasise the importance of returning the sublimated starting material to the solution and the stepwise formation of products. These features are not observed under dielectric heating. Both tungsten and molybdenum hexacarbonyl dissolved rapidly with little or no sublimation observed and only very minor amounts of the mono-substituted product were isolated. This may be assumed to be a result of the elevation of the reflux temperature to 6 °C above the conventional boiling point.

The lack of observed sublimation may be explained by localised dielectric heating, exaggerated by the lack of mixing. In the early stages of heating bubbles are seen to form

at the surface of the starting material. These were not thought to be pyridine vapour because reflux conditions are not achieved for several minutes, by which time the starting material had dissolved and the solution had become highly coloured. The starting material is non-polar and does not absorb microwave energy, thus only the outer surface is warmed by the solvent. As the hexacarbonyl gains energy via the pyridine rather than through any direct heating process a reaction is favoured relative to simple sublimation.

Good yields of the bis-pyridyl product were rapidly obtained using this system. Care needs to be taken with the volume of solvent used - if too little is used solid product can build up on the vessel wall above the solvent head, leading to hot-spots, on one occasion this resulted in serious cracking of the vessel and complete product breakdown. Only black solids were observed on the cracked vessel surface.

Table 2.3 shows some comparative results obtained by heating $M(CO)_6$ in pyridine using a CEM LDV system. Only the bi-substituted product was isolated using this apparatus which is based on closed Teflon vessels. Once again no products could be isolated from chromium hexacarbonyl, even when lower temperatures were employed. Tungsten and molybdenum hexacarbonyl rapidly give quantitative yields of the

Table 2.3: Substitution of $M(CO)_6$ by pyridine. Heated under pressure in the MDS 2000 oven

Metal	time / min.	T / °C	$M(CO)_4py_2$ yield / %
W	20	200	95
Mo	10	140	75
	10	200	95
	20	200	75
Cr	20	90	0
	20	200	0

bisubstituted pyridyl products, $M(CO)_4py_2$.

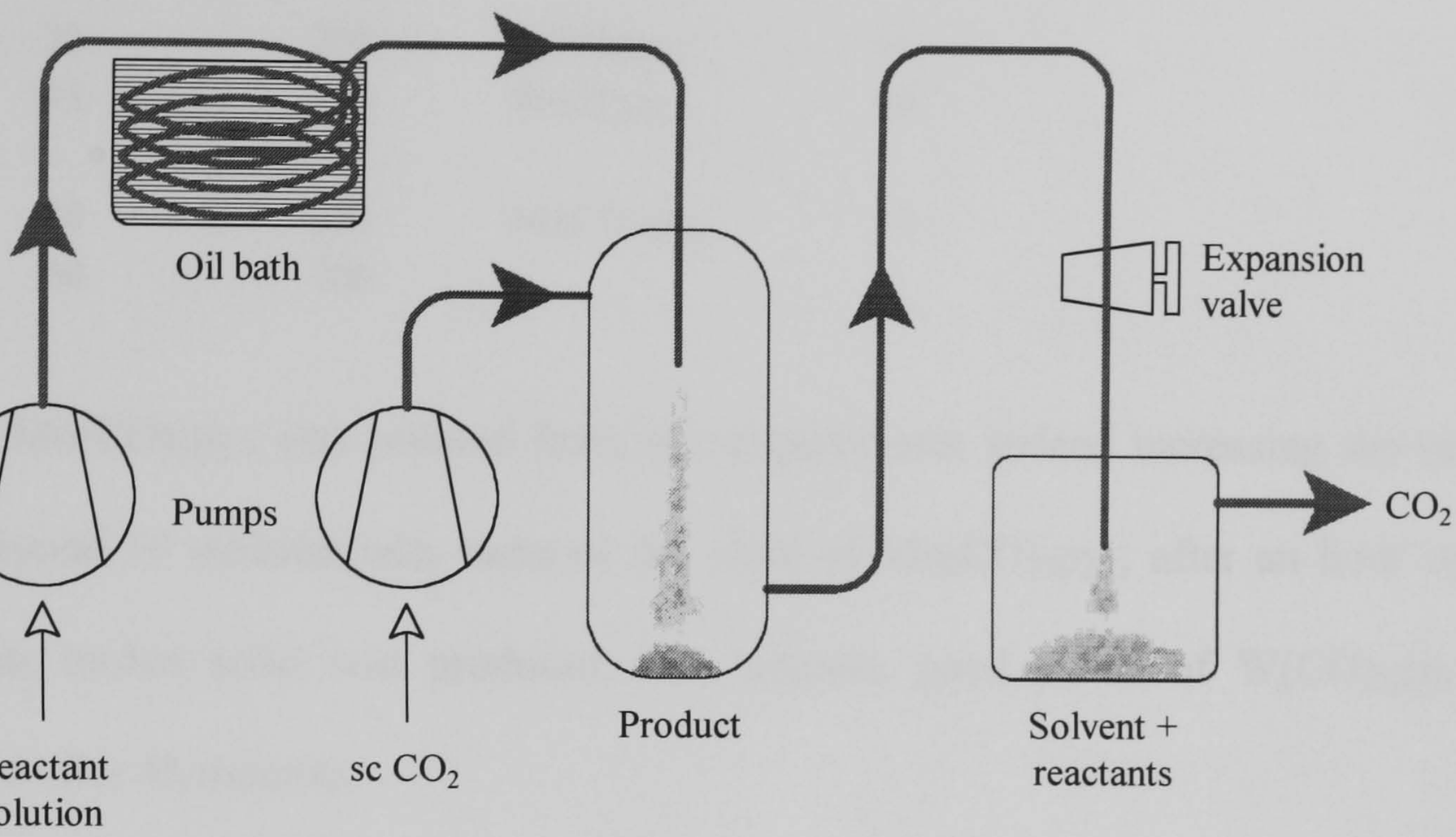


Figure 2.8: ROSA reactor[10]

Poliakoff[10] has reported similar results for tungsten using his ROSA (Reaction in Organics with Supercritical Antisolvents) system. The basic experimental set-up for ROSA is shown in Figure 2.8: A 1 % (w/v) solution of $W(CO)_6$ in pyridine is pumped through a tubular reactor at 215 °C with a flow rate such that the overall residence time is 30 minutes. The solution is then pumped into a chamber of $scCO_2$ where the product precipitates as yellow needles. The solution then passes through an expansion valve, vapourising the $scCO_2$ and allowing the recovery of solvent.

Direct comparison of the conditions used in the ROSA reactor is beyond the thermal capabilities of the LDV. Consequently some experiments, using more extreme conditions, were performed, using the Pyrex autoclave (**Vessel 2**) and the STAR 2 oven. Some results from these experiments are summarised in Table 2.4.

Table 2.4: Substitution of $M(CO)_6$ by pyridine. Heated under pressure in the STAR 2 oven, ***Vessel 2***

Metal	time / min	T / °C	Products	yield / %
W	30	200	$W(CO)_4py_2$	83
	45	200	$W(CO)_3py_3$	60
Mo	30	200	$Mo(CO)_4py_2$	72
	60	200		

No $Mo(CO)_3py_3$ was isolated from any experiments, indeed increasing the reaction time beyond 10 minutes only reduced the yield of $Mo(CO)_4py_2$; after an hour only an insoluble brown solid was produced. For tungsten good yields of $W(CO)_3py_3$ were obtained after 45 minutes.

In summary, good yields of $Mo(CO)_4py_2$, $W(CO)_4py_2$ and $W(CO)_3py_3$ may be obtained using microwave dielectric heating. Reactions using pressurised vessels require shorter heating times than those using reflux conditions at atmospheric pressure and give greater yields. Of the three pressurised systems examined (LDV, **Vessel 2** and ROSA) the LDV's allow rapid synthesis of bis-pyridyl products in near quantitative yields. The tri-substituted product $W(CO)_3py_3$ requires longer reaction times which cannot be safely sustained within an LDV. Good yields were obtained from the Pyrex autoclave (**Vessel 2**). In all the systems examined relatively high temperatures are generated, thus it has not been possible to isolate the more thermally sensitive chromium compounds for which indirect substitution methods remain necessary.[9]

2.4.2. 2,2'-bipyridine

Stibbard has reported virtually quantitative yields for the synthesis of $M(CO)_4$bipy for all Group 6 metal hexacarbonyls after heating $M(CO)_6$ with 2,2'-bipyridine under reflux

in toluene for approximately two hours.[11] Toluene is a poor solvent for dielectric heating; a 20 cm^3 sample heated in the STAR 2 oven was not observed to reflux, the highest measured temperature being 100 °C. Consequently toluene was replaced with chlorobenzene for the microwave experiments.

Table 2.5 summarises some results for the reflux experiments. Data from reference 11 is compared with experiments heating $M(CO)_6$ and 2,2'-bipyridine under reflux in chlorobenzene, using either an electric mantle or the STAR 2 microwave oven. Chlorobenzene is observed to reach 143 °C under dielectric heating conditions, some 11 °C above its conventional boiling point. As a result the reaction is generally complete more quickly under dielectric heating conditions. The most dramatic result is observed for tungsten, where the required reaction time is halved. An apparently even greater reduction in overall rate for molybdenum hexacarbonyl is actually due to poor optimisation of the original literature conditions.

Table 2.5: Substitution of $M(CO)_6$ by bipyridine under reflux conditions. (literature data in italics)

Metal	Solvent	Energy source	time / min	Yield / %	Ref.
Cr	*toluene*	*electromantle*	*120*	*94*	*11*
	chlorobenzene	electromantle	90	80	
	chlorobenzene	STAR 2	90	92	
Mo	*toluene*	*electromantle*	*90*	*93*	*11*
	toluene	electromantle	30	92	
	chlorobenzene	electromantle	30	90	
	chlorobenzene	STAR 2	30	94	
W	*xylene*	*electromantle*	*120*	*99*	*11*
	chlorobenzene	electromantle	120	91	
	chlorobenzene	STAR 2	60	98	

In autoclave experiments it was discovered that acetonitrile had an activating effect. These results are summarised in Table 2.6. Quantitative yields are rapidly achieved in 30 minutes or less using acetonitrile, a halving of the overall reaction time, without the temperature being raised.

Table 2.6: Substitution of $M(CO)_6$ by bipyridine in an autoclave (CEM LDV)

Metal	Solvent	time / min.	T / °C	Yield / %
Cr	acetonitrile	30	140	99
	chlorobenzene	30	140	53
Mo	acetonitrile	10	140	81
	chlorobenzene	30	140	99
W	acetonitrile	30	140	88
	chlorobenzene	30	140	32

The activating effect of acetonitrile as a solvent may be assumed to be due to *in-situ* generation of $M(CO)_x(NCCH_3)_y$, (where x = 4 - y and y = 1 or 2). Such compounds are well known reactive intermediates. However, attempts to isolate the air and moisture sensitive, acetonitrile substituted products were generally unsuccessful, revealing the limitations of the LDV's for such compounds. Heating $Mo(CO)_6$ in dry acetonitrile in an LDV sealed under nitrogen gave green or brown solutions from which stable products could not be isolated. Attempts were also made to synthesise $M(CO)_5py$ by heating $M(CO)_6$ in a dilute acetonitrile solution of pyridine. These experiments also failed to yield isolable products.

Further substitution has proved difficult; Han *et al*[12] report a photochemical process, using the 313 nm line from a mercury lamp (no yields are reported) and Chisholm *et al*[13] report a 59 % yield for $Mo(CO)_2(bipy)_2$ requiring a slow initialisation process: a tetralin

solution of $Mo(CO)_4$bipy and excess bypyridine is raised to its boiling point over three hours, whilst nitrogen is bubbled through the solution. Once at reflux the solution is heated for a further 30 minutes. Several attempts were made to adapt this process for use in the Pyrex autoclave, generally using shorter ramp times but only starting materials were recovered.

Thus $M(CO)_4$bipy can be synthesised most effectively by dielectric methods using an activating solvent (acetonitrile) in an autoclave at moderate temperatures and pressures.

2.5. Limitations of the new vessel

2.5.1 Vessel failures

We have reported above some successful uses of the new vessel in the STAR 2 oven.

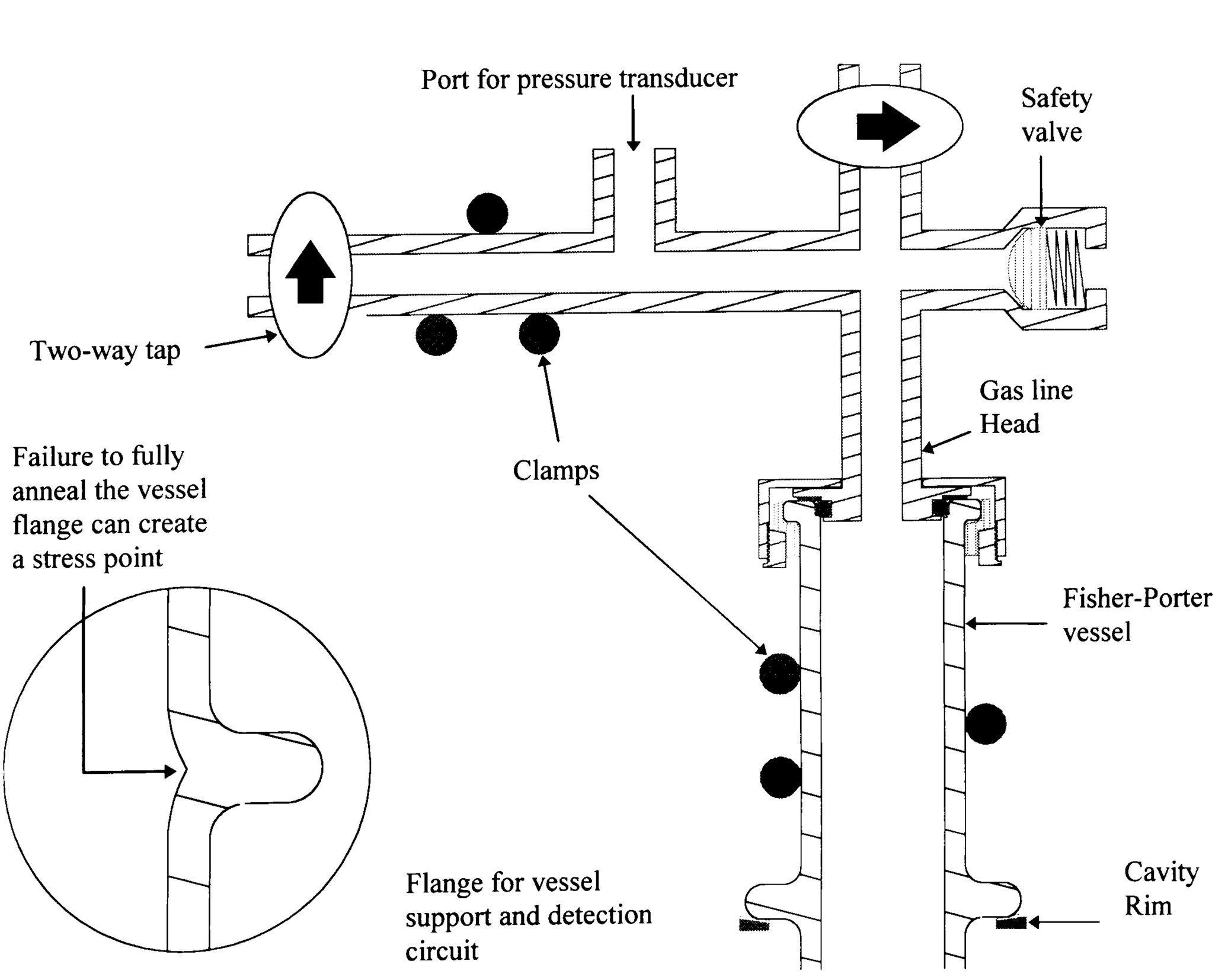


Figure 2.9: Vessel 2, showing clamp and support points.

These have generally occurred at moderate temperatures and pressures. Nonetheless several vessel failures occurred under these conditions. With one exception, the failure of the vessel totally shattered the glass of both the vessel and the cavity liner. It is a testament to the rugged design of the STAR 2, that cleaning the cavity and replacing the liner are simple if tedious tasks and the oven can soon be made operational again. In the exceptional case, the vessel broke cleanly about the flange, pointing to a failure to fully anneal that surface, resulting in an internal stress point (see insert in Figure 2.9). For the other failures the fragmentation of the debris makes pinpointing the exact cause difficult. A possible cause lies in the design and support of the apparatus: in order to minimise the thickness of glass required the vessel diameter is kept to 30 mm, approximately half that of the oven cavity. The gas line and pressure head is both heavy and unsymmetrical and is therefore supported by a clamp at one end (see Figure 2.9). To ensure the vessel sits centrally in the cavity a second clamp is placed about the upper neck of the vessel. The two clamps exert perpendicular forces and although care is taken to ensure the vessel sits securely it seems likely that slight shifts in vessel alignment would create unequal stresses at the clamping points.

Several issues arise as a result of the vessel failures. Obviously it limits the scope of the apparatus, particularly with regard to expensive or toxic reagents, secondly repeated failures are most unnerving. As we do not currently have an automated method for detecting vessel failure and immediately cutting the oven power it also imposes a requirement that all reactions are watched constantly, effectively limiting its use for long reaction times.

The inherent fragility of **Vessel 2** results from several design compromises. Temperature is monitored by an infra-red detector at the base of the cavity. For accurate temperature measurement the vessel wall should be as thin as possible, however reducing the wall thickness requires a corresponding reduction in vessel diameter which leads to problems in siting the vessel base accurately above the thermometer.

An alternative design is shown in Figure 2.10. The flange has been removed and the gas line head rests directly upon the cavity rim. By extending the 'neck' of the gas line and arranging the components in a more symmetrical manner it may be possible to secure the position of the vessel using only one clamp. Such a design, if feasible, would remove much of the external stress upon the vessel.

Although a modified design may be expected to suffer fewer explosive failures, better safety features should also be developed. A possible solution would be a cut-off switch

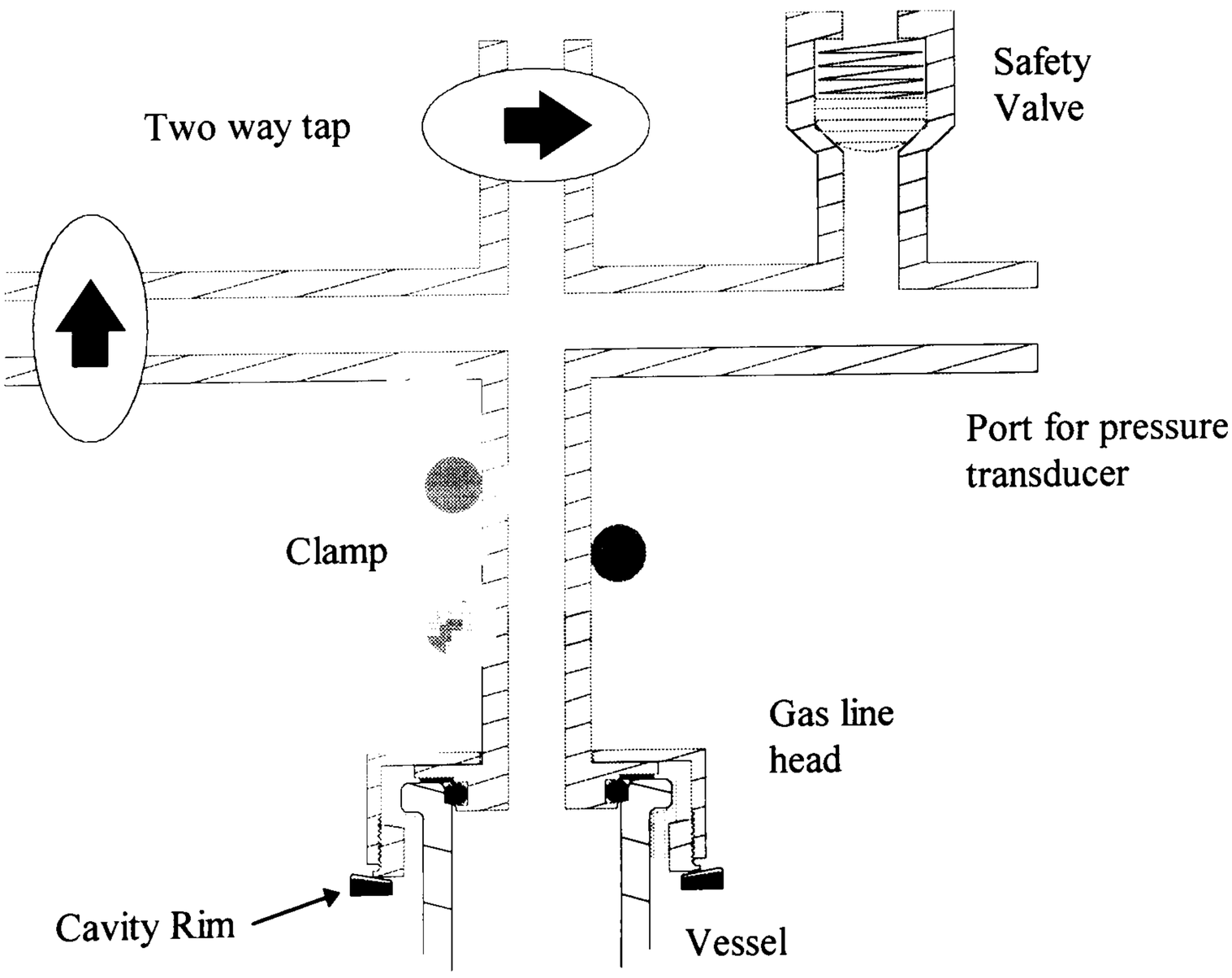


Figure 2.10 Some possible simple alterations for ***Vessel 2***

for the oven power, designed to activate when vessel failure (i.e. sudden and total loss of pressure) is detected; ideally such developments would be combined with a method for fully monitoring and controlling the pressure within the vessel.

2.5.2 Seal failure

The pressure seal in the Pyrex autoclave is a polymer o-ring. The most common material for such seals is Viton, which has a safe working temperature limit of 215 °C. This does not represent a significant advance on the temperature range offered by the LDV system. Extension of these limits will require alternative materials; silicon based polymers have been considered but are not generally available in the required form.

2.6. Summary

A range of vessels designed for use in a microwave cavity have been examined and evaluated. The MDS 2000 oven, using PTFE autoclaves has been shown to be advantageous for moderate conditions. By heating solvents beyond their standard boiling points substantial reductions in overall reaction time may be achieved. However, the system is not well adapted for air and moisture sensitive reactions.

The STAR 2 oven allows heating under reflux conditions and the apparatus is easily connected to standard laboratory glassware. As a result of heating above the nucleation limited boiling point, some reductions in overall reaction time are possible.

Attempts to adapt a Fischer-Porter style Pyrex autoclave for the STAR 2 oven have met with mixed results. The vessel has been shown to be useful for several reactions although technical problems remain with the pressure seal and overall vessel strength, limiting its use under rigorous conditions. It is noteworthy that a recent commercial

design by Milestone[14] capable of using either a glass or TFM vessel does not recommend using the glass vessel at pressures above 2.5 bar.

2.7. Experimental

Unless otherwise specified, reagents were purchased from Aldrich and used as supplied.

$[Ru_3(bipy)_3](PF_6)_2$

$RuCl_3 \cdot 3H_2O$ (0.14 g, 0.52 mmol), 2,2'-bipyridine (0.30 g, 2.0 mmol) and NEt_3 (1.5 cm^3, 11 mmol) were placed in **Vessel 2** with 10 cm^3 methanol and stirred briefly. The vessel was then sealed under a nitrogen atmosphere. The oven was set with a maximum temperature of 120 °C and TAP (time at parameter) of 10 minutes. The reaction conditions were reached within 2 minutes, with the pressure at 9 ± 1 atm. After cooling the red-brown solution was transferred to a Schlenk flask containing 10 cm^3 of a 0.25 M solution of KPF_6. The resulting orange precipitate was recrystallised from methanol ($[Ru_3(bipy)_3](PF_6)_2$, 0.44 g, 98 %).

$[Ru_3(bipy)_3](PF_6)_2$

MS FAB$^+$: 715 (M^+), 570 (M^+- PF_6), 413 (M^+ - (PF_6 + $C_{10}H_8N_2$))

CHN analyses: Found C 41.9, H 2.7, N 9.6. *Calc. C 41.9, H 2.9, N 9.8*

$[Ru(C_7H_8)Cl_2]_2$

$RuCl_3 \cdot 3H_2O$ (0.17 g, 0.67 mmol) and cycloheptatriene (1.0 cm^3, 9.6 mmol) were placed in **Vessel 2** with 9 cm^3 ethanol and stirred briefly. The vessel was then sealed under a nitrogen atmosphere. The oven was set with a maximum temperature of 130 °C and TAP of 9 minutes. The reaction conditions were reached within 2 minutes, with the pressure at 7 ± 0.5 atm. After cooling, red-brown crystals were filtered and washed with methanol. (0.095 g, 54 %).

$[Ru(C_7H_8)Cl_2]_2$

MS FAB$^+$: 492 (M^+ - Cl)

CHN analyses: Found C 31.7, H 3.0, N 0. *Calc. C 31.8, H 3.0, N 0.*

$Mo_2(acetato)_4$

$Mo(CO)_6$ (0.26 g, 0.98 mmol) and acetic anhydride (1.0 cm^3, 11 mmol) were placed in **Vessel 2** with 9 cm^3 glacial acetic acid. The vessel was then sealed under a nitrogen atmosphere. The oven was set with a maximum temperature of 195 °C and TAP of 30 minutes. The reaction conditions were reached within 6 minutes, with the pressure at 7 ± 0.5 atm. After cooling, yellow needles were filtered and washed with methanol. ($Mo_2(acetato)_4$, 0.13 g, 65 %)

$Mo_2(acetato)_4$

MS FAB$^+$: 428 (M^+)

CHN analyses: Found C 22.2, H 2.7, N 0. *Calc. C 22.4, H 2.8, N 0.*

Substitution of $M(CO)_6$ by py. Heated under reflux in the STAR 2 oven

For details of times and yields see Table 2.2. A typical procedure is described below.

$Mo(CO)_6$ (0.13 g, 0.5 mmol) was placed in a standard Pyrex STAR 2 vessel with 10 cm^3 of pyridine and the apparatus flushed with nitrogen. The oven was set with a maximum temperature of 130 °C and TAP of 30 minutes. Effervescence is observed at the solid surface while the solution rapidly turns orange. The solution colour darkens as the reaction progresses. The solution achieves reflux within three minutes, although the temperature sensor does not record a maximum (122 °C) for another 6 minutes. No sublimation of the starting material is observed in the part of the vessel above the cavity choke. After cooling 10 cm^3 of hexane was added to the reaction solution. The resulting precipitate was washed with hexane and recrystallised from pyridine and pentane. ($Mo(CO)_4py_2$, 0.17 g , 95 %)

$Mo(CO)_4py_2$

MS EI: 289 ($M^+ - C_5H_5N$), 259 ($M^+ - (C_5H_5N + CO)$), 233 ($M^+ - (C_5H_5N + 2CO)$), 205 ($M^+ - (C_5H_5N + 3CO)$)

CHN analyses: Found C 45.9, H 2.6, N 7.6. *Calc. C 45.9, H 2.7, N 7.6*

IR (CH_3CN): ν_{CO} 2024 (w), 1908 (m), 1881 (vs), 1840 (m, sh) cm^{-1}
lit. (CH_3CN): *2025 (w), 1907 (m), 1881 (vs), 1839 (m, sh)[8] cm^{-1}*

$W(CO)_4py_2$

MS EI: 375 ($M^+ - C_5H_5N$), 347 ($M^+ - (C_5H_5N + CO)$), 319 ($M^+ - (C_5H_5N + 2CO)$), 291 ($M^+ - (C_5H_5N + 3CO)$)

CHN analyses: Found C 36.9, H 2.2, N 6.1. *Calc. C 37.0, H 2.2, N 6.2*

IR ($CHCl_3$): ν_{CO} 2010 (w), 1888 (m), 1870 (vs) 1828 (m, sh) cm^{-1}
lit. ($CHCl_3$): *2012 (w), 1888 (m), 1869 (vs), 1828 (m, sh)[8] cm^{-1}*

Substitution of $M(CO)_6$ by py. Heated under pressure in the MDS 2000 oven

For details of times and yields see Table 2.3. A typical procedure is described below.

$Mo(CO)_6$ (0.13 g, 0.5 mmol) was placed in an LDV with 20 cm^3 of pyridine. The vessel was flushed with nitrogen and then sealed. The oven was set with a maximum temperature of 200 °C and TAP of 20 minutes. After cooling the vessel was opened to reveal a red-brown solution. This was transferred to a flask containing 20 cm^3 hexane and stored overnight in a freezer. The resulting precipitate was washed with hexane and recrystallised from pyridine and pentane. ($Mo(CO)_4py_2$, 0.14 g, 75 %)

Substitution of $M(CO)_6$ by py. Heated under pressure in the STAR 2 oven

For details of times and yields see Table 2.4. A typical procedure is described below.

$W(CO)_6$ (0.18 g, 0.5 mmol) was placed in **Vessel 2** with 10 cm^3 pyridine. The vessel was then sealed under a nitrogen atmosphere. The oven was set with a maximum temperature of 200 °C and TAP of 30 minutes. The reaction conditions were reached within 5 minutes, with the pressure at 8 ± 1 atm. After

cooling 10 cm^3 of hexane was added to the reaction solution. The resulting precipitate was washed with hexane and recrystallised from pyridine and pentane. ($W(CO)_4py_2$, 0.19 g, 83 %)

$W(CO)_3py_3$

MS EI: 426 (M^+ - C_5H_5N), 398 (M^+ - (C_5H_5N + CO)), 370 (M^+ - (C_5H_5N + 2CO))

CHN analyses: Found C 42.7, H 3.1, N 8.2. *Calc.. C42.8, H 3.0, N 8.3*

Substitution of $M(CO)_6$ by bipy. Heated under reflux in the STAR 2 oven

For details of times and yields see Table 2.5. A typical procedure is described below.

$Mo(CO)_6$ (0.13 g, 0.5 mmol) and 2,2'-bipyridine (0.24 g, 1.5 mmol) were placed in a standard Pyrex STAR 2 vessel with 10 cm^3 of chlorobenzene and the apparatus flushed with nitrogen. The oven was set with a maximum temperature of 150 °C and TAP of 30 minutes. Effervescence is observed at the solid surface while the solution rapidly turns red. The solution colour darkens as the reaction progresses. The solution is under reflux within two minutes, although the temperature sensor does not record a maximum (143 °C) for another 5 minutes. No sublimation of the starting material is observed in the part of the vessel above the cavity choke. After cooling the reaction solution was stored overnight in a freezer. The resulting precipitate was washed with hexane. ($Mo(CO)_4$bipy, 0.16 g, 90 %)

$Cr(CO)_4$bipy

MS FAB^+: 320 (M^+), 292 (M^+ - CO), 264 (M^+ - 2CO)

CHN analyses: Found C 52.4, H 2.4, N 8.6. *Calc. C 52.5, H 2.5, N 8.7*

IR ($CHCl_3$): ν_{CO} 2009 (m), 1907 (vs), 1886 (m,sh), 1833 (s). cm^{-1}
lit. ($CHCl_3$): *2010 (m), 1908 (vs), 1888 (sh), 1833 (s).*[11] *cm^{-1}*

$Mo(CO)_4$bipy

MS FAB^+: 364 (M^+), 338 (M^+ - CO), 310 (M^+ - 2CO)

CHN analyses: Found C 46.0, H 2.1, N 7.6. *Calc. C 46.1, H 2.2, N 7.7.*

IR ($CHCl_3$): ν_{CO} 2014 (m), 1911 (vs), 1883 (m), 1830 (s) cm^{-1}
lit. ($CHCl_3$) *2014 (m), 1911 (vs), 1882 sh, 1830 (s).*[11] *cm^{-1}*

$W(CO)_4$bipy

MS FAB^+: 452 (M^+), 424 (M^+ - CO), 396 (M^+ - 2CO)

CHN analyses: Found C 37.0, H 1.7, N 6.1. *Calc. C 37.2, H 1.8, N 6.2.*

IR ($CHCl_3$): ν_{CO} 2007 (m), 1901 (vs), 1880 (m,sh), 1828 (s) cm^{-1}
lit ($CHCl_3$. *2008 (m), 1900 (vs), 1880 (sh), 1829 (s).*[11] *cm^{-1}*

Substitution of $M(CO)_6$ by bipy. Heated under pressure in the MDS 2000 oven

For details of times and yields see Table 2.6. A typical procedure is described below.

$Mo(CO)_6$ (0.13 g, 0.5 mmol) and 2,2'-bipyridine (0.24 g, 1.5 mmol) were placed in an LDV liner with 20 cm^3 acetonitrile. The vessel was sealed and the oven set at 140 °C for 10 minutes. After cooling the vessel was opened to reveal a red-brown solution which was stored in a freezer overnight. The resulting

precipitate was washed with hexane and recrystallised from acetone to give maroon crystals of $Mo(CO)_4$bipy (0.14 g, 80 %)

2.8. References

1 *CEM MDS 2000 Manual,* CEM Corporation, Matthews, North Carolina, 28106 (1992)

2 *CEM STAR2 Manual,* CEM Corporation, Matthews, North Carolina, 28106 (1996)

3 D.R. Baghurst and D.M.P. Mingos, *J. Chem. Soc. Dalton Trans,.* (1992) 1151

4 R.A. Palmer and T.S. Piper, *Inorg. Chem.,* **5** (1966) 864

5 G. Winkhaus and H. Singer, *J. Organomet. Chem.,* 7 (1967) 487

6 D. Holste and H. Schafer, *Z. Anorg. Allg. Chem.,* **391** (1972) 263

7 W. Hieber and E. Romberg, *Z. Anorg. Allg. Chem.,* **221** (1935) 349

8 C. S. Kraihanzel and F. A. Cotton, *Inorg. Chem.,* **2** (1963) 533

9 T. S. A. Hor, *Inorg. Chim. Acta,* **143** (1988) 3

10 M. Poliakoff, *Proc. 4th Intl. Symp. on Supercritical Fluids*, (Sendai, Japan); Tohoku University Press, Sendai, Japan 1997, **Vol C**, 757

11 M. H. B. Stibbard, *J. Chem. Soc. A* (1962) 4713

12 Y. J. Yan and A. J. Lees, *Inorg. Chim. Acta,* **147** (1988) 45

13 M. Chisholm, *Inorg. Chem.* **23** (1984) 2298

14 Milestone Ethos Microwave Reactor, Via Fatebenefratelli, 1/5 24010 Sorisole (BG), Italy, www.milestonesci.com.

Chapter Three

Transition Metal Carbonyl Cluster Synthesis

3.1. Introduction

A metal cluster has been defined as 'a group of two or more metal atoms where direct and substantial metal-metal bonding is present.'[1] The field is barely 35 years old, yet the range of cluster compounds which have been isolated has been extended from those with 'two or more' metal atoms to $[H_2Pt_{38}(CO)_{44}]^{2-}$, where the metal atoms adopt a face centred cubic, close-packed arrangement.[1] Even larger clusters have also been identified, e.g. $Ru_{55}(P\text{-}^tBu_3)_{12}Cl_{20}$[2] and $[Pd_{561}Phen_{60}O_{60}][PF_6]_{60}$[3] with sizes more usually associated with metal colloids.[4] However, these clusters have not been structurally characterised.

Transition metal clusters have been proposed as models for metal surfaces by Meutterties.[5] In particular he proposed that they are good models for the interpretation of the surface chemistry of heterogeneous catalysts. Studies have also been made on the catalytic properties of clusters in their own right, although there is still considerable debate on the identities of the active species.[4] The development of new and improved synthetic methods to metal cluster compounds remains an important prerequisite to such studies.

3.2. Carbonyl Cluster Synthesis

Carbon monoxide is the most important ligand for the stabilisation of clusters of the late transition metals. Four general methods for the syntheses of metal carbonyl clusters have been developed:[1]

Thermal condensation;

Redox condensation;

Base-promoted CO loss;

Oxidative coupling.

Table 3.1. Preparation of high nuclearity ruthenium clusters by reflux thermolysis.

Starting Material	Solvent	Time / h	Product	% yield wrt ruthenium	Ref.
$Ru_3(CO)_{12}$	Methanol	6	$[HRu_6(CO)_{18}]^-$	80	6
	Ethanol	3	$[HRu_6(CO)_{18}]^-$	90	
		18	$[HRu_6(CO)_{18}]^-$	a	7
			$[H_2Ru_{10}(CO)_{25}]^{2-}$	27	
	Methanol - water	40	$[HRu_6(CO)_{18}]^-$	a	8
			$[H_2Ru_{10}(CO)_{25}]^{2-}$	a	
			$[H_2Ru_8(CO)_{21}]^{2-}$	a	
			$[HRu_{11}(CO)_{27}]^{3-}$	15	
	Acetonitrile	20	$[HRu_{11}(CO)_{27}]^{3-}$	90	7
	Mesitylene (10 %) - n-heptane	100	$[HRu_{10}C(CO)_{24}]^-$	35	9
	di-n-butyl ether	6	α-$H_4Ru_4(CO)_{12}$	10	10
			$Ru_6C(CO)_{17}$	30	
$[Ru_6(CO)_{18}]^{2-}$	diglyme	0.2	$Ru_6C(CO)_{17}$	100	
		1	$[Ru_6C(CO)_{16}]^{2-}$	96	11
	tetraglyme	80	$[Ru_{10}C_2(CO)_{24}]^{2-}$	35	12

a) Yield not given. Products listed in order of elution

Thermal condensation simply involves the heating of a saturated low-nuclearity carbonyl cluster, leading to carbonyl loss and subsequent condensation of the metal fragments. Heating under reflux in high boiling solvents and vacuum pyrolysis have both successfully been used. The reaction is rarely specific; vacuum pyrolysis of $Os_3(CO)_{12}$ in a sealed tube at 210 °C for 12 hours gives a mixture of $Os_6(CO)_{18}$ (80 % yield), $Os_5(CO)_{16}$, $Os_7(CO)_{21}$ and $Os_8(CO)_{23}$ (> 10 %).[13] Separation is usually by thin layer chromatography although fractional crystallisation has also been used. Table 3.1 and

Table 3.2 summarise some reported yields of clusters produced by reflux thermolysis. For ruthenium and osmium this has become the major route for the synthesis of high nuclearity clusters.

Table 3.2. Preparation of osmium carbonyl clusters by reflux thermolysis.

Starting Material	Solvent	Time / h	Product	% yield wrt osmium	Ref.
$Os_3(CO)_{12}$	n-butanol		$[H_4Os_{10}(CO)_{24}]^{2-}$	'low'	14
$[HOs_3(CO)_{11}]^-$	Propan-2-ol	4	$HOs_3(CO)_{10}(O^iBu)$	20	15
			$[H_3Os_4(CO)_{12}]^-$	'main product'	
$HOs_3(CO)_{10}(O^iBu)$	Propan-2-ol	17	$[HOs_8(CO)_{22}]^-$	10	15
			$H_4Os_4(CO)_{12}$	'main product'	
			$[HOs_{10}C(CO)_{24}]^-$	5	
$Os_6(CO)_{18}$	Propan-2-ol	68	$[HOs_8(CO)_{22}]^-$	30	15
			$H_4Os_4(CO)_{12}$	21	
			$[HOs_{10}C(CO)_{24}]^-$	5	
$[Os_6(CO)_{18}]^-$	Triglyme	24	$[Os_{10}C(CO)_{24}]^{2-}$	35	11

The majority of medium sized ruthenium and osmium clusters have been prepared by redox condensation reactions. The preferred reducing agent is sodium and solvents are usually heated under reflux. Using this method[11] $[Ru_6(CO)_{18}]^{2-}$ has been prepared in 78 % yield from $Ru_3(CO)_{12}$, by heating in dry tetrahydrofuran for 5 hours, and $[Os_6(CO)_{18}]^{2-}$ in 65 % yield from $Os_3(CO)_{12}$ in diglyme. Redox condensation has also been employed in 'build-up' reactions, such as the preparation of $[Ru_{10}N(CO)_{24}]^-$ from $[Ru_6N(CO)_{16}]^-$ and $Ru_3(CO)_{12}$ in refluxing diglyme.[16]

Base-promoted CO loss is the primary method for the production of medium sized iridium clusters.[17] Depending on the conditions used, either $[Ir_8(CO)_{22}]^{2-}$ or $[Ir_6(CO)_{15}]^{2-}$ can be isolated by stirring $Ir_4(CO)_{12}$ with potassium hydroxide in methanol. Similarly reaction of a tetrahydrofuran solution of $Ru_3(CO)_{12}$ with potassium hydroxide in either methanol or water yields $[HRu_3(CO)_{11}]^-$ and $[Ru_6(CO)_{18}]^{2-}$ respectively.[18]

Oxidation of anionic species under a carbon monoxide atmosphere can be used to prepare simple neutral clusters. Treatment of $[Ru_6C(CO)_{16}]^{2-}$ and $[Os_6(CO)_{18}]^{2-}$ with ferric chloride in such conditions yields $Ru_6C(CO)_{17}$ and $Os_6(CO)_{18}$ respectively.[11] Coupling of anionic species is also possible; $[Ir_{12}(CO)_{24}]^{2-}$ has been produced by treating $[Ir_6(CO)_{15}]^{2-}$ with $[Cu(NCMe)_4]^+$ in refluxing tetrahydrofuran.[19]

Table 3.3. Preparation of carbonyl clusters on inorganic surfaces.

Precursor	Support	Gas flow over the support	Time / hr	T / °C	Product	Yield / %	Ref.
$RuCl_3$	SiO_2	CO (5 atm)	24	110	$[Ru(CO)_3Cl_2(HOSi\equiv)]$	97	20
$[Ru(CO)_3Cl_2(HOSi\equiv)]$ + Na_2CO_3	SiO_2	CO	48	110	$Ru_3(CO)_{12}$	82	
$[Ru(CO)_3Cl_2(HOSi\equiv)]$ + K_2CO_3	SiO_2	CO	10	150	$K_2[Ru_6C(CO)_{16}]$	68	
$Os_3(CO)_{12}$	MgO	CO	4	275	$[Os_5C(CO)_{14}]^{2-}$	65	21
H_2OsCl_6	MgO	CO/H_2 (1:1)	5	275	$[Os_{10}C(C()_{24}]^{2-}$	65	
$Ir(CO)_2(acac)$	γ-Al_2O_3	CO	10	100	$[Ir_6(CO)_{15}]^{2-}$	a	22
			15	r.t.	$[Ir_8(CO)_{22}]^{2-}$	a	24

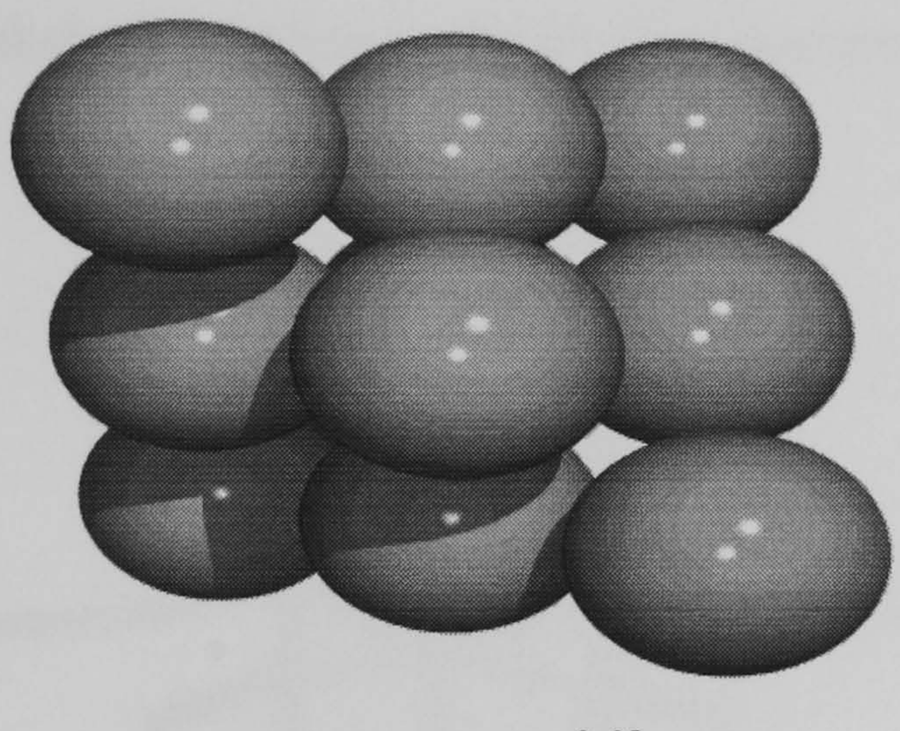
a) Yield not given.

It is possible to carry out solvent free organometallic syntheses by adsorbing the starting materials onto a metal oxide support.[23] Recently this approach has been applied to cluster syntheses. Small clusters or monometallic fragments have been introduced onto the surface and heated under CO or CO/H_2 mixtures. Using this method either $[Ir_8(CO)_{22}]^{2-}$ or $[Ir_6(CO)_{15}]^{2-}$ have been prepared by heating $Ir(CO)_2(acac)$ on γ-alumina with a range of surface hydroxylation at higher temperatures.[24] Table 3.3 summarises some reported yields for surface-mediated cluster synthesis.

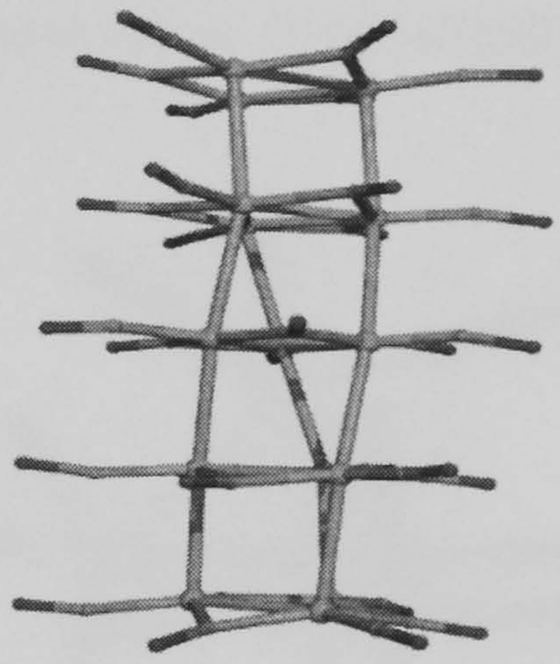
3.3. Cluster Structures

The structures of the majority of transition metal cluster cores are based on spherical deltahedra, i.e. structures where the vertices are arranged upon the surface of a sphere and

form triangular faces. Clusters of nuclearity of less than 7 may generally be described by these structures (e.g. tetrahedra, octahedra). For higher nuclearity clusters 'condensed' structures are formed by joining or capping standard deltahedra. For pseudo-spherical, condensed clusters, close-packed structures may be formed, however it is also possible to produce clusters with columnar structures by condensing faces (see Figure 3.1).



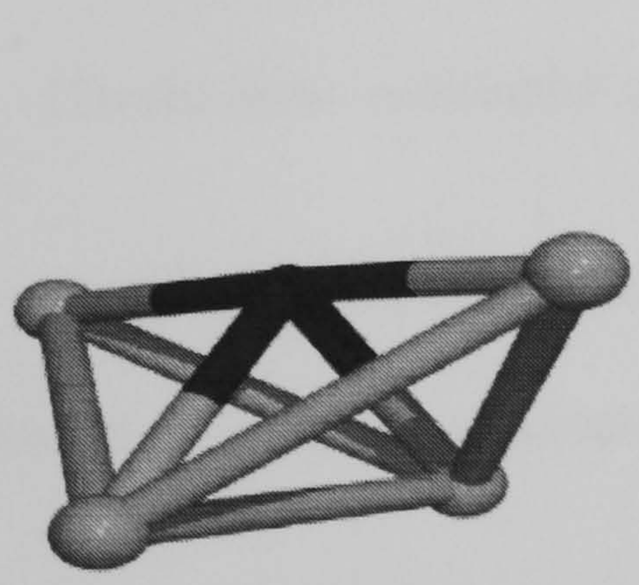
$[H_4Os_{10}(CO)_{24}]^{2-}$ [25]



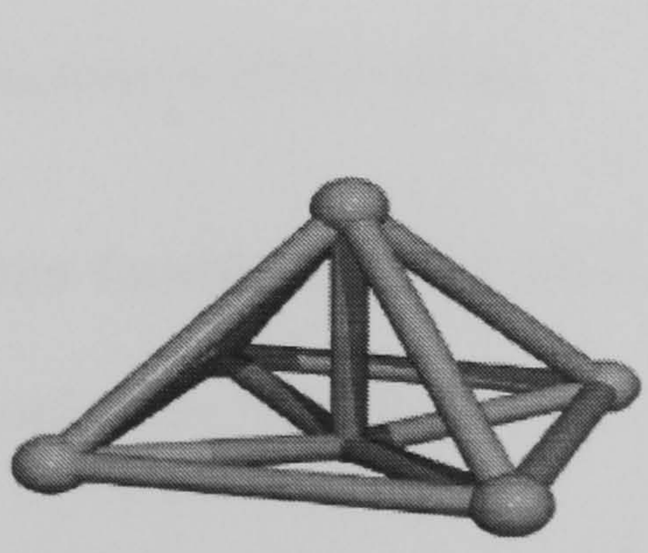
$[Pt_{15}(CO)_{30}]^{2-}$ [26]

Figure 3.1. Structures of $[H_4Os_{10}(CO)_{24}]^{2-}$, a condensed cluster with face centred cubic packing and $[Pt_{15}(CO)_{30}]^{2-}$, a columnar cluster.

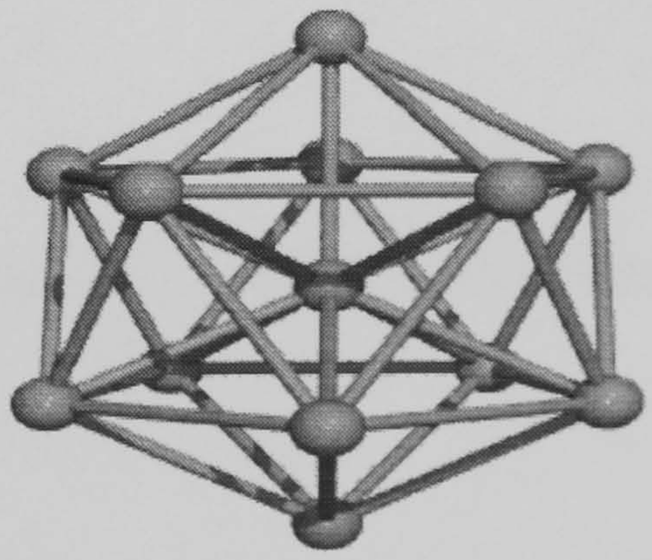
Atoms may be inserted within cavities in the cluster core, providing their radii are sufficiently small. For octahedra the only known examples contain carbon, nitrogen or hydrogen atoms. For lower nuclearity clusters incorporation of nitrogen or carbon atoms requires expansion of the metal skeleton, e.g. in $Ru_5C(CO)_{15}$ the carbon sits in the base of a square pyramid[1], whereas $[Ru_4N(CO)_{12}]^-$ adopts a 'butterfly' structure.[29] Hydrogen



$[Ru_4N(CO)_{12}]^-$ [27]



$Ru_5C(CO)_{15}$ [14]

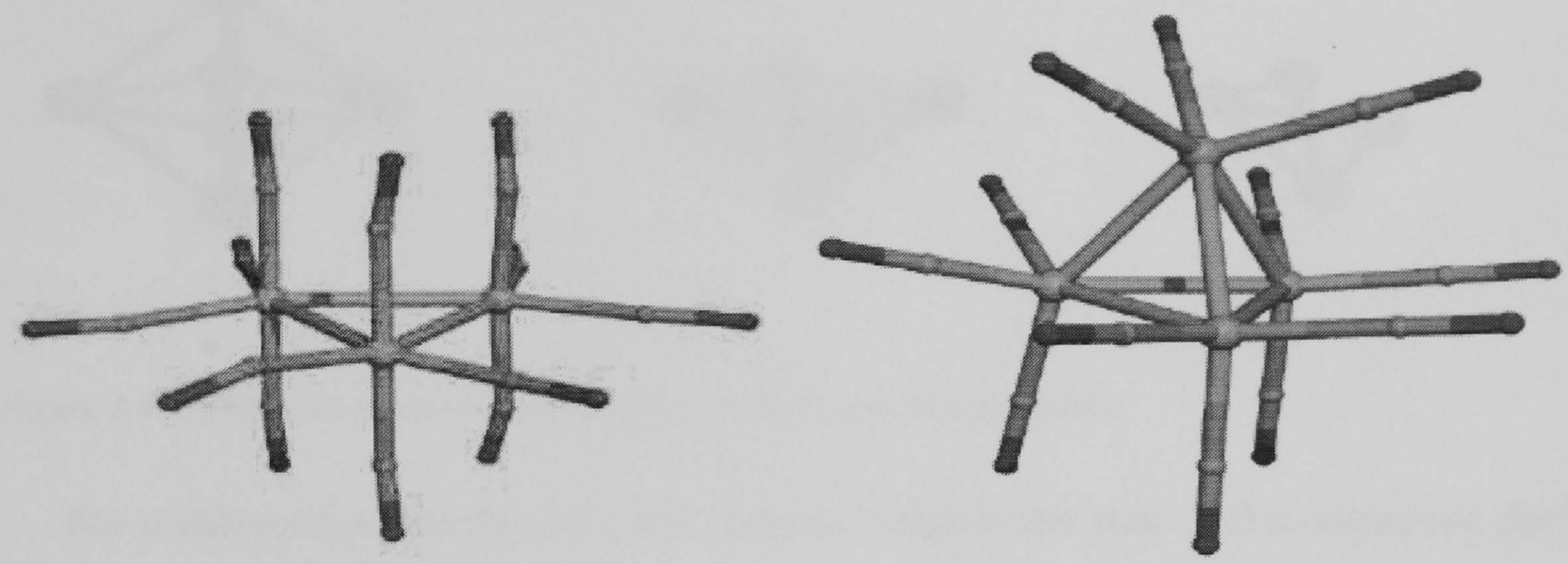


$[Rh_{12}Sb(CO)_{27}]^{3-}$ [28]

Figure 3.2. Examples of clusters with interstitial atoms

atoms can also be found in tetrahedral cavities; this is believed to be the location for three of the hydrides in $[H_4Os_{10}(CO)_{24}]^{2-}$.[14] As the size of the cluster increases larger atoms may be incorporated (see Figure 3.2).

The structures of cluster compounds have been rationalised using the polyhedral skeletal electron pair theory (PSEPT).[1] This relates the number of electron pairs involved in skeletal bonding to the cluster geometry. The basic rules can be summarised as follows.



$M_3(CO)_{12}$ (M = Ru, Os[30]) - 48 electrons $Ir_4(CO)_{12}$[31] - 60 electrons

Figure 3.3. Examples of ring and three-connected cluster compounds.

Ring and three-connected structures can be described in terms of localised, two centre, two electron bonds. The metal-metal bonds correspond to the polyhedral edges. The polyhedral electron counts (pec) are:

$16n$ for rings with n vertices.

$15n$ for three-connected structures with n vertices.

For four-connected structures formal, localised bonds cannot be assigned. However, delocalised bonding schemes lead to the following pec's:

$14n + 2$ for four-connected structures where the n vertices lie on a spherical surface.

Other simple polyhedra are derived from spherical deltahedra (*closo* structures) by the removal of one (*nido*) or two (*arachno*) vertices. The characteristic pec's are:

14 n + 2 for a *closo* deltahedron with n vertices

14 n + 4 for a *nido* deltahedron with n vertices

14 n + 6 for a *arachno* deltahedron with n vertices

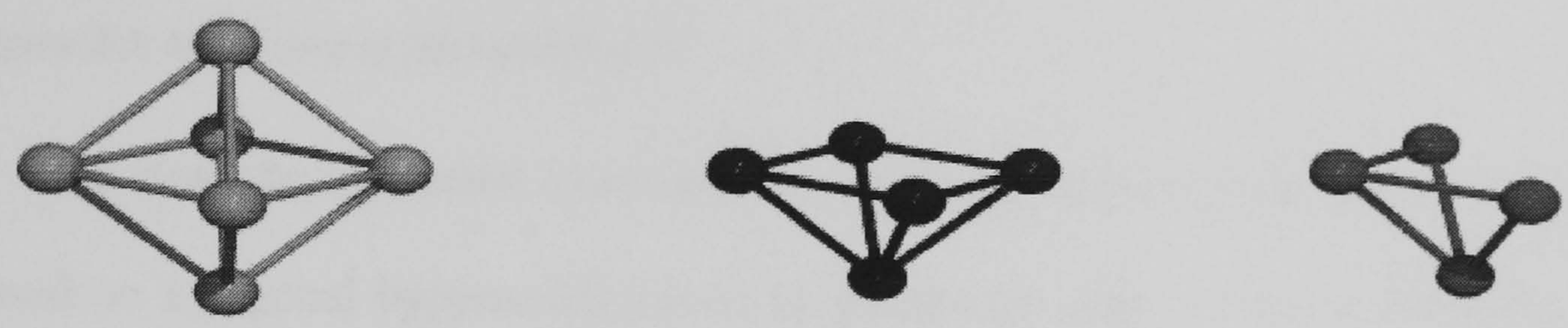


Figure 3.4. closo, nido *and* arachno *polyhedra derived from the octahedron.*

For condensed polyhedra the total electron count is the sum of the respective pec's, minus the electron count characteristic of the common atoms. These characteristic electron counts are:

18 for a shared vertex

34 for a shared edge

48 for a shared triangular face

62 for a shared square face

It can easily be shown that a transition metal atom bridging the edge of a deltahedron adds 14 electrons to the pec and capping a triangular face adds 12 electrons. From these principles apparently complex structures can easily be rationalised.

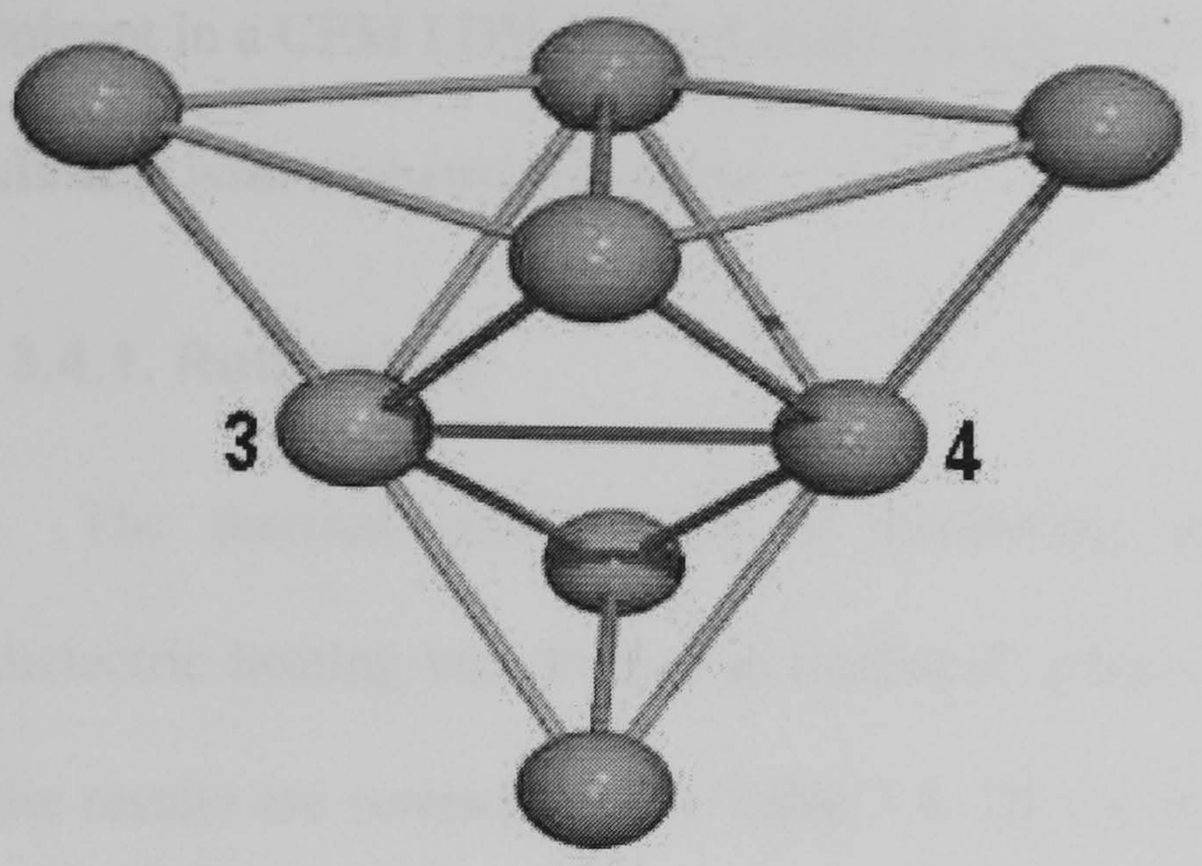


Figure 3.5. Metal core of $[HOs_8(CO)_{22}]^-$.[15]

The structure illustrated above can be considered as two tetrahedrons (*nido* structures based on a trigonal bypyramid) joined by a common edge {Os(3) and Os(4)}, with two caps on the upper tetrahedron. Thus the electron count is;

$2 \times 60 - 34 + 2 \times 12 = 110$

corresponding exactly to that for $[HOs_8(CO)_{22}]^-$ ($8 \times 8 + 2 \times 22 + 1 + 1 = 110$).

3.4. Dielectric Thermolysis

Synthesis of carbonyl clusters by reflux thermolysis generally involves the use of low boiling polar solvents and long reaction times or high boiling, viscous solvents such as glymes which can lead to problems during workup. The CEM LDV's allow rapid heating of volatile, polar solvents to temperatures beyond their atmospheric boiling points. Organic reactions performed under similar conditions have shown up to twentyfold reductions in overall reaction times.[32] In the cluster thermolysis reactions a small amount of the simple carbonyl clusters (i.e. $Ru_3(CO)_{12}$, $Os_3(CO)_{12}$ and $Ir_4(CO)_{12}$) were heated in a

solvent in a CEM LDV. A brief study was also made of the substitution reactions of these clusters with triphenylphosphine.

3.4.1. Ruthenium

The thermal condensation of $Ru_3(CO)_{12}$ under high-temperature and pressure dielectric heating was studied in methanol, ethanol, tetrahydrofuran and acetonitrile and the results are summarised in Table 3.4. Of the three metal carbonyl systems examined, ruthenium gave the most promising results.

$Ru_3(CO)_{12}$ showed no evidence of reaction (tested by solution infrared spectroscopy) after 20 minutes of heating in either tetrahydrofuran or a 50:50 mix of methanol and water.

Table 3.4. Preparation of high nuclearity ruthenium clusters by dielectric heating.

Starting Material	Solvent	Time / min	Product	% yield wrt ruthenium
$Ru_3(CO)_{12}$	Methanol	10	$[HRu_6(CO)_{18}]^-$	55
	Ethanol	10	$[HRu_6(CO)_{18}]^-$	65
			$[H_2Ru_{10}(CO)_{25}]^{2-}$	5
	Acetonitrile (stock)	10	$[HRu_{11}(CO)_{27}]^{3-}$	80
			$[H_2Ru_{10}(CO)_{25}]^{2-}$	> 5
			$[Ru_6C(CO)_{16}]^{2-}$	5
	Acetonitrile (dried)	10	$[HRu_{11}(CO)_{27}]^{3-}$	70
			$[Ru_6C(CO)_{16}]^{2-}$	10
			$[H_2Ru_{10}(CO)_{25}]^{2-}$	> 5
$Ru_3(CO)_{12}$ + $(PPh_3)_2NCl$ (1:2)	Methanol	10	$[HRu_6(CO)_{18}]^-$	47
$Ru_6C(CO)_{17}$	Acetonitrile	10	$[Ru_6C(CO)_{16}]^{2-}$	90
			$[Ru_{10}C_2(CO)_{24}]^{2-}$	> 10

The reactions studied in methanol and ethanol gave very similar results and can be considered together. The average temperatures and pressures maintained within the LDV

were 120 °C and 4.5 atm for methanol and 130 °C and 5.0 atm for ethanol. The major product has been identified as $[HRu_6(CO)_{18}]^-$, isolated in up to 65 % yield after 10 minutes of heating. Conventional thermolysis requires 3 hours (see Table 3.1) however, the cluster can also be produced in 80 % yield, by stirring $Ru_3(CO)_{12}$ with excess aqueous base for 90 minutes, followed by careful acidification.[18] Thus, the dielectric thermolysis reaction proceeds 9 times more quickly than the fastest conventional synthesis, with comparable yields.

The infrared spectrum of $[HRu_6(CO)_{18}]^-$ shows one major band in the carbonyl region at 2020 cm^{-1}, suggesting broadly similar carbonyl environments. This, together with the unusually low-field ^1H nmr signal observed for the hydride (16.54 ppm) was the initial evidence for placing the hydride inside the octahedron.[18] This structure (see Figure 3.6) has since been confirmed by X-ray crystallography and neutron diffraction studies.[18]

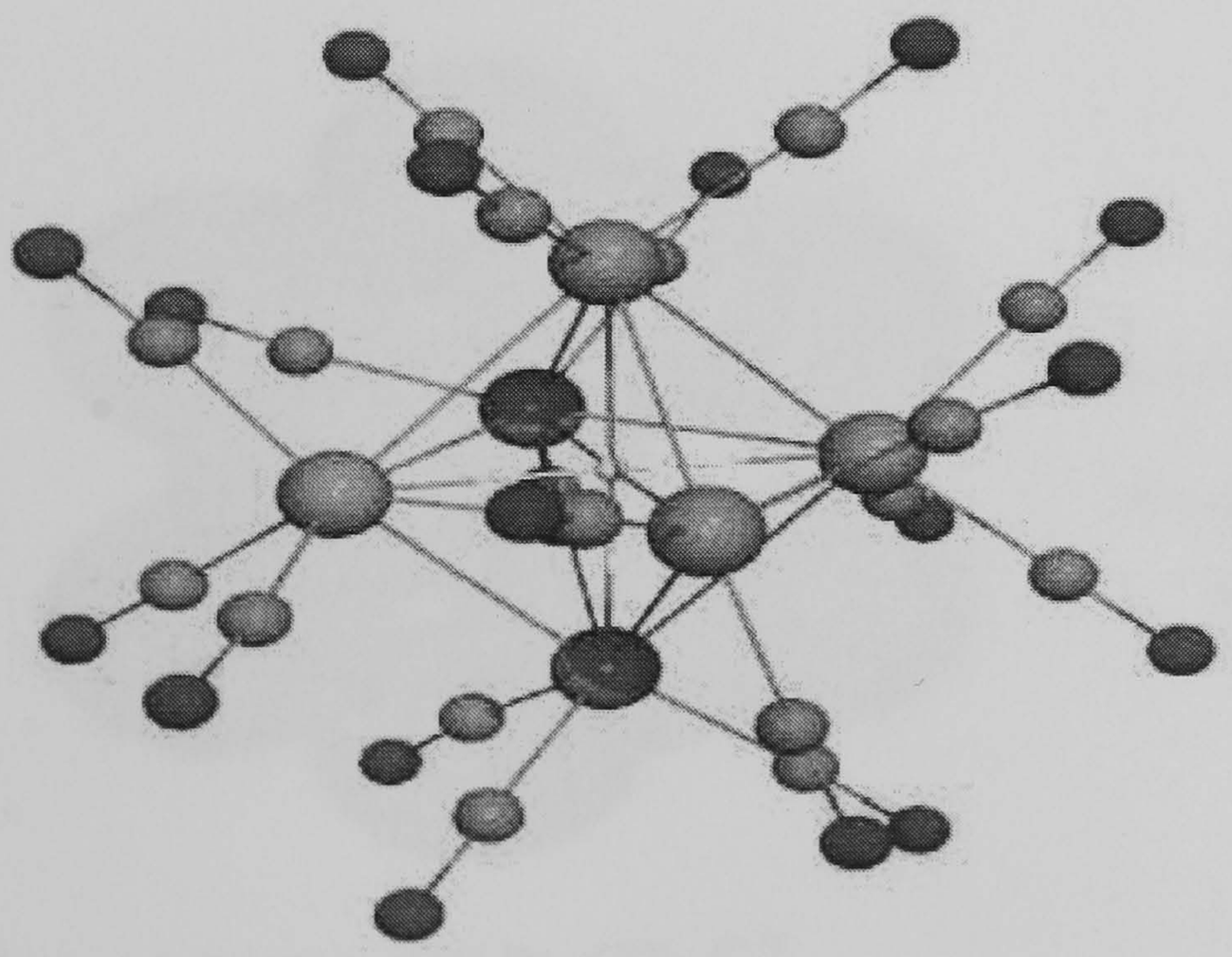


Figure 3.6. Structure of $[HRu_6(CO)_{18}]^-$.[18]

The decanuclear dihydride $[H_2Ru_{10}(CO)_{25}]^{2-}$ was only observed when ethanol and acetonitrile were used as solvents for dielectric thermolysis, presumably as a result of the

more vigorous conditions compared with methanol (acetonitrile is heated to 140 °C and 4.0 atm). Higher yields have been obtained by refluxing $Ru_3(CO)_{12}$ in ethanol for 12 hours.[33] This also gave a large amount of black solid. It is possible that increased reaction times or more severe conditions would increase the yield of $[H_2Ru_{10}(CO)_{25}]^{2-}$ from the dielectric thermolysis reaction in ethanol: both methods initially produce $[HRu_6(CO)_{18}]^-$ which has been shown to be an intermediate in the reaction.[33] However, as there is a significant likelihood of the solid by-product containing ruthenium particles, extended reaction times could lead to dangerous hot-spots building up in the dielectric vessel, which could damage the expensive fibre-optic temperature probe.

Reflux thermolysis of a 50:50 mix of methanol:water also yields $[H_2Ru_{10}(CO)_{25}]^{2-}$. As the reaction time is extended the yield of this product is reduced and $[HRu_{11}(CO_{27}]^{3-}$ becomes the favoured product.[8]

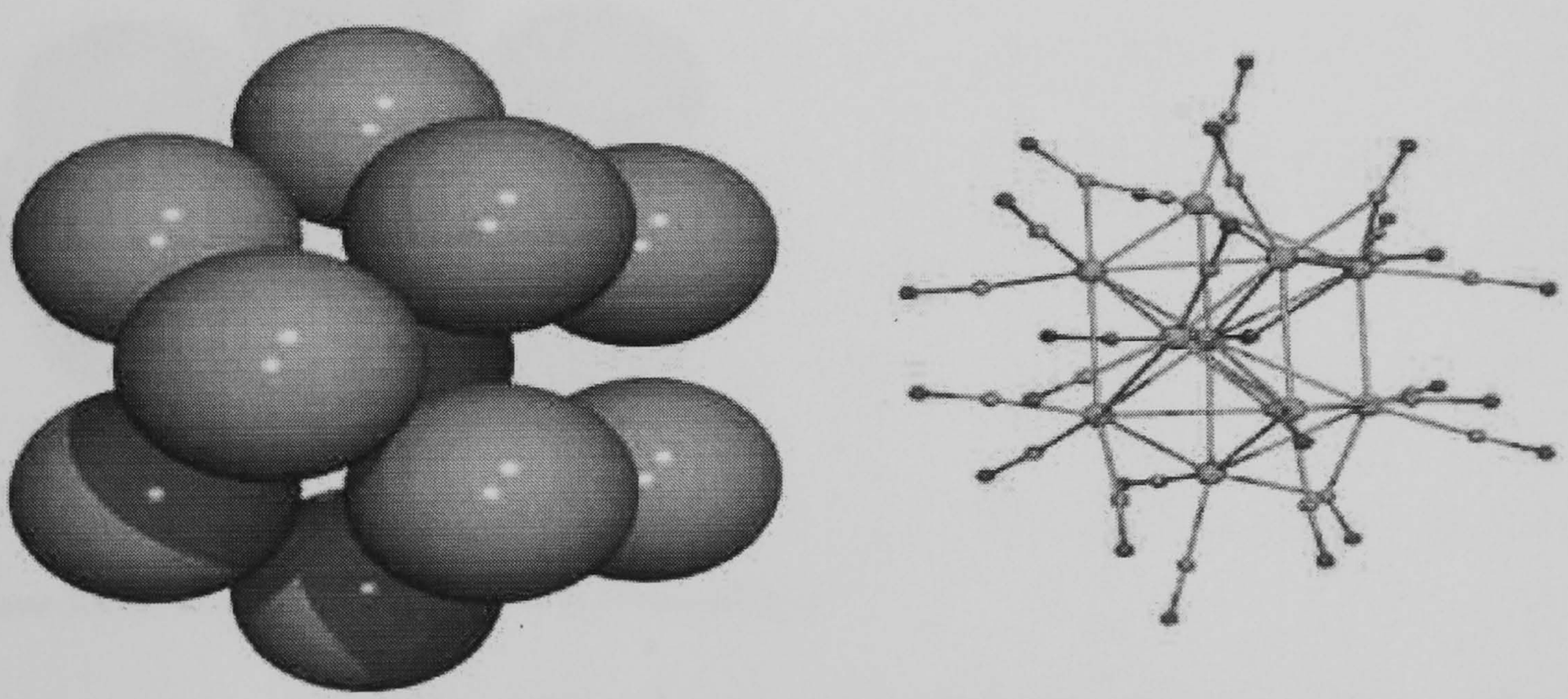


Figure 3.7. Structure of $[H_2Ru_{10}(CO)_{25}]^{2-}$.[33]

The metal core in most ruthenium decanuclear structures can be considered as an octahedron with 4 faces capped, as in $[H_4Os_{10}(CO)_{24}]^{2-}$ (see Figure 3.1). Such a structure

can also be regarded as derived from a face centred cubic unit cell.[33] However the structure of $[H_2Ru_{10}(CO)_{25}]^{2-}$, reproduced above, shows clear ABA ordering of metal atom layers and thus may regarded as a hexagonal close packed array, as observed in the bulk metal. The locations of the hydride ligands have yet to be determined for this cluster. No obvious positions on the cluster surface can be inferred from the X-ray structure. Thus it seems likely that they occupy interstitial positions.[33]

The major product from high-temperature thermolysis in acetonitrile is $[HRu_{11}(CO)_{27}]^{3-}$ isolated in 80 % yield. Reflux thermolysis yields 90 % after 20 hours.[7] Thus the dielectric method leads to a 120 fold reduction in the reaction time. The decrease in yield with the use of dried acetonitrile suggests that traces of water in the solvent are the probable source of the hydride ligand.

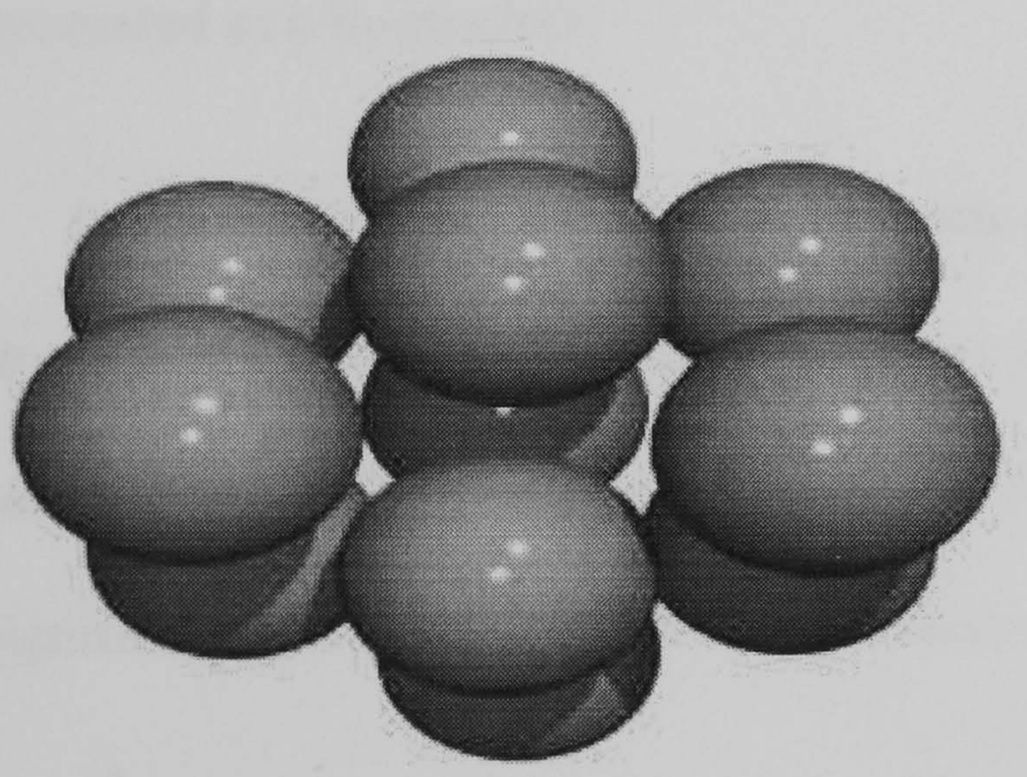


Figure 3.8. Structure of the metal core in $[HRu_{11}(CO)_{27}]^{3-}$ [7]

The metal core in $[HRu_{11}(CO)_{27}]^{3-}$ represents a fragment of an hcp lattice, although for electron counting purposes it may be considered as the condensation of two octahedra and two trigonal bipyramids. Once again, the hydride has not been unequivocally located

yet it seems likely, especially in light of the nmr data (δ -5.47 ppm) that it resides in one of the octahedral cavities.

Yields of $[Ru_6C(CO)_{16}]^{2-}$ obtained from dielectric heating in acetonitrile are low, even after drying the solvent to minimise the formation of hydrido clusters. A more convenient synthesis involves heating $Ru_3(CO)_{12}$ with sodium in refluxing diglyme:[11] $[Ru_6C(CO)_{16}]^{2-}$ can be precipitated in 90 % yield after 12 hours.

The dielectric thermolysis of $Ru_6C(CO)_{17}$ in acetonitrile unfortunately only yields $[Ru_{10}C_2(CO)_{24}]^{2-}$ as a minor product. It has been obtained (along with a ruthenium mirror) in 35 % yield by refluxing $[Ru_6(CO)_{18}]^{2-}$ in diglyme for 80 hours.[11] Greater yields could possibly be obtained from dielectric heating if increased reaction times were used. However, such reactions would carry a risk of vessel failure if ruthenium metal is generated as a by-product.

In summary, two products have been obtained in good yields from the dielectric thermolysis of $Ru_3(CO)_{12}$ for 10 minutes in a microwave cavity: $[HRu_6(CO)_{18}]^-$ from methanol and ethanol and $[HRu_{11}(CO)_{27}]^{3-}$ from acetonitrile. For both these compounds a significant decrease in overall reaction time was observed.

Two products; $[Ru_6C(CO)_{16}]^{2-}$ and $[H_2Ru_{10}(CO)_{25}]^{2-}$ have been obtained in low yield. As lengthy purification procedures are required the dielectric heating approach holds few advantages in the preparation of these clusters.

The use of Teflon autoclaves in a microwave cavity to rapidly heat volatile, polar solvents beyond their atmospheric boiling points has been shown to be an effective

method for the synthesis of some ruthenium carbonyl clusters. This approach is limited to systems where the products have a high thermal stability, as metal particles may cause hot spots which damage the vessels or temperature probe. However for some of the systems considerable reductions in overall reaction time have been observed, compared to conventional reflux methods.

3.4.2. Osmium

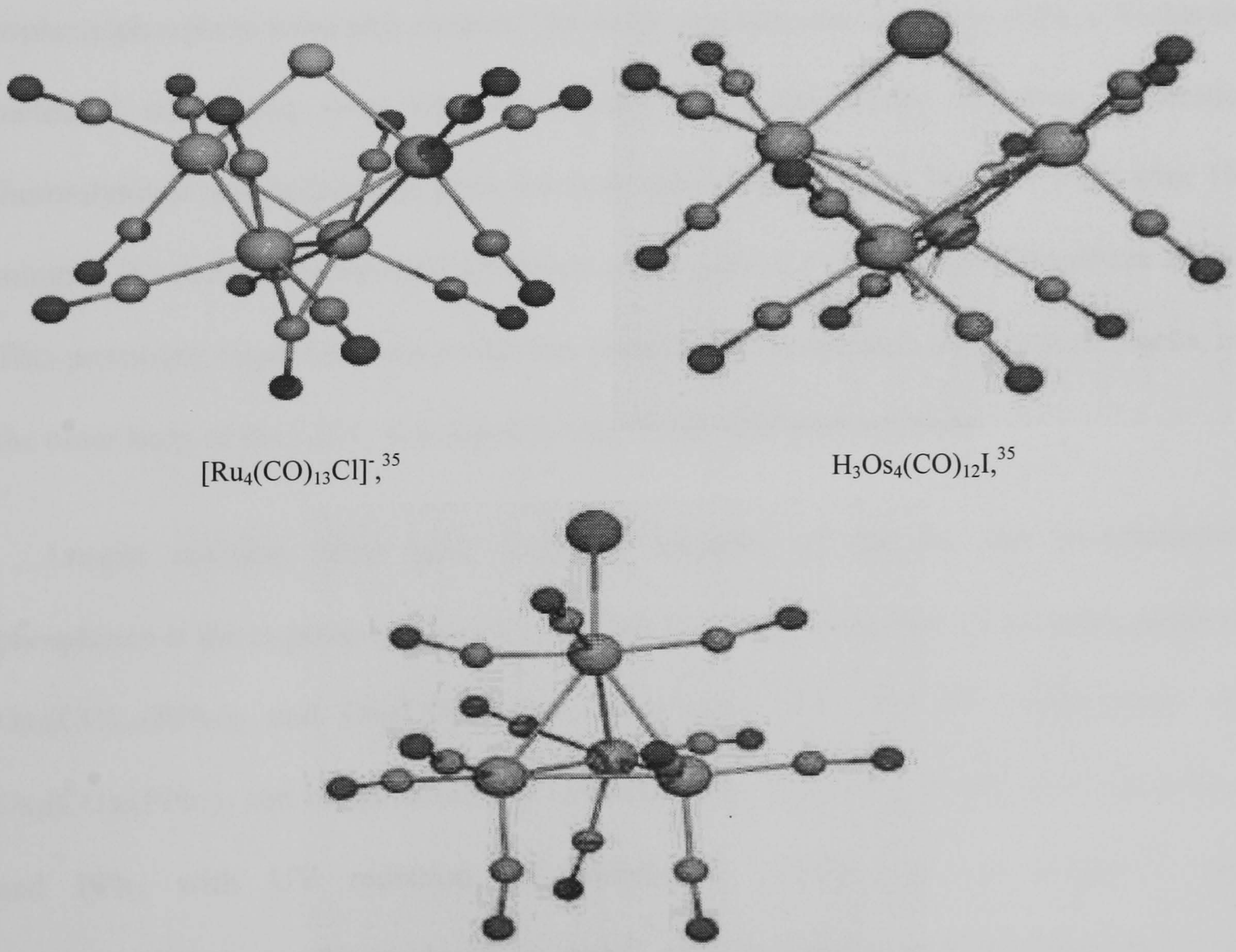
The thermal condensation of $Os_3(CO)_{12}$ under high temperature and pressure dielectric heating was studied in the following solvents; methanol, tetrahydrofuran, acetonitrile and chlorobenzene and the results are summarised in Table 3.5. The reactions were less promising than those described above for ruthenium.

There was no evidence of a reaction having occurred, as detected by infrared spectroscopy and spot TLC, after 30 minutes heating in methanol, tetrahydrofuran or chlorobenzene (at temperatures of 120, 120 and 170 °C respectively). A variety of products, in very low yields, were produced in acetonitrile, however reproducibility was poor and separation difficult (a problem with all the osmium experiments was the tendency of unreacted $Os_3(CO)_{12}$ to spread over the TLC plate).

Table 3.5. Preparation of Osmium clusters by dielectric thermolysis

Starting Material	Solvent (25 cm^3)	Time / min	Products	% yield wrt to osmium
$Os_3(CO)_{12} + (PPh_3)_2NCl$	Acetonitrile	15	$[H_2Os_4(CO)_{13}Cl]^-$	45
$Os_3(CO)_{10}(NCMe)_2 + (PPh_3)_2NCl$	Acetonitrile (30 cm^3)	15	$[H_2Os_4(CO)_{13}Cl]^-$	20
$Os_3(CO)_{12} + 5\ PPh_3$	Tetrahydrofuran	15	$Os_3(CO)_{11}(PPh_3)$	85
			$Os_3(CO)_{10}(PPh_3)_2$	5

In an attempt to increase the yield by forming a stable anionic cluster, $(PPh_3)_2NCl$ (PPN) was added to the reaction mixture. This still gave no reaction in methanol. With acetonitrile one red-brown product was obtained in low yield. The yield did not increase when the reaction time was increased to 20 minutes. This compound has been identified as $[H_2Os_4(CO)_{13}Cl]PPN$ on the basis of ^1H nmr, mass spectrometry and elemental analyses. This compound has not been reported previously, however the related clusters $H_3Os_4(CO)_{12}Cl$ and $[H_2Os_4(CO)_{12}Cl]PPN$ have been produced by stirring $[H_3Os_4(CO)_{12}(NCMe)_2]BF_4$ and $(PPh_3)_2NCl$ in acetonitrile[34] and $[Ru_4(CO)_{13}Cl]PPN$ has been reported from the reaction of $Ru_3(CO)_{12}$ and $(PPh_3)_2NCl$ in dry, refluxing tetrahydrofuran.[35]



$[Ru_4(CO)_{13}Cl]^-$,[35] $H_3Os_4(CO)_{12}I$,[35] $[H_2Os_4(CO)_{12}I]^-$,[35]

Figure 3.9. Osmium and ruthenium carbonyl clusters with bridging and terminal halides

Both $[Ru_4(CO)_{13}Cl]^-$ and $H_3Os_4(CO)_{12}I$ have bridging halides, giving a pec of 62. consistent with the *arachno*, butterfly structure shown in Figure 3.9. The 60 electron cluster $[H_2Os_4(CO)_{12}I]^-$ has a terminal iodide and adopts a tetrahedral structure. If the new compound $[H_2Os_4(CO)_{13}Cl]^-$ is assumed to have a terminal chloride the pec is 62, giving a butterfly cluster. This is the only structure that satisfies the PSEPT rules.

Dielectric thermolysis of $Os_3(CO)_{10}(NCMe)_2$ with $(PPh_3)_2NCl$ in acetonitrile also gave $[H_2Os_4(CO)_{13}Cl]^-$. As for $Os_3(CO)_{12}$, no increase in yield was observed on increasing the reaction time. A slight increase was observed on increasing the volume of solvent.

The substitution of $Os_3(CO)_{12}$ in methanol and tetrahydrofuran with triphenylphosphine were also studied. The major product was $Os_3(CO)_{11}(PPh_3)$. Yields in methanol were poor, even after 40 minutes (25 % maximum). However, dielectric thermolysis in tetrahydrofuran gave the monosubstituted product in 85 % yield after 15 minutes. No previously reported syntheses give a yield for $Os_3(CO)_{11}(PPh_3)$ above 20 %. This promising result has been somewhat undermined by the high incidence of cracks, in the outer body of the LDV, developed during tetrahydrofuran reactions.

Longer reaction times gave increased amounts of the di- and tri-substituted phosphines at the expense of $Os_3(CO)_{11}(PPh_3)$. However, even after 30 minutes, yields of $Os_3(CO)_{10}(PPh_3)_2$ and $Os_3(CO)_9(PPh_3)_3$ were only 15 % and 5 % respectively. As $Os_3(CO)_9(PPh_3)_3$ can be quantitatively synthesised by irradiating a mixture of $Os_3(CO)_{12}$ and PPh_3 with UV radiation, of wavelength 320 nm, for 30 minutes[36] and $Os_3(CO)_{10}(PPh_3)_2$ can be produced in 'good' yield by stirring $Os_3(CO)_{10}(NCMe)_2$ with

excess PPh_3 for 30 minutes,[37] there seems little advantage in using dielectric syntheses for the more substituted osmium carbonyl phosphine cluster compounds.

In summary, the osmium carbonyl cluster, $Os_3(CO)_{12}$ has been shown to be stable to short, high-temperature, dielectric thermolysis. Addition of $(PPh_3)_2NCl$ to the reaction mixture stabilises the osmium cluster sufficiently to produce the new compound $[H_2Os_4(CO)_{13}Cl]PPN$. Substitution by triphenylphosphine in tetrahydrofuran gives high yields of $Os_3(CO)_{11}(PPh_3)$. Unfortunately, the degradative effects of tetrahydrofuran upon the reaction vessel limited the development of this otherwise promising result.

3.4.3. Iridium

The thermal condensation of $Ir_4(CO)_{12}$ under high temperature and pressure dielectric heating was studied in methanol, tetrahydrofuran, acetonitrile and chlorobenzene. The results were not at all promising. However, since no iridium clusters are prepared by conventional reflux thermolysis, this is not surprising.

There was no evidence of reaction in methanol at 120 °C. Thermolysis in acetonitrile (140 °C) showed evidence (spot TLC) of several products. However, these decomposed on the TLC plates. Attempts to precipitate pure compounds from solution failed and gave a black, insoluble product.

The reaction of $Ir_4(CO)_{12}$ in both tetrahydrofuran (120 °C) and chlorobenzene (170 °C) gave the same compound, in very low yield and the results are summarised in Table 3.6. The yield did not improve when the reactions were performed under a nitrogen atmosphere or on extension of the reaction time to 30 minutes. The brown solid has been isolated as a PPN salt. It decomposes, in air, over a period of several weeks. The infrared

spectrum shows two bands, at 2053 and 1970 cm^{-1}, suggesting both terminal and bridging carbonyls are present.

Table 3.6. Preparation of Iridium clusters by dielectric heating.

Starting Material	Solvent	Time / min	Products	% yield wrt iridium
$Ir_4(CO)_{12}$	Tetrahydrofuran	15	Unknown	low
	Chlorobenzene	15	Unknown	low
$Ir_4(CO)_{12}$	Acetonitrile	20	$Ir_4(CO)_9(PPh_3)_3$	55
+ 5 PPh_3	Tetrahydrofuran	15	$Ir_4(CO)_9(PPh_3)_3$	100

The substitution reaction of $Ir_4(CO)_{12}$ with excess PPh_3 was studied in tetrahydrofuran and acetonitrile. The tri-substituted phosphine cluster was produced in quantitative yields after 15 minutes heating in tetrahydrofuran at 120 °C. Dielectric thermolysis of $Ir_4(CO)_{12}$ in acetonitrile, at 140 °C, only yielded 55 % of $Ir_4(CO)_9(PPh_3)_3$, however, no lower substituted compounds were isolated. The tri-substituted phosphine cluster can also be synthesised by stirring $Ir_4(CO)_{12}$ with excess PPh_3, in a solution of potassium hydroxide in methanol saturated with carbon monoxide, for 2 hours at 50 °C. $Ir_4(CO)_9(PPh_3)_3$ precipitates in 80 % yield from this reaction.[38]

3.4.4. Summary

This part of the project has attempted to evaluate the usefulness of performing the microwave induced thermal condensation of small carbonyl clusters of ruthenium, osmium and iridium in sealed pressure vessels. Some success was acheived with $Ru_3(CO)_{12}$ and one new compound isolated from the reaction of $Os_3(CO)_{12}$ and $(PPh_3)_2NCl$.

The results parallel those achieved using conventional heating methods: iridium carbonyl clusters are not generally synthesised by reflux thermolysis and adapting the

syntheses to dielectric heating has not led to promising results. Osmium carbonyl clusters generally require long thermolysis times under conventional heating methods; attempts to adapt these syntheses to dielectric heating have not produced promising results. More aggressive reaction conditions may lead to more promising results, however the current restrictions of the LDV limit the development of this approach. Many ruthenium clusters are prepared by thermolysis at relatively low temperatures and the dielectric heating technique has been shown to substantially reduce the reaction time for some of these compounds.

3.5. Surface-mediated Syntheses

A diverse range of organic reactions, e.g. functional group protection and deprotection, aromatic substitution, cycloaddition, alkylation and condensation[32] have been performed by adsorbing the reactants onto an inorganic oxide and heating them in a microwave oven. Inorganic chemists have also examined the possibilities of surface-mediated synthesis; Several groups have examined surface mediated syntheses of metal carbonyl clusters, starting from small clusters[21,39] or monometallic fragments.[24,20,22] A recent review has compared the reactions and catalytic potential of such species with their molecular analogues[40] in solution; several surface supported species have been shown to be noticeably more stable to catalytic conditions than their solution counterparts.

Much organic surface-mediated synthesis has used simple equipment: The reactants are slurried with the support for a short time and the impregnating solution removed. The resulting solid is then simply placed in a beaker and heated in a standard domestic

microwave oven. For small scale reactions an external 'bed' of support has been used, to maximise the absorption of microwave radiation.[41]

The CEM STAR2 oven appeared to offer several advantages for this method, specifically temperature control. It was also anticipated that the external bed would be unnecessary, as the oven has a small, single-mode cavity rather than the large multi-mode cavities found in domestic ovens. For these reactions the standard STAR 2 vessel was adapted as shown in Figure 3.10.

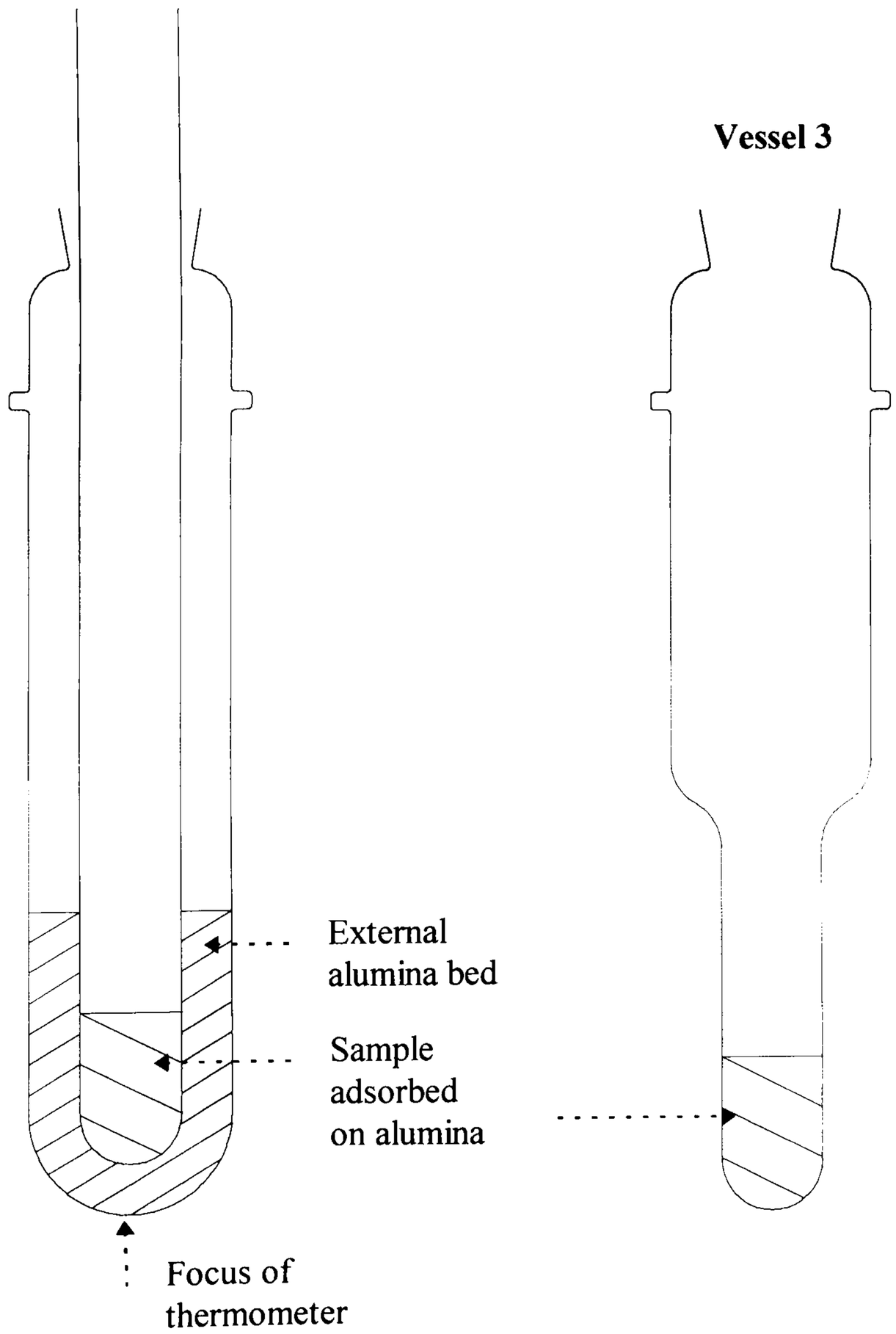


Figure 3.10. Apparatus for surface mediated reactions in a STAR 2 oven

This method was used to investigate the surface-mediated pyrolysis of $Ru_3(CO)_{12}$ and $Os_3(CO)_{12}$ under a variety of conditions

3.5.1. Ruthenium

$Ru_3(CO)_{12}$ was dispersed on an oven-dried alumina surface at 1 and 2.5 % w/w ratios. Infra-red spectra of the resulting solid are identical to that of a KBr disc of the pure cluster, indicating simple physisorbtion has occurred. Samples were sealed in **Vessel 3** under a CO or N_2 atmosphere and heated to 150 and 200 °C for 10 minutes. After extraction in polar solvents and solution metathesis with $(PPh_3)_2NCl$ the alumina surface was a dark grey. Only $Ru_3(CO)_{12}$ was found in the extracted solutions.

Low temperature (100 °C) experiments were slightly more successful; low yields of $[HRu_6(CO)_{18}]^-$ were extracted from the surface after metathesis with $(PPh_3)_2NCl$. These results are summarised in Table 3.7.

*Table 3.7. Alumina supported $Ru_3(CO)_{12}$ heated to 100°C in **Vessel 3***

Ru ratio / (w/w %)	Vessel atmosphere	time / min	$Ru_3(CO)_{12}$ / % yield	$[HRu_6(CO)_{18}][PPN]$ / % yield
1.0	N_2	30	33	3.7
1.0	CO	30	34	1.6
2.5	CO	30	51	0.8

The yields of $[HRu_6(CO)_{18}]^-$ are too low to conclusively examine the effects of changing conditions, although a nitrogen atmosphere and low dispersion level give the best results. Extraction proceeds in two stages. The final solid (pale orange, with no apparent colour change during reaction) is stirred in dichloromethane, to remove purely physisorbed species and then in an acetone solution of $(PPh_3)_2NCl$. After the second extraction stage the solid is a pale yellow and shows two broad bands in the carbonyl

region of the i.r. spectrum. These are attributed to the surface species $[Ru(CO)_x(OAl\equiv)_2]_n$ by analogy with the known silica-supported species $[Ru(CO)_2(OSi\equiv)_2]_n$ (ν_{CO} 2069 (s). 2005 (s) cm^{-1}) and $[Ru(CO)_3(OSi\equiv)_2]_n$ (ν_{CO} 2138 (m), 2069 (s), 2014 (m) cm^{-1}).[42]

Roberto *et al*[20] have reported 65 % yields of $[HRu_6(CO)_{18}]^-$ from the silica-supported $[Ru(CO)_3Cl_2(HOSi\equiv)]$ after 48 hours at 80 °C under a CO atmosphere. The surface is also impregnated with a thirty-fold excess (wrt ruthenium) of aqueous K_2CO_3. The physisorbed species $[Ru(CO)_x(OH)_2]_n$ (x = 2,3) has been identified as the major intermediate, formed by interaction of the starting material and surface water. By varying the carbonate to ruthenium ratio, reaction temperature and atmosphere either $Ru_3(CO)_{12}$, $[HRu_3(CO)_{11}]^-$, $H_4Ru_4(CO)_{12}$, $[HRu_6(CO)_{18}]^-$ or $[Ru_6C(CO)_{16}]^{2-}$ can be isolated, with good selectivity.

Thus far the potential for surface-mediated dielectric syntheses of ruthenium carbonyl clusters appears limited. As the conditions in dielectric and conventionally heated surface-mediated synthesis are much closer than those in solution reactions it is unlikely that dramatic reductions in reaction time will occur. The work of Roberto *et al*[20] indicates some possible future lines of inquiry; particularly with respect to the effects of surface water and the control of surface basicity through addition of K_2CO_3, but it is noteworthy that many of these syntheses require reaction times in excess of 24 hours. For reactions where there is a potential for reduction to pure metal surfaces, leading to arcing, use of such extended reaction times will necessitate the development of suitable monitoring and control systems.

3.5.2. Osmium

$Os_3(CO)_{12}$ was dispersed over an oven dried alumina surface at 1 and 2 % ratios (w/w). It was heated using both the 'external bed' method and **Vessel 3** (see Figure 3.10). For the reactions using **Vessel 3** the effects of temperature, osmium dispersion, gas atmosphere and reaction upon the overall yield were examined.

Reactions using an external bed of alumina as a heating 'jacket' were performed with a 1 % (w/w) dispersion of $Os_3(CO)_{12}$ and run for 20 minutes in the CEM STAR 2 oven. The temperature limit was set at 200 °C (monitored by an infra-red detector focused on the external bed) and after heating had been stopped a thermocouple was inserted into the sample. This indicated that the reaction temperature in the sample was at least 250 °C, uncomfortably close to the limit at which reduction to osmium metal has been observed in Cariss tube pyrolyses (275 °C).[13] The sample was a pale brown, with dark red-brown spot. After extraction with an acetone solution of $(PPh_3)_2NCl$, $[Os_{10}C(CO)_{24}]^{2-}$ was isolated in 42 % yield. Despite this promising result further experiments did not use the external bed due to the temperature control difficulties and the risk of reduction to osmium metal with consequent arcing.

The experiments using **Vessel 3** initially concentrated upon reproducing the results achieved with the external bed, thereby allowing an estimation of the sample reaction conditions using that apparatus.

Table 3.8. summarises the results for some short experiments examining the effects of osmium carbonyl dispersion over the alumina surface. The main product is $[H_3Os_4(CO)_{12}][PPN]$, its yield is low and unaffected by dispersion ratios. The minor

product, $[Os_{10}C(CO)_{24}][PPN]_2$ occurs in yields too low to allow the drawing of any firm conclusions, although lower dispersions and a carbon monoxide atmosphere appear to be unfavourable.

Table 3.8. Alumina supported $Os_3(CO)_{12}$ heated to 200 °C with a range of surface dispersions

Os ration (%, w/w)	time / minutes	vessel atmosphere	$[H_3Os_4(CO)_{12}][PPN]$ / % yield	$[Os_{10}C(CO)_{24}][PPN]_2$ / % yield
1.0	10	N_2	8.2	
2.5	10	N_2	7.2	4.6
1.0	20	N_2	8.4	1.9
1.0	20	CO	5.1	
2.5	20	CO	4.9	

The samples for the above experiments were prepared by grinding the osmium carbonyl and alumina in a pestle and mortar, followed by stirring under hexane for at least 30 minutes, prior to solvent evaporation. This gave an evenly coloured yellow powder, even under 50x magnification. After heating had concluded the surface was an even orange colour. However, the samples for the experiments using the external bed were prepared by rapid, brief stirring of the reactants under hexane, followed by solvent evaporation. After heating the surface was a pale tan colour, with dark red-brown spots. It was postulated that the higher yields in the external bed experiment might therefore be due to localised superheating of relatively large particles of $Os_3(CO)_{12}$. Consequently a series of experiments, at uneven dispersions, was performed. Some doubt was thrown on the initial postulate when it proved difficult to repeatedly produce a surface dispersion of $Os_3(CO)_{12}$ that was visibly uneven at 50x magnification. It was found to be necessary to separate the $Os_3(CO)_{12}$ between 100 and 120 mesh (the alumina is 100 mesh) and slurry with alumina and hexane on a rapidly rotating rotavac. This resulted in a sample that was

pale yellow to the naked eye but under the microscope particles of $Os_3(CO)_{12}$ were visible.

These samples were prepared with an overall osmium loading of 2.5 % (w/w) and heated for 20 minutes at 200 °C. Although the sample showed spots of colour after heating , rather than an even tone, it was pale orange rather than red-brown. The results are summarised in Table 3.9. The major product was $[HOs_5(CO)_{15}][PPN]$, only trace amounts of $[H_3Os_4(CO)_{12}][PPN]$ were isolated. The formation of the pentaosmium cluster was favoured when the reaction was performed under a carbon monoxide atmosphere. Yields of $[Os_{10}C(CO)_{24}]^{2-}$, although higher than those seen for the evenly dispersed samples (Table 3.8), remain low.

Table 3.9. Alumina supported $Os_3(CO)_{12}$, heated to 200 °C, for 20 minutes, with an uneven surface dispersion. (Overall Os ratio 2.5 % w/w)

vessel atmosphere	$[H_3Os_4(CO)_{12}][PPN]$ / % yield	$[HOs_5(CO)_{15}][PPN]$ / % yield	$[Os_{10}C(CO)_{24}][PPN]_2$ / % yield
CO		27.1	7.9
N_2	0.9	15.3	9.5

Table 3.10. summarises the results of some experiments examining the effect of reaction time. No dramatic effects are observable in the time range examined, although the unfavourable effect of a carbon monoxide atmosphere on the yield of $[Os_{10}C(CO)_{24}]^{2-}$

Table 3.10. Alumina supported $Os_3(CO)_{12}$ heated to 200 °C for a range of times, surface dispersion 1 % Os w/w

time / minutes	vessel atmosphere	$[H_3Os_4(CO)_{12}][PPN]$ / % yield	$[Os_{10}C(CO)_{24}][PPN]_2$ / % yield
10	N_2	8.2	
20	N_2	8.4	1.9
30	N_2	9.2	2.2
10	CO	5.1	
20	CO	5.1	

is again evident.

The results for some samples heated for 20 minutes with increasing reaction temperatures are summarised in Table 3.11. Both $[H_3Os_4(CO)_{12}]^-$ and $[Os_{10}C(CO)_{24}]^{2-}$ were isolated from these reactions, with the yield of the decanuclear cluster increasing, in favour of $[H_3Os_4(CO)_{12}]^-$ as the reaction temperature was raised. For the high temperature reactions the hindering effect of a carbon monoxide atmosphere is noticeably reduced.

Table 3.11. Alumina supported $Os_3(CO)_{12}$, heated for 20 minutes

Os ratio (%, w/w)	temperature / °C	vessel atmosphere	$[H_3Os_4(CO)_{12}][PPN]$ / % yield	$[Os_{10}C(CO)_{24}][PPN]_2$ / % yield
1.0	200	N_2	8.4	1.9
1.0	200	CO	5.1	
1.0	225	N_2	2.5	4.8
1.0	250	N_2	0.5	9.7
2.5	275	N_2		15.6
2.5	275	CO	3.2	13.6

Attempts to extend the conditions examined had only partial success. Increasing the heating time for reactions performed at 275 °C beyond 25 minutes resulted in deposition of osmium metal on the vessel walls, causing arcing and in one case the apparent formation of a plasma. These effects were generally more exaggerated under a carbon monoxide atmosphere than with nitrogen. Reasonable yields of $[Os_{10}C(CO)_{24}]^{2-}$ have been isolated from such experiments (the largest, at 20 % was achieved after 28 minutes, the reaction was halted when the arcing changed from intermittent flashing to an bright incandescence) but as the vessel is unusable afterwards they have not been examined in detail.

For all the systems examined only small (> 5 %) amounts of $Os_3(CO)_{12}$ have been extracted from the surface after reaction. Infra-red spectra (KBr disc) of the final surface reveals carbonyl bands at 2127 m, 2034 vs,br and 1970 m, br. These have been identified as Os^{II} surface species[43] and can be extracted in ethanolic $(PPh_3)_2NCl$ solution after treatment with dilute hydrochloric acid as $[Os(CO)_2Cl_4]^{2-}$ or $[Os(CO)_3Cl_3]^-$.

3.5.3. Summary

Adaptation of a STAR2 reaction vessel to allow controlled, direct dielectric heating of small clusters adsorbed on alumina has been shown to be a viable technique, although monitoring problems remain; particularly for systems where deposition of metal particles and arcing are possible.

For $Ru_3(CO)_{12}$ the results are not very promising: relatively high temperatures (above 100 °C) have merely resulted in cluster breakdown.

Under the range of conditions studied $[H_3Os_4(CO)_{12}]^-$ was our most ubiquitous product. The highest yield obtained was 15 % ,after heating for an hour at 250 °C. Production of this cluster was generally favoured by moderate conditions and long reaction times. Roberto *et al* have also generated this cluster, on silica from $[Os(CO)_3Cl_2]_2$ and K_2CO_3, under 1 atmosphere of CO, extracting quantitative yields after 24 hours at 150 °C.[44] A range of small osmium clusters were prepared, using the same conditions and a range of temperatures; at 150 °C the major product was $[H_3Os_4(CO)_{12}]^-$, at 200 °C $[H_2Os_4(CO)_{12}]^{2-}$ and at 265 °C $[Os_5C(CO)_{14}]^{2-}$.[45]

Small yields (27 %) of $[HOs_5(CO)_{15}]^-$ could be extracted from samples prepared with uneven surface distributions of $Os_3(CO)_{12}$. This cluster has previously been isolated in

small yields from pyrolysis of $Os_3(CO)_{11}py$ in an evacuated Cariss tube (38 % was extracted after heating for 15 hours at 250 °C)[46] along with $H_4Os_4(CO)_{12}$, $Os_3(CO)_{10}py$ and $[Os_{10}C(CO)_{24}]^{2-}$. As this cluster is only produced from samples with discrete particles of $Os_3(CO)_{12}$ it cannot be described as surface-mediated, the support is acting mostly as a heat sink. Whilst the natural development of this result would seem to be the direct dielectric heating of $Os_3(CO)_{12}$ our current apparatus does not immediately seem amenable to such experiments. A cavity in which a nmr tube sized vessel could be used is a possible solution, although the problems of temperature control and monitoring are likely to be considerable for such a system.

Formation of $[Os_{10}C(CO)_{24}]^{2-}$ required high temperatures. Under a CO atmosphere this led to cluster breakdown to osmium metal and subsequent arcing. Although originally produced by vacuum pyrolysis of $Os_3(CO)_{11}py$ (65 % yield after 64 hours at 250 °C)[46] surface activated syntheses have generally proved more efficient: Gates *et al* extracted a 65 % yield from H_2OsCl_6 on MgO, under flowing CO/H_2, after 4 hours at 275 °C[21] and Roberto *et al* reported 81 % from α-$[Os(CO)_3Cl_2]_2$ and Na_2CO_3 on silica, under H_2, after 24 hours at 200 °C.[45]

3.6. Experimental

Thermolysis of $Ru_3(CO)_{12}$ in methanol

50 mg $Ru_3(CO)_{12}$ (0.08 mmol) and 20 cm^3 methanol were sealed inside a CEM Lined Digestion Vessel. The vessel was heated at 120 °C, creating an average pressure of 4.5 atm, for 10 minutes. After cooling to room temperature the vessel was opened, revealing a red-brown solution. 25 mg $(PPh_3)_2NCl$ (0.14 mmol) was added and the solution stirred for an hour. After concentration the solution was purified by TLC (acetone:hexane 3:2) yielding a broad orange band and a broad brown band. Extraction of the orange band in acetone gave $[HRu_6(CO)_{18}][PPN]$ (28.4 mg, 55 % yield wrt Ru). The brown band could not be extracted from the TLC plate.

$[HRu_6(CO)_{18}][PPN]$

MS FAB^+:	1111 (M^+); (M^+ - n28) observed for n= 0 - 16	
CHN analyses:	Found C 39.3, H 2.0, N 0.7. Calc C 39.3, H 1.8, N 0.7	
IR(CH_2Cl_2): ν_{CO}	2022 (vs), 1957 (w)	cm^{-1}
lit. (CH_2Cl_2):	*2020 (s), 1953 (vw)*[18]	*cm^{-1}*
^1H nmr ($(CD_3)_2CO$)	16.5 ppm	
lit. (CD_2Cl_2)	*16.5*[18] *ppm*	

Thermolysis of $Ru_3(CO)_{12}$ in ethanol

50 mg $Ru_3(CO)_{12}$ (0.08 mmol) and 20 cm^3 ethanol were sealed inside a CEM Lined Digestion Vessel. The vessel was heated at 130 °C, creating an average pressure of 5.0 atm, for 10 minutes. After cooling to room temperature the vessel was opened, revealing a red-brown solution. 25 mg $(PPh_3)_2NCl$ (0.14 mmol) was added and the solution stirred for an hour. Separation by TLC (acetone:hexane 3:2) gave $[HRu_6(CO)_{18}][PPN]$ (42.3 mg, 65 % yield wrt Ru) and $[H_2Ru_{10}(CO)_{25}][PPN]_2$ (3.4 mg, 5 % yield wrt Ru). A stationary brown band remained on the TLC plate.

$[H_2Ru_{10}(CO)_{25}][PPN]_2$

CHN analyses:	Found C 42.6, H 2.1, N 0.9. Calc C 42.7, H 2.3, N 1.0
IR(CH_2Cl_2): ν_{CO}	2061 (w), 2011 (vs), 1995 (m, sh), 1957 (m), 1772 (m) cm^{-1}
lit. (CH_2Cl_2):	2058 (vw), 2015 (s, sh), 2008 (vs), 1992 (m, sh), 1950 (w) 1772 (m, br)[7] cm^{-1}

Thermolysis of $Ru_3(CO)_{12}$ in acetonitrile

50 mg $Ru_3(CO)_{12}$ (0.08 mmol) and 20 cm^3 acetonitrile were sealed inside a CEM Lined Digestion Vessel. The vessel was heated at 140 °C, creating an average pressure of 4.0 atm, for 10 minutes. After cooling to room temperature the vessel was opened, revealing a red-brown solution. 25 mg $(PPh_3)_2NCl$ (0.14 mmol) was added and the solution stirred for an hour. Separation by TLC (acetone:hexane 3:2) gave, in order of elution $[H_2Ru_{10}(CO)_{25}][PPN]_2$ (1.7 mg, 3 % yield wrt Ru), $[Ru_6C(CO)_{16}][PPN]_2$ (5.3 mg, 5 % yield wrt Ru) and $[HRu_{11}(CO)_{27}][PPN]_3$ (59.7 mg, 80 % yield wrt Ru).

$[Ru_6C(CO)_{16}][PPN]_2$

MS FAB^+: 1067 (M^+); (M^+ - n28) observed for n= 0 - 12

CHN analyses: Found C 51.5, H 2.7, N 1.2. *Calc C 51.3, H 2.9, N 1.3*

IR(CH_2Cl_2): ν_{CO} 1977 (vs), 1917 (m), 1778 (m) cm^{-1}
lit. (CH_2Cl_2):[11] *2048 (vw), 2032 (w), 1977 (s), 1918 (m) 1780 (m) cm^{-1}*

$[HRu_{11}(CO)_{27}][PPN]_3$

MS FAB^+: 1869 (M^+); (M^+ - n28) observed for n= 0 - 25

CHN analyses: Found C 42.5, H 2.1, N 1.0. *Calc C 42.7, H 2.3, N 1.2*

IR(CH_2Cl_2): ν_{CO} 1992 (vs), 1960 (w, sh), 1758 (m) cm^{-1}
lit. (CH_2Cl_2):[7] *2051 (vw), 1993 (vs), 1780 (m, br) cm^{-1}*

^1H nmr ($(CD_3)_2CO$) -5.3 ppm
lit. (CD_2Cl_2)[7] *-5.5 ppm*

Thermolysis of $Ru_6C(CO)_{17}$ in acetonitrile

50 mg $Ru_6C(CO)_{17}$ (0.05 mmol) and 20 cm^3 acetonitrile were sealed inside a CEM Lined Digestion Vessel. The vessel was heated at 140 °C, creating an average pressure of 4.0 atm, for 10 minutes. After cooling to room temperature the vessel was opened, revealing a red-brown solution. 50 mg $(PPh_3)_2NCl$ (0.28 mmol) was added and the solution stirred for an hour. Separation by TLC (acetone:hexane 3:2) gave, in order of elution $[Ru_{10}C_2(CO)_{25}][PPN]_2$ (6.3 mg, 8 % yield wrt Ru) and $[Ru_6C(CO)_{16}][PPN]_2$ (85.1 mg, 90 % yield wrt Ru)

$[Ru_{10}C_2(CO)_{25}][PPN]_2$

CHN analyses: Found C 42.9, H 2.1, N 0.9. *Calc C 43.2, H 2.2, N 1.0*

IR (CH_2Cl_2): ν_{CO} 2004 (vs) cm^{-1}
(thf): 2043 (w), 2005 (vs), 1962 (w, sh), 1796 (m) cm^{-1}
lit. (thf):[12] 2046 (w), 2003 (vs), 1962 (w,sh), 1922 (w, sh), 1798 (m) cm^{-1}

Thermolysis of $Os_3(CO)_{12}$ in acetonitrile

50 mg $Os_3(CO)_{12}$ (0.06 mmol), 25 mg $(PPh_3)_2NCl$ (0.14 mmol) and 20 cm^3 acetonitrile were sealed inside a CEM Lined Digestion Vessel. The vessel was heated at 140 °C, creating an average pressure of 4.0 atm, for 10 minutes. After cooling to room temperature the vessel was opened, revealing a red solution. The solution was filtered over silica and removed. Recrystallisation by slow evaporation of acetone gave $[H_2Os_4(CO)_{13}Cl][PPN]$ (31.1 mg, 45 % yield wrt Os)

$[H_2Os_4(CO)_{13}Cl][PPN]$

MS FAB^+: 1162 (M^+), (M^+-35-n28) observed for n = 0 to 12

CHN analyses: Found C 34.8, H 2.3, N 0.9. *Calc. C 35.2, H 1.9, N 0.8*

IR (CH_2Cl_2): ν_{CO} 2070 (w), 2031 (s) 2011 (vs), 1971 (m) cm^{-1}

^1H nmr ($(CD_3)_2CO$): -10.2 (1), -20.1 (1) ppm

Thermolysis of $Os_3(CO)_{12}$ and PPh_3 in tetrahydrofuran

50 mg $Os_3(CO)_{12}$ (0.06 mmol), 75 mg PPh_3 (0.29 mmol) and 20 cm^3 tetrahydrofuran were sealed inside a CEM Lined Digestion Vessel. The vessel was heated at 120 °C, creating an average pressure of 4.0 atm,

for 15 minutes. After cooling to room temperature the vessel was opened, revealing an orange solution. Separation by TLC (acetone:hexane 3:2) gave $Os_3(CO)_{11}PPh_3$ (53.6 mg, 85 %) and $Os_3(CO)_{10}(PPh_3)_2$ (3.7 mg, 5 %).

$Os_3(CO)_{11}PPh_3$

CHN analyses: Found C 30.7, H 1.2, N 0.0. *Calc. C 30.5, H 1.3, N 0.0.*

IR (CH_2Cl_2): ν_{CO} 2054 (s), 2033 (m), 2017 (vs), 1999 (w) 1987 (m) 1977 (w) cm^{-1}
lit. (CCl_4): *2055 (s), 2035 (ms), 2019 (s), 2000 (m), 1989 (m), 1978 (m) cm^{-1}*

^{31}P ($(CD_3)_2CO$) -4.3 ppm

$Os_3(CO)_{10}(PPh_3)_2$

CHN analyses: Found C 40.0. H 2.4, N 0.0. *Calc. C 39.7, H 2.2, N 0.0*

IR (CH_2Cl_2): ν_{CO} 2083 (w), 2030 (s), 2010 (m), 1996 (s), 1965 (m), 1950 (w) cm^{-1}
lit. (CCl_4): *2085 (m), 2030 (s), 2012 (m), 1998 (s), 1969 (m), 1951 (w) cm^{-1}*

Thermolysis of $Ir_4(CO)_{12}$ and PPh_3 in tetrahydrofuran

50 mg $Ir_4(CO)_{12}$ (0.05 mmol), 75 mg PPh_3 (0.29 mmol) and 20 cm^3 tetrahydrofuran were sealed inside a CEM Lined Digestion Vessel. The vessel was heated at 120 °C, creating an average pressure of 4.0 atm, for 15 minutes. After cooling to room temperature the vessel was opened, revealing an orange solution. The solution was filtered over silica and removed. Recrystallisation by slow evaporation of thf gave $Ir_4(CO)_9(PPh_3)_3$ (81.2 mg, 99 %)

$Ir_4(CO)_9(PPh_3)_3$

CHN analyses: Found C 41.5, H 2.4, N 0.0. *Calc. C 41.9, H 2.5, N 0.0.*

IR (CH_2Cl_2): ν_{CO} 2043 (m), 1989 (vs, br), 1788 (s, br) cm^{-1}
lit. (PhCl):[47] *2040 (m), 1980 (s, br), 1960 (sh), 1780 (m,br) cm^{-1}*

^{31}P ($(CD_3)_2CO$): 19.8 (2), -16.0 (1) ppm
lit.:[48] *20.0 (2), -17.4 (1) ppm*

Surface-mediated synthesis of $Os_3(CO)_{12}$ and $Ru_3(CO)_{12}$

A range of experimental conditions were used, the details are discussed in the text and summarised in Table 3.7 toTable **3.11**. A typical procedure is described below.

50 mg (0.06 mmol) $Os_3(CO)_{12}$ and 1.25 g oven-dried alumina (Os 2.5 % w/w) were evenly ground in a mortar and the slurried with hexne for 30 minutes. The solvent was removed and the solids transferred to **Vessel 3**, which was sealed under nitrogen. The vessel was placed in a STAR 2 cavity and heated for 10 minutes at 200 °C. After cooling the resulting pale orange solid was slurried with 25 mg (0.14 mmol) $(PPh_3)_2NCl$ in 30 cm^3 acetone for 30 minutes. After filtration the alumina was colourless. The pale orange solution was separated by TLC (acetone:hexane, 3:2) yielding $[H_3Os_4(CO)_{12}]PPN$ (4.8 mg, 7.2 % wrt to Os) and $[Os_{10}C(CO)_{24}][PPN]_2$ (2.8 mg, 4.6 % wrt to Os)

$[H_3Os_4(CO)_{12}]PPN$

MS FAB^+: 1100 (M^+), (M^+ - n28) observed for n = 0 to 8

CHN analyses Found C 35.3, H 1.0, N 1.0. *Calc. C 35.5, H 1.1, N 0.9*

IR (CH_2Cl_2): ν_{CO} 2045 (vs), 2022 (vs), 1999 (s) 1978 (m) cm^{-1}
lit. (CH_2Cl_2):[21] *2046 (s), 2021 (s), 1998 (s), 1979 (m) cm^{-1}*

$[Os_{10}C(CO)_{24}][PPN]_2$

MS FAB^+: 2586 (M^+), (M^+ - n28) observed for n =0 to 14

CHN analyses Found C 32.2, H 1.0, N 0.8. *Calc. C 32.1, H 0.8, N 0.8.*

IR (CH_2Cl_2): ν_{CO} 2034 (s), 1988 (m) cm^{-1}
lit. (CH_2Cl_2):[46] *2033 (s), 1986 (s) cm^{-1}*

$[HOs_5(CO)_{15}]PPN$

MS FAB^+: 1372 (M^+), (M^+ - n28) observed for n = 0 to 10

CHN analyses Found C 32.2, H 0.9, N 0.6. *Calc. C 32.3, H 0.9, N 0.7*

3.7. References

1 D.M.P. Mingos and D.J. Wales, *Introduction to Cluster Chemistry*, Prentice-Hall Inc. (1990)

2 J.-O. Malm, J.-O. Bovin, A. Petford-Long, D.J. Smith, G. Schmid and N. Klein, *Angew, Chem. Int. Engl.* **27** (1988) 555

3 M.N Vargaftik, V.P. Zagorodnkov, I.P. Stolarov, I.I. Moiseev, D.I. Kochubey, V.A. Likholobov, A.L. Chuvilin and K.I. Zamaraev, *J. Mol. Cat.* **53** (1989) 315

4 L.N. Lewis, *Chem. Rev.* **93** (1993) 2693

5 E.L. Meutterties, *J. Organomet. Chem.* **200** (1980) 177

6 P.L. Dyson, *Personal Communication.*

7 P.J. Bailey, M.A Beswick, B.F.G. Johnson, J. Lewis, M. McPartlin, P.R. Raithby and M.D.R de Arellano, *J. Chem. Soc. Dalton Trans.* (1996) 3515

8 P.J. Bailey, M.A. Beswick, B.F.G. Johnson, J. Lewis, P.R. Raithby and M.C.R. de Arellano, *J. Chem. Soc. Dalton Trans.*, (1992) 3159

9 P.J. Bailey, M.J. Duer, B.F.G. Johnson, J. Lewis, G. Conole, M. McPartlin, H.R. Powell and C.E. Anson, *J. Organomet. Chem.* **383** (1990), 441

10 B.F.G. Johnson, J. Lewis and I.G. Williams, *J. Chem. Soc. A*, (1970) 901

11 C.T. Hayward and J.R. Shapley, *Inorg. Chem.* **21** (1982), 3816

12 C.T. Hayward, J.R. Shapley, M.R. Churchill, C. Bueno, A.L. Rheingold, *J. Am. Chem. Soc.* **104** (1982) 7347

13 C.R. Eady, B.F.G.Johnson and J. Lewis, *J. Chem. Soc. Dalton Trans,* (1975), 2606

14 D. Braga, J. Lewis, B.F.G. Johnson, M. McPartlin, W.J.H. Nelson and M.D. Vargas, *J. Chem. Soc. Chem. Commun.* (1983) 241

15 D. Braga, K. Henrick, B.F.G. Johnson, J. Lewis, M. McPartlin, W.J.H. Nelson and M.D. Vargas, *J. Chem. Soc. Chem. Commun.* (1982) 419

16 P.J. Bailey, G.C. Conole, B.F.G. Johnson, J. Lewis, M. McPartlin, A. Moule and D.A. Wilkinson, *Angew. Chem. Int. Ed. Engl.* **30** (1991) 1706

17 M. Angoletta, L. Malatesta and G. Caglio, *J. Organomet. Chem.* **94** (1975), 99

18 C.R. Eady, P.F. Jackson, B.F.G. Johnson, J. Lewis, M.C. Malatesta, M. McPartlin and W.J.H. Nelson, *J. Chem. Soc. Dalton*, (1980) 383

19 R.D. Pergola, F. Demartin, L. Garlaschelli, M. Manasserro, S. Martinengo, N. Masciocchi and P. Zanello, *Inorg. Chem.* **32** (1993) 3670

20 D. Roberto, E. Cariati, E. Lucenti, M. Respini and R. Ugo, *Organometallics* **16** (1997) 4531

21 H.H. Lamb, A.S. Fung, P.A. Tooley, J. Puga, T.R. Krause, M.J. Kelly and B.C. Gates, *J. Am. Che. Soc.* **111** (1989) 8367

22 A. Zhao and B.C. Gates, *J. Am. Chem. Soc.* **118** (1996) 2458

23 H.H. Lamb, B.C. Gates and H. Knözinger, *Angew. Chem. Int. Ed. Engl.* **27** (1988) 1127

24 A. Zhao and B.C. Gates, *Langmuir*, **13** (1997) 4024

25 A. Bashall, L.H. Gade, J. Lewis, B.F.G. Johnson, G.J. McIntyre, M. McPartlin, *Angew. Chem., Int. Ed. Engl.*, **30** (1991) 1164

26 J.C. Calabrese, L.F. Dahl, P. Chini, G. Longoni, S. Martinengo, *J. Am. Chem. Soc.*, **96** (1974) 2614

27 S. Harris, M.L. Blohm, W.L. Gladfelter, *Inorg. Chem.*, **28** (1989) 2290

28 J.L. Vidal and J.M. Troup, *J. Organomet. Chem.* **213** (1981) 351

29 M.L Blohm and W.L. Gladfelter, *Organometallics*, **4** (1985) 45

30 E.R. Corey and L.F. Dahl, *Inorg.Chem.* **1**, (1962) 521

31 M.R. Churchill, J.P. Hutchinson, *Inorg. Chem.*, **17** (1978) 3528

32 S. Caddick, *Tetrahedron,* **51** (1995) 10403

33 P.J. Bailey, E. Charalambous, J. Hoyle, B.F.G Johnson, J. Lewis and M. McPartlin, *J. Chem. Soc. Chem. Commun*, (1990) 1443

34 J. Purga, A. Arce, R.A. Sanchez-Delgado, J. Asciano, A. Andriollo, D. Braga and F. Grepioni, *J. Chem. Soc. Dalton*, (1988) 913

35 G.R. Steinmetz, A.D. Harley, G.L. Geoffroy, *Inorg. Chem.* **19** (1980) 2985

36 D.R. Tyler, M. Altobelli and H.B. Gray, *J. Am. Chem. Soc.* **102** (1980) 3022

37 M. Tachikawa and J. Shapley, *J. Organomet. Chem.* **124** (1977) C19

38 A.J. Drakesmith and R. Whyman, *J. Chem. Soc. Dalton*, (1973), 362

39 D. Roberto, E. Lucennti, C. Roveda and R. Ugo, *Organometallics* **16** (1997), 5974

40 S.L. Scott and J-M. Basset, *J. Mol. Cat.* **86** (1994) 5

41 G. Bram, A. Loupy, M. Madjoub, E. Guitierrez and E. Ruiz-Hitzky, *Tetrahedron*, **45** (1990) 5167

42 G.M. Zanderighi, C. Dossi, R. Ugo, R. Psaro, A. Theolier, A. Choplin L. D'Ornelas and J-M. Basset, *J Organomet. Chem.* **296** (1985) 127

43 R. Psaro, R. Ugo, G.M. Zanderighi, B. Besson, A.K. Smith and J-M Basset, *J Organomet. Chem.* **213** (1981) 215

44 D. Roberto, E. Cariati, R. Psaro and R. Ugo, *Organometallics*, **13** (1994) 734

45 D. Roberto, E. Cariati, R. Ugo and R. Psaro, *Inorg. Chem.* **35** (1996) 2311

46 P.F. Jackson, B.F.G. Johnson, J. Lewis, W.H. Nelson and M. McPartlin, *J. Chem. Soc. Dalton,* (1982) 2099

47 D.C. Sonnenberger and J.D. Atwood, *Organomet.* **1** (1982) 694

48 G.F. Stuntz and J.R. Shapley, *J. Am. Chem. Soc.* **99** (1977) 607

Chapter Four

Dielectric Parameters and their Influence on Solvent Heating

4.1. Introduction

This Chapter summarises a wide variety of dielectric data gathered from the literature and supplemented by recent measurements in our laboratories. The effects of molecular structure upon the observed dielectric properties are examined and the relationship between these properties and the observed heating rates are probed. Much of this data has been published in a recent review.[1]

The dielectric properties of a material in an electromagnetic field vary with the applied frequency and temperature. During the early development of dielectric heating von Hippel and co-workers assembled a large database of the dielectric properties of common substances, foodstuffs and materials.[2] Recently, as exposure of biological tissue to microwave and radio frequency electromagnetic radiation has increased, considerable effort has been directed towards the measurement of the dielectric properties of biological materials.[3,4] The dielectric analysis of pharmaceutical materials has become increasingly important, and the results have been summarised in a recently published book.[5] However, the availability of data for the commonly used organic solvents remains poor, even though there has been a great interest in dielectric heating as a method for accelerated chemical synthesis during the last ten years.[6] This is partly a matter of focus, since much of the literature data was gathered as part of the examination of solution structures, the dielectric parameters of interest for dielectric heating need to be extracted from them.

4.2. Fundamental Theory[6,7,8]

Collins[9] defines a dielectric as 'a substance or medium that can sustain an electric field.' In conductive materials the charge carriers are free to move throughout the medium. When the movement of the charge carriers is restricted polarisation occurs instead. Such a material acts as a capacitor. Polarisation within the dielectric is considered to be due to the sum of various components;

$$\alpha_t = \alpha_e + \alpha_a + \alpha_d + \alpha_i$$

where α_t is the total polarisation and

α_e, the electronic polarisation, arises from the realignment of electrons around specific nuclei;

α_a, the atomic polarisation, results from the relative displacement of nuclei due to the unequal charge distribution within the molecule;

α_d, the dielectric polarisation, results from the orientation of permanent dipoles by the electric field; and

α_i, the interfacial polarisation or Maxwell Wagner effect, occurs when charge builds up at interfaces.

The electronic and atomic polarisation relaxation frequencies are much larger than those for the dielectric polarisation and at microwave frequencies it is this effect which predominates. The interfacial polarisation relates to the charge accumulated at the surface

of a conductive particle in a non-conducting medium. Its importance in the microwave region is unclear.

4.2.1. Dielectric Polarisation

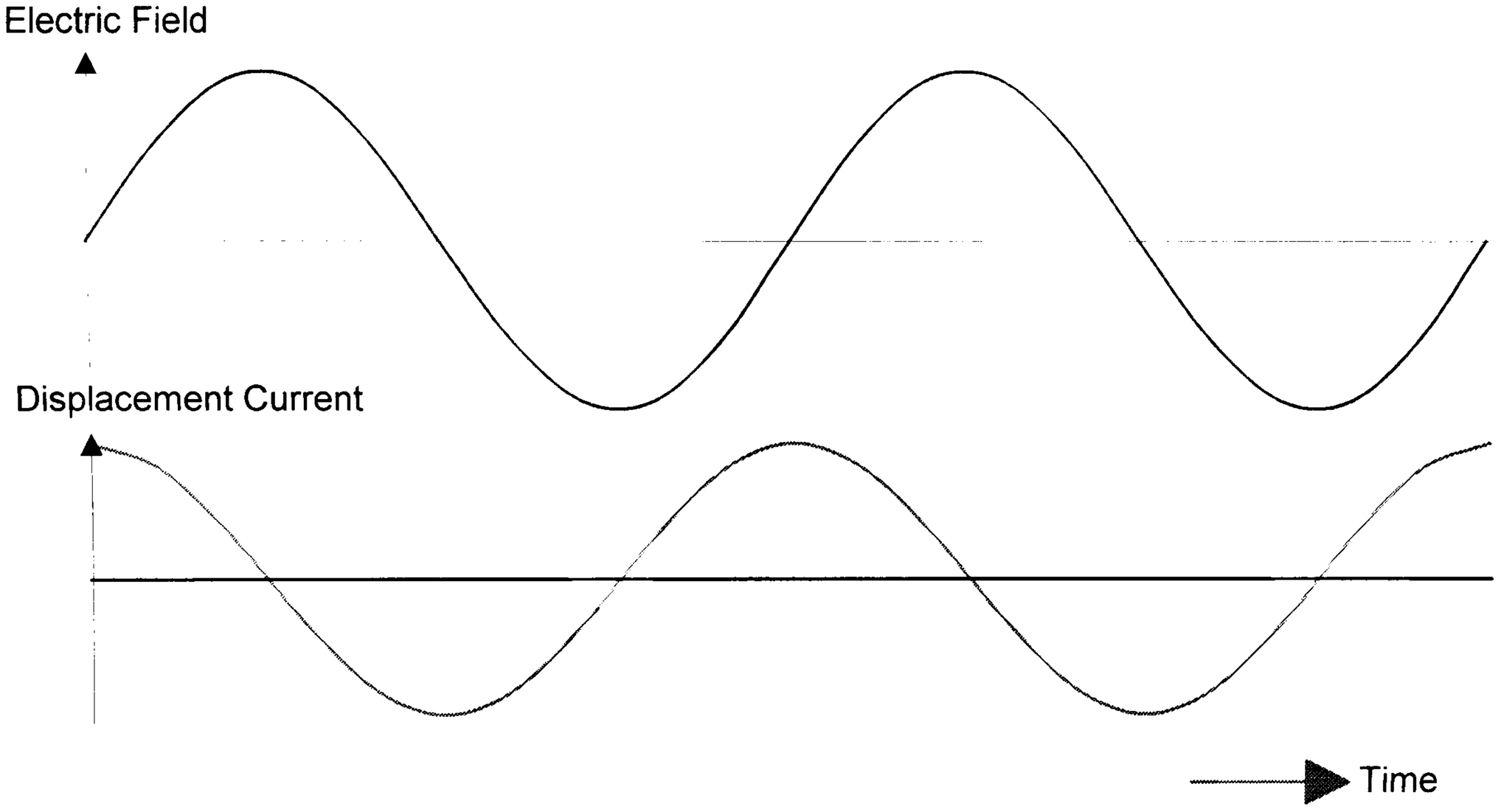


Figure 4.1. Application of a sinusoidal electric field to liquid ideal dielectric (top) and the induced Maxwell displacement current (bottom)

A molecule exposed to an oscillating electric field will align itself with the field. The induced reorientation of charge carriers is equivalent to an electric current, known as the Maxwell displacement current. In an ideal dielectric the orientation of the dipoles follows the electric field exactly and the Maxwell displacement current is 90° out of phase with the external field, as shown in Figure 4.1. At frequencies where the molecular reorientation's keep pace with the external field no heating occurs. As the frequencies of the applied field approach the microwave region of the electromagnetic spectrum the rotation of the dipoles can no longer keep pace with the oscillation of the electric field. This causes a shift in the relative phase of the displacement current, as shown in Figure 4.2. a) and b). For a displacement of less than 90° there is a now a component $\boldsymbol{I} \bullet \sin \delta$ in

phase with the external field leading to resistive heating and the absorption of energy from the electric field.

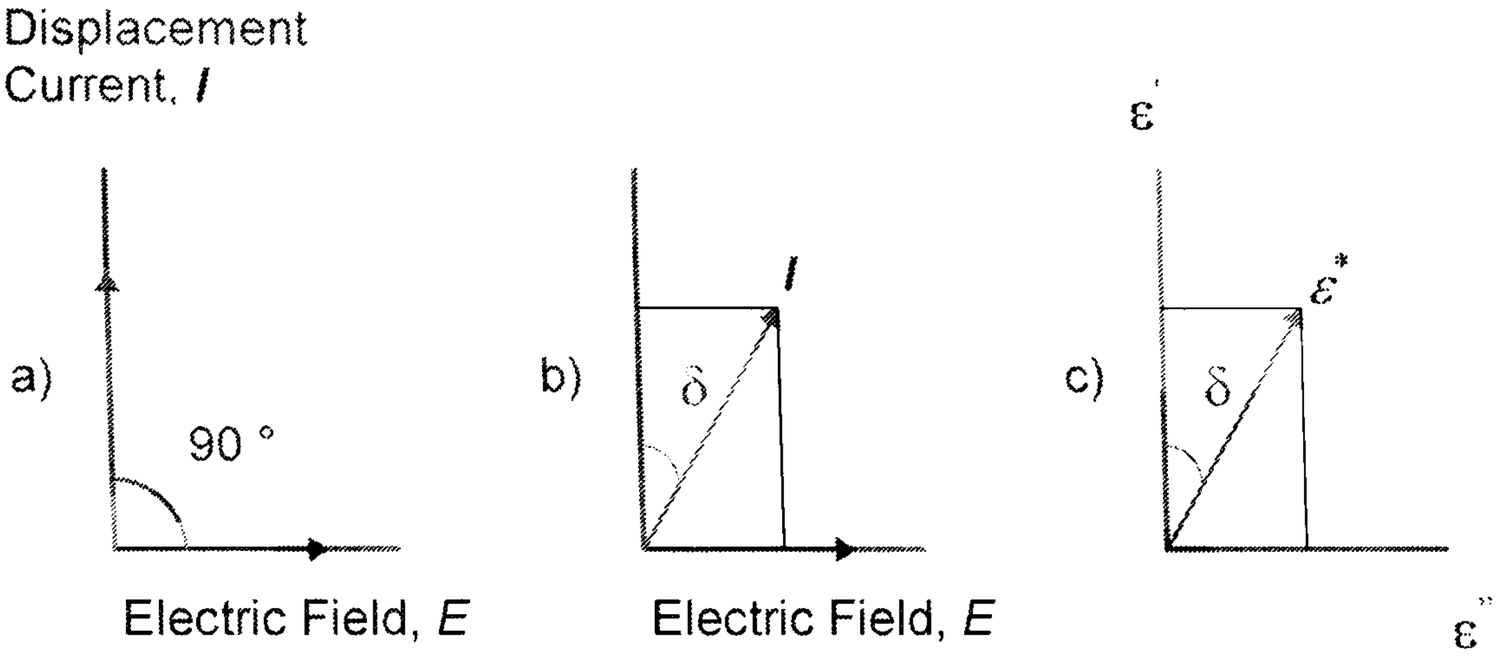


Figure 4.2. Phase diagrams for a) an ideal dielectric where the energy is transmitted without loss b) where there is a phase displacement δ c) the relationship between ε^* ε' and ε''

The ability of a material to store charge is described as its permittivity, usually measured relative to ε_0, the permittivity of free space. At low frequencies, the dipole rotation follows the field oscillation exactly and the relative permittivity is large and approximately constant; this is ε_∞, the infinite dielectric constant. At very high frequencies the dipoles are unable to follow the external field and the relative permittivity falls to a minimum value, referred to as the static dielectric constant ε_s. Here the response is similar to that seen with non-polar materials.

At frequencies where δ differs significantly from 0° the permittivity has a complex character, as shown in Figure 4.2.c);

$$\varepsilon^* = \varepsilon' - j\varepsilon'' \qquad (1)$$

where ε'', the dielectric loss factor, is the permittivity component in phase with the external field and ε' is the real part of the complex permittivity. Here the material

functions as a conductor as well as a dielectric. The ratio of ε" to ε' is equal to tan δ and described as the energy dissipation factor or loss tangent. The loss tangent is frequently used as a 'rule of thumb' guide to the ability of a material to absorb microwave energy at a particular frequency. The reliability of this assumption is examined in Section 4.6., however it is a very simplistic view; accurate evaluation requires the complexity of the electric field pattern, the heat capacity and the sample density to be taken into account.

The frequency dependence of the dielectric parameters are described by the Debye equation;[10]

$$\varepsilon^* = \varepsilon_\infty + \frac{\varepsilon_s - \varepsilon_\infty}{1 + j\omega\tau} \qquad (2)$$

for a single relaxation process with time τ, where ω is the angular frequency; $\omega = 2\pi\nu$

When an external field is removed the dipoles will cease to align with it and adopt random orientations. The relaxation time is a measure of the delay observed in the completion of this process

The Debye equation can be separated into real and imaginary parts thus;

$$\varepsilon' = \varepsilon_\infty + \frac{\varepsilon_s - \varepsilon_\infty}{1 + \omega^2\tau^2} \qquad (3)$$

$$\varepsilon'' = \frac{(\varepsilon_s - \varepsilon_\infty)\omega\tau}{1 + \omega^2\tau^2} \qquad (4)$$

It can be seen that the maximum value for ε" is equal to $(\varepsilon_s - \varepsilon_\infty)/2$ and occurs when $\omega = 1/\tau$. This value of the angular frequency, ω_0, and its associated applied frequency value, $\nu_0 = \omega_0/2\pi$ are the relaxation frequencies.

Debye also derived the following relationship for the relaxation time of a spherical molecule;

$$\tau = \frac{4\pi r^3 \eta}{kT} \qquad (5)$$

where r is the molecular radius, η is the viscosity and k is Boltzmann's constant

The relaxation time is temperature dependent, and since it is related to the rate constant, *k*, for the relaxation process and Arrhenius type analysis may be used to calculate the enthalpy and entropy of the relaxation process. For liquid water $\Delta H^{\ddagger}$ (enthalpy of activation) is 18 kJ mol^{-1} which corresponds roughly to the energy required to break one hydrogen bond. For ice the equivalent value is 55 kJ mol^{-1} thereby suggesting that three hydrogen bonds are involved. Since the water molecules in ice form four hydrogen bonds with neighbouring molecules this observation is consistent with a rotation process that retains one hydrogen bond. The water molecules in liquid water clearly retain some of the structure of ice and it is perhaps better to think of water either as a series of clusters of water molecules which interact with each other or as a statistical assembly of water molecules forming different numbers of hydrogen bonds. As a consequence of the former the relaxation process in the microwave region corresponds to the co-operative rotational movements of molecules within the clusters and between the

clusters, whereas in the latter it is an average relaxation time resulting from the different bonding arrangements adopted in the liquid.

Although the frequencies at which polar molecules become susceptible to dielectric heating approximate to their rotational relaxation frequencies dielectric heating is not a quantum mechanical resonance phenomenon. The energy transfer is not due to transitions between quantised rotational levels, but rather a collective movement of the medium. Debye interpreted dielectric heating as a frictional effect, between the rotating dipole, accelerated by the external radiation and its surrounding molecules. An alternative view is to consider the rotating molecule as a paddle which as it rotates knocks surrounding molecules, increasing their translational energy.

In the liquid phase many different molecular environments are present. Although this dispersion is often mathematically representable as a single relaxation time it is a broad band phenomenon, usually covering at least two decades. As a result of this breadth of dispersion many solvents couple efficiently with microwaves even when their relaxation frequencies are not perfectly matched to the applied field.

4.3. Aqueous Systems

Microwave dielectric heating is still primarily an aqueous phenomenon; all domestic uses and many industrial processes, *e.g.* drying, rely largely on the ability of microwaves to couple with water molecules. Consequently there is a much greater level of data and analysis for the dielectric properties of water and aqueous solutions. The area has recently been comprehensively reviewed by Craig.[5]

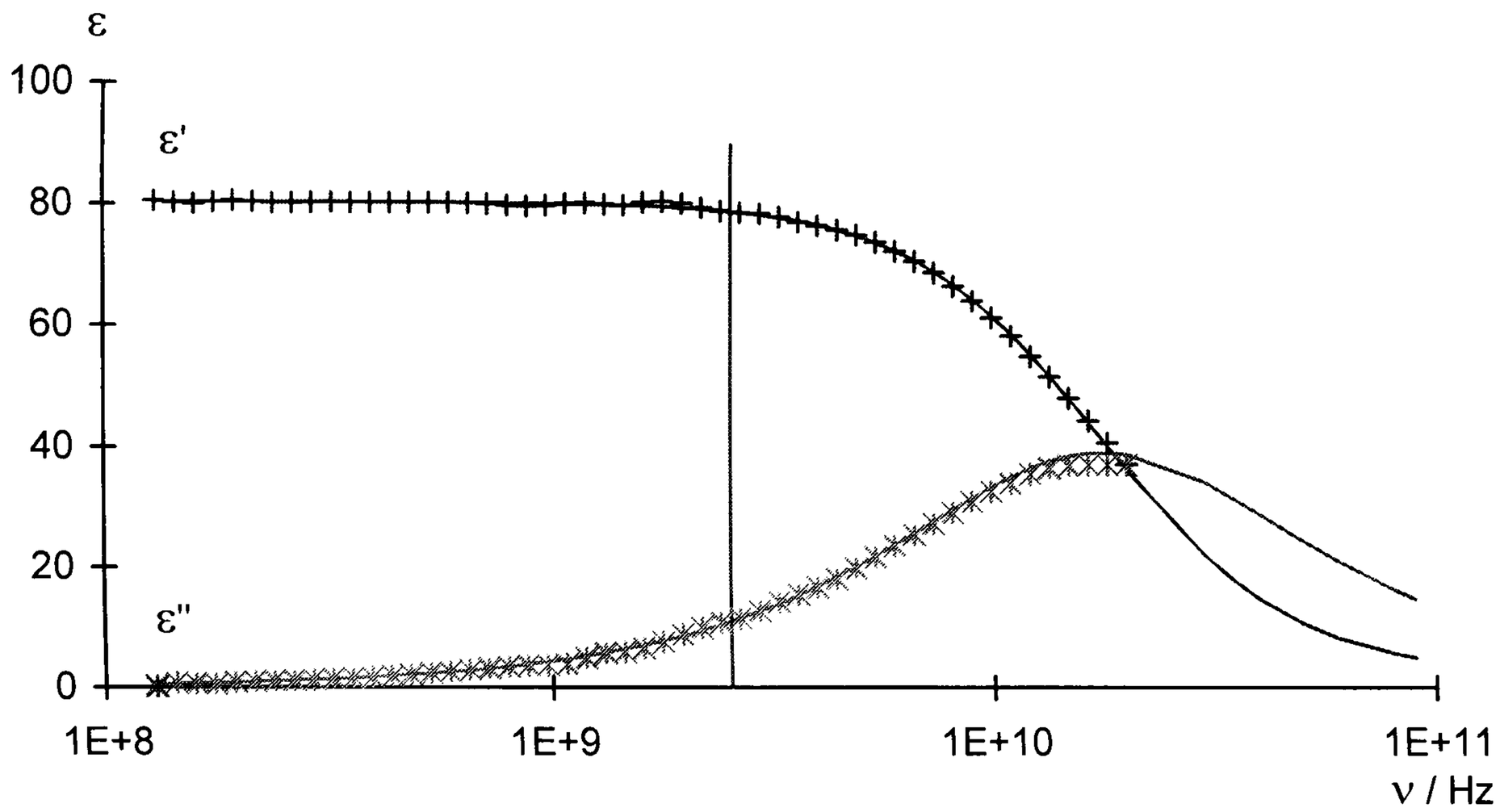


Figure 4.3. The variation of ε' and ε'' with frequency for water at 20 °C

Figure 4.3 shows the variation of ε' and ε'' with frequency for water at 20 °C. The data can be fitted to a single Debye relaxation, as indicated by the solid lines. The relaxation time is 9 ps which corresponds to a relaxation frequency of 17.6 GHz. This is a significant shift from the usual operating frequency of 2.45 GHz (indicated by a vertical bar) and the heating rate observed for water, although large, is far from the maximum obtainable.

The dielectric response of water changes as ionic salts are added; at low concentrations the relaxation time is depressed. It has been proposed that the addition of ions perturbs the hydrogen bonded solution structure; molecules bonding directly to the ions become rotationally fixed, whilst uncoordinated molecules experience less strong hydrogen bonding effects. The resulting increase in rotational freedom leads to a lower relaxation time.[5]

As the ion concentration is increased, relaxation times are extended; concentrated salt solutions have higher relaxation times than that of pure water. In this case it is believed that the increased order in the solution restricts the rotational freedom of the water molecules.

4.3.1. Water-alcohol and water-carbohydrate mixtures

Alcohols and carbohydrates generally are highly miscible with water. In solution they can be considered as organic radicals with pendant hydroxyl groups, capable of forming hydrogen bonds with themselves or the surrounding solvent molecules. Such mixtures tend to show a single relaxation time. For highly similar solvents this can usually be expressed as the average of the two pure components, relative to the molar composition of the solution. In more complex mixtures a broader dispersion than that predicted by the Debye equation (2) is often seen. Several empirical models for such solutions have been formulated; Cole and Cole[11] proposed;

$$\varepsilon^* = \varepsilon_\infty + \frac{\varepsilon_s - \varepsilon_\infty}{1 + (j\varpi\tau)^{(1-\alpha)}} \qquad (6)$$

Here α is a distribution parameter, such that $1 > \alpha \geq 0$ which for $\alpha = 0$ reverts to the Debye equation. It may be considered a measure of the extent to which the distribution is broadened or the dispersion being due to several relaxation processes.

Another model, which is useful for describing the frequency dependence of some sugars and alcohols, is that proposed by Cole and Davidson[12];

$$\varepsilon^* = \varepsilon_\infty + \frac{\varepsilon_s - \varepsilon_\infty}{1 + (j\varpi\tau)^{\beta}} \qquad (7)$$

which reverts to the Debye equation for $\beta = 1$. The Cole-Davidson model has proved useful in situations where a skewed distribution of relaxation times is present.

4.3.1. Aqueous protein solutions[4]

Protein molecules typically have molecular weights several orders of magnitude greater than that of water. This leads to a relaxation dispersion at frequencies much lower than that of pure water. For a moderately sized globular protein, such as haemoglobin this is of the order of 10 MHz. At low protein concentrations the relaxation of the water molecules is largely unaffected by presence of the protein and two distinct relaxation dispersions can be seen, as shown in Figure 4.4: The protein dispersion is labelled β and the water γ. As the concentration of protein increases it influences more of the water molecules; this is described as bound water. The stronger intermolecular forces between bound water and the protein leads to a third dispersion region, between γ and β.

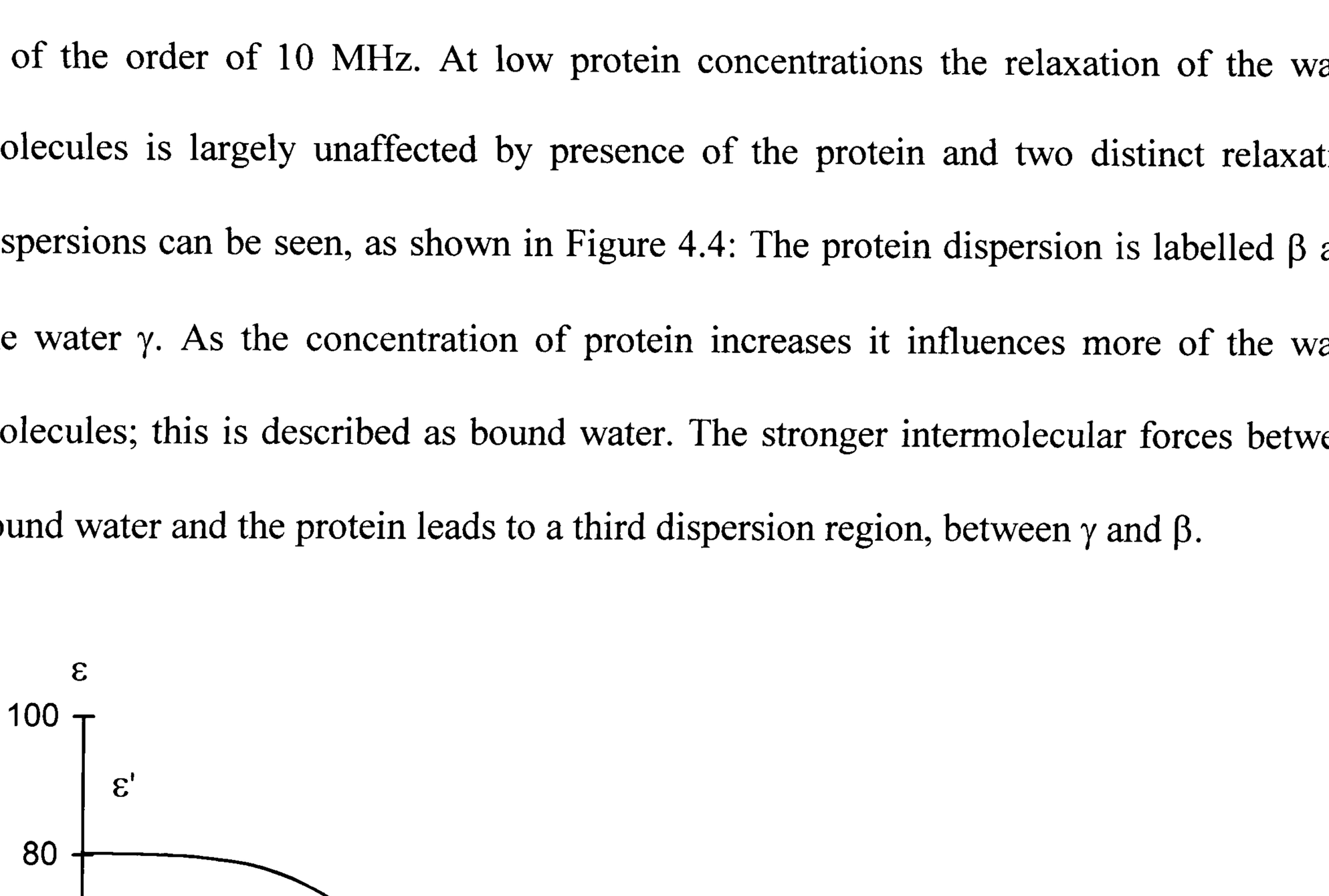


Figure 4.4. Schematic illustration of the dielectric spectrum of an aqueous protein solution.

Grant *et al*[4] have established a linear relationship between the relaxation time of water and the molecular weight of 20 biological molecules with molecular weights of up to 68,000 (haemoglobin), which suggests that the size of the molecule is the predominant influence.

4.3.1. Ionic solutions

The dielectric properties of ionic solutions have been described by Hasted[13] and Craig.[5] Figure 4.5 shows the dispersion curves for three aqueous solutions of potassium chloride. In addition to the dipolar relaxation processes of the water molecules, ionic drift gives rise to Joule heating effects. Each of these processes has a separate loss factor, ε''_d and ε''_i, and an associated conductivity, σ_d and σ_i. The relationship between ε and σ is;

$$\varepsilon'' = \frac{\sigma}{\omega\varepsilon_0} = \frac{\sigma_d + \sigma_i}{\omega\varepsilon_0} \qquad (8)$$

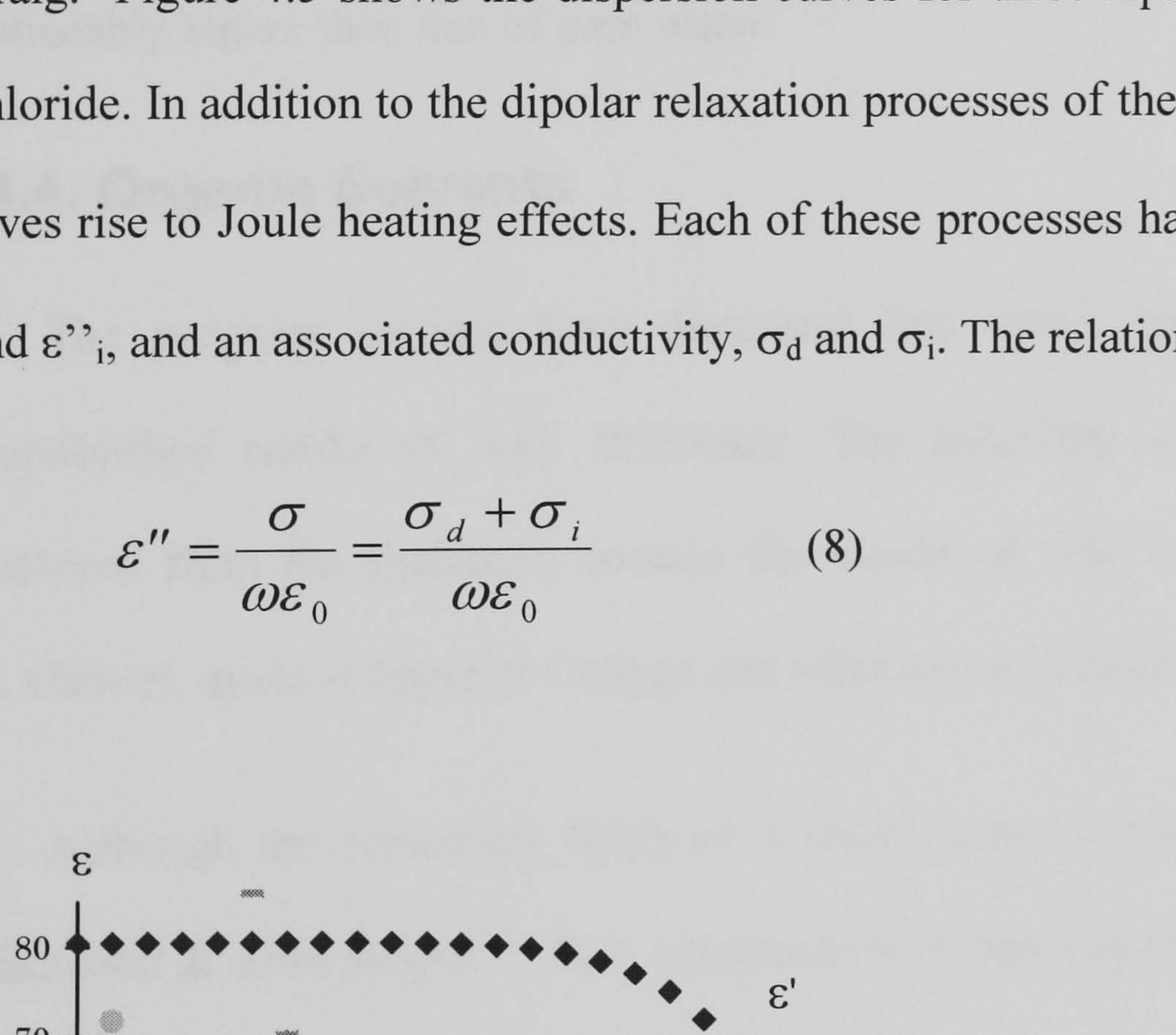


Figure 4.5. Experimental values of the permittivity and total loss factor for KCl solutions with differing concentrations

consequently Eqn (1) can be rewritten as;

$$\varepsilon^* = \varepsilon' - j\left(\varepsilon''_d + \frac{\sigma_i}{\omega\varepsilon_0}\right) \qquad (9)$$

This introduces a component to ε'' that increases with decreasing frequency. As the concentration of ions is increased this component predominates (Figure 4.5). As a practical result the heating rate of an ionic solution, even at low concentrations, is noticeably higher than that of pure water.

4.4. Organic Solvents

The previous sections have discussed data taken from the literature and some unpublished results of A.G. Whittaker. The following sections, in addition to data gathered from the literature, contain the results of new measurements by myself and S. Gabriel, made at Imperial College and Microwave Consultants.

Although the relaxation times of a wide range of organic compounds have been discussed at some length[7,14] little examination of their relevance to dielectric heating has been made.

4.4.1. Alcohols

Alcohols form hydrogen bonds in a similar manner to water, albeit to a lesser extent. They also have similar dipole moments. As a result there are many similarities in their dielectric properties. Table 4.1. summarises the relaxation times for a series of alcohols, listed by chain length and isomer. The relaxation time increases with chain length but does not seem particularly effected by the position of the hydroxyl group in the chain; the

values for the isomeric propanols and butanols are not very different. The unsaturated alcohols tend to have shorter relaxation times than their saturated isomers, this effect is enhanced if the double bond is adjacent to the hydroxyl group. It is possible that this reduction in relaxation time is due to more localised rotational processes arising from the increased rigidity of the molecule; this is considered further in section 4.4.5.

Table 4.1. Relaxation times (at 20 °C) and dielectric properties of aliphatic alcohols compared with water

Compound	Relaxation time τ (ps)	Dipole Moment (Debye)	Loss Tangent @ 2.45 GHz
water*	9.04	1.84	0.123
methanol	51.5	1.70	0.659
ethanol	170	1.69	0.941
propan-1-ol	332	1.68	0.757
propan-2-ol	237	1.66	0.799
butan-1-ol	538	1.66	0.571
butan-2-ol	562		0.447
2-methyl-propan-1ol	644		0.522
pentan-1-ol	792	1.80	0.427
hexan-1-ol	976	1.67	0.344
octan-1-ol	1500		0.157
4-pentene-1-ol	322		0.669
3-pentene-2-ol	169		0.720
3-methyl-2-butene-1-ol	170		0.846
trans-2-hexene-1-ol	277		0.571
benzylalcohol	188		0.667

*1.84 refers to the dipole moment in the vapour phase - in the liquid state it is appreciably higher (ca. 2.5 D).

Although the relaxation times are important in influencing heating rates the breadth of the dielectric loss dispersion is also important. Figure 4.6 shows the dielectric spectra for water and some aliphatic alcohols between 10^8 and 10^{11} Hz. The value of the dielectric increment ($\varepsilon_s - \varepsilon_\infty$) is related by the Kirkwood equation[15] to the correlation factor *g* which

takes into account the highly directional nature of the hydrogen bonds, the dipole moment of the molecule (μ) and the number of molecules in a unit volume (*n*);

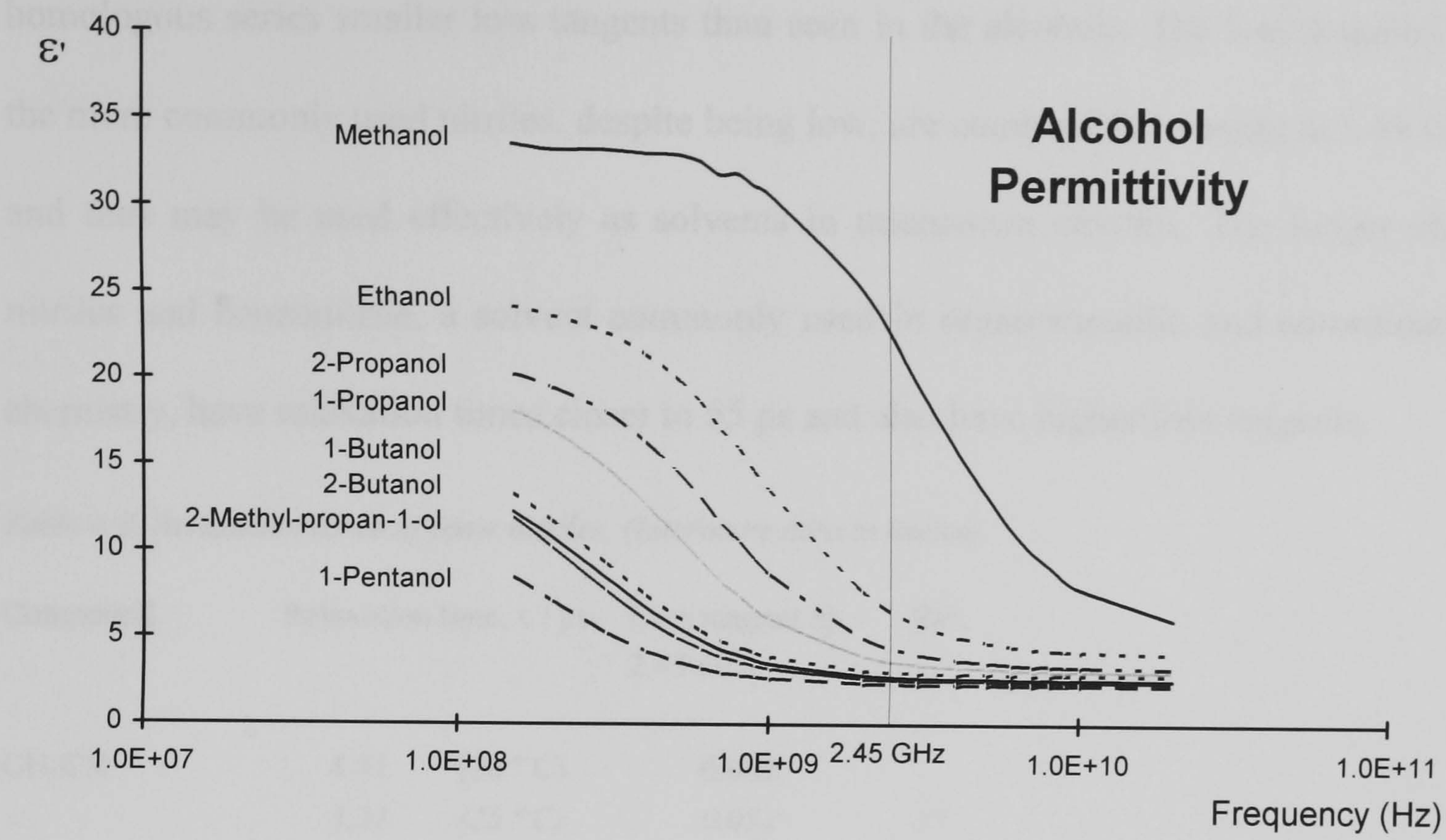
$$\varepsilon_s = \varepsilon_\infty + \frac{gn\mu^2}{2\varepsilon_0 kT} \qquad (10)$$

Table 4.2 Values of static permittivity (ε_s) and Kirkwood correlation factor g *for some non-aqueous solvents.*

Alcohol	ε_s	*g*
methanol	32.8	2.94
ethanol	42.6	3.04
propan-1ol	19.5	3.07
pentan-1-ol	15.8	3.43

For water the *g* parameter is around 2.5 and for alcohols it increases with the chain length; some representative values are given in Table 4.2.

Also shown in Figure 4.6 is a bar at 2.45 GHz, the input frequency for most microwave ovens. This corresponds to a relaxation time of 65 ps, a value straddled by the range of alcohols shown. These alcohols, therefore have relaxation properties which enable them to couple effectively with microwaves at this frequency and have thus proved effective solvents for dielectric heating.[16]



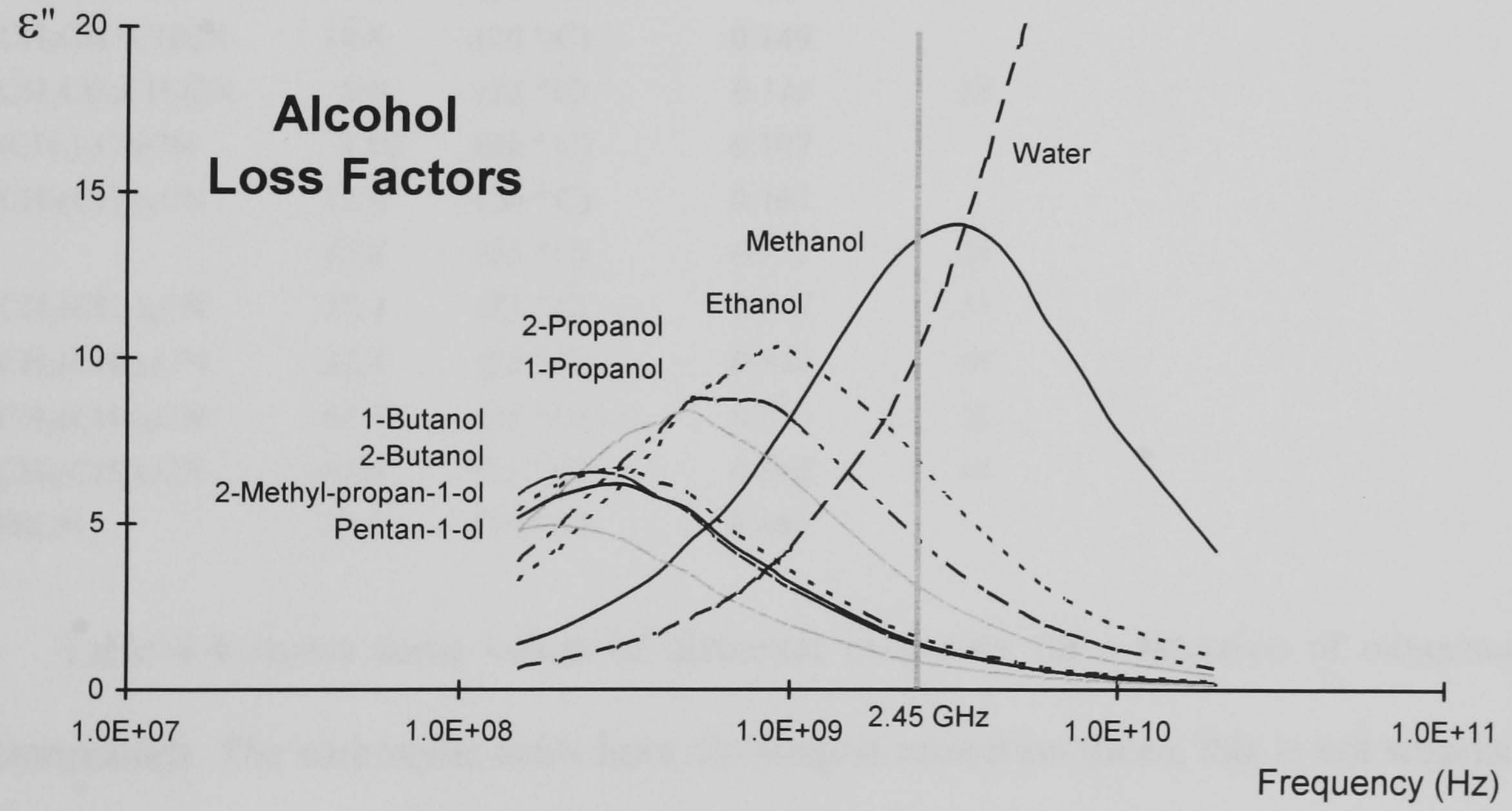


Figure 4.6. Dielectric spectra for water and a range of alcohols

4.4.2. Nitriles, esters, ketones and chlorohydrocarbons

The relaxation times for a series of nitriles are given in Table 4.3., along with values of the loss tangent at 2.45 GHz. The weaker hydrogen bonding in these compounds leads to much shorter relaxation times (4-68 ps) and for the comparable members of the

homologous series smaller loss tangents than seen in the alcohols. The loss tangents for the more commonly used nitriles, despite being low, are comparable to water at 2.45 GHz and thus may be used effectively as solvents in microwave cavities. The longer chain nitriles and benzonitrile, a solvent commonly used in organometallic and co-ordination chemistry, have relaxation times closer to 65 ps and also have higher loss tangents.

Table 4.3. Relaxation times of some nitriles. (Literature data in italics)

Compound	Relaxation time, τ / ps		Loss tangent @ 2.45 GHz	Ref.
CH_3CN	4.47	(20 ° C)	0.062	
	3.21	*(25 ° C)*	*0.052*	*17*
	3.4	*(25 ° C)*	*0.049*	*18*
CH_2=CHCN	5.91	(20 ° C)	0.082	
CH_3CH=CHCN	10.8	(20 ° C)	0.149	
$CH_3CH_2CH_2CN$	*8.9*	*(25 ° C)*	*0.119*	*18*
$(CH_3)_2CHCN$	7.92	(20 ° C)	0.107	
$CH_3(CH_2)_3CN$	12.9	(20 ° C)	0.167	
	13.0	*(25 ° C)*	*0.172*	*18*
$CH_3(CH_2)_4CN$	*17.4*	*(25 ° C)*	*0.215*	*18*
$CH_3(CH_2)_6CN$	*31.4*	*(25 ° C)*	*0.343*	*18*
$CH_3(CH_2)_8CN$	*67.5*	*(25 ° C)*	*0.527*	*18*
$CH_3(CH_2)_9CN$	*64.6*	*(25 ° C)*	*0.500*	*18*
PhCN	33.5	(20 ° C)	0.459	

Table 4.4 shows some values of dielectric properties for a selection of oxygenated compounds. The carboxylic acids have the longest relaxation times, this is not surprising given their strong intermolecular hydrogen bonding capabilities. Analysis of the available amide data is less clear-cut: the relaxation time of dmf, although relatively low is comparable to that of hexanenitrile rather than acetonitrile. Formamide has a relaxation time between that of formic acid and dmf whilst that of methylformamide is larger than them both. This could be attributed to hydrogen bonding, however the value for methylformamide seems unusually high.

Table 4.4. Relaxation times of a series of oxygenated solvents . (Literature data in italics)

Compound	Relaxation time, τ / ps		Loss tangent @ 2.45 GHz	Ref.
Acids				
HCO_2H	*76.7*	*(25 ° C)*	*0.722*	*19*
CH_3CO_2H	*177.4*	*(25 ° C)*	*0.174*	19
Amides				
$HCONH_2$	*37.3*	*(25 ° C)*	*0.561*	*17*
	38.3	*(25 ° C)*	*0.524*	*20*
$HCONH(CH_3)$	*128*	*(25 ° C)*		*17*
	122.9	*(25 ° C)*	*1.610*	20
$HCON(CH_3)_2$	13.05	(20 ° C)	0.161	
	10.2	*(25 ° C)*	*0.142*	20
Esters				
CH_3CO_2Et	4.41	(20 ° C)	0.059	
	3.66	*(40 ° C)*		*21*
$CH_3CO_2C_{16}H_{31}$	*13.3*	*(35 ° C)*		*21*
$C_{17}H_{35}CO_2C_{10}H_{21}$	*30.8*	*(40 ° C)*		*21*
Ketones				
CH_3COCH_3	3.54	(20 ° C)	0.054	
	3.22	*(20 ° C)*	*0.045*	*22*
	3.40	*(25 ° C)*	*0.045*	*23*
$CH_3COCH_2CH_3$	5.90	(20 ° C)	0.079	
$(CH_3)_2CHCOCH_2CH_3$	11.3	(20 ° C)	0.143	
thf, C_4H_8O	3.49	(20 ° C)	0.047	
	4.0	*(25 ° C)*	*0.030*	23
CH_3NO_2	4.51	(20 ° C)	0.064	
$(CH_3)_2SO$	*20.5*	*(25 ° C)*	*0.825*	18
	23.1	*(25 ° C)*		*24*

For the ketones and esters studied the short relaxation times observed are consistent with their lack of hydrogen bonding. For these compounds the molecular size is the most important factor, as may be seen from the data for tetrahydrofuran, with values very similar to those of ethanethanoate, a compound with a comparable molecular mass.

Table 4.5 shows some dielectric properties for a range of haloalkanes. The relaxation times are short, comparable to the ketones and other non-hydrogen bonded compounds discussed in Table 4.4

Table 4.5. Relaxation times of some halogenated alkanes

Compound	Relaxation time, τ / ps		Loss tangent @ 2.45 GHz	Ref.
$CHCl_3$	8.94	(20 ° C)	0.091	
	7.20	*(25 ° C)*	*0.058*	*25*
CH_2Cl_2	3.12	(20 ° C)	0.042	
	2.07	*(20 ° C)*	*0.027*	*26*
CH_2ClCH_2Cl	11.14	(20 ° C)	0.127	
$CHCl_2CH_2Cl$	15.18	(20 ° C)	0.181	
CH_3CCl_3	*5.9*	*(20 ° C)*		*21*
$(CH_3)_2CCl_2$	*6.4*	*(20 ° C)*		*21*
$(CH_3)_3CCl$	*4.8*	*(20 ° C)*		*21*
$(CH)_3CBr$	*6.7*	*(20 ° C)*		*21*

4.4.3. Aromatic Compounds

Table 4.6 summarises the relaxation times and loss tangents of a series of mono-substituted benzene derivatives. The halobenzenes have very similar dipole moments; the increase in their relaxation times can be attributed to the greater molecular volume. Indeed their relaxation times follow Eqn. (5); and this is discussed further in Section 4.5. With the exception of benzyl alcohol, the relaxation times lengthen as the dipole moment

Table 4.6. Relaxation times and dielectric properties of simple aromatic compounds

Compound	Relaxation time, τ / ps	Loss tangent @ 2.45 GHz	Dipole moment / Debye
Chlorobenzene	12.9	0.101	1.69
Bromobenzene	18.0	0.138	1.70
Iodobenzene	27.3	0.157	1.70
Nitrobenzene	43.7	0.589	4.22
Benzonitrile	33.5	0.459	4.68
Benzaldehyde	25.8	0.337	2.84
Benzyl alcohol	188	0.667	

becomes larger. For these molecules the primary intramolecular forces are dipole-dipole interactions. The increasing strength of these forces with the dipole moment is the most likely cause of the longer relaxation times.

4.4.4. Polyalcohols

Table 4.7 provides some comparative data on a series of alcohols which have several OH groups attached to the carbon backbone. These compounds are able to hydrogen bond very extensively and this is reflected in their high viscosities, which in turn correlate with a long relaxation time. The high loss tangents associated with these solvents are particularly noteworthy and it is surprising that they have not been more widely used as solvents for synthetic procedures based on microwave dielectric heating.

It has previously been noted that the activation energy for the relaxation process in water is around 15 - 20 kJ mol^{-1}. For simple aliphatic alcohols the corresponding value is

Table 4.7. Relaxation times and dielectric properties of glycols.

Compound	Relaxation time, τ / ps		Loss tangent @ 2.45 GHz	Viscosity / mPa s	Ref.
Ethanol	170		1.26	1.08	
Ethyleneglycol	112.87		1.35	0.136	
	104.6	*(25 °C)*	*1.17*		27
1,3-Propanediol	*340*	*(25 °C)*	*1.17*		28
1,4-Butanediol	*760*		*0.783*		28
1,5-Pentanediol	*1150*		*0.456*		28
1,7-Heptanediol	*1950*		*0.260*		28
2-Methoxyethanol	35.55		0.410		
	23.7	*(35 °C)*	*0.282*		29
2-Ethoxyethanol	*31.6*	*(35 °C)*	*0.301*		29
2-Butoxyethanol	*36.6*	*(35 °C)*	*0.276*		29
Glycerol	1215.6		0.651	945	
Di(ethylene glycol) methyl ether	*26.1*	*(35 °C)*	*0.310*		29
Di(ethylene glycol) ethyl ether	*35.5*	*(35 °C)*	*0.325*		29
Di(ethylene glycol) butyl ether	*43.6*	*(35 °C)*	*0.303*		29

in the range 16 - 23 kJ mol^{-1} and in polyalcohols, where the extent of hydrogen bonding is very extensive and the viscosities high, it rises to 50 - 130 kJ mol^{-1}.

4.4.5. Intramolecular rotations

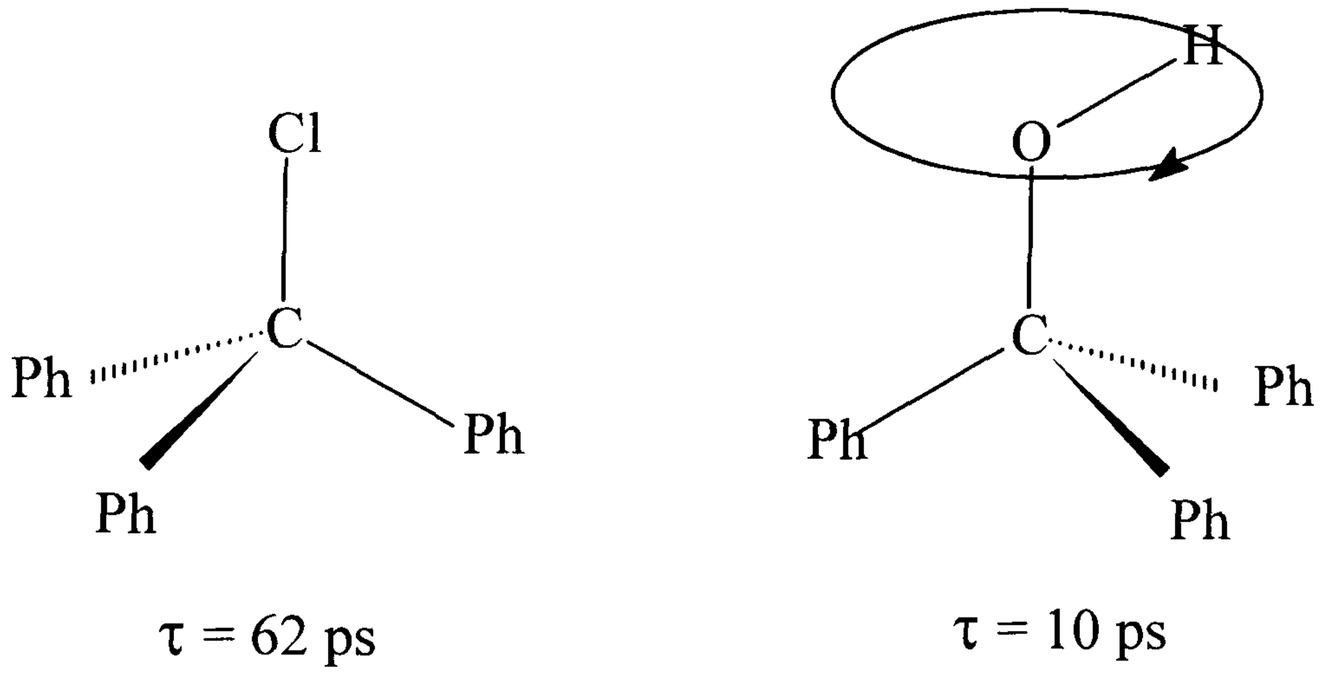


Figure 4.7. Possible localised relaxation processes for Ph_3CX

Dielectric relaxation processes are generally believed to involve the rotation of the entire molecule. For large, relatively rigid molecules with pendant substituents this assumption fails and localised rotational processes are also observed. For example triphenylchloromethane and triphenylhydroxymethane have very different relaxation frequencies and it has been proposed that in the latter case the relaxation time of 10 ps is associated with a rotation of the OH bond relative to the triphenylmethyl fragment (Figure 4.7). In many compounds containing rigid phenyl groups bond rotations are observed; Davies and Meakins[30] were able to discern simultaneously the localised and molecular rotations of tri-*tert*-butylphenol (in decalin) and the relevant dielectric spectrum is illustrated in Figure 4.8.

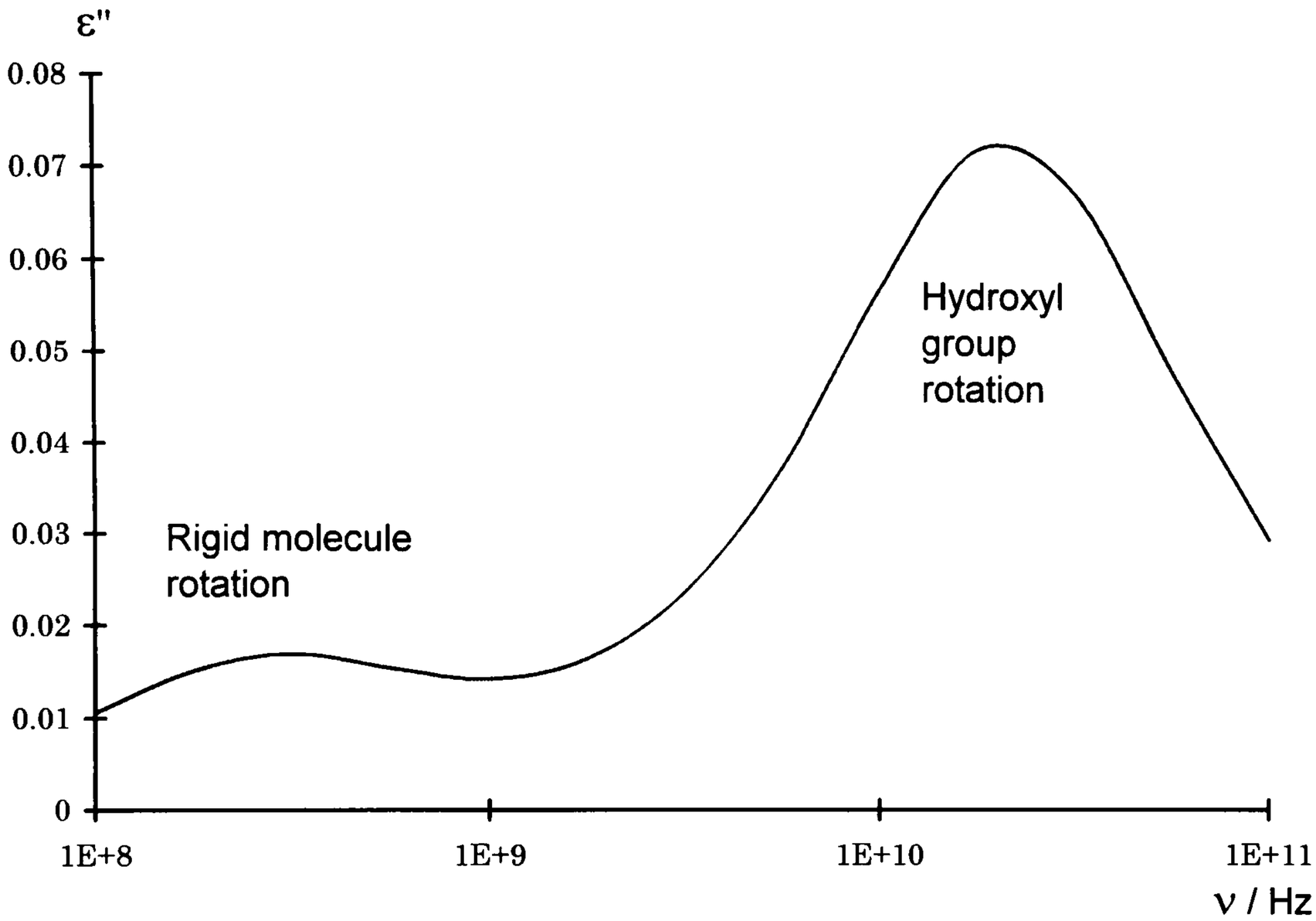


*Figure 4.8. Dielectric absorption of tri-*tert*-butylphenol in decalin (0.76 M) at 20 °C (adapted from ref. 30)*

The data in Table 4.1. shows some relatively short relaxation times for compounds with a CH_2OH group adjacent to a double bond, of particular note is the comparison between pent-4-en-1-ol (322 ps) and pent-3-en-2ol (169 ps). This may be attributed to a localised rotation of the CH_2OH group.

Primary amines anchored to large molecules also show relaxation frequencies which are inconsistent with the rotation of the whole molecule and it has been proposed that it is not a local rotation but an inversion at the nitrogen atom which is responsible. Table 4.8. summarises the data on three amines. The series of *ortho-*, *meta-* and *para-*methoxybenzylamine is particularly interesting since they all show a relaxation time of

Table 4.8. Structure and dielectric parameters of three methoxybenzylamines

	ε_s	Relaxation time, τ / ps
p-methoxy	7.2	25.4
o-methoxy	7.2	28.1, 105
m-methoxy	7.4	29.2

25-30 ps which can be attributed to the inversion of the NH_2 groups, but the *ortho*-isomer shows in addition a second and longer relaxation process at 105 ps, which presumably is associated with the occurrence of intramolecular hydrogen bonding between the NH_2 and the methoxy group.

4.5. Relaxation

Debye predicted that for a spherical molecule with a single relaxation process:

$$\tau = \frac{4\pi r^3 \eta}{kT}$$

emphasising the importance of the radius and solution viscosity. We have collated the data required to test this equation, for a series of alcohols, alkanenitriles and halobenzenes in Table 4.9. Some values could not be found; the viscosity of octanenitrile and the molecular volume for hexanenitrile, octanenitrile and octanol have been estimated using group additivity theory,[31] the estimated values are printed in italics. We have estimated the 'spherical molecular radius' by substituting for;

$$4\pi r = 3V_m/L \qquad (11)$$

where V_m is the molar volume and L is Avogadro's number, in equation (5).

The data derived from the values in Table 4.9. have been plotted in Figure 4.9. The first graph shows the data for the halobenzenes and alkanenitriles. Good agreement with the equation is observed and the gradients are very similar. From this we can infer a single relaxation process involving the whole molecule. The situation is more complex in the alcohol series. A linear relationship is observed for the first three data points, although the

fit, as indicated by the correlation coefficient, is looser than that observed for the other series. The observed gradient for the linear stage is 10 times that observed in the halobenzene and alkanenitrile plots and can be back calculated to give a value for Boltzmann's constant of 1.1×10^{-23}, which has the correct order of magnitude.

Table 4.9. Data required for the evaluation of Debye's equation for dielectric relaxation times

Compound	τ / ps	η_{298} / mPa s	V_m / cm^3 mol^{-1}
acetonitrile	3.4[18]	0.344[32]	52.87[33]
butyronitrile	8.9[18]	0.553[32]	87.87[33]
hexanenitrile	17.4[18]	0.912[32]	*122.85*
octanenitrile	31.4[18]	*1.155*	*157.84*
ethanol	170	1.074[32]	58.70[33]
butanol	538	2.544[32]	91.99[33]
hexanol	976	4.578[32]	125.32[33]
octanol	1500	7.29[32]	*159.25*
benzyl alcohol	188	5.8[32]	122.[33]
chlorobenzene	12.9	0.755[32]	102.42[33]
bromobenzene	18.0	1.074[32]	105.50[33]
iodobenzene	27.3	1.554[32]	111.92[33]

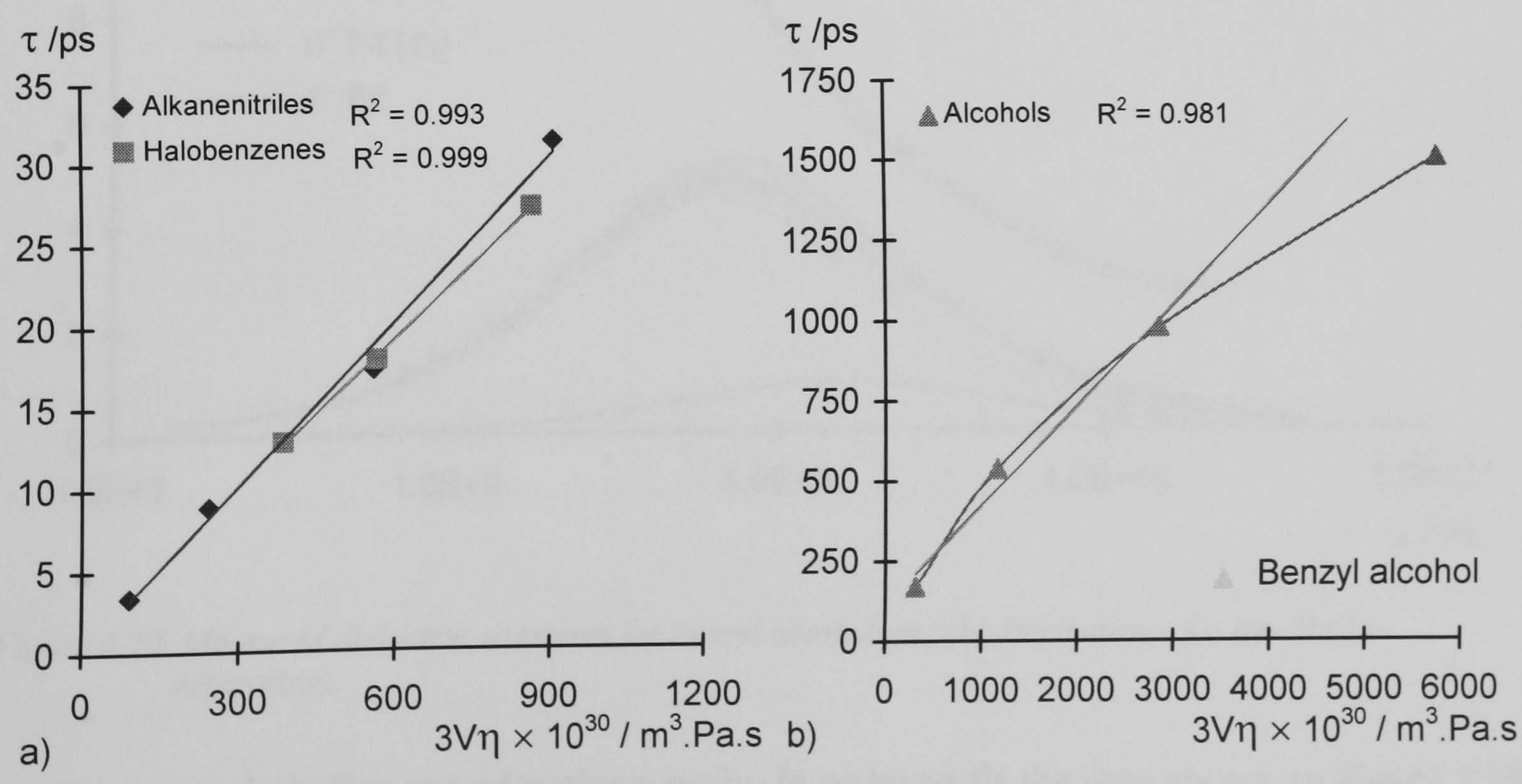


Figure 4.9. Plots of relaxation time τ vs. $3V\eta$ for a) a series of alkanenitriles and a series of halobenzenes; b) a series of alcohols.

Also shown on the graph are the values for octanol and benzyl alcohol which do not conform to the equation at all well. An initial explanation for this discrepancy could be that a secondary relaxation process involving the hydroxyl group only is distorting the data. It is possible to fit the dielectric data for benzyl alcohol to a curve with two Debye relaxation processes, this is shown in Figure 4.10. The secondary relaxation is at 34 ps and the adjusted primary relaxation is 247 ps. Although this results in a higher value for the primary relaxation time, in order to fit this to equation (5) a relaxation time of 1203 ps is required. This corresponds to a relaxation frequency of 0.132 GHz, a value that can in no way be extrapolated from the measured data.

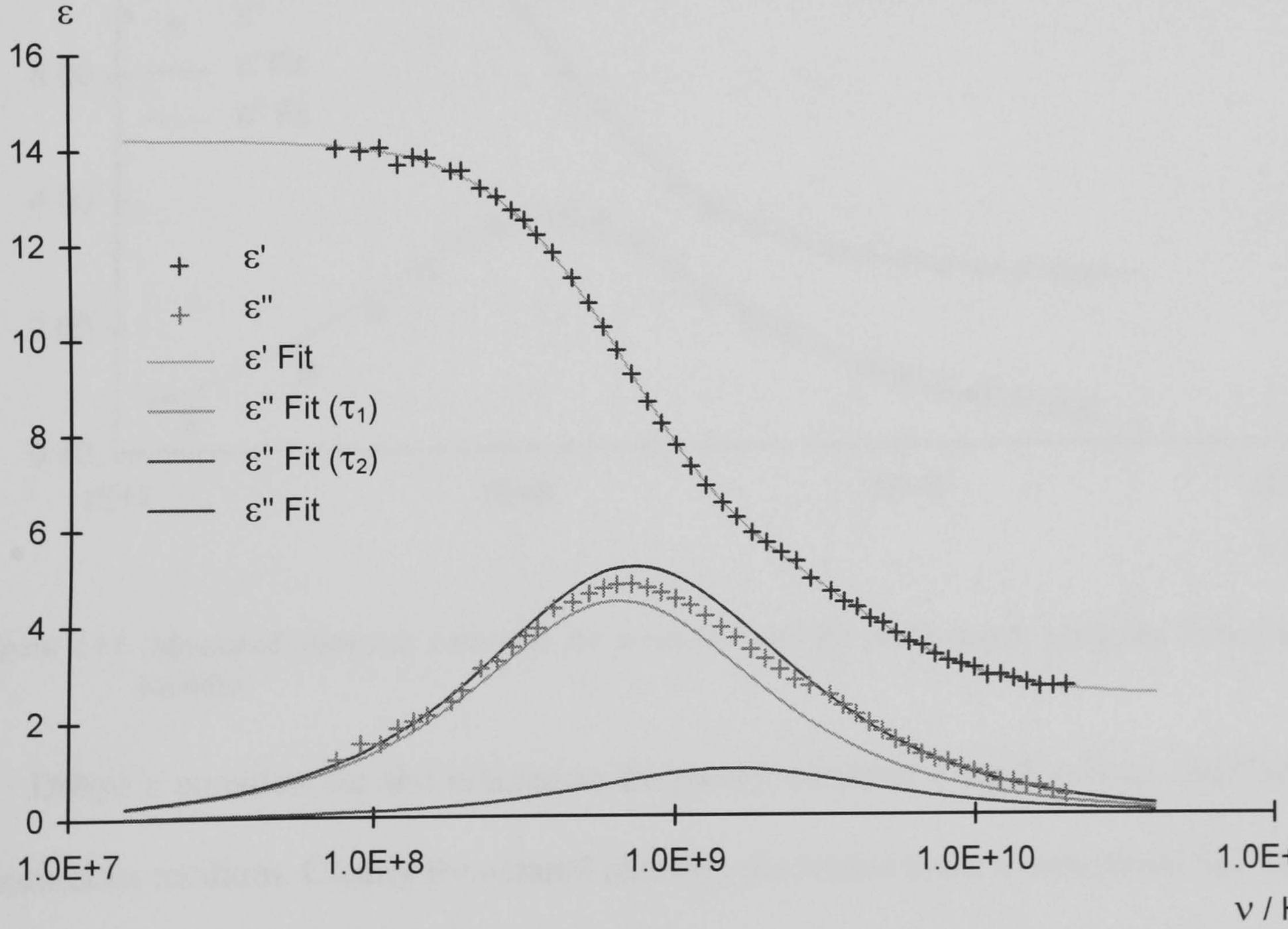


Figure 4.10. Measured dielectric constants for benzyl alcohol and the fitted curves for two Debye relaxations.

For octanol similar considerations apply. In order to fit the data shown in Figure 4.9b to Eqn. (5) a relaxation time of 1900 ps, with a corresponding relaxation frequency of

0.084 GHz is required. It has not been possible to fit a curve for two Debye relaxations to the octanol data, shown in Figure 4.11. Our best fit is achieved using the Cole-Davidson equation, with a relaxation time of 1500 ps and a β value of 0.90. Visual examination of the data reveals that, in any case. any second relaxation frequency would be at a higher value than the observed 0.11 GHz.

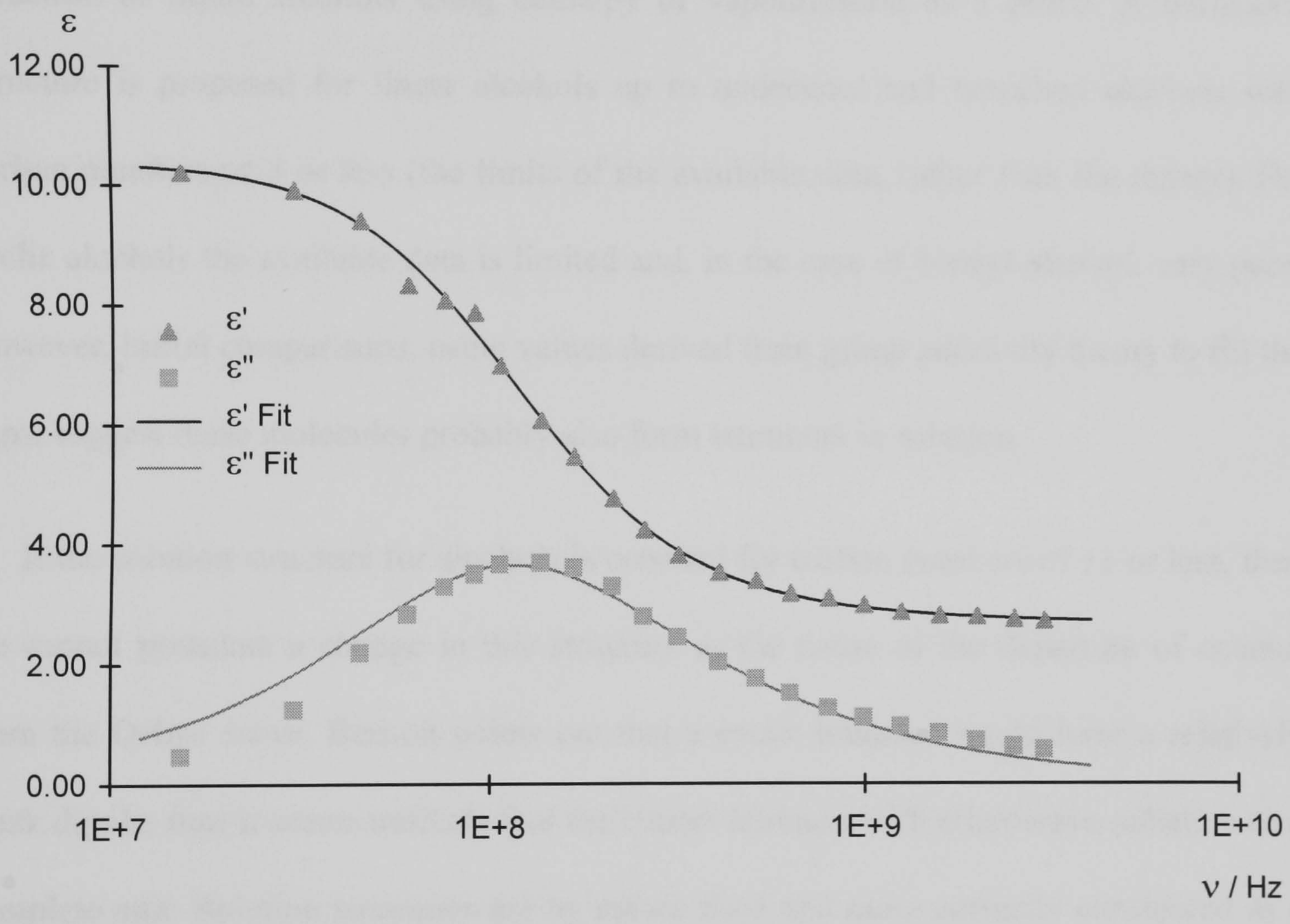


Figure 4.11. Measured dielectric constants for n-octanol and the fitted curves using the Cole-Davidson equation

Debye's equation for the relaxation frequency assumes a rigid sphere, rotating in a continuous medium. Clearly for octanol and benzyl alcohol these assumptions fail but it is hard to see exactly why: If the cause is departure from a spherical shape why does octanenitrile not depart from the curve in a manner similar to octanol ? Why does benzyl alcohol and not the halobenzenes (for benzyl alcohol to lie on a straight line with the

halobenzenes a relaxation time of 107 ps is required). A hydrogen bonding effect seems the most likely cause of the discrepancies.

Alcohols are believed to form 3-dimensional polymers in solution: most of the thermodynamic data favours tetramers (the smallest unstrained polymer), whilst there is some evidence of hexamers from X-ray diffraction studies.[34] Benson[35] has examined the structure of liquid alcohols using enthalpy of vapourisation as a probe. A tetrameric structure is proposed for linear alcohols up to undecanol and branched alcohols with carbon numbers of 5 or less (the limits of the available data, rather than the theory). For cyclic alcohols the available data is limited and, in the case of benzyl alcohol, very poor. However, initial comparisons, using values derived from group additivity theory to fill the gaps, suggest these molecules probably also form tetramers in solution.

If the solution structure for alcohols is constant for carbon numbers of 11 or less, then we cannot postulate a change in this structure as the cause of the departure of octanol from the Debye curve. Benson points out that a cyclic tetramer would have a relatively weak dipole; thus it seems unlikely that the cluster interacts with microwave radiation as a complete unit. Solution structures are by nature fluid and more correctly considered as a time averaged picture. Nonetheless they are more than a conceptual tool; thermodynamic considerations suggest that less than 1 % of a liquid alcohol can be considered as a monomer.

In summary, examination of a series of linear alcohols and alkanenitriles and halobenzenes have shown that Debye's equation for relaxation times gives a linear plot for alkanenitriles, halobenzenes and the early alcohols. Furthermore the early alcohols

follow a gradient of approximately $4\pi/kT$. *n*-Octanol and benzyl alcohol cannot be fitted to these curves. Thermodynamic data suggests that the equilibrium solution structure of octanol and benzyl alcohol should be similar to that of the short chain alcohols. These solution clusters are predicted to have minimal dipoles and thus are unlikely to be involved in the interaction with microwave radiation as complete units. It is possible that the perturbation of the equilibrium structure by microwave radiation does not follow a linear trend as organic chain length increases.

4.6. Heating Rates

In previous sections we have examined the relaxation times and values for tan δ at 2.45 GHz for a variety of solvents, according to the accepted principle that high values of tan δ should give good dielectric heating rates. Here we examine this principle in detail.

In order to gain a fuller understanding of the relationship between the dielectric parameters and the observed heating rates we considered three series of organic solvents, linear alcohols, linear alkanenitriles and halobenzenes. For the alkane derived series members with carbon numbers 2, 4, 6 and 8 were used, in the halobenzene series chlorine to iodine substituents were used. The particular choice of compounds examined was influenced partly by the availability of data for the entire series (only octanol had not been previously reported) and also the fact that the initial members of each series have regularly been used as solvents for synthesis using dielectric heating in our laboratories.

Metaxas and Meredith[8] have discussed the technical aspect of microwave heating; the efficiency of conversion of microwave energy into heat depends on the dielectric and thermal properties of the material. The fundamental relationship is;

$$\begin{aligned} P &= \sigma|E|^2 \\ &= (\omega\varepsilon_0\varepsilon'')|E|^2 \\ &= (\omega\varepsilon_0\varepsilon' \tan\delta)|E|^2 \end{aligned} \qquad (12)$$

where P is the power dissipated per unit volume of a material with conductivity σ. The electric field in the sample is E and ω is the angular frequency.

Assuming negligible heat loss and diffusion, the rate of heating or temperature rise ΔT in a time interval *t* can be expressed as;

$$\begin{aligned} \frac{\Delta T}{t} &= \frac{\sigma|E|^2}{\rho C} \\ &= \frac{\omega\varepsilon_0\varepsilon''}{\rho C}|E|^2 \\ &= \frac{\omega\varepsilon_0\varepsilon' \tan\delta}{\rho C}|E|^2 \end{aligned} \qquad (13)$$

where ρ is the density and C the specific heat capacity.

In practice the electric field strength is dictated by the characteristic shape and dimensions of the cavity, and the field strength within the material is neither known or constant. Moreover the value of *E* is itself strongly dependent on the dielectric properties of the material. Therefore a rigorous numerical analysis is necessary to establish the distribution of the electric field in the cavity and within the sample. This situation has been examined by Dibben and Metaxas.[36]

In our experiments solvents were heated for 30 seconds at 25 % power, using the MDS-2000 oven and CEM LDV's. Two series of experiments were run; one at constant

volume and one at a constant number of moles of sample. The heating rate was monitored using the oven's internal thermometer which was connected to a printer. Some simple experiments, conducted by dipping the probe alternately into beakers of hot and cold water, established a lag in its response of the order of 5 seconds. Consequently the samples were monitored for an additional 10 seconds after heating had concluded and the highest observed temperature recorded.

Table 4.10. Data from the dielectric heating experiments for a range of alcohols.

Compound	ethanol	n-butanol	n-hexanol	n-octanol
tan δ	0.94	0.57	0.34	0.23
ε'	8.00	4.02	3.43	2.77
ε''	7.27	2.30	1.17	0.62
ρ / g cm^{-3}	0.785[37]	0.810[37]	0.814[37]	0.827[37]
Cp_{298} / J K^{-1} mol^{-1}	112.3[38]	177.2[38]	240.4[38]	304.7[39]
Experiments using samples of constant volume				
Sample mass / g	15.2	15.7	15.6	15.4
Sample volume / cm^3	19.3	19.4	19.1	18.7
Moles of sample / mol	0.33	0.21	0.15	0.12
ΔT / K	51	47	40	29
E_{abs} / kJ	1.88	1.77	1.48	1.06
P_{abs} / W	62.8	59.0	49.2	35.4
Experiments using samples with a constant number of moles				
Sample mass / g	15.2	24.2	34.3	44.3
Sample volume / cm^3	19.3	29.8	42.1	53.6
Moles of sample / mol	0.33	0.33	0.34	0.34
ΔT / K	51	32	21	16
E_{abs} / kJ	1.88	1.86	1.66	1.62
P_{abs} / W	62.8	62.0	55.2	54.1

Table 4.10 summarises the data obtained for the alcohols. All the dielectric parameters fall as the series is traversed and the observed temperature rise reflects this. The density rises very slightly across the series. The heat capacity rises evenly, with respect to the relative molecular mass.

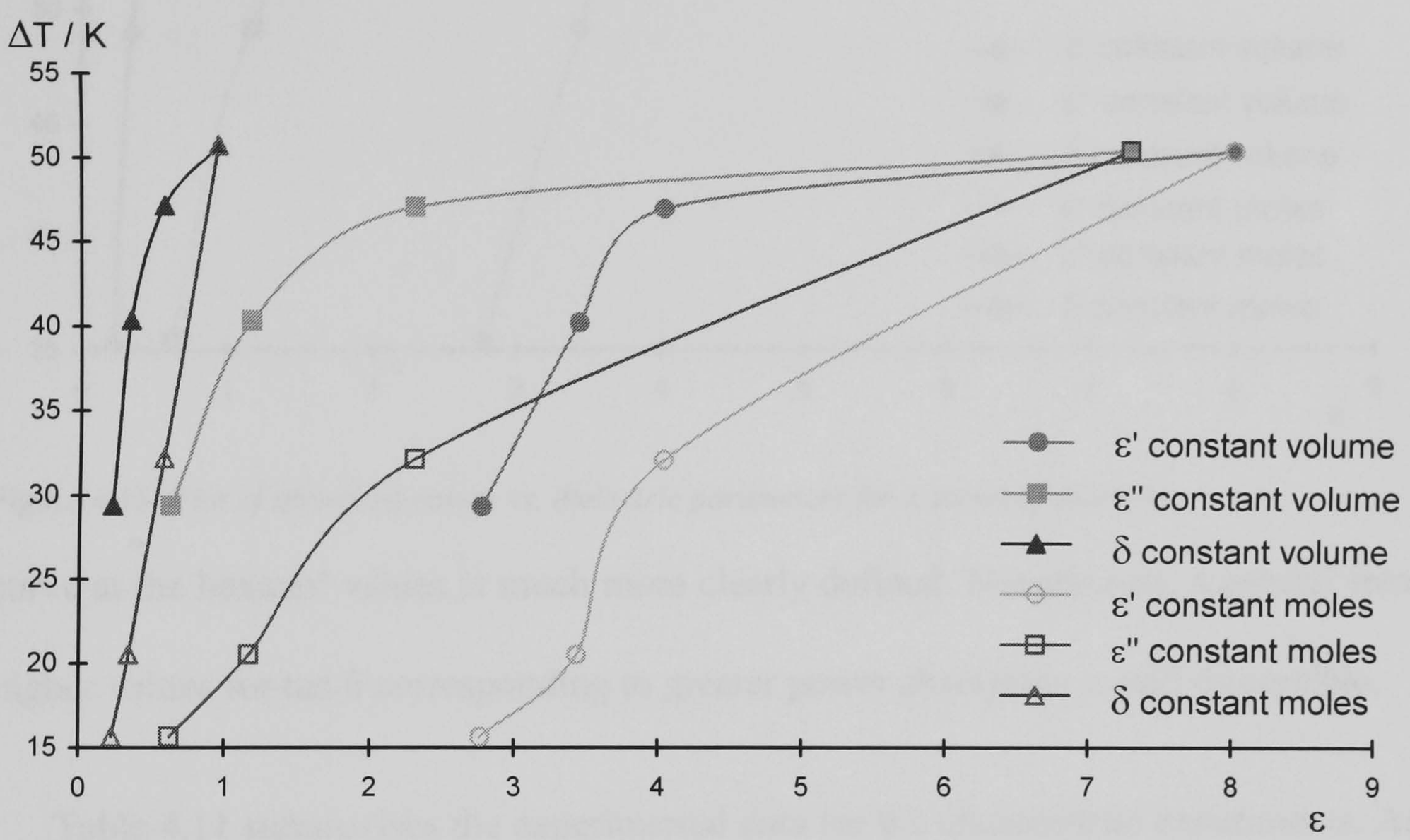


Figure 4.12. Plot of observed temperature rise vs. dielectric parameters for a series of alcohols

Figure 4.12 shows the observed temperature rise plotted against the dielectric parameters. A general correlation between the value of the dielectric parameter and the temperature rise can be seen. For the experiments using a constant number of moles of sample, this variation is approximately linear.

Figure 4.13 shows the power absorbed by the alcohols, plotted against the dielectric parameters. The pattern broadly follows that seen in the temperature rise data, although some aspects are reversed: The constant mole samples show a narrower range of values for absorbed power but a wider range of temperature rise. The deviation from a simple

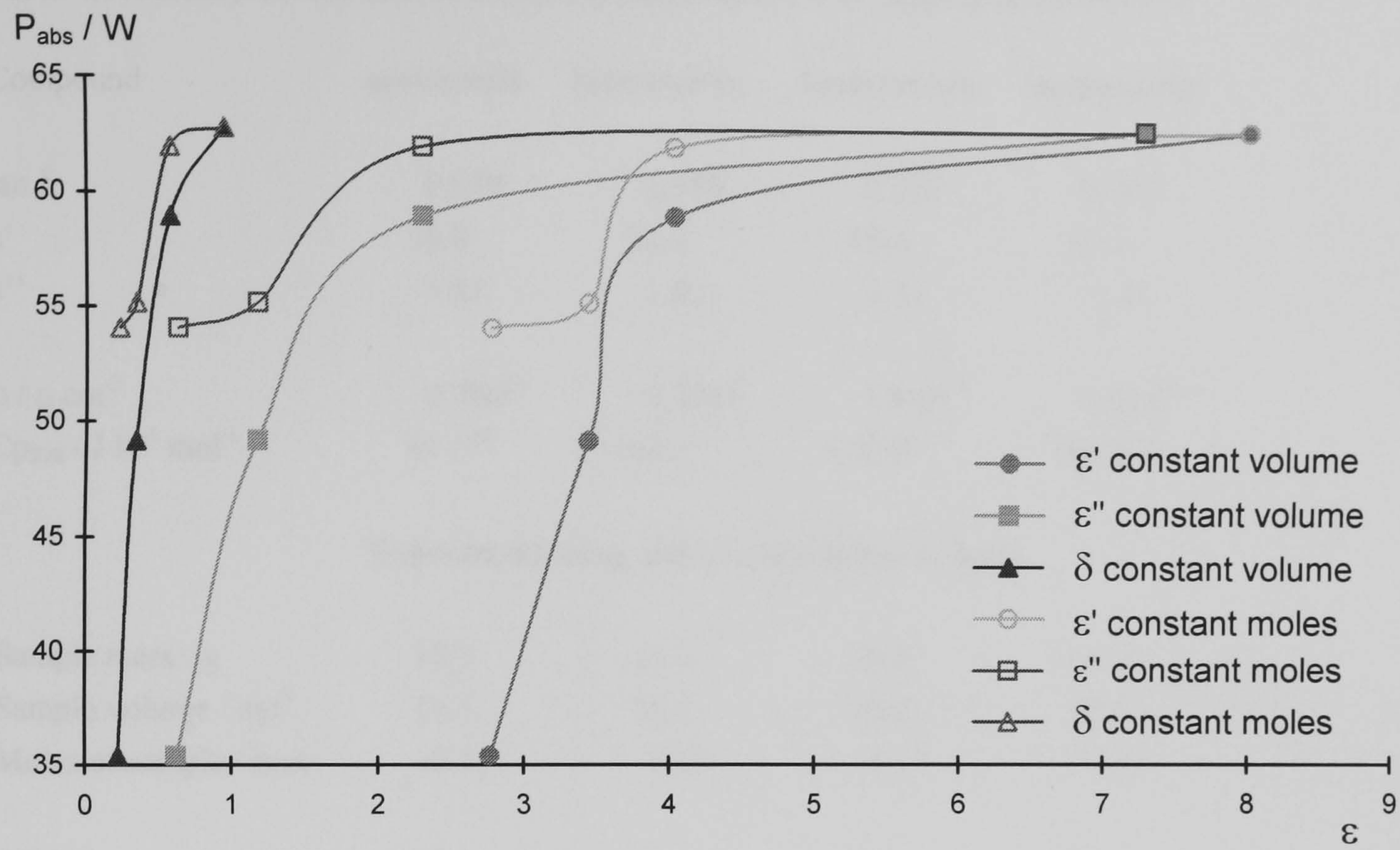


Figure 4.13. Plot of absorbed power vs. dielectric parameters for a series of alcohols

curve at the hexanol values is much more clearly defined. Nonetheless, a general trend of higher values for tan δ corresponding to greater power absorption is still discernible.

Table 4.11 summarises the experimental data for the alkanenitrile experiments. As the carbon number increases the thermodynamic parameters vary in a manner similar to that of the alcohols, indeed the actual values for density and heat capacity are not very different. The dielectric parameters present a very different picture; tan δ and ε'' rise with increasing chain length, whereas ε' falls.

Table 4.11. Data from the dielectric heating experiments for a range of alkanenitriles.

Compound	acetonitrile	butanenitrile	hexanenitrile	octanenitrile
tan δ	0.049	0.119	0.215	0.343
ε'	36.8	21.6	15.4	11.1
ε''	1.81	2.58	3.30	3..81
ρ / g cm^{-3}	0.786[37]	0.794[37]	0.809[37]	0.814[37]
Cp_{298} / J K^{-1} mol^{-1}	91.5[40]	160.1[a]	223.9[a]	287.7[41]
Experiments using samples of constant volume				
Sample mass / g	15.2	15.6	16.7	15.9
Sample volume / cm^3	19.3	19.6	20.2	19.5
Moles of sample / mol	0.37	0.23	0.17	0.13
ΔT / K	28	41	47	50
E_{abs} / kJ	1.60	2.11	2.40	2.40
P_{abs} / W	39.9	52.9	60.1	60.1
Experiments using samples with a constant number of moles				
Sample mass / g	15.2	25.5	37.3	46.8
Sample volume / cm^3	19.3	32.1	46.1	57.5
Moles of sample / mol	0.37	0.37	0.38	0.37
ΔT / K	28	24	21	16
E_{abs} / kJ	1.60	2.43	2.79	2.57
P_{abs} / W	39.9	60.8	69.8	64.5

a) No literature data available. Interpolated values.

Figure 4.14. plots the observed temperature rise against the dielectric parameters for the alkanenitriles. The picture here is more complex than seen in the alcohol series. For the constant volume samples ΔT increases as tan δ and the loss tangent increase whilst for the constant mole samples ΔT falls. This pattern is inverted for the dielectric constant, ε'.

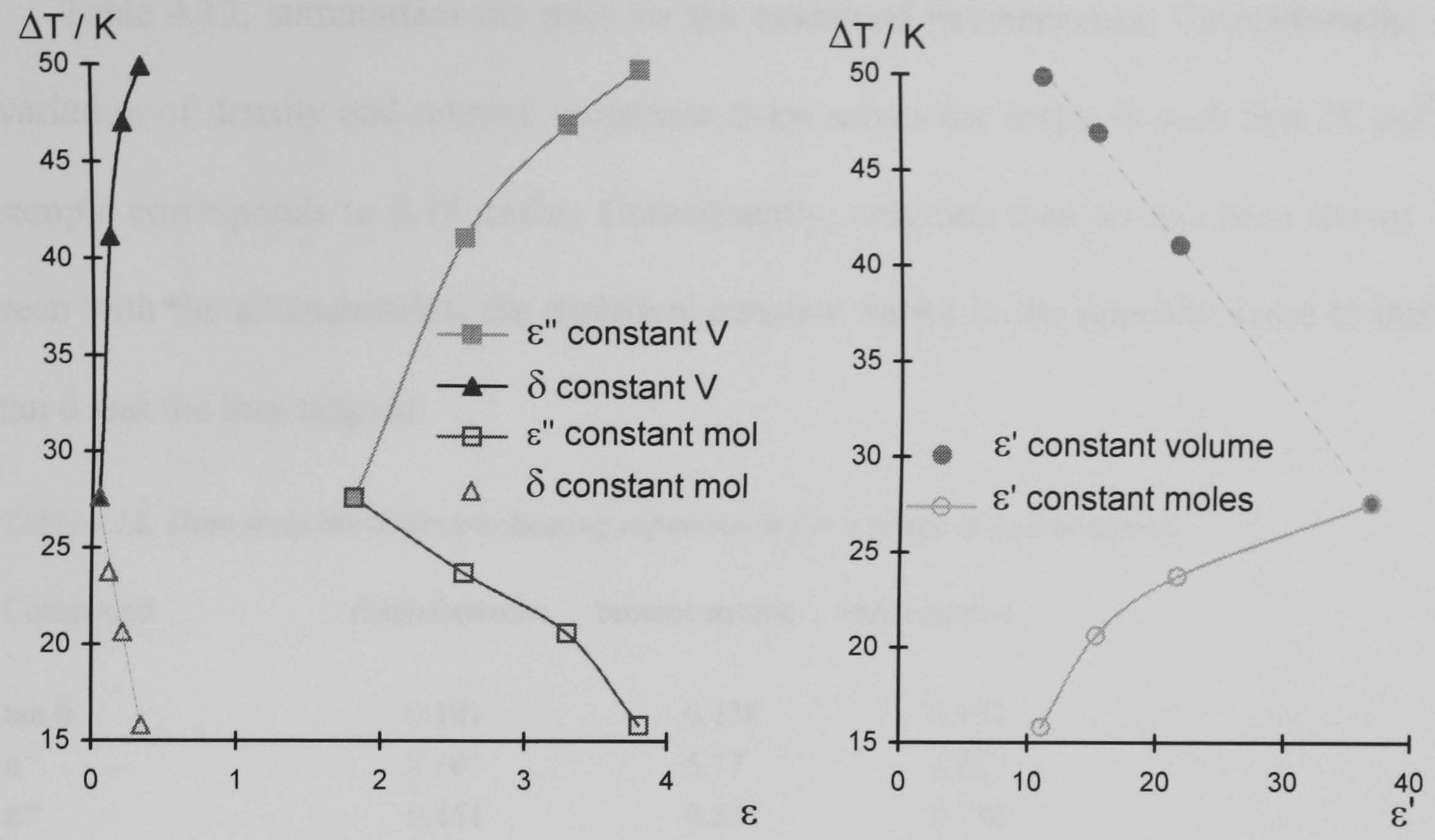


Figure 4.14. Plot of observed temperature rise vs. dielectric parameters for a series of alkanenitriles

In Figure 4.15 the absorbed power has been plotted against the dielectric constants for a series of alkanenitriles. Both data sets (for constant volume or constant moles) show a similar pattern of power absorption, with a maximum value at hexanenitrile. More energy is absorbed in the constant mole data set, despite the lower temperature rises.

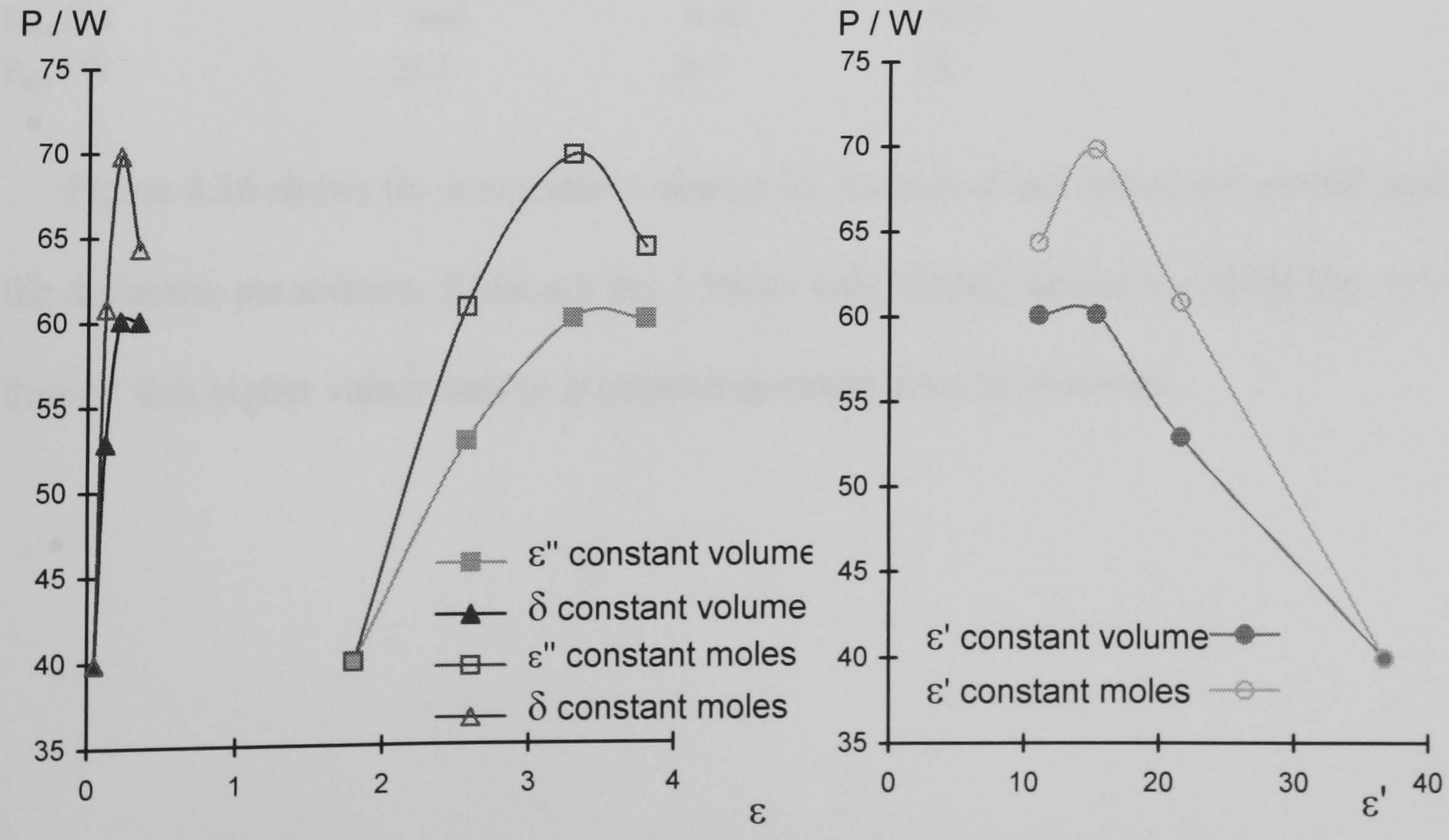


Figure 4.15. Plot of absorbed power vs. dielectric parameters for a series of alkanenitriles

Table 4.12. summarises the data for the examined halobenzenes. Coincidentally, the variation of density and relative molecular mass across the series is such that 20 cm^3 of sample corresponds to 0.18 moles. Consequently, only one data set has been shown. As seen with the alkanenitriles, the dielectric constant varies in the opposite sense to that of tan δ and the loss tangent.

Table 4.12. Data from the dielectric heating experiments for a range of halobenzenes.

Compound	chlorobenzene	bromobenzene	iodobenzene
tan δ	0.101	0.138	0.157
ε'	6.16	5.77	4.82
ε''	0.651	0.835	0.786
ρ / g cm^{-3}	1.11[37]	1.49[37]	1.87[37]
Cp_{298} / J K^{-1} mol^{-1}	150.1[38]	154.3[38]	158.7[38]
Sample mass / g	21.4	28.9	37.4
Sample volume / cm^3	19.4	19.4	20.0
Moles of sample / mol	0.19	0.18	0.18
ΔT / K	24	28	29
E_{abs} / kJ	0.69	0.80	0.84
P_{abs} / W	23.1	26.7	28.1

Figure 4.16 shows the temperature change for a series of halobenzenes, plotted against the dielectric parameters. Although tan δ varies only slightly across the series the 'rule of thumb' that higher values lead to greater temperature rises is observed.

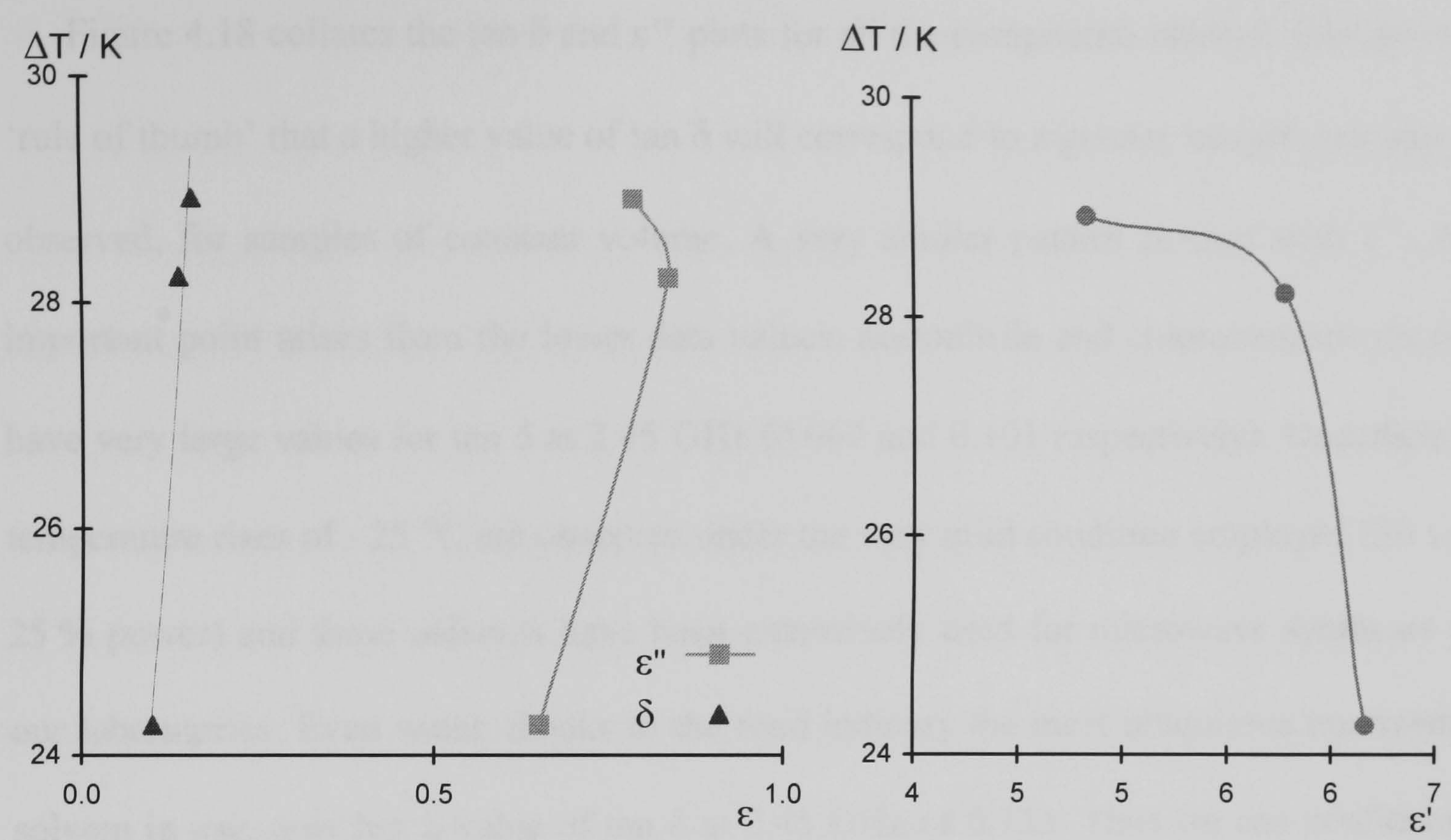


Figure 4.16. Plot of temperature rise vs. dielectric parameters for a series of halobenzenes

The data for power absorption by the halobenzene series, shown in Figure 4.17, follows the same pattern as that for the temperature change, indeed the values are very similar. The data series remains non-linear if a logarithmic scale is used.

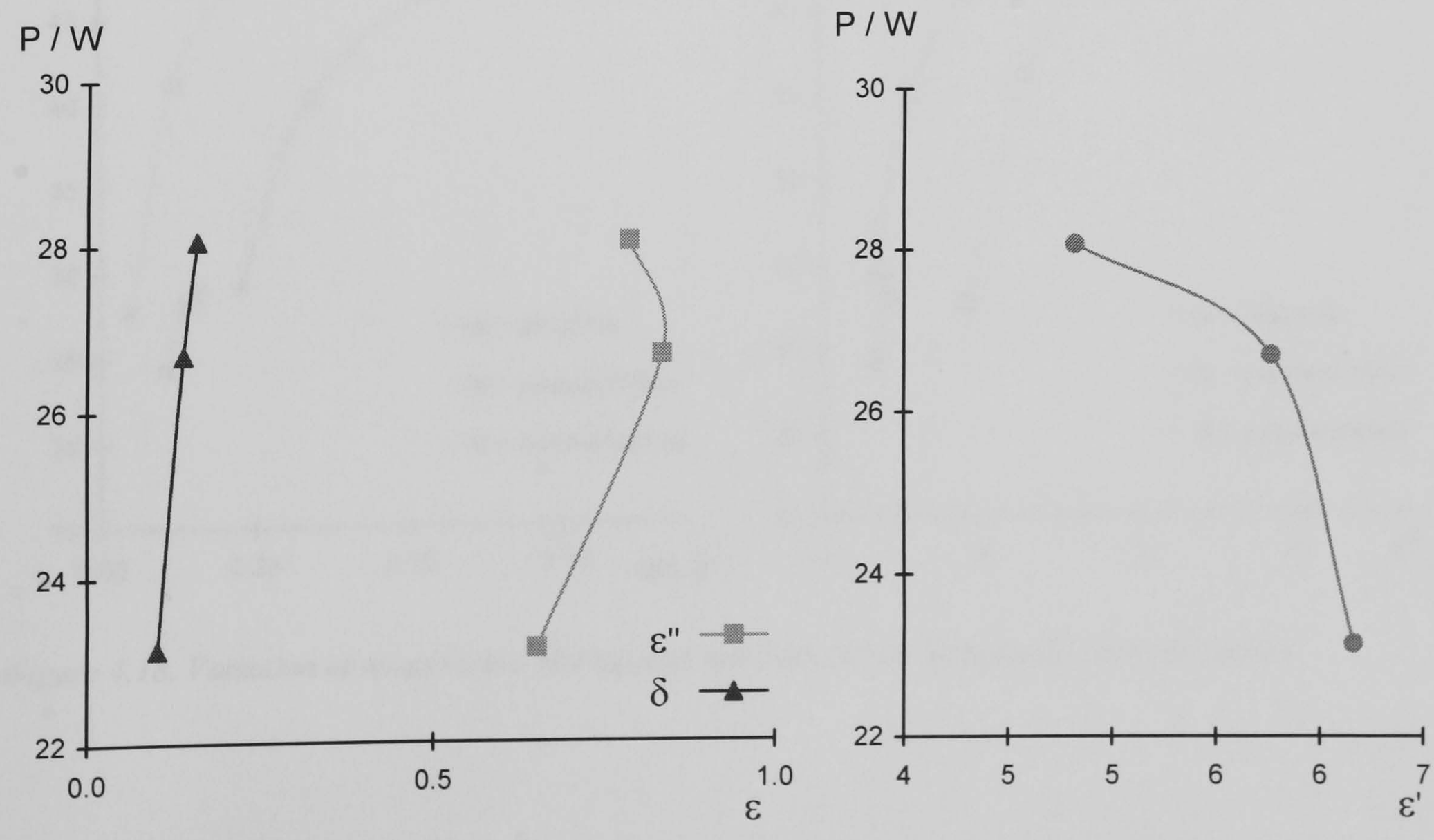


Figure 4.17. Plot of absorbed power vs. dielectric parameters for a series of halobenzenes

Figure 4.18 collates the tan δ and ε'' plots for all the compounds studied. Our general 'rule of thumb' that a higher value of tan δ will correspond to a greater temperature rise is observed, for samples of constant volume. A very similar pattern is seen with ε''. An important point arises from the lower data values; acetonitrile and chlorobenzene do not have very large values for tan δ at 2.45 GHz (0.062 and 0.101 respectively). Nonetheless temperature rises of ~25 °C are observed under the very mild condition employed (30 s at 25 % power) and these solvents have been extensively used for microwave syntheses in our laboratories. Even water, thanks to the food industry the most ubiquitous microwave solvent in use, only has a value of tan δ at 2.45 GHz of 0.123. Thus we can confidently suggest any solvent with a tan δ of greater than 0.1 at 2.45 GHz may be used as a potential solvent for syntheses using microwave dielectric heating.

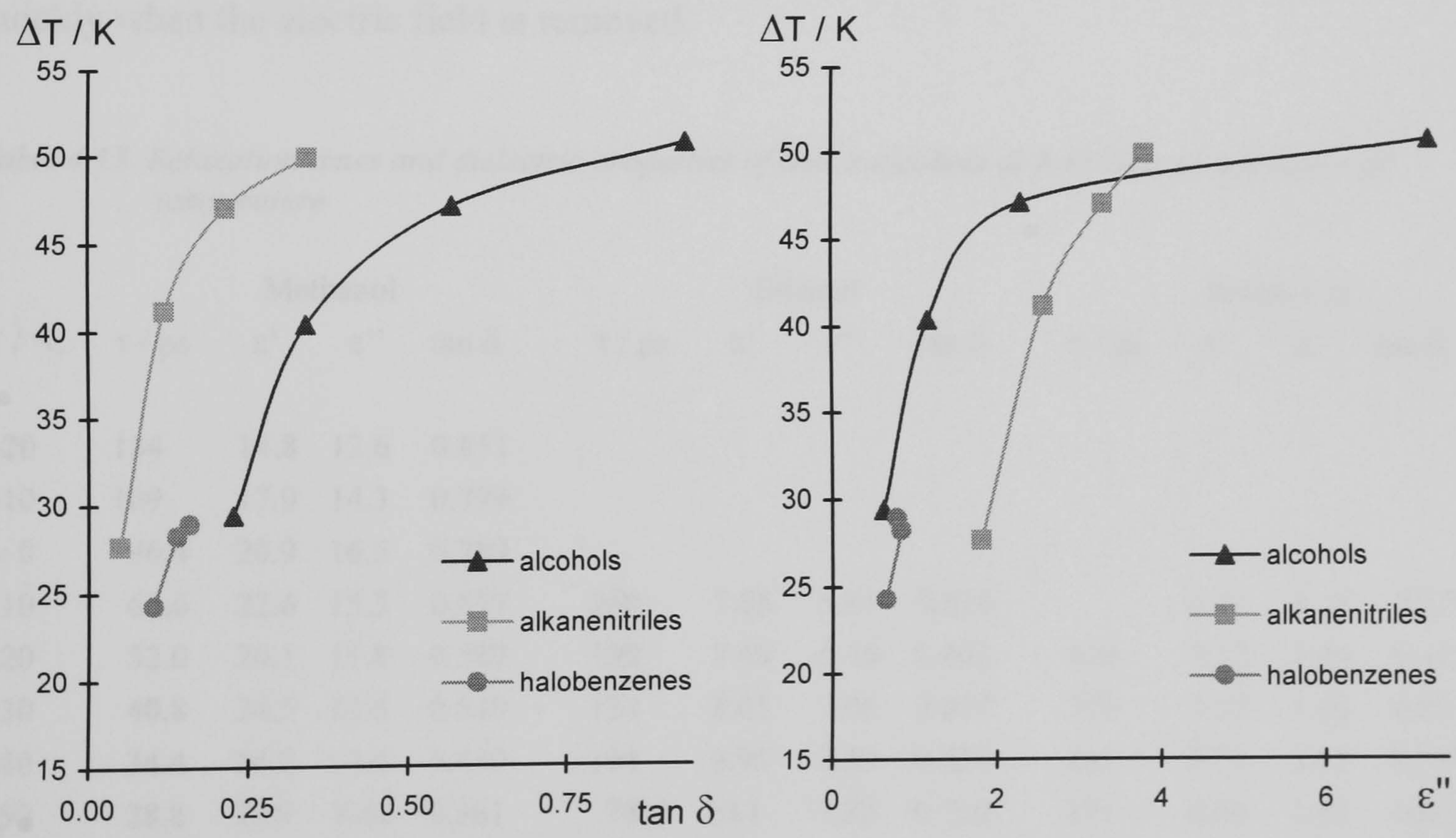


Figure 4.18. Variation of temperature rise against tan δ and ε'' for samples of constant volume

4.7. Temperature dependence

The analysis of heating rates in Section 4.6. has been simplified by ignoring both the effects of temperature dependence and the complex interaction between the electric field and the sample. Whilst this approach has collected useful evidence for the use of tan δ to estimate a solvent's effectiveness in dielectric heating it has also indicated the complexity of the relationships between the dielectric and thermodynamic parameters for solvents. As all these parameters are temperature dependent a full analysis of dielectric heating is highly complex. In this analysis we shall simply examine the available data for the temperature dependence of the dielectric parameters.

The relaxation time of a solvent decreases as the temperature increases, *i.e.* the larger translational motions of the molecules enable them to randomise their position more quickly when the electric field is removed.

Table 4.13. Relaxation times and dielectric properties of linear alcohols at 2.45 GHz as a function of temperature

	Methanol				Ethanol				Butan-1-ol			
T / °C	τ / ps	ε'	ε''	tan δ	τ / ps	ε'	ε''	tan δ	τ / ps	ε'	ε''	tan δ
-20	134	14.8	12.6	0.851								
-10	109	17.9	14.3	0.799								
0	96.4	20.9	16.5	0.789								
10	62.6	22.6	15.3	0.677	269	7.05	5.81	0.824		4.22	1.16	0.275
20	52.0	20.1	11.8	0.587	199	7.49	6.46	0.862	419	3.52	1.45	0.412
30	40.8	24.5	12.5	0.510	134	8.05	7.06	0.877	370	3.55	1.80	0.507
40	34.4	24.2	10.4	0.430	104	8.95	7.39	0.826	231	3.71	2.22	0.598
50	28.8	23.9	8.62	0.361	78.4	10.1	7.28	0.720	171	4.04	2.63	0.651
60	26.6	19.4	6.10	0.314	55.2	11.2	6.76	0.606	121	4.47	2.88	0.644
70					48.8	11.7	6.35	0.542	80.8	5.03	2.92	0.581
80									56.6	5.50	2.67	0.485
90									40.8	5.75	2.28	0.397
100									29.8	5.83	1.77	0.304
110									24.4	5.73	1.33	0.232

Table 4.13 gives some values for the temperature variation of the dielectric parameters for some linear alcohols and the ε'' spectra for ethanol and butanol is shown in Figure 4.19. The spectra clearly show the reduction in τ as the temperature is raised. However the temperature variation of tan δ, dependent as it is on the absolute values of ε' and ε'', is more complex. For methanol the value at 2.45 GHz falls as the temperature is increased whilst for ethanol and butanol tan δ rises and then falls, peaking at ~30 and 50 °C respectively. The temperature at which the relaxation time falls below 65 ps, the inverse of the applied frequency does not obviously have any bearing upon the tan δ values.

For some compounds the ability to absorb microwave energy can increase very rapidly with temperature. For these compounds *thermal runaway* is seen; at a certain value the rate of temperature increase can become exponential. Our data indicates that this is not the case with the alcohols examined but it is known to be a problem for some solids.

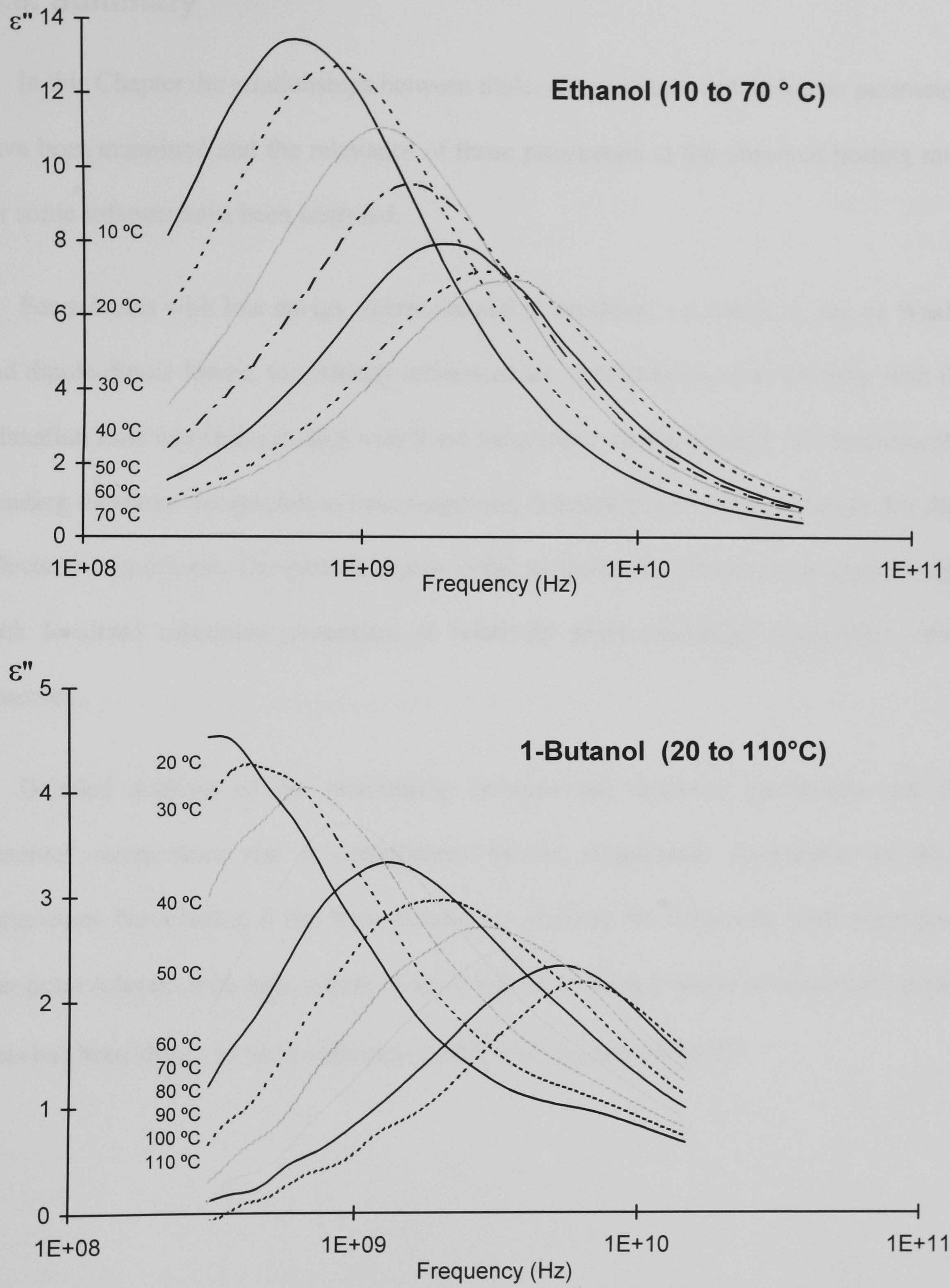


Figure 4.19. Variation of the loss factor as a function of temperature

4.8. Summary

In this Chapter the relationships between molecular structure and dielectric parameters have been examined and the relevance of those parameters to the observed heating rates for some solvents have been analysed.

For solvents with low energy intermolecular interactions, *i.e.* based on van de Waals' and dipole-dipole forces, the primary influences are molecular size and viscosity with the relaxation time increasing in step with these parameters. As the strength of intermolecular bonding increases the relaxation time lengthens; dramatically so when hydrogen bonding effects are significant. The pattern begins to fail as molecules become very large or rigid with localised relaxation processes, at relatively short relaxation times, also being observed.

Detailed analysis of the relationship between the dielectric parameters and the observed temperature rise is complicated by the temperature dependence of those parameters. Nonetheless it has been possible to evaluate the frequently used assumption that polar solvents with high values of tan δ will heat strongly within a microwave cavity. This has been shown to be broadly true, when tan δ is greater than 0.1.

4.9. Experimental

Measurement of dielectric parameters

Samples were purchased from Aldrich and dried over molecular sieves prior to measurement. The measurements for *n*-octanol, dimethylformamide, ethyl acetate, acetone, 2-butanol, tetrahydrofuran, nitromethane, dichloromethane, chloroform, 1,2-dichloroethane and 1,1,2-trichloroethane between 300 kHz and 3 GHz were performed at Imperial college, using a Hewlett Packard 8752A Network Analyser and impedance probe. Other samples and measurements between 130 MHz and 20 GHz were performed by S. Gabriel at King's college London, using an HP 8720 Network Analyser and a custom built probe.[42]

The data was fitted using the program Grafit, written by R.L Leatherbarrow of Imperial college. A non-linear regression analysis was used, with values for the initial data estimated by graphical examination. Initial fits compared a single relaxation using the Debye, Cole-Cole and Cole-Davidson equations and taking χ^2 (the sum of the squares deviation of the calculated minus experimental values) as a measure of fit accuracy. For some samples the high frequency limit (ε_∞) lies beyond the measured data. In these cases it was necessary to hold ε_∞ constant, using the square of the refractive index as an estimated value.

Evaluation of the lag in temperature measurement for the CEM MDS-2000 oven

The MDS-2000 temperature probe is separated from the sample by a Teflon coated Pyrex sheath. Although this is fairly thin some lag in temperature measurement is still observed. A qualitative estimate of this lag was made by inserting the probe and sheath into a beaker of water, whose temperature was also monitored using a thermocouple. For water with an initial temperature of 45 °C 5 s passed before the MDS probe and thermocouple agreed.

Measurement of heating rates

Samples were purchased from Aldrich and dried over molecular sieves prior to use. After sealing in a CEM LDV the samples were heated in the MDS-2000 microwave oven. The temperature was monitored by the built-in fibreoptic probe and the results output to a printer. To ensure clear identification of the initial temperature a 10 s stage at 0 % power was added before the heating stage (30 s at 25 % power). In order to allow for the delay in temperature measurement due to the thermometer's Pyrex sheath a 30 s at 0 % power was added after heating. The temperature at the end of stage one was recorded as the initial temperature and the highest temperature was recorded as the final temperature.

Reproducibility using this method was high; ΔT for different samples varied only by $\pm$ 1 °C

4.10. References

1 C. Gabriel, S. Gabriel, E.H. Grant, B.S.J. Halstead and D.M.P. Mingos, *Chem. Soc. Rev.*, **27** (1998) 213

2 A.R. von Hippel, *Dielectric and Waves*, MIT Press, Massachusetts Institute of Technology, Cambridge Mass. USA, 1954

3 C. Gabriel, S. Gabriel and E. Courtout, *Phys. Med. Biol.*, **41** (1996) 2231

4 E.H. Grant, R.J. Sheppard and G.P. South, *Dielectric Behaviour of Biological Molecules in Solution*, Clarendon Press, Oxford, UK, 1978

5 D.Q.M. Craig, *Dielectric Analysis of Pharmaceutical Systems*, Taylor and Francis, London, UK, 1995

6 D.M.P. Mingos and D.R. Baghurst, *Chem. Soc. Rev.* **20**, (1991) 1; and references therein

7 N.E. Hill, W.E. Vaughan, A.H. Price and M. Davies, *Dielectric Properties and Molecular Behaviour*, van Nostrand, New York 1969

8 A.C. Metaxas and R.J. Meredith, *Industrial Microwave Heating*, Peter Peregrinces, Institution of Electrical Engineers, Essex, 1982

9 P. Hanks, *Collins Dictionary of the English Language,* 2nd ed., William Collins Son and Co. Ltd. Glasgow, (1986)

10 P. Debye, *Phys. Zs.*, **36** (1935) 100

11 K.S. Cole and R.H. Cole, *J. Chem. Phys.* **9** (1941) 341

12 D.W. Davidson and R.H. Cole, *J. Chem. Phys.* **19** (1951) 1484

13 J.B. Hasted, *Aqueous Dilectrics*, Chapman and Hall, London, UK, 1973

14 M. Davies, *Some Electrical and Optical Aspects of Molecular Behaviour*, Commonwealth and International Library of Science, Technology and Liberal Studies, Pergamon Press, Oxford, 1962

15 J.G. Kirkwood, *J. Chem. Phys.* **7** (1939) 911

16 G. Mjetich and K. Whelass, p 455; D.R. Baghurst and D.M.P. Mingos, p 523; *Microwave Enhanced Chemistry*, American Chemical Society, Washington DC, USA, 1997.

17 D. Bertolini, M. Cassetori, G. Salvetti, E. Tombarit and S. Veronesi, *Rev. Sci. Instrumen.* **61** (1990) 450

18 S. N. Helambe, M. P. Lokhande, A. C. Kumbharkhane and S. C. Mehrotra, *Pramana*, **45** (1995) 19

19 U. Kaatze, K. Menzel and R. Pottel, *Jnl. Phys. Chem.* **95** (1995) 324

20 S. M. Puranik, A. C. Kumbharkhane and S. C. Mehrotra, *Indian Jnl. Chem. A*, **32**, (1993) 613

21 C. Clemett and M. Davies, *Trans. Farad. Soc.* **58** (1962) 1705

22 J. K. Vij, T. Grochulski, A. Kocot and F. Hufnagel, *Mol. Phys.* **72** (1991) 353

23 A. C. Kumbharkhane, S. N. Helambe, M. P. Lokhande, S Doraiswamy and S. C. Mehrotra, *Pramana*, **46** (1995) 91

24 U. Kaatze and V. Lünnecke-Gabel, *Jnl. Mol. Liq.*, 1991, **48**, 45

25 J. Goulon, J. L. Rival, J. W. FGleming, J. Chmaberlain and G. W. Chantry, *Chem Phys Lett*, **18** (1973) 211

26 J. K. Vij, F. Hufnagel and T. Grochulksi, *Jnl. Mol. Liq.* **49** (1991) 1

27 A.C. Kumbharkhane, S.M. Puranik and S.C. Mehrotra, *J. Sol. Chem*, **21** (1991) 201

28 F. Wang, R. Pottel and U. Kaatze, *J. Phys. Chem*, **101** (1997) 922

29 H.D. Purohit and R.J. Sengwa, *J. Mol. Liq.* **47** (1990) 53

30 M. Davies and R. Meakins, *J. Chem. Phys.* **26** (1957) 1584

31 R.C. Reid, J.M. Prausnitz, B.E. Poling, *The Properties of Gases and Liquids*, 4th ed., McGraw Hill, New York (1987)

32 CRC Handbook of Thermophysical and Thermochemical Data, CRC Press (1994) 409

33 CRC Handbook of Thermophysical and Thermochemical Data, CRC Press (1994)

34 S. Sarkar and R.N. Joarder, *J. Chem. Phys.* **99** (1993) 2032;
S. Sarkar and R.N. Joarder, *J. Chem. Phys.* **100** (1994) 5118;
K.K. Karmaker, S. Sarkar and R.N. Joarder, *J. Phys. Chem.* **99** (1995) 501;

35 S.W. Benson, *J. Am. Chem. Soc.* **118** (1996) 10645

36 D.C. Dibben and A.C. Metaxas, *J. Microwave Power,* **29** (1994) 242

37 *Aldrich Chemical Catalogue*

38 *CRC Handbook of Chemistry and Physics*, 77th Ed. CRC Press, 5-26

39 *CRC Handbook of Chemistry and Physics*, 77th Ed. CRC Press, 5-14

40 *TRC Thermodynamic Tables, Non-hydrocarbons,* Texas A&M University System (1998)

41 G. Stridh, S. Sunner and C.H. Svensson, *J. Chem. Thermodynamics,* **9** (1977) 1005

42 C. Gabriel, T.Y.A. Chan and E.H. Grant, *Phys. Med. Biol.* **39** (1994) 2183

Chapter Five

Density-functional study of the di-metal decacarbonyls of group 7

5.1. Introduction

Dimanganese decacarbonyl has been considered as a prototype molecule for organometallic systems with a metal-metal single bond. Nevertheless, experimentally determined values for the metal-metal bond dissociation enthalpy span a range of 100 kJ mol^{-1}, despite several studies over the last 25 years.[1,2,3,4,5,6,7] The subject has also attracted considerable theoretical interest, recent papers using Density Functional Theory (DFT) have shown excellent agreement with the observed crystallographic geometries and favoured a value for the metal-metal bond dissociation enthalpy of the order of 115 kJ mol^{-1}.[8]

Less theoretical attention has been paid to mixed metal species of this type, despite some unusual properties. An X-ray crystal structure of $MnRe(CO)_{10}$ has a Mn-Re bond length 0.06 Å less than the mean of the homolytic metal-metal bonds.[9] As with $Mn_2(CO)_{10}$ large differences are reported for measurements of the bond dissociation enthalpy using different techniques: Ionisation potential measurements[10] have suggested a bond enthalpy 50 % greater than that of the average of the single metal compounds (Mn-Mn 94 kJ mol^{-1}, Re-Re 187 kJ mol^{-1}, Mn-Re 210 kJ mol^{-1}) whereas microcalorimetry experiments give an inverted picture, with the mixed metal bond enthalpy 15 % lower than the average (Mn-Mn 159 kJ mol^{-1}, Re-Re 187 kJ mol^{-1}, Mn-Re 145 kJ mol^{-1}).

In seeking to investigate this conundrum using modern theoretical methods limited processing power has precluded the use of relativistic core potentials. Thus we have opted to examine systems with technetium rather than rhenium, as the absence of relativistic corrections are less likely to affect the validity of the calculations for the lighter metal.

5.2. Evaluation of calculation accuracy.

GAUSSIAN basis sets of triple zeta quality are not generally available for technetium. Initial calculations using an extended core potential basis failed to minimise. Thus we have used the double zeta basis set, 3-21g*. In this section we evaluate its effectiveness by comparison with experimental data and some other calculations.

Table 5.1. Geometries for $Mn_2(CO)_{10}$

	X-ray[11]	ED[12]	3-21g*	6-311$^+$g*	Baerends *et al*[8]
rMn-Mn	2.895	2.977	2.808	2.975	3.046
rMn-C_{ax}	1.820	1.803	1.768	1.806	1.820
rMn-C_{eq}	1.859	1.876	1.818	1.855	1.870
rC_{ax}-O	1.150	1.147	1.183	1.159	1.154
rC_{eq}-O	1.140	1.147	1.180	1.156	1.151
aC_{ax}MnC_{eq}	94.88	93.40	93.25	93.29	93.60
aMnC_{eq}O	177.8	178.6	177.4	177.0	177.3

Table 5.1. summarises some calculated geometries for $Mn_2(CO)_{10}$ compared to the X-ray and electron diffraction results. Also shown are the results of a calculation by Baerends *et al*, using the ADF program[13] and a basis set comparable to 6-311$^+$g*. Not surprisingly, the more complex basis set shows better agreement with the experimental results; the most divergent bond length is that for Mn-Mn, approximately 0.1 Å (3 %) longer. The equatorial ligands show a closer fit; diverging by less than 0.02 Å. For the

smaller, 3-21g* basis the overall error is of the order of 3 % for all bond lengths. For both basis sets the divergence in bond angles is less than 2 %.

Table 5.2. shows the calculated geometry of $Tc_2(CO)_{10}$ using the 3-21g* basis. The most divergent bond length is that of the axial CO bond, which is 5% longer than the experimental value. The other parameters are within 2 % of the crystallography measurements.

Table 5.2. Geometries for $Tc_2(CO)_{10}$

	X-ray	3-21g*
rTc-Tc	3.034	2.992
$rTcC_{ax}$	1.900	1.940
$rTcC_{eq}$	2.000	1.999
rC_{ax}-O	1.205	1.183
rC_{eq}-O	1.122	1.180
$aC_{ax}TcC_{eq}$	93.75	92.88
aTcCeqO	177.45	177.77

The bond dissociation enthalpy of the metal-metal bond for these systems is calculated in two stages: first the enthalpy required to break the bond (E_e) is calculated from the comparison of the total energies for dimeric $M_2(CO)_{10}$ and two $M(CO)_5$ radical fragments, held in the geometry of the dimer. Then the energy released in the relaxation of the $M(CO)_5$ fragment (E_R) is calculated.

Table 5.3. Experimental M-M Bond Dissociation Enthalpies for $Mn_2(CO)_{10}$ in kJ mol^{-1}

EI / PES[a]	E / GP[b]	PIMS[c]	KS[d]	PAC[e]	LP[f]	HTMC[g]
171[1]	96[2]	159 ± 21[3]	> 154[4]	159 ± 21[5]	>>176[6]	159[7]

a) Electron Impact mass spectrometry in conjunction with Photoelectron Spectroscopy, b) Equilibrium studies in Gas Phase,

c) PhotoIonisation Mass Spectrometry, d) Kinetic Study, e) Photoacoustic Calorimetry, f) Laser Pyrolysis,

g) High Temperature Microcalorimetry.

Table 5.3 gives a selection of experimental estimates for the Mn-Mn bond dissociation enthalpy. The values vary between 96 and 176 kJ mol^{-1}. By comparison some calculated bond enthalpies are shown in Table 5.4. For the small basis sets the calculated value is relatively large, this can be largely attributed to the basis set superposition effect, after correction for BSSE all theoretical methods agree on a Mn-Mn bond breaking enthalpy of 112 ± 6 kJ mol^{-1}. Our calculation for the bond dissociation energy agrees less well, as a result of the larger value for the relaxation energy. This may also be attributed to basis set incompleteness; the calculations on the $Mn(CO)_5$ fragment are discussed in more detail in Section 5.4.

Table 5.4. Calculated Energy contributions to the M-M Bond Dissociation Enthalpies (D_e) for $Mn_2(CO)_{10}$ in kJ mol^{-1}

Program	GAUSSIAN, this work.		ADF 2.3, ref. 8
Basis set	$6\text{-}311^{+}g^{*}$	3-21g*	tzdf	dz[a]
E_e(Mn-Mn)	126.4	234.7	120.4	165.4
E_e(Mn-Mn) - 2 BSSE		110.4	118.4	108.8
E_R		-18.06	-2.4	-4.0
D_e		74.28	113.6	100.8

a) tzd basis for Mn

We have calculated the optimum geometry and M-M bond 'snapping' enthalpy for $M_2(CO)_{10}$ (M= Mn, Tc). By comparison with experimental data and other DFT calculations we have shown that the 3-21g* basis set gives reasonable geometries and, after correction for basis set superposition error, good bond breaking enthalpies.

5.3. Investigation of the mixed metal system

Figure 5.1. shows the optimised geometry for $MnTc(CO)_{10}$. The final structure is technically within the C_1 point group, rather than C_{4v} although the deviations from a C_{4v} structure involve only differences of 0.0001 Å in bond lengths and 0.01 ° for bond angles.

The most divergent set of values is that of the $C_{ax}MnC_{eq}$ bond angles, the other angles are an order of magnitude closer.

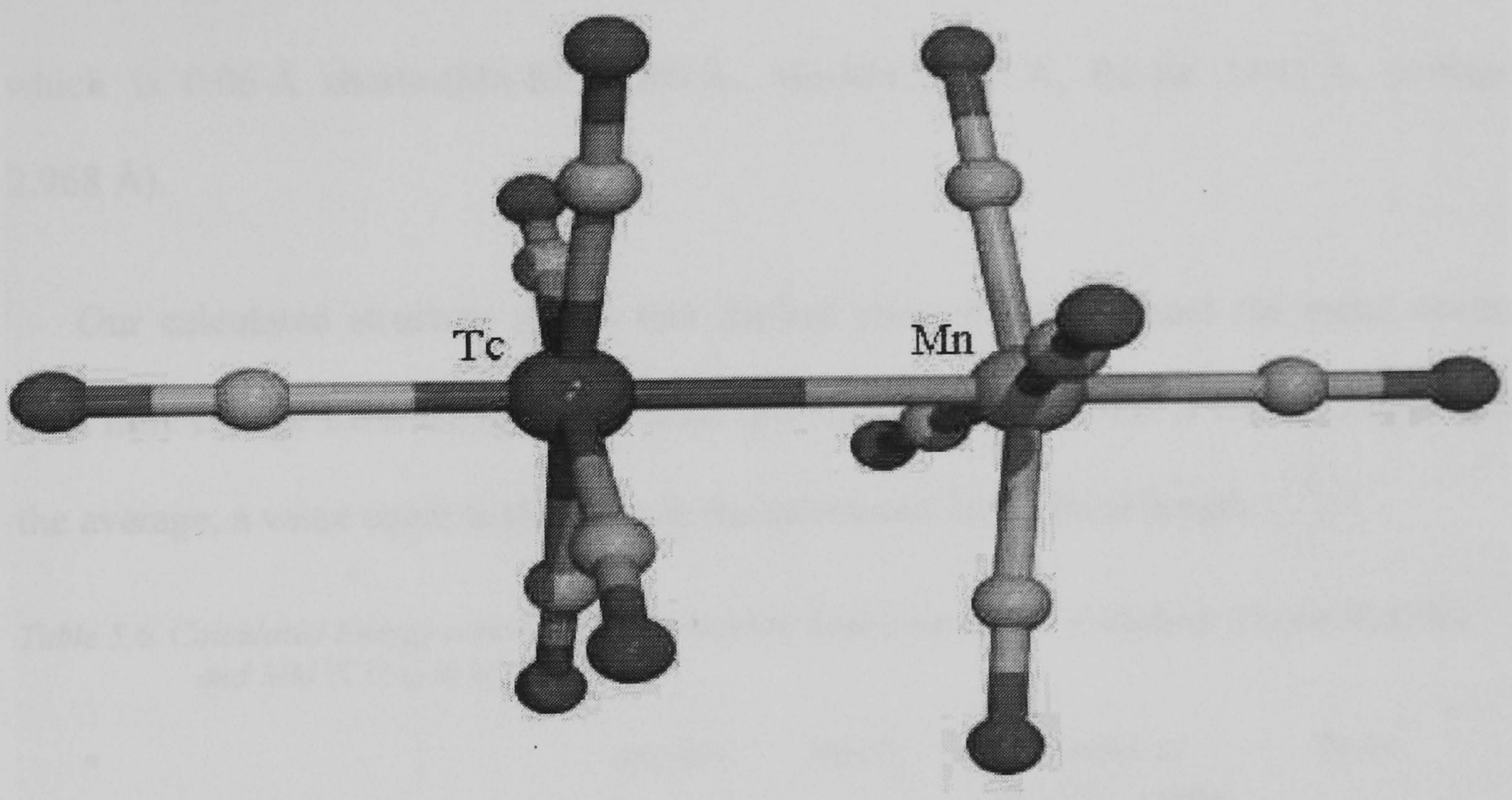


Figure 5.1. Optimised geometry for $MnTc(CO)_{10}$, using a 3-21g basis set.*

Table 5.5. shows the parameters for the calculated $MnTc(CO)_{10}$ geometry, compared to the monometallic species. With the exception of the $C_{ax}MC_{eq}$ bond angles the values do not differ significantly. The crystal structure for $MnRe(CO)_{10}$[9] has been solved for a D_{4d}

Table 5.5. Comparative geometries for calculated $Mn_2(CO)_{10}$, $Tc_2(CO)_{10}$ and $MnTc(CO)_{10}$

	Mn_2	MnTc		Tc_2
		Mn fragment	Tc fragment	
rM-M	2.808	2.933	*(2.900)*	2.992
$rM\text{-}C_{ax}$	1.768	1.774	1.940	1.940
$rM\text{-}C_{eq}$	1.818	1.811	2.005	1.999
$rC_{ax}\text{-}O$	1.183	1.185	1.181	1.183
$rC_{eq}\text{-}O$	1.180	1.184	1.177	1.180
$aC_{ax}MC_{eq}$	93.25	96.69	91.27	92.88
$aMC_{eq}O$	177.36	179.18	177.10	177.77

structure using a composite metal atom, with scattering power intermediate between Mn and Re. This solution only gives one set of ligand bond parameters: The bond lengths in $MnRe(CO)_{10}$ are between those of $Mn_2(CO)_{10}$ and $Re_2(CO)_{10}$, except that for Mn-Re which is 0.06 Å shorter(Mn-Re 2.909 Å; Mn-Mn 2.895 Å, Re-Re 3.041 Å, average 2.968 Å).

Our calculated structure shows two distinct environments around the metal atoms, with little change from the mono-metallic species. The Mn-Tc bond is 0.03 Å longer than the average, a value equal to the error in the calculated Tc-Tc bond length.

Table 5.6. Calculated Energy contributions to the M-M Bond Dissociation Enthalpies (D_e) for $M_2(CO)_{10}$ and $MM'(CO)_{10}$ in kJ mol^{-1}

	Mn-Mn	Mn-Tc	Average of $M_2(CO)_{10}$ values	Tc-Tc
E_e	234	242		240
E_e - 2 BSSE	110	122	*121*	131
E_R $Mn(CO)_5$	-18.06	-8.24		
E_R $Tc(CO)_5$		-9.83		-2.99
D_e	199	224	*217*	234
D_e - 2 BSSE	74.3	104	*99.7*	125

Table 5.6. shows some of the energy contributions to the calculated bond dissociation enthalpies for $M_2(CO)_{10}$ and $MM'(CO)_{10}$. Within experimental error, the calculated bond dissociation enthalpy for the mixed-metal compound is the average of the mono-metallic values.

For $MnRe(CO)_{10}$ two contradictory sets of experimental measurements are available, these are shown in Table 5.7. The differences in the two sets of values are extreme, with the surprising exception of the Re-Re values.

Table 5.7. Experimental bond dissociation energies in kJ mol^{-1}.

Method	Mn-Mn	Mn-Re	average (Mn-Re)	Re-Re	Ref.
Ionisation potential	94	210	*141*	187	10
Microcalorimetry	159	145	*173*	187	7

The negative ion, electron impact mass spectra of the molecules $Mn_2(CO)_{10}$, $MnRe(CO)_{10}$, and $Re_2(CO)_{10}$ has been examined be Meckstroth and Ridge[14] For an ionising electron energy of 4 eV approximately equal intensities of $Mn(CO)_5^-$ and $Mn_2(CO)_9^-$ were observed in the $Mn_2(CO)_{10}$ spectrum. For $MnRe(CO)_{10}$ the main product was $MnRe(CO)_9^-$, with small amounts of $Mn(CO)_5^-$ and $Re(CO)_5^-$ also present whereas for $Re_2(CO)_{10}$ no monometallic fragments were observed at all, even when the ionising energy was increased to 80 eV. Although an increase in metal-metal bond energy down the series is implied by these results no actual figures are given, as the observed results are also affected by the relative stability of the M-CO bonds. However, it is concluded that $D(Mn\text{-}Mn) < D(Mn\text{-}Re) < D(Re\text{-}Re)$ and that $EA(Mn(CO_{)5}) \approx EA(Re(CO)_5) \geq D(Mn\text{-}Re)$, where the electron affinity for $M(CO)_5^-$ is 234 ± 20 kJ mol^{-1}. As this value for the electron affinity is in part derived from the bond energy values of Junk and Svec[10] it supports their high value for the Mn-Re bond energy. However it, implies an Re-Re bond energy higher than either of the observed values.

Our calculations have shown no significant deviation from the mean value for the mixed-metal bond energy for $MnTc(CO)_{10}$. In this section we consider some of the upper occupied molecular orbitals.

Of the four highest occupied molecular orbitals of $Mn_2(CO)_{10}$, three involve metal-metal bonding. The HOMOs are degenerate (about the z-axis) e_3 π^* orbitals, mainly involving manganese d_{xz} or d_{yz}. For the metal fragment aligned with its ligand bonds along the x and y axes (shown to the left in Figure 5.2.) there is no contribution from ligands perpendicular to the metal d orbital. Similarly, on the 'diagonal' fragment there is no contribution from equatorial carbon orbitals. Superficially this electron density plot implies a separation in energy of the two manganese atoms. Thus it should be emphasised that this is only one of a pair of degenerate orbitals. The metal contribution includes some p_x or p_y character, which reduces the orbital density between the metal atoms, leading to the slightly 'squashed' appearance of the d_{xz} orbital.

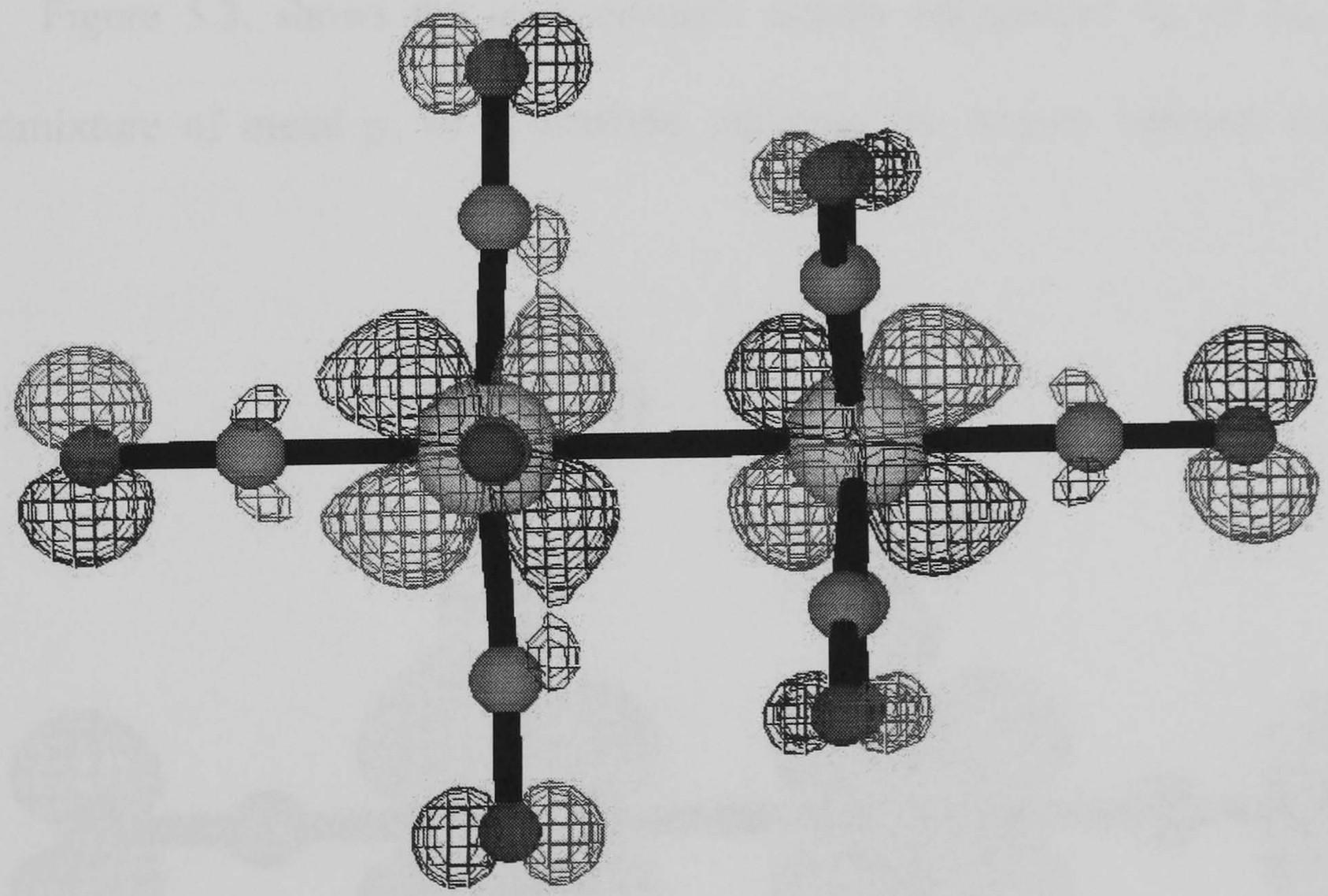


Figure 5.2. e_3 π^* oribtal for $Mn_2(CO)_{10}$.

Below the e_3 π^* orbitals lies the metal-metal a_1 σ orbital, primarily of manganese d_{z2} and p_z character (see Figure 5.4.). As with the HOMO the primary contribution from ligand orbitals involves O p_z.

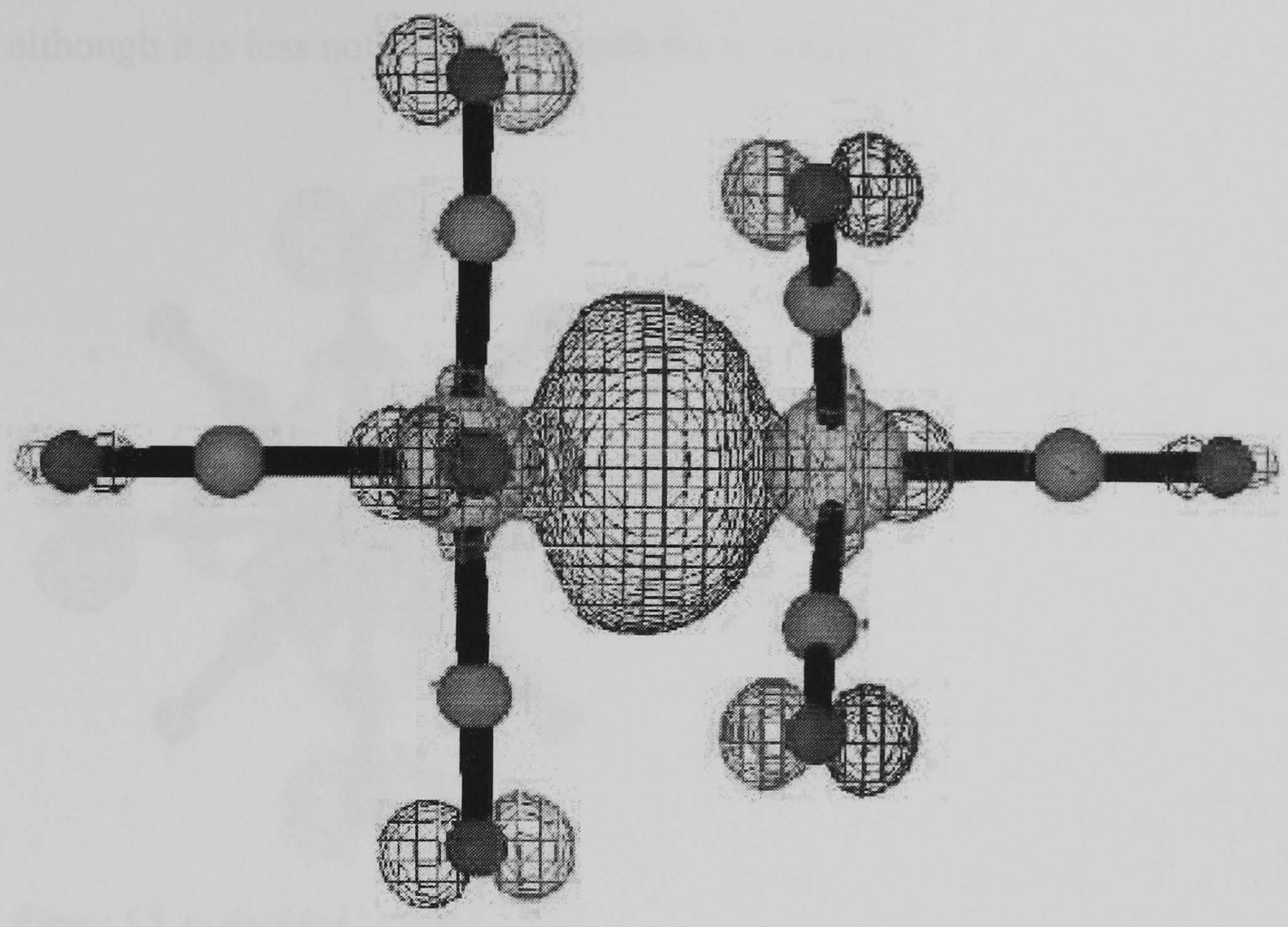


Figure 5.4. a_1 σ orbital for $Mn_2(CO)_{10}$

Figure 5.3. shows the e_1 π orbitals, mainly manganese d_{xz} or d_{yz}. Again there is admixture of metal p_x or p_y orbitals, reducing the density between the metal centres,

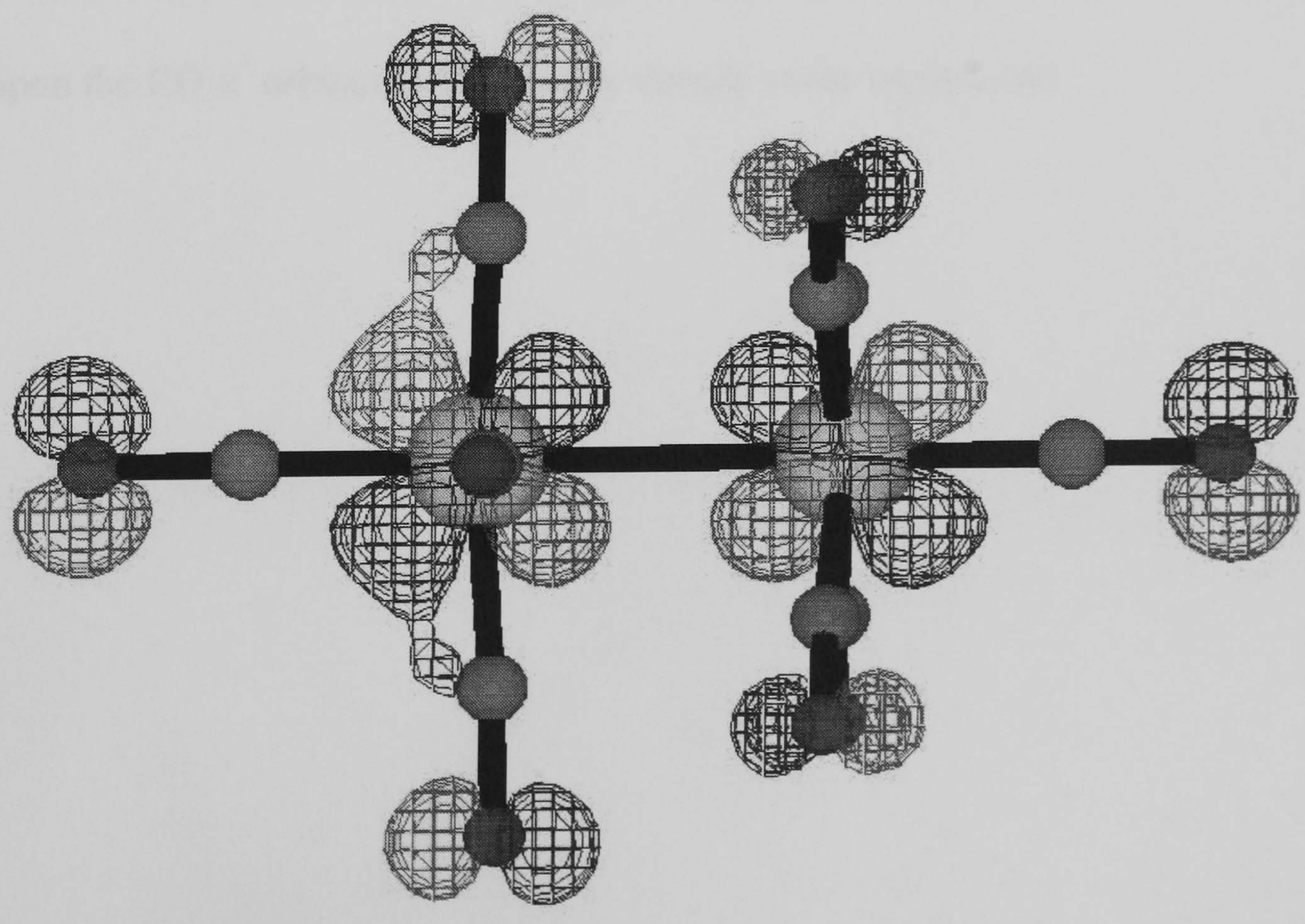


Figure 5.3. e_1 π orbital for $Mn_2(CO)_{10}$

although it is less noticable than with the π^* orbitals.

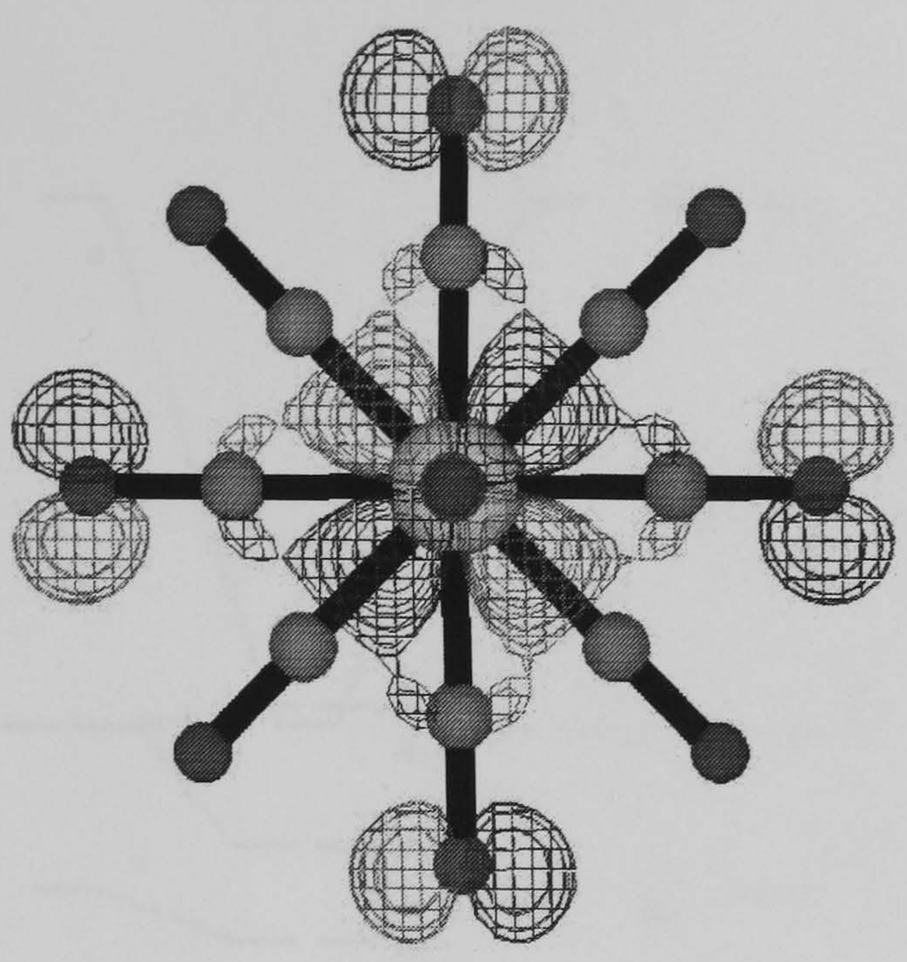


Figure 5.5. e_2 δ orbital for $Mn_2(CO)_{10}$

Below these lie the e_2 δ orbitals, involving either the d_{xy} or d_{x2-y2} of one metal atom and its equatorial π ligands. This set of orbitals is degenerate about the centre of the metal-metal bond. One component is shown in Figure 5.5 projected down the metal-metal bond (z-axis). As with all the high lying orbitals, the ligand contribution is mainly based upon the CO π^* orbital, with a greater density at the oxygen end.

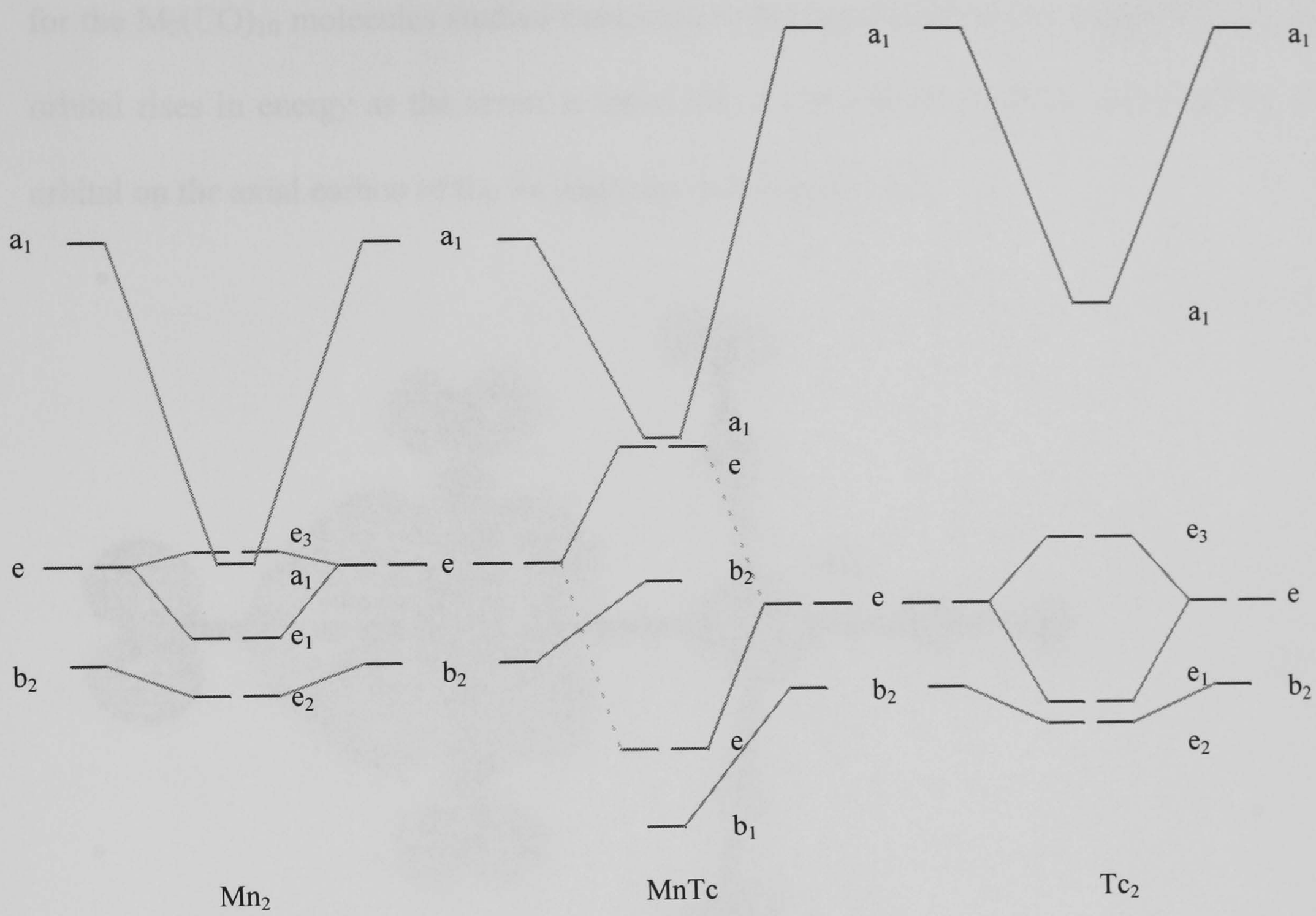


Figure 5.7. Relative energy levels for the upper occupied orbitals of $M_2(CO)_{10}$

Figure 5.7. shows the relative energy levels of the upper occupied molecular orbitals

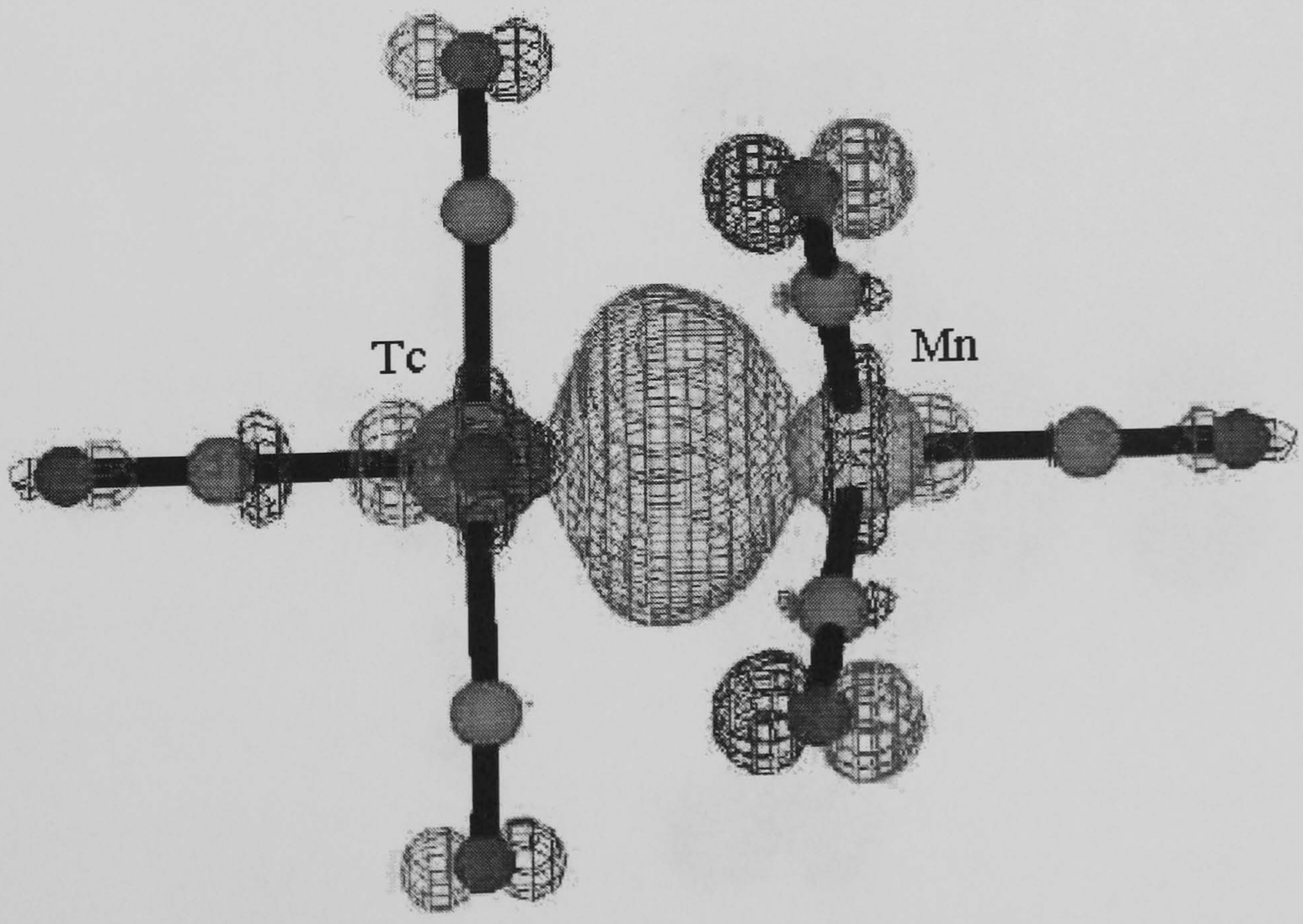


Figure 5.6. Highest occupied molecular orbital (a_1) for $MnTc(CO)_{10}$

for the $M_2(CO)_{10}$ molecules studied compared to the unrelaxed radical fragments. The a_1 orbital rises in energy as the series is traversed, due the presence of an out of phase sp orbital on the axial carbon of the Tc fragment (see Figure 5.6.)

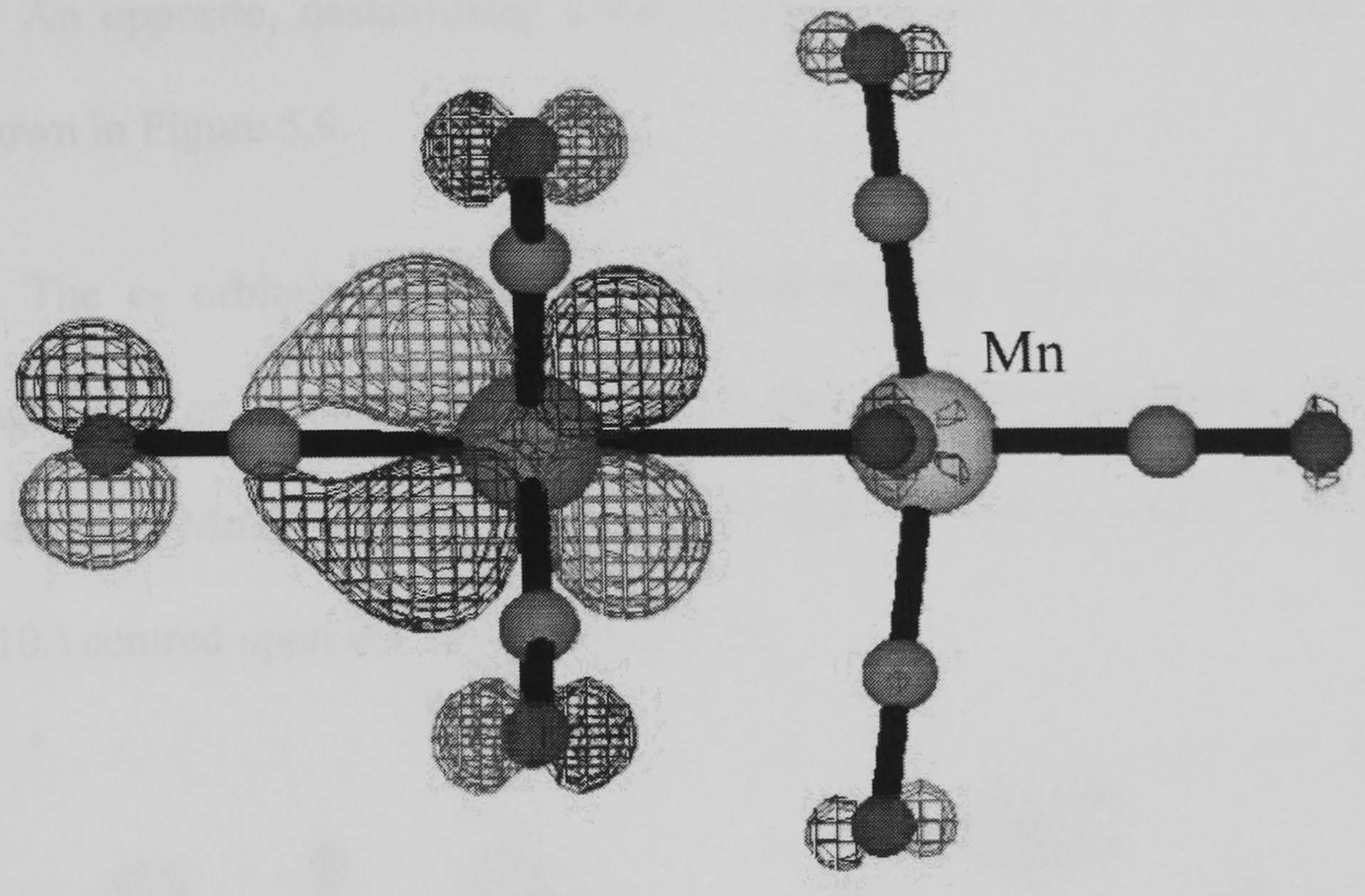


Figure 5.8. Low-lying e orbital for $MnTc(CO)_{10}$, centred on the $Tc(CO)_5$ fragment.

The π and π^* orbitals for $MnTc(CO)_{10}$ differ significantly from their homometallic

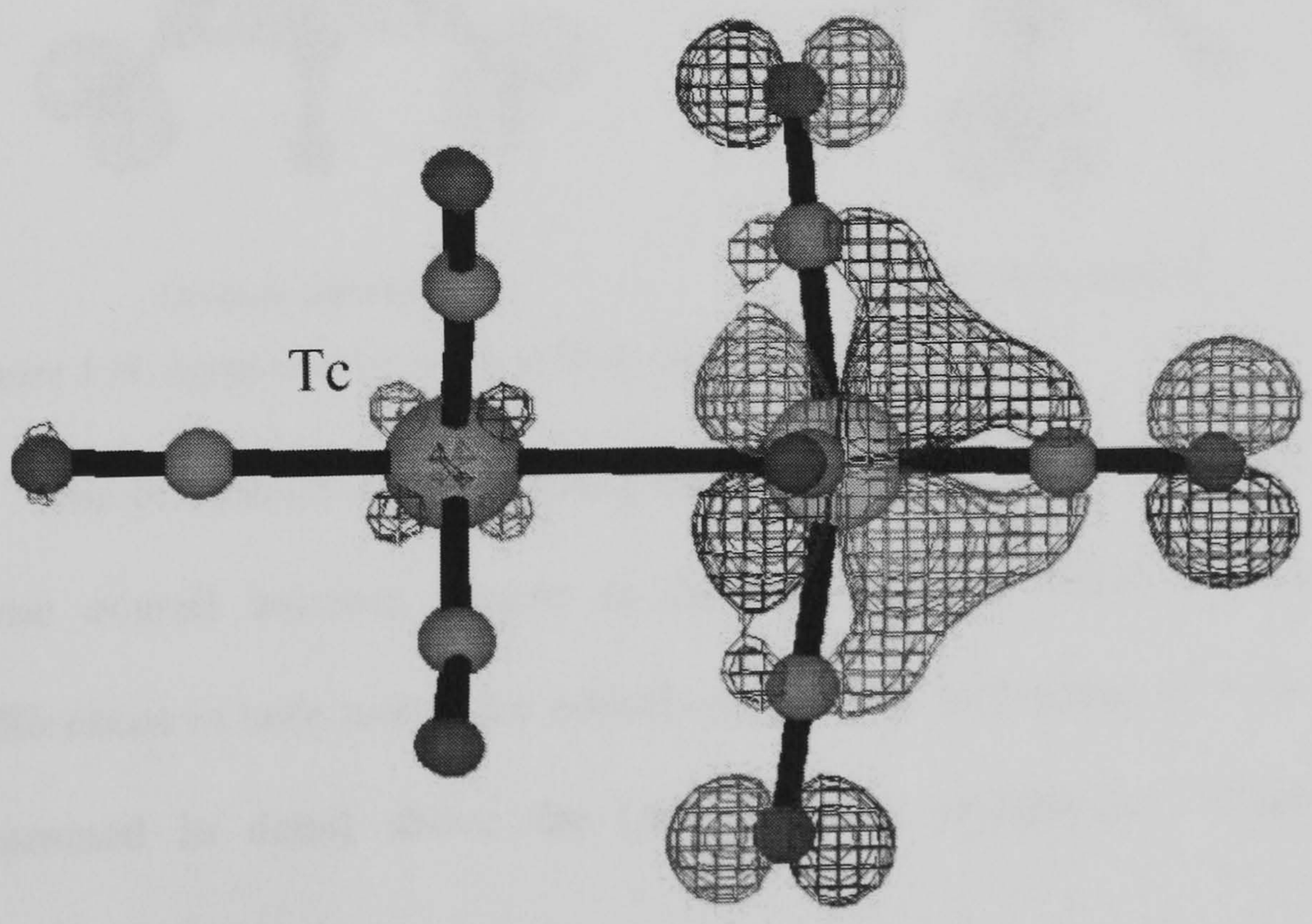
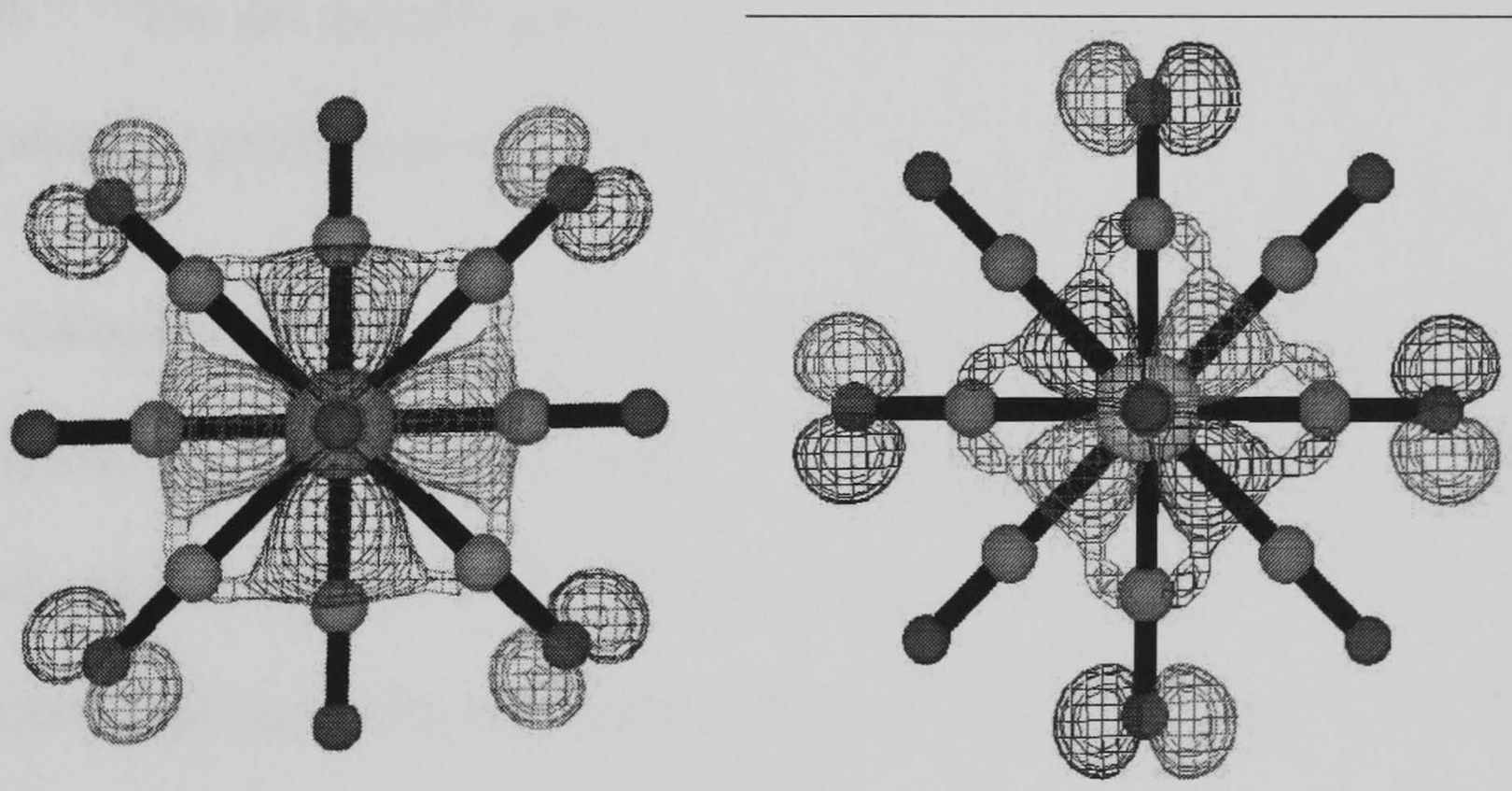


Figure 5.9. High-energy e orbital for $MnTc(CO)_{10}$, centred on Mn.

counterparts. The lower lying orbitals (shown in Figure 5.8.) are centred upon the $Tc(CO)_5$ fragment, with virtually no contribution from any Mn orbitals. As a result this orbital lies considerably lower in energy.

An opposite, destabilising effect is observed for the e orbital pair centred on Mn, shown in Figure 5.9.

The e_2 orbitals represent the π^* back-bonding for the equatorial ligands of one fragment. For the homometallic systems this gives two degenerate orbitals, whereas the equivalent MnTc orbitals are separated, with the lower energy, b_1 orbital (see Figure 5.10.) centred upon the $Tc(CO)_5$ fragment.



Orbitals centred on Tc *Orbitals centred on Mn*

Figure 5.10. Ligand back-bonding orbitals (b_1 and b_2) for MnTc.

This discussion of the bonding has shown that while $MnTc(CO)_{10}$ retains much the same overall bonding pattern as the homometallic species, there are some subtle differences in both molecular orbital composition and energy. For the molecular orbitals examined in detail above the (predominately manganese) destabilised orbitals are

balanced by equivalent stabilising effects on the Tc fragments. This is consistent with the absence of any deviation from the average value for the mixed-metal bond energy.

5.4. Relaxation of the mono-metallic fragments

The calculations discussed previously have involved the separation of the $M_2(CO)_{10}$ molecules into two $M(CO)_5$ fragments held in the geometry of the dimer. For a full comparison with experimental data, the relaxation of the radical fragment should also be considered.

$Mn(CO)_5$ has been isolated in CO and argon matrices. Analysis of the infra-red spectrum from these matrices is consistent with a C_{4v} structure with a $C_{ax}MnC_{eq}$ angle of ~ 96 °.[15] The esr spectrum also implies the C_{4v} structure, with the unpaired electron in an a_1 orbital of predominately d_{z2} character.[16]

Calculations performed using the DFT implementation of the GAUSSIAN[17] suite of programs on the $Mn(CO)_5$ radical with the high level basis set 6-311$^+$g* yield the anticipated structure, which is described in Table 5.8. The relaxation is very slight, the dominant feature being the increase in the angle between the axial and equatorial Mn-C bonds.

Table 5.8. Comparative geometric parameters for $Mn_2(CO)_{10}$ and $Mn(CO)_5$, calculated using GAUSSIAN 94 and a 6-311$^+$g* basis set.

	$Mn_2(CO)_{10}$	$Mn(CO)_5$
$rMn\text{-}C_{eq}$	1.855	1.857
$rMn\text{-}C_{ax}$	1.806	1.816
$rC_{eq}\text{-}O$	1.156	1.156
$rC_{ax}\text{-}O$	1.159	1.160
$aC_{ax}MnC_{eq}$	93.29	96.50
$aMnC_{eq}O$	177.0	179.4

When the basis set is reduced to 3-21g* $Mn(CO)_5$ does not minimise within the C_{4v} point group. If symmetry restraints are removed the geometry converges to an approximately C_{2v} structure, shown in Figure 5.11.a. The $Tc(CO)_5$ structure calculated under these conditions also breaks symmetry, although the final geometry is virtually indistinguishable from C_{4v} (see Figure 5.11.b).

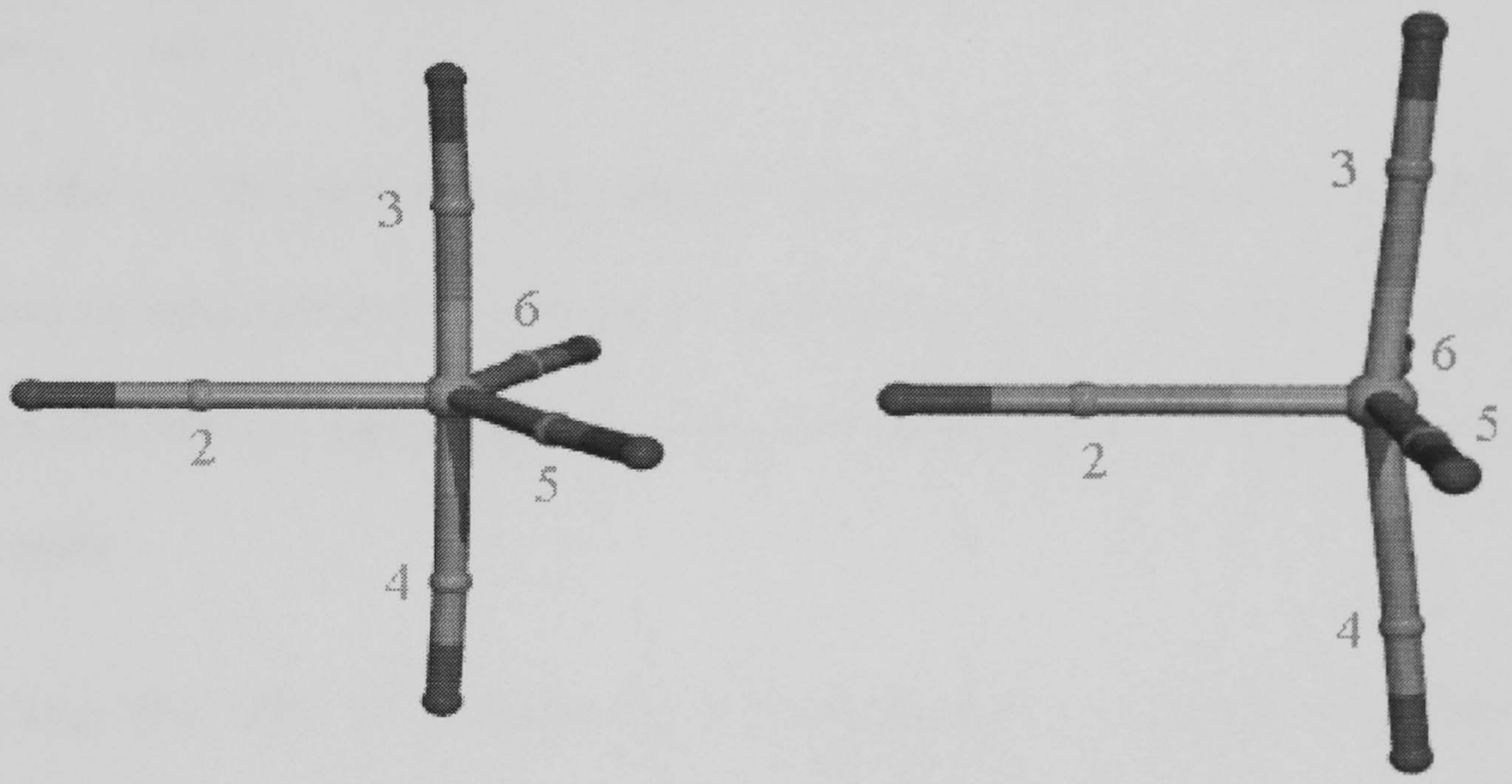


Figure 5.11. Optimised geometries for the $M(CO)_5$ radicals, using GAUSSIAN 98 and a 3-21g basis set*
a) M = Mn *b) M = Tc*

Table 5.9. shows the geometric parameters for the optimised $Mn(CO)_5$ radical. The greatest deviation from a C_{2v} structure is observed for the Mn-C_5 and Mn-C_6 bonds, with bond angles differing by 0.02°, considerably less divergence than that observed between the calculated geometries for $Mn_2(CO)_{10}$ using different basis sets (see Table 5.2). $Tc(CO)_5$ shows an order of magnitude less deviation from C_{2v}; 0.002°. At the level of accuracy shown by $Mn(CO)_5$ it may be considered essentially C_{4v}.

Table 5.9. Geometric parameters for $M(CO)_5$, optimised using GAUSSIAN 98 and a 3-21g basis set.*

$rMn\text{-}C_2$	1.788	$rC_2\text{-}O$	1.184	$rTc\text{-}C_2$	1.910	$rC_2\text{-}O$	1.184
$rMn\text{-}C_3$	1.811	$rC_3\text{-}O$	1.180	$rTc\text{-}C_3$	2.000	$rC_3\text{-}O$	1.181
$rMn\text{-}C_4$	1.811	$rC_4\text{-}O$	1.180	$rTc\text{-}C_4$	2.000	$rC_4\text{-}O$	1.181
$rMn\text{-}C_5$	1.824	$rC_5\text{-}O$	1.182	$rTc\text{-}C_5$	2.000	$rC_5\text{-}O$	1.181
$rMn\text{-}C_6$	1.824	$rC_6\text{-}O$	1.182	$rTc\text{-}C_6$	2.000	$rC_6\text{-}O$	1.181
		$aMnC_2O$	179.99			$aTcC_2O$	180.00
aC_2MnC_3	89.62	$aMnC_3O$	178.51	aC_2TcC_3	95.00	$aTcC_3O$	179.60
aC_2MnC_4	89.63	$aMnC_4O$	178.51	aC_2TcC_4	95.01	$aTcC_4O$	179.60
aC_2MnC_5	109.40	$aMnC_5O$	174.60	aC_2TcC_5	95.03	$aTcC_5O$	179.61
aC_2MnC_6	109.38	$aMnC_6O$	174.60	aC_2TcC_6	95.03	$aTcC_6O$	179.61
aC_5MnC_6	141.22						

As the C_{2v} like geometry only appears under the 3-21g* basis set it may be attributed to basis set incompleteness. A frequency calculation on this structure has yielded only real modes of vibration, indicating that, at this level of calculation, it represents a true energy minimum.

Using the ADF 2.3 program we have been able to minimise the $Mn(CO)_5$ and $Tc(CO)_5$ radicals under both C_{4v} and C_{2v} geometries and the results are shown in Table 5.10. The basis set used was of triple zeta quality with additional polarisation functions for d and f orbitals[18], comparable to 6-311+g*. The divergence's from the C_{4v} geometry are less than those observed using the 3-21g* under GAUSSIAN 98. $Tc(CO)_5$ again shows less deviation, although it clearly belongs to the C_{2v} point group. The differences in energy between the alternate symmetries are small, 1.63 kJ mol^{-1} for $Mn(CO)_5$ and 0.45 kJ mol^{-1} for $Tc(CO)_5$. In both cases the C_{4v} structure has the lower energy.

Table 5.10. Comparative geometries for $M(CO)_5$ optimised under C_{4v} and C_{2v} symmetries using ADF 2.3

	$Mn(CO)_5$		$Tc(CO)_5$	
	C_{4v}	C_{2v}	C_{4v}	C_{2v}
$rM\text{-}C_2$	1.810	1.813	1.939	1.938
$rM\text{-}C_3$	1.854	1.851	2.016	2.013
$rM\text{-}C_4$	1.854	1.851	2.016	2.013
$rM\text{-}C_5$	1.854	1.855	2.016	2.014
$rM\text{-}C_6$	1.854	1.855	2.016	2.014
$rC_2\text{-}O$	1.155	1.156	1.153	1.154
$rC_3\text{-}O$	1.153	1.152	1.150	1.150
$rC_4\text{-}O$	1.153	1.152	1.150	1.150
$rC_5\text{-}O$	1.153	1.154	1.150	1.149
$rC_6\text{-}O$	1.153	1.154	1.150	1.149
aC_2MC_3	95.59	91.07	94.86	94.97
aC_2MC_4	95.59	91.07	94.86	94.97
aC_2MC_5	95.59	102.78	94.86	96.28
aC_2MC_6	95.59	102.78	94.86	96.28
aC_4MC_6		154.44		
aMC_2O	180.00	180.00	180.0	180.00
aMC_3O	177.98	177.91	178.36	179.01
aMC_4O	177.98	177.91	178.36	179.01
aMC_5O	177.98	178.02	178.36	179.76
aMC_6O	177.98	178.02	178.36	179.76

5.5. Conclusion

We have examined the bond breaking enthalpies for $Mn_2(CO)_{10}$, $MnTc(CO)_{10}$ and $Tc_2(CO)_{10}$ using the density functional implementation of GAUSSIAN. The metal-metal bond enthalpy for $MnTc(CO)_{10}$ was found to lie almost exactly between those for $Mn_2(CO)_{10}$ and $Tc_2(CO)_{10}$, in contrast to the experimental results for the $MnRe(CO)_{10}$ compound.

Our investigation of the relaxation geometry of the $M(CO)_5$ radical has yielded a C_{2v} structure. Investigation of this system using ADF 2.3. has shown it to be slightly higher in

energy than the, experimentally observed, C_{4v} system. For the GAUSSIAN program at the 3-21g* level only the C_{2v} symmetry is observed. For all of the calculated $M(CO)_5$ structures the deviation from that of the dimeric $M_2(CO)_{10}$ is very slight, with the M-C_{ax} bond length and the $C_{ax}MC_{eq}$ bond angle showing the greatest change.

5.6. Theoretical Methods

Calculations for this chapter were performed using GAUSSIAN 94[17], GAUSSIAN 98[18] and Amsterdam Density Functional 2.3.[13] All programs used the exchange functional due to Becke[19] and the correlation functional due to Perdew[20]

It was not possible to perform all the calculations on one system. As discussed previously, optimisation of the $Mn(CO)_5$ radical at the 3-21g* level fails to minimise with the experimentally observed C_{4v} point group. This attributed to incompleteness of this low level basis set. Conversely attempts to calculate the $M_2(CO)_{10}$ species using ADF rapidly generate catastrophically large temporary files: The SG Indigo 2 used for ADF calculations has over 2GB free space available, nevertheless this is filled, causing a program failure, during the initial SCF stages. This version of ADF and the SG workstation are obsolete, thus the exact cause has not been traced. Swap file and temporary file errors also occur in the computer logs during the use of XQuest and Netscape, suggesting a hardware cause.

The GAUSSIAN calculations were performed by Edward Griffiths of the Ian Gould group. The Basis Set Superposition Error was calculated by the counterpoise method.[21]

5.7. References

1 J.A. Martinho Simoes, J.C. Schultz and J.L. Beauchamp, *Organometallics*, **4** (1985) 1238

2 D.R. Bidinosti and N.S. McIntyre, *Can. J. Chem.* **48** (1970) 593

3 A.E. Stevens, *PhD Thesis*, California Institute of Technology, 1981

4 A. Marcomini and A. Poë, *J. Am. Chem. Soc.* **105** (1983) 6952

5 J.L. Goodman, K.S. Peters and V. Vaida, *Organometallics*, **5** (1986) 815

6 G.P. Smith, *Polyhedron*, 7 (1988) 1605

7 S.J Addison, J.A. Connor and J.A. Kinkaid, *J. Organomet. Chem.* **554** (1998) 123

8 A. Rosa, A.W. Ehlers, E.J. Baerends, J.G. Snijders and G. te Velde, *J. Phys. Chem.* **100** (1996) 5690

9 A.L. Rheingold, W.K. Meckstroth and D.P. Ridge, *Inorg. Chem.* **25** (1986) 3706

10 G.A. Junk, H.J. Svec, *J. Chem. Soc. A,* (1970) 2102

11 M. Martin, B. Rees and A. Mitschler, *Acta Crystallogr.* **B38** (1982) 6

12 A. Almenningen, G.G. Jacobsen and H.M. Seip, *Acta Chem, Scand.* **23** (1969) 685

13 a) E.J.Baerends, D.E. Ellis and P. Ros., *Chem.Phys.* **2** (1973) 41,
b) G.te Velde, E.J.Baerends, *J.Comp.Phys.* **99** (1992) 84,
c) C.Fonseca Guerra, O. Visser, J.G. Snijders and G. teVelde, *Methods and Techniques in Computational Chemistry-95,* E. Clementi and C. Corongiu. Eds.:STEF: Cagliari (1995) 305

14 W.K. Meckstroth and D.P. Ridge, *J. Am. Chem. Soc.* **107** (1985) 2281

15 S.P.Church, M. Poliakiff, J.A. Timney and J.J. Turner, *J. Am. Chem. Soc.* **103** (1981) 7515

16 M.C.R. Symons and R.L Sweany, *Organomet.* **1** (1982) 834

17 a) *Gaussian 94, Revision E.1*, M.J. Frisch, G.W. Trucks, H.B. Schlegel, P.M.W. Gill, B.G. Johnson, M.A. Robb, J.R. Cheeseman, T. Keith, G.A. Petersson, J.A. Montgomery, K. Raghavachari, M.A. Al-Laham, V.G. Zakrzewski, J.V. Ortiz, J.B. Foresman, J. Cioslowski, B.B. Stefanov, A. Nanayakkara, M. Challacombe, C.Y. Peng, P.Y. Ayala, W. Chen, M.W. Wong, J.L. Andres, E.S. Replogle, R. Gomperts, R.L. Martin, D.J. Fox, J.S. Binkley, D. . Defrees, J. Baker, J.P. Stewart, M. Head-Gordon, C. Gonzalez, and J.A. Pople, Gaussian, Inc., Pittsburgh PA, 1995.
b) *Gaussian 98, Revision A.5*, M.J. Frisch, G.W. Trucks, H.B. Schlegel, G.E. Scuseria, M.A. Robb, J.R. Cheeseman, V.G. Zakrzewski, J.A. Montgomery, Jr., R.E. Stratmann, J.C. Burant, S. Dapprich, J.M. Millam, A.D. Daniels, K.N. Kudin, M.C. Strain, O. Farkas, J. Tomasi, V. Barone, M. Cossi, R. Cammi, B. Mennucci, C. Pomelli, C. Adamo, S. Clifford, J. Ochterski, G.A. Petersson, P.Y. Ayala, Q. Cui, K. Morokuma, D.K. Malick, A.D. Rabuck, K. Raghavachari, J.B. Foresman, J. Cioslowski, J.V. Ortiz, B.B. Stefanov, G. Liu, A. Liashenko, P. Piskorz, I. Komaromi, R. Gomperts, R.L. Martin, D.J. Fox, T. Keith, M.A. Al-Laham, C.Y. Peng, A. Nanayakkara, C. Gonzalez, M. Challacombe, P.M.W. Gill, B. Johnson, W. Chen, M.W. Wong, J.L. Andres, C. Gonzalez, M. Head-Gordon, E.S. Replogle, and J.A. Pople, Gaussian, Inc., Pittsburgh PA, 1998.

18 J.G. Snijders, E.J. Baerends and P. Vernooijs, *At. Nucl. Data Tables,* **26** (1982) 483

19 A.D. Becke, *Phys. Rev.A,* **38** (1988) 3098

20 J.P. Perdew, P*hys. Rev. B,* **33** (1986) 8822

21 S.F. Boys and F. Bernadi, *Mol. Phys.* **19** (1970) 553